



VCU

Virginia Commonwealth University
VCU Scholars Compass

Theses and Dissertations

Graduate School

2017

Discovery and characterization of bile acid and steroid metabolism pathways in gut-associated microbes

Spencer Harris
Virginia Commonwealth University

Follow this and additional works at: <https://scholarscompass.vcu.edu/etd>



Part of the [Microbial Physiology Commons](#)

© Spencer C. Harris

Downloaded from

<https://scholarscompass.vcu.edu/etd/4713>

This Dissertation is brought to you for free and open access by the Graduate School at VCU Scholars Compass. It has been accepted for inclusion in Theses and Dissertations by an authorized administrator of VCU Scholars Compass. For more information, please contact libcompass@vcu.edu.

DISCOVERY AND CHARACTERIZATION OF BILE ACID AND STEROID METABOLISM
PATHWAYS IN GUT-ASSOCIATED MICROBES

A dissertation submitted in partial fulfillment of the requirements for the degree of Doctor of
Philosophy at Virginia Commonwealth University

By

SPENCER C. HARRIS

Bachelor of Science, University of Richmond, 2011

Director: PHILLIP B. HYLEMON

PROFESSOR OF MICROBIOLOGY AND IMMUNOLOGY

Virginia Commonwealth University

Richmond, Virginia

April 2017

Acknowledgements

Many individuals have been instrumental in helping me to succeed during my graduate education at Virginia Commonwealth University. First and foremost, I owe a great debt to my mentor, Dr. Phillip Hylemon. His depth of knowledge and passion for scientific discovery are unparalleled. He stands as a paradigm for how to pursue academic research in its ever-changing landscape. The skills that I learned during my tenure as in his laboratory go well beyond technical proficiencies. He has taught me what it truly means to be on the cutting edge of discovery, to think rationally and independently, and to always question what is presented as fact. The inner fire that drives him is easy to see for anyone that works with him. Some sparks of this fire ignited a similar passion for scientific discovery within me. It is my sincere hope that my fire burns to a similar intensity that it does in Phil in my future scientific career.

I want to thank my lab mates, those that I spent so much time with the past four years. DJ Kang, I appreciate all of the guidance you gave me during my time here. I want to thank Dr. Jason Ridlon for his help during my first few years in lab and continued collaboration for numerous projects. I want to thank Emily Gurley for all the work she does to keep our lab running smoothly. I also want to thank Dr. Zhou and lab members who shared lab space and were always helpful whenever it was needed. Additionally, I want to thank the entirety of the Lipid Research group for their input over the past few years. Specifically I want to thank Patsy Cooper and Genta Kakiyama for their help on numerous projects and teaching me new techniques. I also want to thank the VCU Microbiology and Immunology department, especially Martha VanMeter for all of her assistance throughout my time in the program.

I owe great thanks to the members of my committee; Dr. Cynthia Cornelissen, Dr. Kimberly Jefferson, Dr. William Pandak, and Dr. Arun Sanyal. Their insight and support was instrumental in my graduate education, and I cannot thank them enough for their help in getting me to this point.

The MD-PhD program has been a great source of support during my graduate years. I want to specifically thank the past and current directors; Dr. Archer, Dr. Mikkelsen, and Dr. Donnenberg. Their passionate support of MD-PhD students and sincere desire to see them succeed makes this difficult path more manageable. I also want to thank Sandra Sorrell for all of her help across the years. A special thanks is due to my MD-PhD classmates who are always there to exchange ideas, help with experimental design, or be a supportive friend. I especially want to thank Adam Blakeney, Marc Cantwell, Devin Cash, Sheela Damle, Mackenzie Lind, Nicholas Russell, and Michael Waters. I wish you all the very best in your future careers and I cannot wait to see the amazing work you all will continue to do in the future.

I want to thank all of my friends outside of the VCU community that have supported me. I want to thank my family, especially my two brothers and parents. They are the unwavering foundation on which I stand.

Lastly, I want to thank my girlfriend Natalie. You have been my partner and best friend through these trying years. I cannot thank you enough for your support. You inspire me, keep me focused, and have always been able to make me laugh, especially when I need it the most.

Table of Contents

Table of Contents	iii
List of Figures.....	vi
List of Tables.....	x
List of Symbols and Abbreviations	xii
Abstract.....	xviii
Chapter 1: Introduction.....	1
I. Introduction to the human gut microbiome	1
II. Microbial fermentation of complex carbohydrates in the large intestine.....	2
III. Microbial production of hydrogen gas in the large intestine.....	6
IV. Hydrogen gas utilization by microbes in the large intestine	7
V. Bile acid formation and enterohepatic circulation.....	22
VI. Bile acid metabolism by gut microbes	25
VII. Consequences of bile acid metabolism on microbial and host physiology	31
VIII. Research Objectives	37
Chapter 2: Materials and Methods	39
I. Bacterial strains and materials.....	39
II. Production of radiolabeled secondary bile acids and bile acid metabolism screening.....	40
III. Bile acid metabolite characterization	41
IV. Steroid metabolism screening.....	42
V. Primer design, polymerase chain reaction, and plasmid construction.....	43
VI. C592 genomic sequencing.....	44

VII.	<i>Clostridium scindens</i> VPI 12708 RNA purification and Illumina sequencing	45
VIII.	Protein overexpression and purification	47
IX.	Δ 4,6 reductase and 17 α -HSDH purified enzymatic reactions.....	48
X.	Bioinformatic analysis and statistics	50
Chapter 3: Characterization of novel <i>Eggerthella lenta</i> strain C592		57
I.	Introduction	57
II.	Results	67
	A. Initial screening of C592 primary bile acid metabolism	67
	B. Determination of C592 phylogeny based on 16S sequencing.....	79
	C. Comparison of phenotypic similarities between C592 and <i>Eggerthella lenta</i> ATCC 25559 type strain.....	79
	D. Comparison of bile acid metabolism by C592 and 25559	79
	E. Mass spectrometry characterization of C592 CDCA and DCA metabolites.....	88
	F. Comparison of steroid metabolism by C592 and 25559	91
	G. Whole genomic sequencing of C592 and comparison to <i>E. lenta</i> type strain.....	94
	H. Searching the C592 genome for an explanation for the production of oxo-bile acid derivatives under anaerobic conditions	101
	I. Identifying gene clusters of interest in C592 and 25559	107
	J. Varying atmospheric gases alters C592 and 25559 bile acid and steroid metabolism	129
	K. C592 oxo-bile acid derivatives inhibit 7 α -dehydroxylation <i>in vitro</i>	141
III.	Discussion.....	149
Chapter 4: <i>Clostridium scindens</i> ATCC 35704 Δ 4,6 reductase gene discovery		162

I. Introduction	162
II. Results	167
III. Discussion.....	181
Chapter 5: <i>Clostridium scindens</i> VPI 12708 RNAseq and 17 α -HSDH gene discovery.....	183
I. Introduction	183
II. Results	188
III. Discussion.....	205
Chapter 6: Summary and Perspectives	209
Literature Cited.....	218
Vita	240

List of Figures

Figure 1.1. Chemical structure of major short chain fatty acids produced by gut-associated microbes	4
Figure 1.2. Biochemistry of the methanogenesis pathway in archaea from CO ₂	9
Figure 1.3. Biochemistry of sulfidogenesis in gut microbes from sulfate and taurine.....	13
Figure 1.4. Diagram of acetate formation via the Wood Ljungdahl pathway	18
Figure 1.5. Schematic of RNF complex and ATP synthase in acetogens	20
Figure 1.6. Chemical structure of primary bile acids and their conjugates	24
Figure 1.7. Diagram of bile salt biotransformations by gut bacteria.....	28
Figure 3.1. Diagram of reductive digoxin inactivation by <i>Eggerthella lenta</i>	60
Figure 3.2. TLC of whole cell extracts from various fecal bacterial strains induced by cholic acid to metabolize [24- ¹⁴ C]-cholic acid	69
Figure 3.3. Conversion of [24- ¹⁴ C]-cholic acid by allocholic acid- and cholic acid-induced C592	71
Figure 3.4. Conversion of [24- ¹⁴ C]-chenodeoxycholic acid by chenodeoxycholic acid-induced C592	73
Figure 3.5. TLC separation of organic extracts from <i>C. scindens</i> VPI 12708 and C592 bile acid-induced whole cell conversions of [24- ¹⁴ C]-cholic acid	76
Figure 3.6. TLC separation of organic extracts from <i>C. scindens</i> VPI 12708, <i>C. absonum</i> , and C592 CDCA-induced whole cell conversions of [24- ¹⁴ C]-chenodeoxycholic acid.....	78
Figure 3.7. TLC separation of chenodeoxycholic acid-induced C592 and <i>Eggerthella lenta</i> ATCC 25559 whole cell metabolism of [24- ¹⁴ C]-chenodeoxycholic acid.....	83

Figure 3.8. TLC separation of cholic acid-induced C592 and <i>Eggerthella lenta</i> ATCC 25559 whole cell metabolism of [24- ¹⁴ C]-cholic acid	85
Figure 3.9. TLC separation of deoxycholic acid-induced C592 and <i>Eggerthella lenta</i> ATCC 25559 whole cell metabolism of [24- ¹⁴ C]-deoxycholic acid.....	87
Figure 3.10. C592 chenodeoxycholic acid metabolite separation and MS characterization.....	90
Figure 3.11. C592 deoxycholic acid metabolite separation and MS characterization	93
Figure 3.12. C592 metabolizes testosterone to androstenedione under inert N ₂ gas.....	96
Figure 3.13. Summary of C592 and 25559 bile acid and neutral steroid metabolic potential	98
Figure 3.14. Mauve alignment of C592 and <i>E. lenta</i> type strain genomes	103
Figure 3.15. Overall C592 BlastKOALA results	106
Figure 3.16. C592 encodes genes annotated to be involved in the Wood Ljungdahl pathway..	109
Figure 3.17. KEGG map of C592 arginine metabolism genes and the link to Kreb’s cycle.....	112
Figure 3.18. Gene cluster alignment of “ <i>bai</i> -like” operon from C592 and 25559.....	117
Figure 3.19. Gene cluster alignment of the putative cardiac glycoside reductase operon from C592 and 25559.....	119
Figure 3.20. Gene cluster alignment of RNF complex operon from C592 and 25559	121
Figure 3.21. Gene cluster alignment of energy-conserving hydrogenase operon from C592 and 25559	124
Figure 3.22. Gene cluster alignment of ATP synthase operon from <i>E. lenta</i> strains C592 and 25559	126
Figure 3.23. Quantitation of C592 and 25559 metabolites of CDCA when grown overnight under inert N ₂ gas	136

Figure 3.24. Quantitation of C592 and 25559 metabolites of CDCA when grown overnight under CO ₂ gas.....	138
Figure 3.25. Quantitation of C592 and 25559 metabolites of CDCA when grown overnight under H ₂ gas	140
Figure 3.26. <i>C. scindens</i> VPI 12708 metabolism of CA and CDCA does not change under anaerobic CO ₂ or H ₂ atmospheric gas	143
Figure 3.27. <i>C. scindens</i> VPI 12708 recognizes C592 CDCA metabolites but is unable to effectively 7 α -dehydroxylate	145
Figure 3.28. Coculture of <i>C. scindens</i> VPI 12708 and C592 inhibits 7 α -dehydroxylation of CDCA.....	147
Figure 3.29. Illustration of C592 whole cell redox balancing with bile acids under low H ₂ partial pressure.....	154
Figure 3.30. Illustration of C592 whole cell redox balancing with bile acids under high H ₂ partial pressure.....	159
Figure 4.1. Schematic of 7 α -dehydroxylation pathway in <i>Clostridium scindens</i> ATCC 35704	165
Figure 4.2. Schematic representation of the reactions catalyzed by squalene desaturase and the oxidation of 3-dehydro-4-DCA to 3-dehydro-DCA in the 7 α -dehydroxylation pathway	170
Figure 4.3. Overexpression and purification of rEDS08212.1 from <i>C. scindens</i> ATCC 35704	172
Figure 4.4. Autoradiograph of thin layer chromatography separation of rEDS08212.1 reaction products from [24- ¹⁴ C]-3-dehydro-DCA.....	175
Figure 4.5. LCMS-IT-TOF analysis of rEDS08212.1 reaction products	177

Figure 4.6. Maximum likelihood phylogenetic tree of EDS08212.1 from <i>Clostridium scindens</i> ATCC 35704	180
Figure 5.1. Biotransformations of cortisol by gut microbes.....	186
Figure 5.2. <i>Clostridium scindens</i> VPI 12708 exhibits inducible 17 α -HSDH activity	190
Figure 5.3. <i>Clostridium scindens</i> VPI 12708 produces a secondary metabolite from androstenedione that maintains the 4-ene-3-keto moiety	192
Figure 5.4. NMR analysis of <i>Clostridium scindens</i> VPI 12708 androstenedione metabolite confirms epitestosterone formation	194
Figure 5.5. Overall transcriptomic heatmap of <i>Clostridium scindens</i> VPI 12708 induced with numerous bile acid and steroid molecules.....	202
Figure 6.1. Model of <i>Eggerthella lenta</i> C592 bile acid metabolism <i>in vivo</i>	214

List of Tables

Table 2.1. Bacterial strains used in the present study.....	51
Table 2.2. Primers used in the present study.....	52
Table 2.3. Plasmids used in the present study.....	56
Table 3.1. Overnight growth comparison between C592 and <i>E. lenta</i> ATCC 25559.....	80
Table 3.2. De novo hybrid assembly of the five largest contigs from C592 genomic sequencing.....	99
Table 3.3. Nucleotide level comparisons between C592 NODE_1 contig and the <i>E. lenta</i> type strain closed genome.....	100
Table 3.4. CDS protein annotation comparison between C592 and <i>Eggerthella lenta</i> type strain.....	104
Table 3.5. Wood Ljungdahl pathway homologous genes in C592 and <i>E. lenta</i> ATCC 25559..	110
Table 3.6. Annotated reductase in C592 and <i>E. lenta</i> ATCC 25559 genomes.....	113
Table 3.7. Annotated arginine and agmatine metabolism genes in <i>E. lenta</i> strain C592.....	127
Table 3.8. Annotated glutamate and histidine decarboxylating genes in <i>E. lenta</i> strain C592..	128
Table 3.9. Annotated genes from Krebs's cycle in <i>E. lenta</i> strain C592.....	130
Table 3.10. Annotated genes for arginine biosynthesis in <i>E. lenta</i> strain C592.....	133
Table 4.1. Flavin reductases identified in the genome of <i>Clostridium scindens</i> ATCC 35704.	168
Table 5.1. Induction of bile acid inducible operon of <i>Clostridium scindens</i> VPI 12708 by cholic acid and allocholic acid.....	196
Table 5.2. Genes upregulated in <i>Clostridium scindens</i> VPI 12708 in response to androstenedione induction.....	198

Table 5.3. Putative 17 α -HSDH genes from <i>Clostridium scindens</i> VPI 12708 screened for activity	203
---	-----

Symbols and Abbreviations

°	degree
%	percent
α	alpha
β	beta
Δ	delta
ΔG°'	standard free energy change
μCi -	microcurie
μL	microliter
μM	micromolar
11β-OHAD	11β-hydroxyandrostenedione
AB	antibiotic
ACA	allocholic acid
ADP	adenosine diphosphate
AMP	adenosine monophosphate
amu	atomic mass unit
ASBT	apical sodium-codependent bile acid transporter
ATP	adenosine triphosphate
BA7	bile acid 7α-dehydroxylation
bai	bile acid-inducible
BHI	brain heart infusion extract

bp	base pair
BSEP	bile salt export pump
BSH	bile salt hydrolase
C	celcius
C#	carbon (corresponding number on steroid backbone)
CA	3 α ,7 α ,12 α -trihydroxy-5 β -cholan-24-oic acid
CCK	cholecystokinin
CDCA	3 α ,7 α -dihydroxy-5 β -cholan-24-oic acid
CDI	<i>Clostridium difficile</i> infection
CFU	colony forming unit
CH ₄	methane
CO	carbon monoxide
CO ₂	carbon dioxide
CoA	coenzyme A
COG	Clusters of Orthologous Groups
CRC	colorectal cancer
DCA	3 α ,12 α -dihydroxy-5 β -cholan-24-oic acid
DNA	deoxyribonucleic acid
Ech	energy-conserving hydrogenase
EDTA	ethylenediaminetetraacetic acid
EGFR	epidermal growth factor receptor
ESI	electrospray ionization
FAD	flavin adenine dinucleotide

Fd	ferredoxin
FGF	fibroblast growth factor
FMN	flavin mononucleotide
FXR	farsenoid X receptor
g	gram
G protein	guanine nucleotide-binding protein
GC	gas chromatography
H ₂	dihydrogen gas
H ₂ S	hydrogen sulfide
HCl	hydrochloric acid
HDAC	histone deacetylase
HPLC	high pressure liquid chromatography
HSDH	hydroxysteroid dehydrogenase
IPTG	isopropyl beta-D-1-thiogalactopyranoside
iso	isomerized
IT	ion trap
J	joule
K	potassium
KEGG	Kyoto Encyclopedia of Genes and Genomes
kPa	kilopascal
L	liter
LB	lysogeny broth
LC	liquid chromatography

LCA	3 α -hydroxy-5 β -cholan-24-oic acid
LCB	localized collinear blocks
M	molar
m/z	mass/charge ratio
M _{2,3}	muscarinic receptors 2 and 3
mg	milligram
min	minute
mL	milliliter
mM	millimolar
MRM	multiple reaction monitoring
mRNA	messenger ribonucleic acid
MS	mass spectrometry
N	Normality
N ₂	dinitrogen gas
Na	sodium
NaCl	sodium chloride
NAD	nicotinamide adenine dinucleotide (oxidized)
NADH	nicotinamide adenine dinucleotide (reduced)
NADP	nicotinamide adenine dinucleotide phosphate (oxidized)
NADPH	nicotinamide adenine dinucleotide phosphate (reduced)
nM	nanomolar
NTCP	sodium taurocholate cotransporting polypeptide
OD	optical density

OST	organic solute transporter
OTU -	operational taxonomic unit
oxo	oxidized
PCR	polymerase chain reaction
psi	pounds per square inch
PXR	pregnane-activated receptor
Rf	retardation factor
RNA -	ribonucleic acid
RNAseq -	ribonucleic acid sequencing
RNF	Rhodobacter nitrogen fixation
RPM -	revolutions per minute
rRNA	ribosomal ribonucleic acid
R _T	retention time
S1PR2	sphingosine-1 phosphate receptor 2
SCFA	short chain fatty acid
SDS	sodium dodecyl sulfate
SSC	saline sodium citrate
TEG	triethyleneglycol
tet	tetracycline
TGR	transmembrane guanine nucleotide-binding protein receptor 5
THF	tetrahydrofolate
TLC	thin layer chromatography
TOF	time of flight

Treg	peripheral regulatory T cell
UC	ulcerative colitis
UDCA	3 α ,7 β -dihydroxy-5 β -cholan-24-oic acid
UPLC	ultra performance liquid chromatography
UV	ultraviolet
V	volt
VDR	vitamin D receptor
WLP	Wood Ljungdahl pathway
wt	weight

Abstract

DISCOVERY AND CHARACTERIZATION OF BILE ACID AND STEROID METABOLISM PATHWAYS IN GUT-ASSOCIATED MICROBES

Spencer Harris, B.S.

A dissertation submitted in partial fulfillment of the requirements for the degree of Doctor of Philosophy at Virginia Commonwealth University

Virginia Commonwealth University, 2017

Major Director: Phillip Hylemon, Ph.D.

Professor, Department of Microbiology and Immunology

The human gut microbiome is a complex microbial ecosystem residing in the lumen of our gastrointestinal tract. The type and amounts of microbes present in this ecosystem varies based on numerous factors, including host genetics, diet, and environmental factors. The human gut microbiome plays an important role in normal host physiological functions, including providing energy to colonocytes in the form of short-chain fatty acids. However, gut microbial metabolites have also been associated with numerous disease states. Current tools for analyzing the gut microbiome, such as high-throughput sequencing techniques, are limited in their predictive ability. Additionally, “-omic” approaches of studying the complex array of molecules, such as transcriptomics (RNA), proteomics (proteins), and metabolomics (previously identified physiologically active molecules), give important insight as to the levels of these molecules but do not provide adequate explanations for their production in a complex environment. With a

better physiological understanding of why specific metabolites are produced by the gut microbiome, more directed therapies could be developed to target their production. Therefore, it is immensely important to study the specific bacteria that reside within the gut microbiome to gain a better understanding of how their metabolic actions might impact the host. Within this framework, this study aimed to better understand the production of secondary bile acid metabolites by bacterial in the gut microbiome. High levels of secondary bile acids are associated with numerous pathophysiological disorders including colon cancer, liver cancer, and cholesterol gallstone disease. In the current study, three bile acid metabolizing strains of bacteria that are known members of the gut microbiome were studied. A novel strain of *Eggerthella lenta* was identified and characterized, along with the type strain, for its ability to modulate bile acid and steroid metabolism based on the atmospheric gas composition. Additionally, it was shown that the oxidation of hydroxyl groups on primary bile acids by *E. lenta* C592 inhibited subsequent 7 α -dehydroxylation by *Clostridium scindens*. The gene involved in the production of a Δ 4,6-reductase enzyme, responsible for catalyzing two of the final reductive steps in the 7 α -dehydroxylation pathway, was putatively identified and characterized in *Clostridium scindens* ATCC 35704. Lastly, the transcriptomic profile of *Clostridium scindens* VPI 12708 in the presence of numerous bile acids and steroid molecules was studied. These studies contribute significantly to the understanding of why specific bile acid metabolites are made by members of the gut microbiome and suggest ways of modulating their production.

Chapter 1: Introduction

Introduction to the human gut microbiome

The human body can be thought of as a vehicle used by trillions of microscopic passengers. In fact, the number of prokaryotic cells associated with our bodies outnumbers our own eukaryotic cells by an order of magnitude (1). The overall conglomeration of microbes making up the “human microbiome” varies based on numerous factors including: diet, environment, and host genetics, among others (2). There has been significant effort by scientists to better understand this complex microbial community. Next generation nucleic acid sequencing, along with advances in both computational and bioinformatic analysis, allows for whole-genomic sequencing from both isolated strains in culture and those isolated via single-cell sorting (3) as well as reconstruction of these individual genomes in more complex microbial communities (4) and even modeling bacterial metabolic potentials (5). In tandem with these high-throughput analyses, the assignment of bacterial strains into operational taxonomic units (OTUs) is accomplished via comparison against 16S sequencing data. The utilization of OTU classification has important implications, as it is used to predict metabolic potential of complex microbial ecosystems. It is on the basis of OTU assignment that the observation was made that in spite of vast variation of microbial constituents, there is maintenance of metabolic potential across different individuals (2).

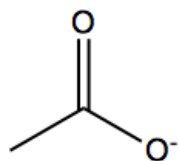
Within this association between humans and microbes, a large amount of attention has been paid to the lumen of the large intestine. The anaerobic environment here harbors the highest

concentration of microbes in the human body, as well as a vast host mucosal layer allowing for direct interaction with the microbes. With over 10^{13} prokaryotic cells (6), the number of microbial genes eclipses our own by over 100-fold. The “human gut microbiome” refers to this incredibly diverse microbial ecosystem and under normal physiological conditions it establishes a symbiotic relationship with us. The gut microbiome has important, established roles in producing energy sources for gut epithelial cells (7), modulating host immunity (8, 9), and preventing colonization by harmful pathogens (9). This, however, is only the beginning of our understanding of the complex interplay between gut-associated microbes and their hosts.

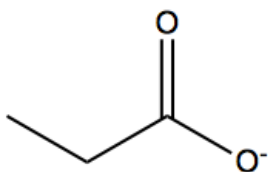
Microbial fermentation of complex carbohydrates in the large intestine

As with many niches in symbiotic ecosystems, there is usually an evolutionary “opening” that allows for abundant but otherwise unused byproducts and nutrients to be exploited for energy production, respiration, or used for other cellular processes. The most quantitatively important example of this phenomenon in the large intestine is the plant-derived complex carbohydrates that escape absorption and metabolism in the small intestine. Resistant starches undergo anaerobic fermentation by bacteria, forming short chain fatty acids (SCFAs) (10). The three major SCFAs produced in human large intestine include acetate, propionate, and butyrate (11). Figure 1.1 depicts the structure of these three major SCFAs. SCFAs are present at a concentration of 13-130mM in the lumen of the gut (12), and are rapidly absorbed by the surrounding epithelial cells. Butyrate is favored by the colonic epithelial cells as an energy source (12), but all SCFAs are an important source of energy for intestinal epithelial cells, contributing to an estimated 3-9% of our calorie intake per day (7).

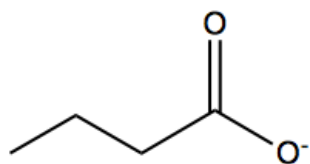
Figure 1.1: Chemical structure of major short chain fatty acids produced by gut-associated microbes



acetate ($\text{C}_2\text{H}_3\text{O}_2^-$)



propionate ($\text{C}_3\text{H}_5\text{O}_2^-$)



butyrate ($\text{C}_4\text{H}_7\text{O}_2^-$)

Both propionate and acetate are detected in portal circulation (12, 13), but propionate is mostly metabolized by the liver, leaving acetate as the major SCFA reaching systemic circulation (13). It is important to note that SCFA production varies widely and is impacted by bacterial species present, gut transit time, pH, hydrogen partial pressure, and the availability of complex carbohydrate substrates (14-16).

Landmark studies have been performed comparing the contributions of genetics, environmental, and dietary factors towards predisposition to colorectal cancer (CRC). Native Africans eating a diet rich in complex carbohydrates and low in animal protein had a significantly lower rate of CRC compared to African Americans eating a “Western diet” low in complex carbohydrates but high in fats and animal protein (17, 18). The mechanism by which increased complex carbohydrates play into prevention of CRC has been a topic that has received a lot of attention.

Both butyrate and propionate have been shown to have beneficial effects on colonocytes and gut-associated immune cells, and also impact colorectal tumor growth. On normal colonic epithelial cells, SCFAs aid in the maintenance of normal physiological functions by sustaining the integrity of the mucosal barrier (19, 20), regulating inflammatory responses (9, 21), and cell growth/differentiation (22, 23). Butyrate and propionate are inhibitors of histone deacetylases (HDACs), leading to induction of apoptosis in CRC cell lines (24, 25). SCFAs also impact peripheral regulatory T cells (T_{reg}) through the same HDAC inhibition, leading to an upregulation of forkhead box P3 (FOXP3) and enhancement of the T_{reg} population and anti-inflammatory function, under normal conditions (26). Because of the dual functionality of

preventing CRC cell proliferation and maintaining homeostatic conditions, the production of SCFAs in the colon has been suggested as a means of reducing the occurrence of CRC.

Microbial production of hydrogen gas in the large intestine

SCFAs are not the only end products of the fermentative actions of gut microbes on carbohydrates in the colon. Both carbon dioxide (CO₂) and hydrogen gas (H₂), found in abundance in the colon, are byproducts of anaerobic bacterial fermentation (27). The majority of CO₂ produced by gut-associated microbes is either absorbed into circulation through the enterocytes or is immediately utilized by other microbes in the vicinity (28). On the other hand, approximately 60-70% of H₂ produced remains after utilization by other microbes to be excreted via breath or flatus (28). Upwards of 13L per day of H₂ can be produced in the human colon (29), while germ-free animal studies show negligible hydrogen gas production until introduced to fecal slurries containing gut microbes (30). The amount of H₂ found in the lumen of the large intestine varies based on numerous factors, but is mainly impacted by the rate of production versus the rate of utilization of H₂ by various members of the gut microbiota (14, 28, 29).

H₂ producers are relatively abundant in the gut microbiota. Hydrogen production is common within the Firmicutes and Bacteroidetes phylum, the two major constituents colonizing the colon. *In vitro* studies have shown that members of the genera Roseburia (31), Ruminococcus (32), Eubacterium (33-35) generate H₂. Another means of microbial H₂ production is through the oxidation of ferredoxin, pyridine nucleotides, and formate by microbial hydrogenases. Through this process, anaerobic bacteria are able to rid their cells of reducing equivalents and maintain

intracellular redox balance. Genes encoding various hydrogenases are widespread throughout bacteria known to inhabit the colon, especially in the Bacteroidetes phylum (36).

Hydrogen gas utilization by microbes in the large intestine

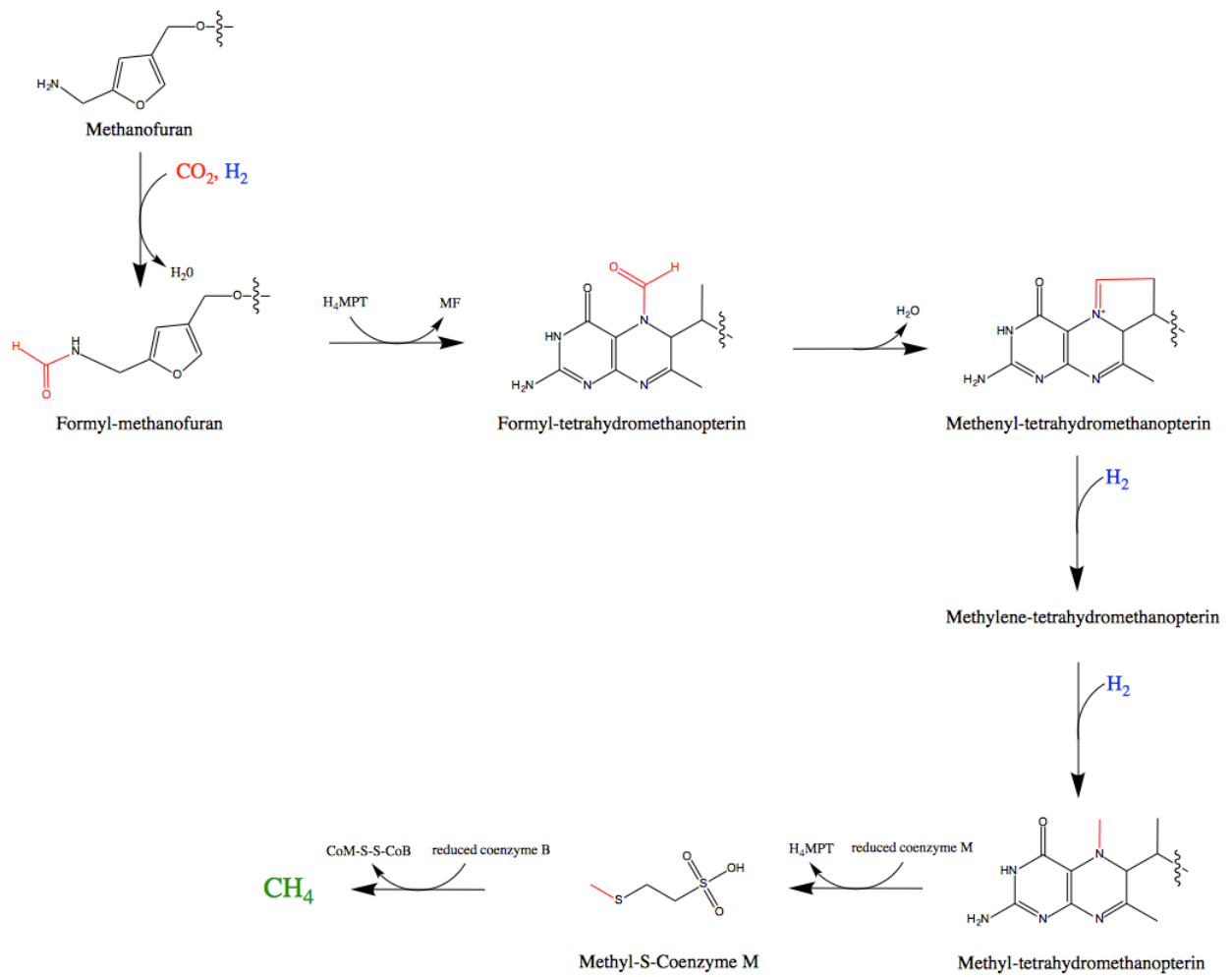
Because H₂ is a major byproduct produced by many gut bacteria, microbes able to utilize it as a substrate would have an evolutionary advantage in the gut microbiota. One such group of H₂ utilizers is methanogens, a group of archaea that are able to reduce CO₂, methanol, or acetate to methane gas (CH₄), using H₂ as an electron donor (37). CH₄ is an entirely microbial-derived product, as it is neither made nor utilized by our own cells (38). The reduction of CO₂ to CH₄ is carried out by a series of dehydrogenases and reductases, forming an electron transport chain (38). CO₂ is first reduced and attached to methanofuran as a formyl group, then affixed to tetrahydromethanopterin, undergoes a dehydration followed by two reductive steps, is transferred to its next carrier sulfhydryl-coenzyme M along with the generation of a Na⁺ gradient, and undergoes a final reduction resulting in CH₄ (39, 40) (Figure 1.2).

This process is energetically favorable, the resulting change in free energy (ΔG°) = -131 kJ/mol and leads to approximately one mol ATP generated for each mol CH₄ formed (41).

Methanobrevibacter smithii is the most numerically prominent methanogen found in the gut microbiome and can be present in up to 10¹⁰ CFU/g in stool (42). Presence of methanogens in the gut microbiome is impacted by diet (17, 38), host genetics (43), and environmental factors (17). Early studies on methanogens in humans used breath assays to determine presence of CH₄

Figure 1.2: Biochemistry of the methanogenesis pathway in archaea from CO₂

Conversion of CO₂ and H₂ to methane via methanogenesis in *Methanobrevibacter* species starts by the fixation of CO₂ with H₂ to methanofuran. The resulting formyl group is then transferred to tetrahydromethanopterin. After a dehydration step, the resulting molecule undergoes two successive reductive steps (requiring additional H₂). The resulting methyl group is then transferred to reduced coenzyme M. The last step requires reduced coenzyme B and the nickel-containing porphinoid F₄₃₀, and results in the production of methane.



Adapted from (44)

producers (45). Detection of CH₄ in a breath assay is indicative of relative activity of methane producers, although the lack of CH₄ detection was not necessarily indicative of their absence (46). More modern molecular techniques have been developed to screen for a highly conserved methanogenic gene, i.e. coenzyme M reductase (*mcrA*) (47, 48). Studies have shown that methanogens are found in colonic samples at rates ranging from less than 10³ to over 10⁹ CFU/g stool (49).

Methanogens have been implicated to have various effects on human health. For instance, patients with terminal ileal disease, Crohn's disease, and ulcerative colitis (UC) have been shown to have significantly lower amounts of CH₄ excretion compared to healthy controls (50-54).

Moreover, gene copy number of *mcrA* is significantly reduced in patients with UC (47).

Whether the lack of methanogens contributes to or is merely a symptom of these disorders remains to be elucidated, although the reduced gut microbial diversity found in these disorders may contribute to the reduction in methanogenesis. There is less definitive data surrounding the effects methanogens may play on CRC, and the data that exists is mixed. Older reports indicate increased amounts of CH₄ in patients with CRC versus control patients (55, 56), while newer ones show no difference or less methanogens in patients with CRC versus control patients (57, 58).

In the colon, methanogens are not the only group of microbes that are able to utilize H₂.

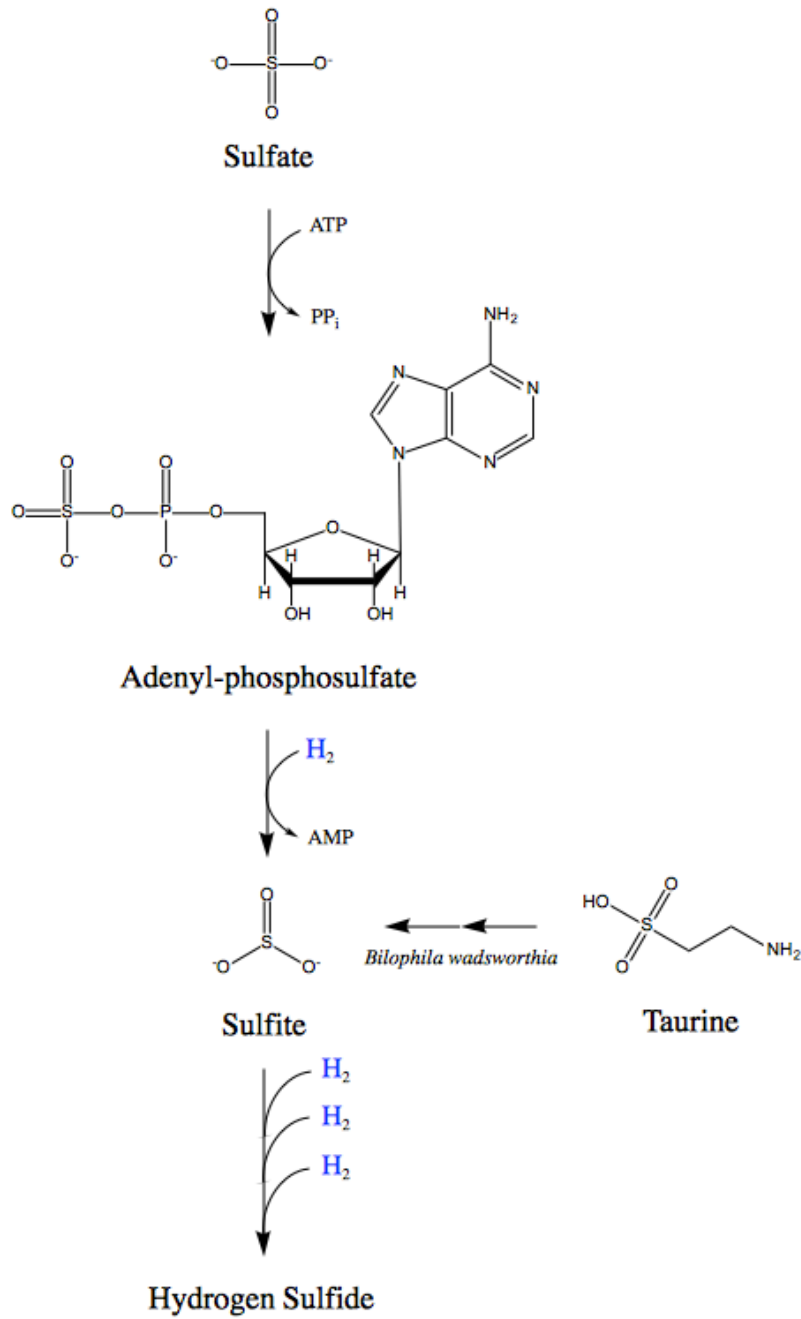
Sulfate reducing bacteria, are able to reduce sulfate (SO₄²⁻) as their terminal electron acceptor, forming hydrogen sulfide gas (H₂S or HS⁻). This reaction is able to utilize reducing equivalents from numerous electron donors, including lactate, pyruvate, ethanol, formate, SCFAs, and amino

acids (59, 60), although H₂ appears to be the preferred electron donor for the most prevalent sulfate reducing bacteria found in the gut microbiome (61). Similar to methanogenesis, reduction of sulfate to hydrogen sulfide gas is carried out through an electron transport chain (62) (Figure 1.3). Sulfate and ATP are first linked via an ATP-sulfurylase to form adenosine-5'-phosphosulfate, which then undergoes reduction via APS-reductase leading AMP and sulfite (SO₃⁻⁻) (62). Sulfite then undergoes three successive reductive steps leading to H₂S (63). This process is even more energetically favorable under physiological conditions than methanogenesis, resulting in $\Delta G^\circ = -152.2$ kJ/mol, although the overall ATP generation is estimated to still be 1 mol ATP per mol H₂S formed (41).

Sulfate reducing bacteria with the highest activity and affinity for H₂ are found within the genus *Desulfovibrio* (59) and are known members of the gut microbiome at a level of 10⁴ to 10¹¹ CFU/g wet weight (46, 64). Newer molecular techniques screening for genes conserved in sulfate reduction have confirmed sulfate-reducing bacteria are relatively ubiquitous in the human gut microbiome (65, 66). In addition to using numerous electron donors, sulfate can come from numerous sources both endogenous and exogenous, including secreted mucin, non-absorbed proteins, sulphur-containing amino acids, and taurine (a source of sulfite) (63, 64, 67). Since both sulfate-reducing bacteria and methanogens in the gut microbiota compete for the same pool of H₂, the deciding factor is the availability of sulfate for hydrogen sulfide production. Energetically, hydrogen sulfide generation is a more favorable reaction than methanogenesis. While presence of one strain is not mutually exclusive of the other, screening tests of human fecal samples have shown that patients usually harbor either methanogens or sulfate-reducing

Figure 1.3: Biochemistry of sulfidogenesis in gut microbes from sulfate and taurine

In the process of hydrogen sulfidogenesis from sulfate, adenosine triphosphate is first linked to sulfate via ATP sulfurylase. This molecule is then reduced, forming AMP and sulfite. Sulfite can also be liberated from bile acid conjugate taurine via bacteria such as *B. wadsworthia* (68). Sulfite then undergoes three successive reductions (via dissimilatory sulfite reductases) to ultimately produce hydrogen sulfide.



Adapted from (63)

bacteria (46), although in situations of abundant H₂ there are reports of both being present and active (59, 60, 69). *In vivo* studies comparing methanogenesis and H₂S production in mouse models confirm that when both methanogens and H₂S producers are present and available sulfate is abundant, H₂S production dominates and methanogenesis along with viable methanogens are below the limits of detection (70, 71). By reducing the amount of sulfate available, methanogenesis has been shown to recover (71), suggesting a direct inverse link between H₂S production and methanogenesis and confirming that sulfate-reducing bacteria out-compete methanogens for utilization of H₂.

High levels of H₂S have been reported to have deleterious effects on human health. Several studies have suggested a link between ulcerative colitis and gut microbial H₂S production (72, 73) while others have refuted this claim (74). There is a demonstrated link between UC and a western diet high in protein and sulfur-containing amino acids (75, 76). Similarly, removal of such foods from the diet of UC patients results in an improved outcome (76). Another source of sulfite, taurine from conjugated bile salts, has been shown to be increased in the lumen of the large intestine in individuals eating a western diet (77, 78). Studies have also suggested a link between bacteria able to liberate sulfate from conjugated bile acids and the development of colitis in mice (68). In addition to ulcerative colitis, H₂S production has been associated with CRC. In a mouse model of colonic dysplasia, mice given a source of sulfate had significantly more colonic dysplasia than those treated with a source of sulfate plus metronidazole, suggesting both H₂S is formed by gut microbes and that it is associated with dysplasia (79). Stool H₂S levels in CRC cancer patients have been shown to be increased (80). However, a concurrent

increase in H₂S producing bacteria was not significant, suggesting that H₂S producing activity instead of presence of H₂S producing bacteria is more predictive for CRC (81, 82).

One suggested link between H₂S and CRC is the H₂S-mediated inhibition of acyl-CoA dehydrogenase in colonocytes, the enzyme responsible for butyrate oxidation (83, 84).

Inhibition of butyrate oxidation leads to increased epithelial permeability, decreased absorption of ions, as well as membrane lipid and mucus formation (85). Even at physiological concentrations, H₂S has been shown to be cause DNA damage in colonocytes, at least partially via stimulation of reactive oxygen species (ROS) (86, 87). In addition to direct DNA damage, H₂S can induce inflammatory and DNA damage repair pathways in human intestinal cells (88). Levels of the enzyme thiosulphate sulphotransferase, responsible for detoxifying H₂S, are significantly reduced in patients with CRC (89). Taken as a whole, H₂S is a likely culprit for creating and maintaining an environment that can, over time, lead to the formation of CRC in individuals that have sufficient substrates promoting H₂S formation in the colon.

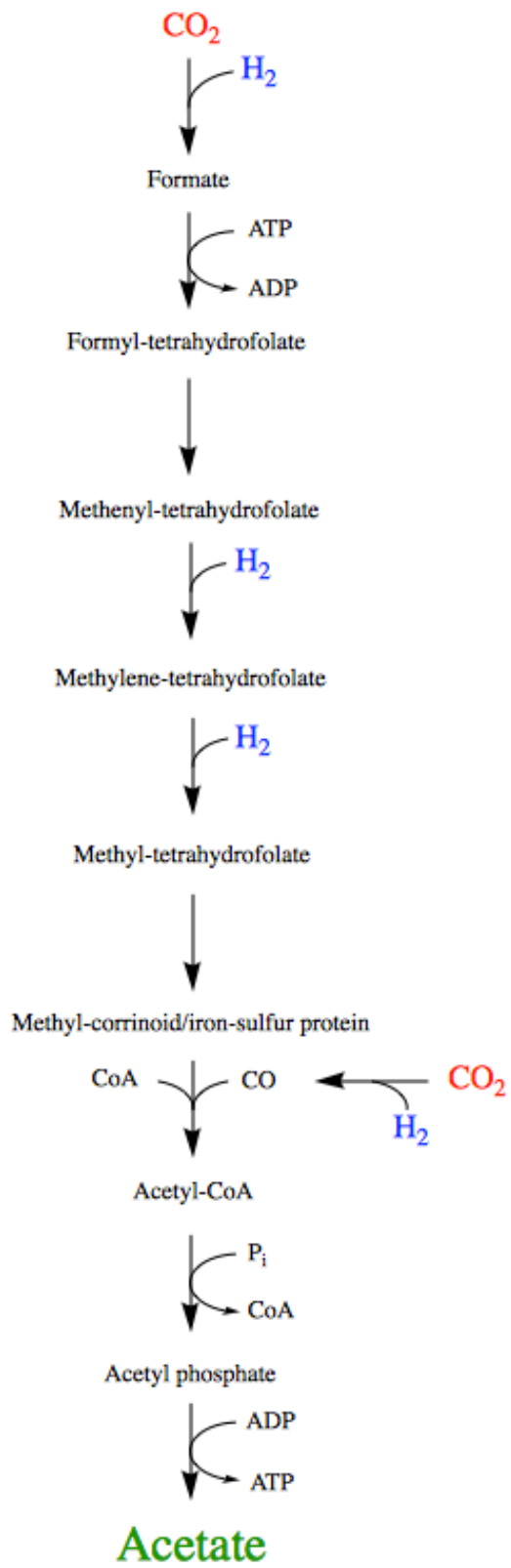
A third mechanism of utilizing H₂ produced by gut microbial fermentation is through acetogenesis. Acetogenesis is the process by which bacteria fix CO₂ and molecular H₂ to form acetate. The study of acetogenesis takes its roots in the study of gas metabolism by anaerobic soil bacterium, as one of the first reports of this “new type of glucose fermentation” was found in a strain of *Clostridium thermoaceticum* isolated from manure (90). Subsequent studies by Harland Wood and Lars Ljungdahl elucidated enzymatic pathway responsible for autotrophic synthesis of acetate from CO₂ known as the Wood-Ljungdahl pathway (WLP) (91). The WLP is a multi-step enzymatic pathway that utilizes eight reducing equivalents and two CO₂ to form

acetate (Figure 1.4). The overall reaction yields even less energy than methanogenesis or sulfidogenesis, with a $\Delta G^{\circ} = -95\text{kJ/mol}$ (41). ATP is generated from ADP during the final substrate-level phosphorylation of acetyl-CoA to acetate (92). However, more recently it has been suggested that instead of acetogenesis being a pathway of energy production, it is a means of regenerating oxidized pyridine nucleotides and ferredoxin to maintain intracellular redox equilibrium (93). As many of these bacteria are found in anaerobic environments and electron acceptors are at a premium, the ability of acetogens to use CO_2 as an electron acceptor via the WLP gives them an evolutionary advantage. In addition, the majority of acetogens are able to use a multitude of different electron acceptors and electron donors, making them good at adapting to the energy and redox requirements of their environment (94).

In addition to harboring the genes for the WLP, most acetogens additionally have membrane bound hydrogenases that are able to interconvert their reducing equivalents in an electron transport chain. One of the best-characterized examples of this is the *Rhodococcus* nitrogen fixation (RNF) complex originally characterized in an electron transporter associated with nitrogenases (95-97). The RNF complex, found in numerous strains of acetogens, couples the oxidation of ferredoxin (Fd) to the reduction of pyridine nucleotides and the generation of either a Na^+ or H^+ membrane gradient (98) (Figure 1.5). This process is reversible and can help cycle reducing equivalents between various electron carriers (99, 100). The gradient produced by the RNF complex can then be utilized to generate additional ATP, coupling acetogenesis to an ATP-generating process in the cell in addition to regenerating oxidized electron carriers (93, 98). Not all acetogens harbor RNF complexes, although those that do not usually encode some membrane-bound energy conserving hydrogenase system capable of interconverting reducing

Figure 1.4: Diagram of acetate formation via the Wood-Ljungdahl Pathway

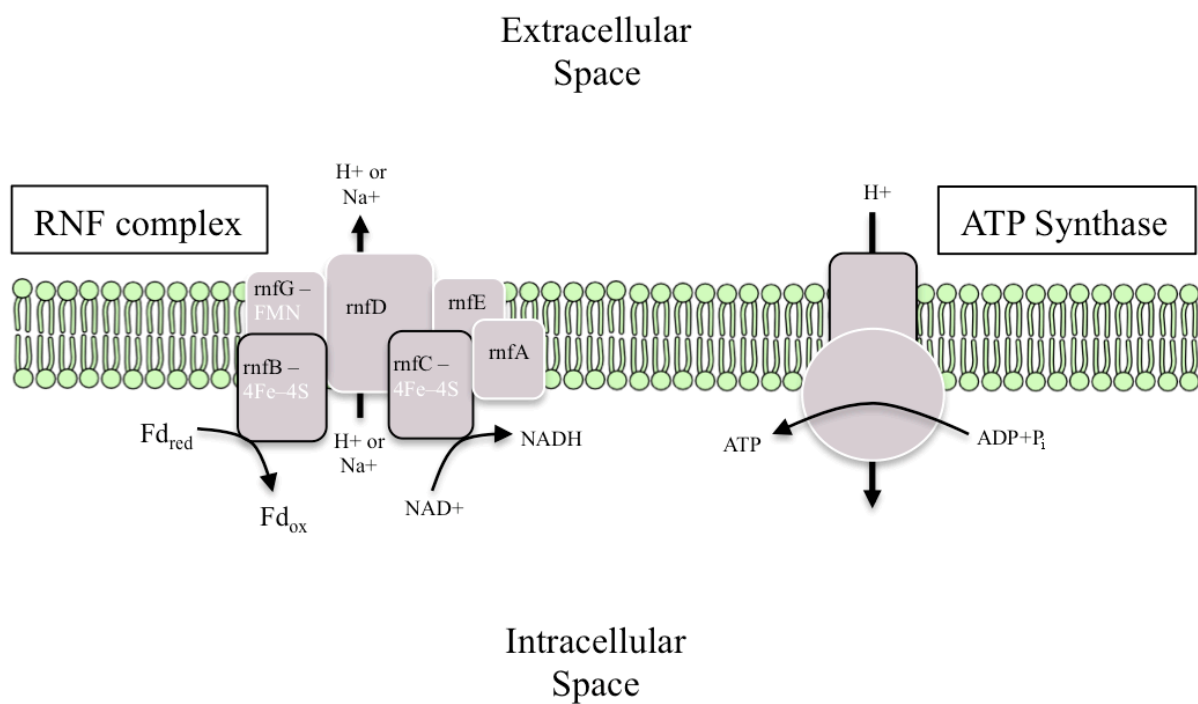
The multistep process of CO₂ fixation to acetate starts with the fixation of carbon dioxide by formate dehydrogenase. Formate is then linked to tetrahydrofolate (requiring ATP) via formyl-tetrahydrofolate synthetase. Formyl-tetrahydrofolate is then recognized by a cyclohydrolase, forming methenyl-THF. This molecule undergoes two successive reductive steps by methylene-THF dehydrogenase and methylene-THF reductase, respectively. The resulting methyl-group is transferred to a corrinoid/iron sulfur protein via a methyltransferase. Then, along with CoA and carbon monoxide (from reduction of CO₂ by a carbon monoxide dehydrogenase), the methyl group is used to generate acetyl CoA via acetyl-CoA synthase. This acetyl-CoA then undergoes substrate-level phosphorylation, ultimately leading in the production of acetate and the generation of ATP. This process is energy-neutral (1 mol ATP used/1 mol ATP generated per mol acetate), but requires a significant amount of reducing equivalents (four reducing equivalents/mol acetate) (101).



Adapted from (101)

Figure 1.5: Schematic of RNF Complex and ATP Synthase in Acetogens

RNF complex is a multi-subunit NADH/ferredoxin oxidoreductase capable of reversibly oxidizing reduced ferredoxin forming reduced NADH and generating a proton or Na⁺ gradient. Other transmembrane machinery can utilize this gradient for transport or for energy generation, such as an ATP synthase.



Adapted from (98)

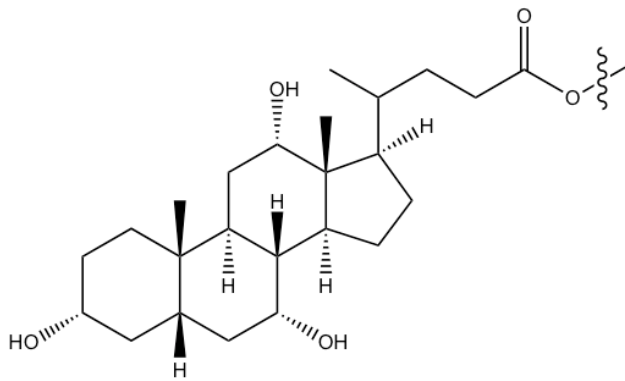
equivalents whilst generating an ion gradient (98, 102, 103). More recently, acetogenesis has begun to garner interest as an alternative pathway of H₂ elimination in the lumen of the large intestine. Due to the contributions of CH₄ production of livestock to global warming (104), acetogens have been suggested as a potential alternative probiotic in the rumen of cattle (105). The largest group of characterized acetogens present in mammalian gut microbiomes is from the *Firmicutes* phylum (106). However, unlike the methanogenesis and sulfidogenesis, the acetogenesis phenotype has also been identified in other phyla, making acetogens a more diverse group of H₂ utilizers (107). Studies have shown that in humans, acetogenesis during glucose fermentation by gut microbes contributes to up to a third of the total amount of acetate produced (11). Much less is known about contributions acetogens may have on human health. Since acetogens, in contrast with methanogens and sulfidogens, are a more heterogenous group of organisms, traditional means of molecular screening testing are less effective, though some studies that have screened genes from the acetogenic pathways in stool samples have found them at rates of 10³ – 10⁷ genes/g stool (49). Based on the energetics, acetogenesis is the least energetically favorable reaction behind methanogenesis and sulfidogenesis. However, *in vivo* data suggests acetogens are the most quantitative potential H₂ utilizers present in the gut microbiome (11, 106). Taken together, this suggests that acetogenic utilization of H₂ in the colon may be the prevalent method in humans that harbor neither active methanogens nor active H₂S producers. Ultimately, acetogenesis in the human colon can be influenced by numerous factors that impact microbial fermentation, the levels of available CO₂ and H₂, the presence of methanogens or sulfidogens, and presence of sulfate or sulfite for reduction.

Bile acid formation and enterohepatic circulation

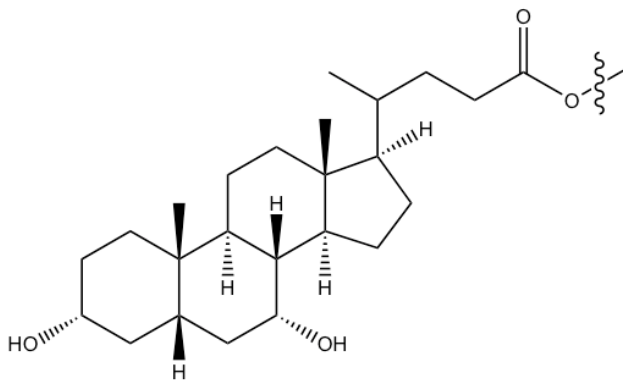
Under normal physiological conditions, microbial fermentation of complex carbohydrates and amino acids in the colon is quantitatively the most prevalent reaction occurring. However, other exogenous and endogenous molecules also enter the lumen of the large intestine where they become substrates for microbial conversion. One such group of molecules is bile acids, sterol molecules synthesized by hepatocytes from cholesterol. The two major bile acids produced in humans are cholic acid ($3\alpha, 7\alpha, 12\alpha$ -trihydroxy- 5β -cholan-24-oic acid; CA) and chenodeoxycholic acid ($3\alpha, 7\alpha$ -dihydroxy- 5β -cholen-24-oic acid, CDCA) (Figure 1.6). Bile acids are conjugated to either taurine or glycine forming bile salts, resulting in their characteristic amphipathic nature. Bile salts are actively secreted across the canalicular membrane of hepatocytes via the bile salt export pump (BSEP) (108), and subsequently stored and concentrated in the gallbladder during the interdigestive phase. Upon the arrival of fatty acids and/or amino acids reaching the duodenum, enteroendocrine cells in the mucosal lining of the duodenum secrete cholecystokinin (CCK). CCK stimulates release of pancreatic enzymes, inhibits gastric emptying, and induces the gallbladder to constrict (109). This constriction causes the stored bile salts through the cystic duct, common bile duct, ampulla of Vater, and finally through the relaxed sphincter of Oddi into the lumen of the duodenum (110). Once in the lumen of the small intestine, bile salts serve to aid in the sequestration and absorption of lipids and lipid soluble vitamins (A,D,E,K) via the formation of micelles (111). Bile salts activate pancreatic lipase, producing monoglycerides and free fatty acids, which become key components of the mixed micelles (112). Due to their high concentration and detergent-like actions, bile salts also help to prevent overgrowth of bacteria in the small

Figure 1.6: Chemical structure of primary bile acids and their conjugates

Primary bile acids

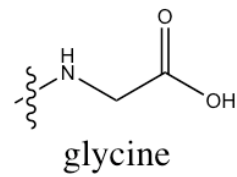


cholic acid

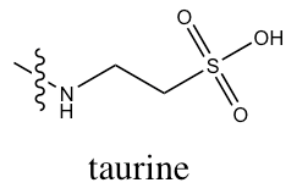


chenodeoxycholic acid

Bile acid conjugates



glycine



taurine

intestine (113). Once the bile salts reach the terminal ileum they are actively transported across the apical membrane of ileal enterocytes via the apical sodium-codependent bile acid transporter (ASBT) (108). They are then transported across the apical membrane of enterocytes via the OST α /OST β transporter (114) and enter portal circulation. When they reach the liver, bile salts are highly efficiently taken up through active transport across the sinusoidal membrane of hepatocytes via Na⁺ taurocholate cotransporting polypeptide (NTCP) and returned to the pool of bile salts (115), thus completing a process known as enterohepatic circulation. Enterohepatic circulation of bile salts is only approximately 95% effective, allowing 400-800mg/day of bile salts to escape into the large intestine where they become substrates for numerous microbial biotransformations (113).

Bile acid metabolism by gut microbes

Beginning in the ileum and occurring in earnest once in the large intestine, the first reaction bile salts undergo is deconjugation of bile acids from their taurine or glycine conjugate via bile salt hydrolases (BSH) (116). Typically the ratio of glycine:taurine conjugation in humans is 3:1, however this is impacted by diet. It has been shown that individuals on a “Western diet” have predominantly taurine conjugation, while individuals on a vegetarian diet shift towards glycine conjugation (77, 78). BSH activity is widely present in the microbes populating both the large and small intestines. Gram-positive commensal bacteria with BSH activity include *Clostridium* (117, 118)), *Enterococcus* (119), *Bifidobacterium* (120, 121), and *Lactobacillus* (122, 123). BSH activity is less widespread in commensal Gram-negative bacteria, but include members of *Bacteroides* genus (124). Gut-associated archaea *Methanobrevibacter smithii* and

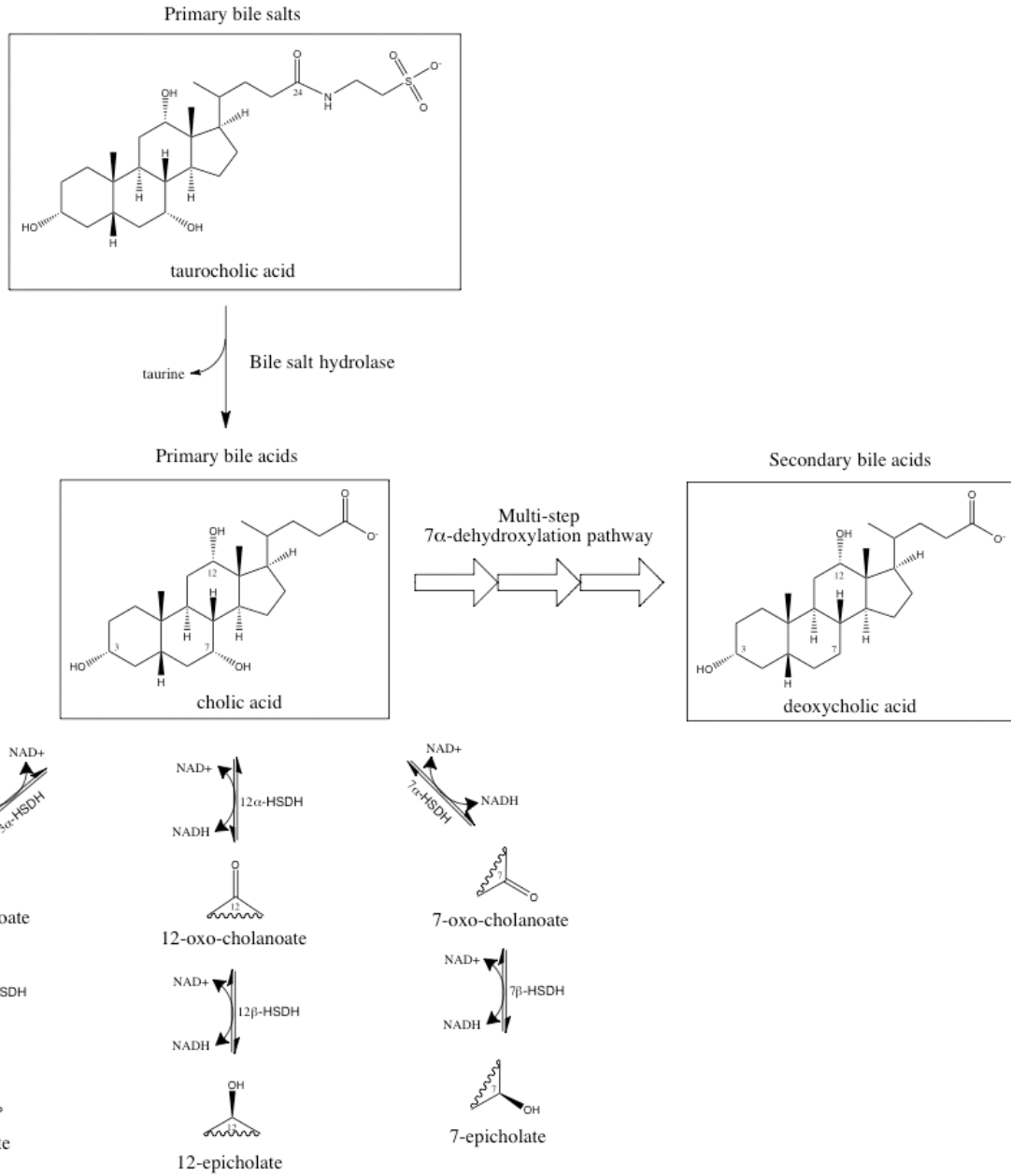
Methanosphaera stadtmanae have also been found to have BSH activity (116). BSH enzymes specifically hydrolyze the *N*-acyl bond on the 24th carbon that is responsible for linking the amino acid conjugate to the bile acid (Figure 1.7) (125). Studies that have characterized BSH activity from purified enzymes show that their pH sensitivities tend to be between 5-6, are located intracellularly, and have higher activity on glycine-conjugated bile salts (121, 126-128).

Once bile acids are liberated from their conjugate, they become substrates for numerous microbial biotransformations. 7 α -dehydroxylation is a process by which a small group of bacteria within the *Clostridia* genus are able to remove the hydroxyl group from the seventh carbon of both CA and CDCA forming secondary bile acids deoxycholic acid (3 α , 12 α -dihydroxy-5 β -cholen-24-oic acid; DCA) and lithocholic acid (3 α -monohydroxy-5 β -cholen-24-oic acid; LCA), respectively (113) (Figure 1.7). This process is unique to gut microbes, as hepatocytes do not produce secondary bile acids nor are they found in fecal samples of germ free animals (129, 130). Studies measuring fecal bile acid composition show that secondary bile acids form the major constituency (113), suggesting that even though only approximately 0.0001% of gut microbes harbor the 7 α -dehydroxylation pathway (131), it is the most quantitatively significant biotransformation of primary bile acids by gut microbes after BSH. In metagenomic analyses, *C. scindens*, a well-characterized 7 α -dehydroxylating species, has been shown to be a member of the “core gut microbiome” in humans, due to its high rate of prevalence in human fecal samples (132). DCA, and to a smaller degree LCA, both passively diffuse across the epithelial barrier and enter portal circulation, where they are reabsorbed by the liver and

Figure 1.7: Diagram of bile salt biotransformations by gut bacteria

Endogenous bile salts are produced by the liver and then undergo biotransformation by gut microbes. Bile acids are liberated from their conjugates by microbial bile salt hydrolases.

Primary bile acids then undergo numerous further reactions, such as oxidation and epimerization (bottom) or 7 α -dehydroxylation (right).



Adapted from (Ridlon 2016)

accumulate in the bile acid pool, since human hepatocytes cannot perform 7α -hydroxylation (133).

While bile acids had seen usage as “liver tonics and laxatives” earlier, contemporary scientific interest in both primary bile acids and secondary bile acids began after determination of their chemical structure in 1932 (134). In 1946, an effective method for developing cortisone from DCA was developed (135). Three years later the use of cortisone in patients was shown to cause significant improvement in patients dealing with rheumatoid arthritis (136). However, since at the time the only source for DCA was from bile isolates from livestock, pharmaceuticals began to worry there would not be enough supply to cover the demand for cortisone (134), and as a result plant sterols became used as a more widespread and effective precursor to cortisone (137). As such, interest in bile acids dwindled but for a few dedicated laboratories. However, work on bile acids continued in a Swedish laboratory run by Sune Bergström where means of tracking H^3 and ^{14}C incorporation into bile acids (138), as well as GC and MS techniques for measurements of bile acids were developed (139). Bergstrom and colleagues were the first to distinguish primary bile acids, made by the host, and secondary bile acids, made by commensal intestinal microbes (140, 141). In this earliest work of determining the pathway for microbial conversion of primary bile acids to secondary bile acids, it was proposed that the mechanism was a two-step process with a single intermediate, cholen-6-oic acid (142). However, subsequent work by Hylemon et al. of CA-induced conversion of $[24-^{14}C]$ -CA by *Clostridium scindens* showed the formation of numerous bile acid metabolites (143). MS identification of the metabolites and chemical synthesis and introduction to CA-induced *Clostridium scindens* showed DCA was the major end product, suggesting these were intermediates in the formation of DCA (143). Taken

together, it was suggested that the formation of secondary bile acids by 7 α -dehydroxylating bacteria was an inducible, multi-enzymatic process.

Although 7 α -dehydroxylation of primary bile acids leads to the most abundant end products, there are several other biotransformations that bile acids can undergo in the large intestine. Members of the intestinal microbiota have genes that encode a variety of pyridine nucleotide-dependent hydroxysteroid dehydrogenases (HSDH). HSDHs are widely distributed throughout various members of the gut microbiota (113). Gut microbes are known to be capable of oxidation and reduction of the hydroxyl groups on the 3-, 7-, and 12- carbons of bile acids (Figure 1.7). The epimerization of bile acid hydroxyl groups ($\alpha \leftrightarrow \beta$) requires two position-specific bile acid α - and β - HSDHs, which generate a stable oxo-bile acid intermediate i.e., 7 α -hydroxy \leftrightarrow 7-oxo \leftrightarrow 7 β -hydroxy. Bacterial bile acid HSDHs differ in their pH optima, pyridine nucleotide specificity (NAD(H), NADP(H), or both), subunit molecular weight, and gene regulation (113). Amino acid sequence analysis suggests that most bacterial HSDHs in the gut microbiota belong to the short-chain alcohol/polyol dehydrogenase family (113). Bile acid HSDHs have been found and characterized in numerous genera inhabiting the lumen of the colon, including *Bacteroides* (144, 145), *Clostridium* (146-148), *Escherichia* (149), *Eggerthella* (150), *Eubacterium* (151-154)), *Peptostreptococcus* (155), and *Ruminococcus* (156, 157).

Bile acids with oxidized hydroxyl groups (oxo-bile acids) have been shown to be present in fecal bile acids (158-160), portal circulation (161, 162), and human serum (163). Interestingly, the hydroxyl groups on dihydroxy-bile acids (DCA, CDCA) have been shown to be more sensitive to microbial oxidoreduction than trihydroxy-bile acids (CA) (164). Also, cholecystectomised

patients have been shown to have increased levels of oxo-bile acid derivatives in enterohepatic circulation (165). This observation is likely that due to the increased levels of bile acids being seen by the gut microbes in cholecystectomised patients leading to increased microbial biotransformation. The extent of epimerization and the accumulation of oxo-bile acids appears to be influenced by the oxidation/reduction potential of the local cellular environment. For example, the formation of oxo-bile acids may be more favorable in bacteria associated closer to the mucosal edges, where there is a higher redox potential than further inside the lumen of the intestines (125).

Consequences of bile acid metabolism on microbial and host physiology

To understand the effects of microbial biotransformations of bile acids on host and microbial physiology, it is important to first discuss the effects that bile acids have on normal host physiology. Near the turn of the millennium, it was discovered that endogenous bile acids were ligands for the orphan nuclear receptor farsenoid X receptor (FXR) (166, 167). Under normal physiological conditions, primary bile acids CA and CDCA activate FXR in enterocytes, leading to expression of fibroblast growth factor 15/19 (FGF15/19) (168). FGF15/19 then acts on the hepatic FGFR4 receptor in hepatocytes and, among other effects, leads to a down-regulation of CYP7A1, the rate-limiting enzyme of bile acid synthesis (169). Through this pathway, bile acids are able to effectively inhibit their own synthesis.

Soon after the discovery of FXR activation by bile acids, it was shown that transmembrane G-coupled protein receptor 5 (TGR-5), a widely distributed receptor throughout human cells, is

activated by bile acids (170, 171). TGR-5 is a $G\alpha_s$ receptor that leads to an increase in intracellular c-AMP (172). It has been reported that activation of TGR-5 can lead to the release of glucagon-like peptide 1 (GLP-1), which has roles in glucose homeostasis as well as appetite suppression (173). Subsequent work also showed bile acids as ligands for pregnane-activated receptor (PXR) (174), vitamin D receptor (VDR) (175), sphingosine-1 phosphate receptor 2 (S1PR2) (176), and some muscarinic receptors ($M_{2,3}$) (177).

While primary bile acids have been shown to be agonists for many different receptors, the potency of their activation differs based on their substituents. In addition, secondary bile acids produced by gut microbes have differing and sometimes more potent agonist properties than primary bile acids. In the case of FXR, primary bile acid CDCA appears to be the most potent activator, but both secondary bile acids LCA and DCA are more potent than CA (167). Similarly, PXR appears to be most potently activated by LCA (174), VDR by 3-oxo-LCA (175), and TGR-5 by DCA and LCA (170). Taken together, this suggests that not only can bile acids modulate the structure of the gut microbiome, but the microbes can also modulate host physiology by the creation of secondary bile acid “hormones” (178).

In addition to modulating normal host physiology, bacterial bile acid metabolites such as DCA and LCA also have roles in pathophysiological disorders. There is a body of evidence suggesting a link between secondary bile acids (DCA and LCA) and numerous gastrointestinal diseases, including colon cancer (67), liver cancer (179), and cholesterol gallstone disease (131). Both LCA and DCA levels are increased in fecal samples of CRC patients compared to control (180). In African Americans, when compared to rural, native Africans, a high-fat diet is

correlated with increased levels of DCA/LCA as well as an increased rate of CRC (18). DCA and LCA have been shown to be effective enhancers of mutagenesis (181, 182), and in rats endogenous levels of secondary bile acids led to increased CRC tumor numbers and invasiveness (183). In addition, rats supplemented with DCA show decreased production of protective SCFAs when compared to control, along with significant changes to the makeup of the gut microbiota away from SCFA-producing bacterial species (184).

The mechanism by which DCA and LCA may contribute to the formation of CRC is an area of significant study. Based on their hydrophobicity, DCA and LCA can cause membrane perturbations in colonocytes (185). Chronic exposure to secondary bile acids has been shown to lead to resistance to apoptosis and enhanced cell proliferation in many epithelial cell lines (186, 187). Secondary bile acids have been shown to generate reactive oxygen and reactive nitrogen species, can cause DNA double-stranded breaks, and inhibit DNA repair mechanisms (188, 189). They also cause NF- κ B activation in intestinal epithelial cells, which can promote CRC development (126, 188, 190-192). It has been suggested that DCA may directly stimulate CRC progression through activation of protein kinase C, which effects growth regulation, differentiation, and apoptosis (193). DCA has also been shown to cause hypomethylation of DNA, leading to increased transcription of proto-oncogenes (194). In CRC cells, DCA has been shown to phosphorylate β -catenin, causing increased invasiveness (195). DCA can also prevent apoptosis in CRC cells via activation of EGFR, NF- κ B, and Akt (188, 196, 197). While secondary bile acids themselves have not been shown to be carcinogenic (67), they produce an environment both in the microbiota (decreased production of protective SCFAs) and in the enterocytes themselves that promotes progression of CRC. These effects on colonocytes also

seem to be dose-dependent, as low concentrations of bile acids and secondary bile acids appear to be protective, while higher concentrations have deleterious effects.

Even oxidized or epimerized bile acids have differing effects on host physiology. 3-oxo-LCA has been shown to be the most potent agonist for the VDR (175). Epimerization of the 7 α -hydroxyl group on CDCA yields a much more hydrophilic and therefore less toxic metabolite ursodeoxycholic acid, which has been shown to be protective against CRC-inducing effects of DCA (157). Recent studies reported that 7-oxo-lithocholic acid acts as a competitive inhibitor of human hepatic 11 β -HSDH-1 (198). 11 β -HSDH-1 is responsible for converting 7-oxo-LCA back to CDCA, however it also catalyzes the activation of cortisol from cortisone (199). When 7-oxo-LCA is in high enough concentrations, it acts as a competitive inhibitor preventing production of active cortisol. 7-oxo-LCA and ursodeoxycholic acid are both less potent agonists of FXR than the endogenous bile acid they are formed from, CDCA (167). Since the expression of the antimicrobial peptide cathelicidin is controlled by FXR in enterocytes, it follows that by lessening the affinity of bile acids for FXR, an otherwise susceptible microbe could increase its fitness in the lumen of the large intestine. The full extent to which alteration in bile acid hydroxyl oxidation or epimerization effects host metabolism is a field that requires more significant study.

The effects of bile salt biotransformations is not restricted to host-microbe interactions, as there are many microbe-microbe interactions that occur as a result of bile salt metabolism. Taurine can be found conjugated to primary bile acids and is more prevalent in the bile acid pool of those eating a Western diet (78). When liberated from bile acids through BSH activity by microbes in

the intestinal tract, taurine becomes a substrate for further bacterial metabolism. Microbes are able to utilize taurine as an energy source via Stickland fermentation (200). In addition, the formation of H₂S through metabolism of taurine by *Bacteroides* has been shown to enhance 7 α -dehydroxylation by *Clostridium* sp. in germ-free mice colonized with both bacterial strains (201). Addition of taurocholic acid to a low-fat diet in IL-10 deficient mice led to a bloom of sulfate-reducing bacteria and induced colitis (68). These effects seem to be specific for taurine conjugation, as glycine liberated from bile salts has not been shown to be a source of sulfate for H₂S production nor does it induce 7 α -dehydroxylation.

Bile acid 7 α -dehydroxylation has recently been shown to have consequences for *Clostridium difficile* colonization and growth in the gastrointestinal tract. *C. difficile* infection, the causative agent of antibiotic-associated diarrhea and colitis, is a significant health concern for patients taking broad-spectrum antibiotics (202). An estimated 29,000 deaths are attributed to *C. difficile* infection (CDI) in the US every year (203), and the numbers are expected to increase as the aging population becomes more colonized. Although rates of *C. difficile* colonization vary significantly, it has been reported that up to 90% of healthy neonates and infants, 15% of healthy adults, and 51% of elderly patients are asymptomatic *C. difficile* carriers (204). Treatment of patients with broad-spectrum antibiotics, especially in hospital settings, leads to a decreased level of protective gut microbes which allows for the over proliferation of *C. difficile* which tend to be resistant in their spore form (205). Once induced to germinate in the GI tract, increased *C. difficile* proliferation leads to overproduction of vegetative cells that produce toxin A and B causing diarrhea and severe colitis in some patients (206). In patients with relapsing *C. difficile* infection, approximately 17% of patients do not respond to metronidazole or vancomycin

treatment (207). However, fecal transplants of gut microbiota from healthy donors have been shown to be a successful treatment, with 81% having resolution of CDI after the first fecal infusion and 94% having resolution after a second fecal infusion (208). Initial reports indicated an increased fecal bacterial diversity in fecal-infused CDI patients, as well as an increase in *Bacteroidetes* and *Clostridium* sp. as well as a decrease in *Proteobacteria* species (208). A more directed attempt to ascertain the gut microbes that were responsible for resistance to CDI suggested that *Clostridium scindens*, the group of bacteria responsible for production of secondary bile acids, was strongly associated with inhibition of *Clostridium difficile* colonization and antibiotic-induced CDI in animal models and human patients (209). Earlier work on *C. difficile* linked bile salts and bile acids to germination of spores, showing that when CA, TCA, or DCA were added germination of *C. difficile* spores occurred (210, 211). Later work by Sorg et al showed *C. difficile* specificity for specific bile acids, as taurocholate, cholate, and deoxycholate induced germination *in vitro* but chenodeoxycholate did not (212). It was later shown by the same group that chenodeoxycholate competitively inhibits taurocholate germination of *C. difficile* spores (213). More recent work found a germinant receptor (CspC) in *C. difficile* was recognized specifically by 12 α -hydroxylated bile acids (214). Binding to this receptor led to the release of Ca²⁺ dipicolinic acid from the inside of the spore and subsequent influx of water, ultimately leading to growth into a vegetative cell (214). Some recent studies have shown that secondary bile acids inhibit *C. difficile* growth *in vitro* (215) and that ursodeoxycholic acid inhibits *C. difficile* growth and sporulation (216). Since *C. scindens* are the major producers of secondary bile acids, it would follow that these secondary bile acids are the mechanism by which *C. scindens* is associated with protection against CDI. However, experimental proof of *C. difficile* growth inhibition by physiological concentrations of secondary

bile acids *in vitro* or *in vivo* is lacking. Furthermore, a molecular mechanism by which DCA inhibits growth (as opposed to germination) is also absent. More work to determine the interplay between these bacteria in the colon is necessary, but the potential for a probiotic to prevent against CDI is an exciting prospect.

Research Objectives:

The research described in this thesis is aimed at better understanding numerous mechanisms by which gut-associated bacteria metabolize bile acid and steroid molecules and how this metabolism is linked to overall microbial physiology in the anaerobic environment of the colon. Within this framework, three objectives were pursued. The first objective was the characterization of a novel strain of *Eggerthella lenta*, screening and comparing its ability to metabolize various primary and secondary bile acids and steroid molecules, and linking its unique pattern of bile acid metabolites with specific gene clusters linked to acetogenesis. The second objective was the discovery of a gene in *Clostridium scindens* ATCC 35704 responsible for the production of a $\Delta 4,6$ -reductase that catalyzes two of the three reductive steps of the 7α -dehydroxylation pathway. The third objective was the utilization RNA-seq analysis to determine the transcriptomic changes in *Clostridium scindens* VPI 12708 treated with various steroid and bile acids, with the ultimate goal of locating the gene encoding a 17α -hydroxysteroid dehydrogenase responsible for production of epitestosterone from androstenedione. The work in this thesis gives better insight into the 7α -dehydroxylation pathway in *Clostridium scindens*. In addition, a unique interplay between atmospheric gases, bile acid oxidation, and 7α -

dehydroxylation was discovered and evidence put forth to characterize *Eggerthella lenta* as an acetogen.

Chapter 2: Materials and Methods

Bacterial strains and materials

Clostridium scindens ATCC 35704 obtained from ATCC, *Clostridium scindens* VPI 12708 obtained from Virginia Polytechnic Institute, *Clostridium absonum* ATCC 27555 obtained from ATCC, and human fecal isolates C592, I10, SA14, 19BHI, KS11, SO46, SO77 from collaborators at Ryukyus University in Okinawa, Japan are maintained as -80°C glycerol stocks in our laboratory. *Eggerthella lenta* ATCC 25559 was acquired commercially (ATCC). Before further analysis, strains were propagated on brain heart infusion (BHI) agar plates and grown under anaerobic conditions in Brewer jar with AnaeroPack (Mitsubishi) for 48 hours at 37°C, and colonies were picked and grown individually. Unless otherwise noted, bacterial strains were grown in liquid BHI broth (Becton, Dickinson) in round bottom flasks anaerobically under 100% N₂ gas atmosphere (Airgas), supplemented with 5g/L yeast extract (Becton, Dickinson), 1g/L cysteine HCl (Sigma) and 40mL/L of a salt solution containing 0.2g CaCl₂, 0.2g MgSO₄, 1g K₂HPO₄, 1g KH₂PO₄, 10g NaHCO₃ per liter. When arginine (Sigma) was used, it was added separately to the media to a final concentration of 5g/L (0.5% wt/volume) or 10g/L (1% wt/volume). Chenodeoxycholic acid (3 α -, 7 α - dihydroxy-5 β -cholan-24-oic acid; CDCA), cholic acid (3 α -, 7 α -, 12 α -trihydroxy-5 β -cholan-24-oic acid; CA), and deoxycholic acid (3 α -, 12 α -dihydroxy-5 β -cholan-24-oic acid, DCA) were obtained from Sigma. Allocholic acid (3 α -, 7 α -, 12 α -trihydroxy-5 α -cholan-24-oic acid; ACA), androst-4-ene-3,17-dione (androstenedione), androst-4-en-17 β -ol-3-one (testosterone), and androst-4-en-17 α -ol-3-one (epitestosterone) were obtained from Steraloids. [24-¹⁴C]-labeled CDCA and CA were obtained from American

Radiochemicals. [24-¹⁴C] DCA and lithocholic acid (3 α -monohydroxy-5 β -cholen-24-oic acid; LCA) were produced biologically. Before addition to culture, bile acids were suspended in methanol to a concentration of 10mM before being diluted to their final concentration in culture media.

Production of radiolabeled secondary bile acids and bile acid metabolism screening

For numerous experiments, [24C-¹⁴C]-bile acid biotransformation to secondary metabolites was screened. Unless otherwise noted, bile acid biotransformation profiles were investigated in whole cell cultures grown at 37°C overnight in anaerobic BHI medium under 100% N₂ atmospheric gas. For primary bile acid biotransformation screens, cultures were grown in the presence of 25 μ M bile acids and 1 μ Ci labeled bile acids. For secondary bile acid metabolism screens, cultures were grown in the presence of 25 μ M secondary bile acids with varying amounts of analogous [24-¹⁴C]-labeled bile acids. Culture growth was monitored using UV spectrophotometry (BioMate 3), monitoring at 600nm. Once adequate growth was observed, cultures were acidified to pH = 3.0 by adding 1N HCl (Sigma) and confirmed via pH meter. Cultures were then extracted with 2x volume ethyl acetate (Fischer Scientific). The organic layer was isolated and concentrated under a stream of N₂ gas. Organic extracts were then suspended in methanol, spotted, and run on silica gel TLC plates (J.T. Baker) with a 75:20:2 benzene:dioxane:acetic acid (Sigma) mobile phase. Plates were exposed to MS autoradiographic film (Kodak) overnight and bands corresponding to bile acid metabolites were scraped off and quantified using liquid scintillation spectrophotometry (RPI Budget-Solve; Tri-Carb 2100TR). These biotransformation of [24-¹⁴C]-labeled bile acids experiments were run alongside unlabeled

bile acid biotransformation experiments, separated on the same TLC plates as described above, and the corresponding unlabeled bands were scraped and isolated for future MS analysis.

Bile acid metabolite characterization

For future MS analysis, 100mL C592 cultures were grown to stationary phase as stated above in the presence of 25 μ M CDCA or DCA with and without [24-¹⁴C] radiolabel. Bile acid metabolites were extracted, separated, and isolated as stated above and then underwent LC-MS analysis. LC-MS analysis was run on a Shimadzu UPLC coupled with a Shimadzu LCMS-IT-TOF System (Shimadzu Corporation, Kyoto, Japan). The LC operating conditions were as follows: LC column, C-18 analytical column (Capcell Pak C18, Shiseido, Japan), 250 mm \times 2 mm i.d., particle size - 3 μ m (C18 (RP18, ODS, Octadecyl); mobile phase, H₂O containing 0.1% formic acid (A), and acetonitrile containing 0.1% formic acid (B); total flow rate of mobile phase, 0.2 ml/min; total run time including equilibration, 41 minutes. The initial mobile phase composition was 70% mobile phase A and 30% mobile phase B. The percentage of mobile phase B was changed linearly over the next 5 minutes until 35%. Over the next 25 minutes, the percentage was increased to 98% linearly. After that the percentage was maintained for 5 minutes, the mobile phase composition was allowed to return to the initial conditions and allowed to equilibrate for 5 minutes. The injection volume was 10 μ L. The mass spectrometer (LCMS-IT-TOF) was operated with an electrospray ionization (ESI) source in both positive and negative ion mode with multiple reaction monitoring (MRM). The nebulizer gas pressure was set at 150kPa with the source temperature of 200 $^{\circ}$ C and the gas flow at 1.5L/min. The detector voltage was 1.65kV. High-purity nitrogen gas was used as collision cell gas. The raw

chromatograph and mass spectrogram data were processed with the LC solution Workstation software (Shimadzu). For further characterization of C592 CDCA metabolites, as well as the production of 3-dehydro-DCA for putative Δ 4,6-reductase screening, radiolabeled CDCA, DCA, putative 7-oxo-CDCA, and putative 7-oxo-isoCDCA were treated with 0.25 unit/mL purified 3 α -hydroxysteroid dehydrogenase (Sigma) for one hour in the presence of 150 μ M NAD⁺ (Sigma) in 0.1M Tris-HCl buffer (pH 8.0). Enzymatic reaction was quenched with ethyl acetate and separated on TLC as described above.

Steroid metabolism screening

Similar to bile acid metabolism screening, steroid metabolism screening was performed in whole cell cultures grown at 37°C overnight in anaerobic BHI media under 100% N₂ gas. For whole cell biotransformation screening of androstenedione, testosterone, and epitestosterone metabolism, cultures were grown in the presence of 25 μ M of the steroid molecule. Once adequate growth was observed, growth was quenched with the addition of 2x volume ethyl acetate. The organic layer was then isolated, the solvent evaporated, and the extract suspended in 500 μ L methanol. One hundred microliters were injected and run on high-pressure liquid chromatography (Agilent) using a C-18 reverse phase column (Agilent Eclipse XDB-C18), 50:50 methanol:water mobile phase at a flow rate of 1mL/min, as adapted from previous work in (217). Absorbance of steroid metabolites was monitored at 240nm by UV-Vis spectroscopy. The *C. scindens* VPI 12708 androstenedione metabolite was fractionally collected and sent for NMR analysis, which was performed as previously described (217). For TLC separation of 11 β -OHAD and hydrocortisol cell culture biotransformation screens, organic extracts were run

similarly to described above except for the use of a different mobile phase: 5:25:0.2 isooctane; ethyl acetate; glacial acetic acid.

Primer design, polymerase chain reaction, and plasmid construction

Genomic DNA from *C. scindens* ATCC 35704, *C. scindens* VPI 12708, and C592 were isolated as described previously (218). Genomic DNA was then used as template for further PCR and genomic sequencing. A streptavidin tag engineered into the reverse primer (for EDS08212.1 and various putative 17 α -HSDH candidates) or the forward primer (various putative 17 α -HSDH candidates) and genes to test for activity were PCR amplified, restriction digested, and ligated into expression vectors. Generic 16S primers (16s357F, 16s1392R) and ExTaq polymerase kit (Takar) were used for initial 16S screening of *Eggerthella lenta* strain C592.

Methods for PCR amplification and plasmid construction are based on previously published methods (217). The gene encoding the putative Δ 4,6 reductase, EDS08212.1, was PCR amplified using the TITANIUM TAQ PCR Kit (Clontech) using primers designed to include the *E. coli* ribosome binding site and KpnI restriction site on the forward primer and a streptavidin-affinity peptide encoding sequence and BamHI restriction site on the reverse primer. The PCR product was purified through gel electrophoresis, underwent restriction endonuclease treatment (KpnI and BamHI), and was ligated into the pSport1 expression vector. Recombinant plasmid was transformed into chemically competent *E. coli* DH5 α cells via heat shock method, plated, and grown for 16 hours at 37 °C on lysogeny broth (LB) agar plates supplemented with ampicillin (100 μ g/mL). A single colony from each transformation was inoculated into LB

medium (5 mL) containing ampicillin (100 µg/mL) and cultivated overnight at 37°C with agitation. The cells were subsequently centrifuged (3220 x g, 15 min, 4 °C) and plasmids were extracted from the resulting cell pellet using the QIAprep Spin Miniprep kit (Qiagen, Valencia, CA). The foreign DNA inserts in the recombinant plasmids were sequenced to confirm the correctness of the gene sequence (Virginia Commonwealth University Nucleic Acid Sequencing Core Facility, Eurofins Genomics). Similar methods were used for putative 17 α -HSDH genes of interest. In some cases, troubleshooting changes were made via altering the streptavidin tag presence and location (C-terminal tag, N-terminal tag, or No strep tag), varying restriction endonuclease sequences, and utilization alternative expression vectors (pASK-IBA15plus and pASK-IBA43plus).

C592 genomic sequencing

Genomic DNA (1.5µg) was sheared in a gTube (Covaris, Woburn, MA) for 1 minute at 6,000 rpm in an Eppendorf MiniSpin plus microcentrifuge (Eppendorf, Hauppauge, NY). The sheared DNA was converted into a Nanopore library with the Nanopore Sequencing kit SQK-NSK007 (Oxford Nanopore, UK). The library was sequenced on a SpotON Flowcell MK I (R9) flowcell for 48 hours, using a MinION MK 1B sequencer. Basecalling was performed in real time with the software Metrichor version 2.40.17. Poretools v-0.5.1 software (219) was used to extract sequences from Oxford Nanopore MinION output file folder, and then converted to fastq format. FastQC v-0.11.2 software was also used to further access quality scores and other attributes of the data set. A Perl script was then used to trim adaptors from the raw nanopore reads. The adapter trimmed reads were used to blast against NCBI Ecoli_strK12_MG1655 genome. Reads

with greater than 95% alignment to this genome were removed. 2,113,230 reads from the Illumina paired end MiSeq run and 14,023 reads from Oxford Nanopore sequencing platform were used for de novo hybrid assembly with SPAdes-v3.9.0 (220). The assembly produced 245 contigs, five of which were 500 base pairs and longer. The top five contigs were selected to blast NCBI NT database. Nucleotide level comparisons between *Eggerthella lenta* DSM 2243 genome and the longest contig from the assembly were done with the dnadiff program from MUMmer v-3.23 (221). Annotation comparisons between *Eggerthella lenta* DSM 2243 genome and the longest contig were made with Prokka v-1.11 (222). Annotated CDS file for the longest C592 contig were then imported into Geneious v9.1.3 for Mauve alignment and further analysis, as well as utilized to form KEGG maps via BlastKOALA (223).

***C. scindens* VPI 12708 RNA purification and Illumina sequencing**

After -80°C stock of *C. scindens* VPI 12708 was grown overnight at 37°C in BHI broth, a 1% inoculum was transferred to 100mL BHI containing 25µM of either: cholic acid, allocholic acid, androstenedione, cortisol, or only BHI (for uninduced control) along with relevant [24-¹⁴C]-bile acid. Cells were allowed to grow to early-log phase, an additional 25µM of the inducing molecules were added, and then at mid-log phase cells were pelleted by centrifugation. Pelleted cells were immediately suspended in RNALater (Ambion) and placed in -80°C freezer. Supernatant was extracted and the metabolism of all four molecules in culture was confirmed via TLC and HPLC analysis, as outlined above.

Isolation of mRNA from *C. scindens* VPI 12708 follows a similar procedure to previously published work (Ridlon 2013). Cell pellets were suspended in 500 μ L lysis buffer (200mM NaCl, 20mM EDTA, in diethylpyrocarbonate-treated water) and then transferred to 2mL bead beating tubes (Sarstedt). To each tube, 1mL 5:1 acid phenol (Ambion), 200 μ L 20% SDS (Ambion), and 200 μ L zirconium beads was added. Cells were then disrupted on max RPM on a Mini-BeadBeater (Biospec Products) for one-minute increments twice and placed on ice in between. Samples were then centrifuged to separate the aqueous and phenol phases. The aqueous phase was isolated and subsequently washed with an additional 1mL of 5:1 acid phenol, and then separated again via centrifugation. The nucleic acids in the purified aqueous phase were precipitated by addition of 2x volume of 2-propanol (Sigma), 100 μ L ammonium acetate (Ambion), and 1 μ L glycoblue (Ambion). Samples were incubated at -80°C overnight, centrifuged for 30 minutes, and the pellet isolated. RNA was isolated from the nucleic acid samples using the Ambion “Megaclear” kit, according to the manufacturers instructions. Purified RNA samples were treated 2x with DNase (Takara), following manufacturers instruction. Resulting RNA was checked for purity via a 1.6% denaturing gel electrophoresis (for 16S and 23S bands) as well as via RT-PCR to check for contaminating genomic DNA following the Clontech manufacturer instructions.

Purified total RNA then underwent mRNA enrichment protocol, following a similar procedure to previously published work from our lab (217). Custom biotinylated TEG-spaced oligonucleotides were designed against *C. scindens* VPI 12708 16S and 23S rRNA sequences. Dynabeads M-280 Streptavidin (Invitrogen) were made RNase free and then bound to oligonucleotides by resuspending beads in 500 μ L DEPC 0.5x SSC containing 360 pmol of each

oligonucleotide. Beads were captured using Promega magnetic stand (Promega). After oligonucleotide beads were isolated, the rRNA capture-hybridization protocol was run using a Biorad C1000 thermocycler (Biorad). Total RNA (1µg) was suspended in 35uL 6x SSC, heated to 70°C for 5 minutes, cooled to 0°C for 3 minutes, and then 150uL of oligonucleotide-bound beads were added. The mixture was then incubated at 68°C for 30 minutes. Beads were magnetically captured using the Promega stand, and the supernatant containing the enriched mRNA was isolated and precipitated as described above. Total RNA and enriched mRNA were compared using Bioanalyzer to see a distinct drop in the bands corresponding to rRNA subunits before RNAseq analysis.

mRNA-enriched *C. scindens* VPI 12708 samples were then used to create libraries for Illumina whole transcriptome sequencing using the NEBNext Ultra RNA Library Prep Kit for Illumina, following manufacturer's instructions (NEBNext). Samples were then run using MiSeq instrumentation using a 2 x 300 bp recipe. Resulting reads were then aligned to a previously annotated *C. scindens* VPI 12708 genome using the BowTie2 algorithm.

Protein overexpression and purification

For the putative $\Delta 4,6$ -reductase gene expression, pSport-EDS08212 plasmid was transformed into *E. coli* BL-21 CodonPlus (DE3) RIPL chemically competent cells by the heat shock method and grown overnight at 37 °C on LB agar plates supplemented with ampicillin (100 µg/mL). After 16 hours, five isolated colonies were used to inoculate 10 mL of fresh LB medium supplemented with antibiotics and grown at 37 °C for 6 hours with vigorous aeration. The pre-

cultures were then added to fresh LB medium (1L), supplemented with the same antibiotic at the same concentrations, and grown with vigorous aeration at 37 °C. At OD₆₀₀ of ~0.3, isopropyl β-D-1-thiogalactopyranoside (IPTG) inducer was added to each culture at a final concentration of 0.1mM and the temperature was decreased to 16 °C. Following 16 hours of culturing, cells were pelleted by centrifugation (4,000 x g, 30 min, 4 °C). Cells were then suspended in buffer (20mM sodium phosphate buffer pH 7.0, 0.1M NaCl, 15% glycerol, 10mM 2-mercaptoethanol) and treated with lysozyme (5ug/mL) on ice for 1 hour. Cell suspension was then run through a French press at 1,500 psi and following cell extract was centrifuged (30min, 16,000g, 4°C). Recombinant EDS08212.1 gene product was then purified using Strep-Tactin® resin (IBA) as per manufacturing protocol. The recombinant protein was eluted using an elution buffer composed of 20mM Tris-HCl, 150mM NaCl, 20% glycerol, 10mM 2-mercaptoethanol pH 7.9 and 2.5mM desthiobiotin. Protein purity was assessed using both sodium dodecyl sulfate-polyacrylamide gel electrophoresis (SDS-PAGE) and Western blotting using the Strep Tag II antibody (IBA). The purified protein concentration was determined via the Bradford Assay (BioRad). The same methods were used for the overexpression and purification of putative 17α-HSDH enzymes from *C. scindens* VPI 12708 with minor adjustments. Constructs lacking a streptavidin tag were not purified on a Strep-resin column nor were visualized via Western blot hybridization.

Δ4,6-reductase and 17α-HSDH purified enzyme reactions

To test the oxidation of 3-dehydro-DCA by EDS08212.1, we used a standard buffer composed of 20mM sodium phosphate (pH 7.0), 100mM NaCl, 20% glycerol, and 10mM 2-mercaptoethanol.

When utilized, pyridine nucleotides (NAD⁺, NADP⁺, NADH, NADPH) were added at 150μM final concentration. 3-dehydro-DCA was added at 30μM final concentration. The reaction was initiated by addition of 0.5μg purified rEDS08212 to 1ml reaction buffer and was terminated after 6 hrs at 37°C by addition of 75μl 1N HCl, and was extracted and chromatographed as described above.

Similar methods were used for testing purified putative 17α-HSDH enzymes. Buffers used included 20mM sodium phosphate (pH 7.0) or 100mM sodium acetate buffer (pH 5.5) with either 10mM 2-mercaptoethanol or 1mM dithiothreitol (Sigma). When utilized, pyridine nucleotides (NAD⁺, NADP⁺, NADH, NADPH) were added at 150μM final concentration. 1μg purified recombinant putative 17α-HSDH enzymes were added to each 1mL reaction volume. In the case of whole cell extract assays, up to 100ug of whole cell protein extract was added per 1mL reaction volume. Aerobic metabolism of androstenedione and epitestosterone was tested by monitoring changes in pyridine nucleotide oxidation states spectrophotometrically by absorption at 340nm over time. Alternatively, aerobic metabolism of the steroid molecules was screened by extraction of reaction mixtures and separation on HPLC as described above. Anaerobic metabolism used the same reaction buffers that had been made anaerobic under N₂ stream. The metabolism of substrates was tracked via HPLC separation, as described above. Additionally, *E. coli* BL-21 CodonPlus (DE3) RIPL transformed with putative 17α-HSDH gene plasmid constructs were grown aerobically and anaerobically, induced with IPTG at early log phase, and inoculated with 25μM androstenedione or epitestosterone. Whole cell conversion of these steroids was then screened via extraction and HPLC separation, as described above.

Bioinformatics analysis and statistics

Phylogenetic analysis of EDS08212.1 by maximum-likelihood was performed using RAxML 8.2.0 (224), with gamma-distributed heterogeneity rates, automatically selected empirical substitution model, and 100 bootstrap pseudoreplicates. Selection and alignment of sequences from the NCBI nr database were performed as previously described (217). The resulting tree was drawn in Dendroscope (225) and cosmetic adjustments were performed in Inkscape.

For *C. scindens* VPI 12708 RNAseq analysis, significance was assessed using a false discovery rate corrected p-values of 0.05, which were calculated and assessed using this cut-off. RNAseq was utilized to make a heatmap using a distance metric of $1-(\text{abs}(\text{pearson correlation}))$, and the “ggplot” and “heatmap.2” R packages.

Table 2.1: Bacterial strains used in the present study

Strain	Source
<i>Clostridium scindens</i> VPI 12708	VPI
<i>Clostridium scindens</i> ATCC 35704	ATCC
<i>Clostridium absonum</i> ATCC 27555	ATCC
<i>Eggerthella lenta</i> ATCC 25559	ATCC
<i>Eggerthella lenta</i> strain C592	Collaborators at Ryukyus University
I10	Collaborators at Ryukyus University
SA14	Collaborators at Ryukyus University
19BHI	Collaborators at Ryukyus University
KS11	Collaborators at Ryukyus University
SO46	Collaborators at Ryukyus University
SO77	Collaborators at Ryukyus University
<i>E. coli</i> BL21 (DE3)	New England Biolabs
<i>E. coli</i> Top10	Thermo Fischer

Table 2.2: Primers used in the present study

Primer	Use	Sequence (5' – 3')
16s357F	Fwd: C592 16S amplification	CTCCTACGGGGAGGCAGCAA
16s1392R	Rev: C592 16S amplification	ACGGGCGGTGTGTRC
16s35704cap1	<i>C. scindens</i> VPI 12708 rRNA depletion	GCGTTACTGACTCCCATGGTGTGACGG/3BioTEG/
16s35704cap2	<i>C. scindens</i> VPI 12708 rRNA depletion	CTTGCGAACGTACTCCCCAGGTGGACTA/3BioTEG/
16s35704cap3	<i>C. scindens</i> VPI 12708 rRNA depletion	GCTTCGGTCTTATGCGGTATTAGCAGCC/3BioTEG/
23s35704cap1	<i>C. scindens</i> VPI 12708 rRNA depletion	CCAGGGTAGCTTTTATCCGTTGAGCGA/3BioTEG/
23s35704cap2	<i>C. scindens</i> VPI 12708 rRNA depletion	GACAGTGCCCAAATCATTACGCCTTTCG/3BioTEG/
23s35704cap3	<i>C. scindens</i> VPI 12708 rRNA depletion	AACCTGTTGTCCATCGGCTACGGC/3BioTEG/
23s35704cap4	<i>C. scindens</i> VPI 12708 rRNA depletion	GGACATGGATAGATCACCCGGTTTCG/3BioTEG/
23s35704cap5	<i>C. scindens</i> VPI 12708 rRNA depletion	GACACCTCCGGATCAAAGGGTATTTGCC/3BioTEG/

Primer	Use	Sequence (5' – 3')
pSport112708_00455NTERM	Rev: Cs12708_00005_00084	GTCGACTTATTCCTCAGCCTGCTC
Rnew	w/ N-terminal Strep tag	
pSport112708_00455NTERMF	Fwd: Cs12708_00005_00084	CTGCAGATTAGAGAGGTGGATAACATGTGG- -AGCCACCCGCAGTTCGAAAAAATTTATTT
	w/ N-terminal Strep tag	
CLONE12708_00455F	Fwd: Cs12708_00005_00084	CACTGCTCATGGTGACCTATTTCTA
	no tag	
CLONE12708_00455R	Rev: Cs12708_00005_00084	GCTATCATCTTCACCTCTCATCATT
	no tag	
pSport_00455_CF	Fwd: Cs12708_00005_00084	TAATCTGCAGATTAGAGAGGTGGATAAC
	w/ C-terminal Strep tag	
pSport_00455_CR	Rev: Cs12708_00005_00084	ATATGTCGACTTATTTTTTCGAACTGCGGGT- -GGCTCCATTTCCTCAGCCTGCTC
	w/ C-terminal Strep tag	
pASK_64_18 Forward	Fwd: Cs12708_00064_00018	GGATCCAATTCATATACAGTA
	in pASK p43 and p15 vectors	
p43_68_18_R	Rev: Cs12708_00064_00018	CCATGGCCTATTCGCTCG
	in pASK p43	

Primer	Use	Sequence (5' – 3')
p15_64_18_R	Rev: Cs12708_00064_00018 in pASK p15	ATGCATCCATGGCTCCTTATATTCGCTCG
Cs12708_64_18F	Fwd: Cs12708_00064_00008 in pSport1 with N-terminal Strep tag	GTCGACGGATCCCGGAGAATGAAT- -TCATATACAGTA
Cs12708_64_18R	Rev: Cs12708_00064_00008 in pSport1 with N-terminal Strep tag	AAGCTTCTATTTTTCGAACTGCGGGTG- -GCTCCATATTCGCTCGACTTTCTG
Cs12708_114_9_NF	Fwd: Cs12708_00114_00009 in pSport1 with N-terminal Strep tag	CTGCAGAAAAGGAAGGGGATGATAGG
Cs12708_114_9_NR	Rev: Cs12708_00114_00009 in pSport1 with N-terminal Strep tag	GGATCCTTATTTTTCGAACTGCGGGTGG- -CTCCAAACAAGCGTCCAGCC
Cs12708_114_9_NoTagF	Fwd: Cs12708_00114_00009 in pSport1 no tag	GTCGACCTGCAGGATAGGATGAAGAA- -TTTATTTGAT
Cs12708_114_9_NoTagR	Rev: Cs12708_00114_00009 in pSport1 no tag	ATGCATGGATCCAATTGTCTAAACAAG- -CGTCAA

Primer	Use	Sequence (5' – 3')
Cs12708_124 _9_NF	Fwd: Cs12708_ 00124_00009 in pSport1 with N-terminal Strep tag	CTGCAGAAAGGAGAACAAAAAGGA
Cs12708_124 _9_NF	Rev: Cs12708_ 00124_00009 in pSport1 with N-terminal Strep tag	GGATCCTTATTTTTCGAACTGCGGGTGGCT- -CCATATCAACGGTTCATA

Fwd – Forward; Rev – Reverse; 3BioTEG – 3' Biotin with triethyleneglycol (TEG) spacer

Table 2.3: Plasmids used in the present study

Plasmid	Description	Source
pCR TM Blunt II-TOPO®	Kanamycin resistance, designed for blunt-end ligation	Thermo Fischer
pSPORT-1	Ampicillin resistance, contains lac-promotor for expression in <i>E. coli</i> cells	Thermo Fischer
pASK-IBA43plus	Ampicillin resistance, contains C-terminal Strep-tag, tet- promotor expression vector	IBA
pASK-IBA15plus	Ampicillin resistance, contains N-terminal Strep-tag, tet- promotor expression vector	IBA

Chapter 3: Characterization of novel *Eggerthella lenta* strain C592

Introduction:

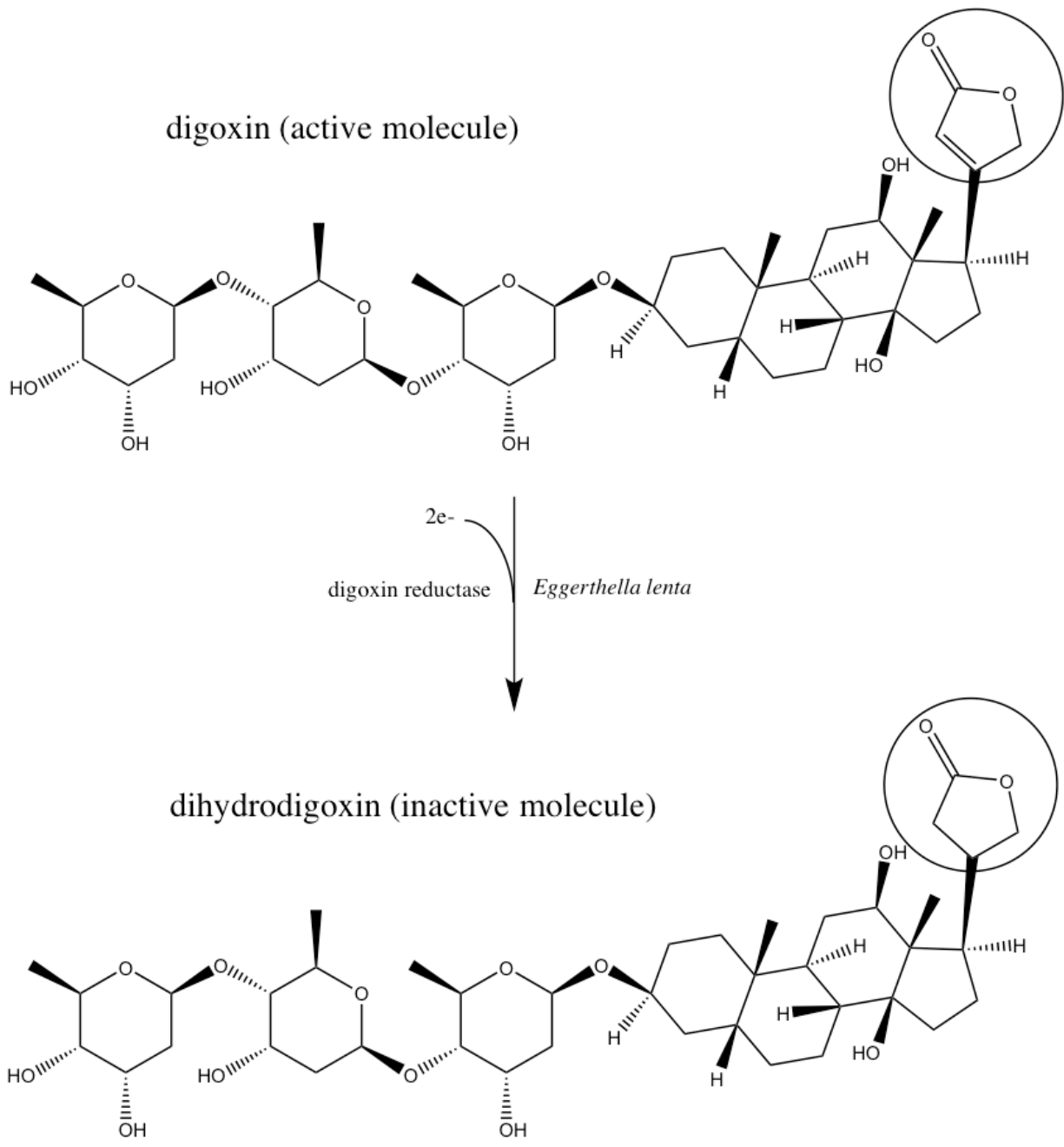
Significant effort is underway studying the human gut microbiome and how it impacts human health. The first step in this process is to obtain a basic understanding of the makeup of this microbial community. The advent of next generation sequencing, along with advances in computational power have provided the ability to assign functional characterization organisms based on clusters of orthologous groups (COG) and Kyoto Encyclopedia of Genes and Genomes (KEGG) databases, allows scientists to gain insight into the effects microbes may have on each other and the host (226). However, the reference genomes that guide predictive annotations of novel microbial strains only account for a third of the entire metagenomic data received from high-throughput shotgun sequencing of fecal samples (227). A complementary approach is to attempt to assign strains to OTUs based on 16S DNA sequence (2). However, in doing so it is very easy to miss significant differences that may exist among species within a specific OTU. These significant differences are evident when studying the gut “sterolbiome”, the genes involved in bile acid and steroid metabolism. For example, within the same species, *Clostridium scindens* strains have been shown to have varying ability to metabolize steroids. *C. scindens* ATCC 35704 encodes a steroid 17,20-desmolase which is absent from its sister strain *C. scindens* VPI 12708 (217). Additionally, *C. scindens* VPI 12708 has been shown to have unique 17 α -HSDH activity that is not found in *C. scindens* ATCC 35704 (228). Understanding and characterizing the sterolbiome’s potential to biotransform these molecules in humans is

important because even small modifications to the base structure of bile acids and steroids can have significant physiological effects, even at nanomolar concentrations (167, 229, 230).

One bacterial strain that has garnered significant attention in the study of the human gut sterolbiome is *Eggerthella lenta*. Within the class *Actinobacteria* and the family *Coriobacteriaceae*, *E. lenta* is a non-motile, non-sporulating, gram-positive short rod-shaped bacterium usually found in pairs or chains (231). The first isolation of what would later be named *Eggerthella lenta* was from normal adult fecal samples by Arnold H. Eggerth in 1935, and classified under the *Bacteroides* genus, although no type strain was obtained (232). Soon after, the first reported type strain for *Eggerthella lenta* was isolated from a rectal tumor and added to the Prevot collection under the *Eubacterium* genus classification (231). It was later transferred to the *Eggerthella* genus after further characterization and phylogenetic analysis (233, 234).

E. lenta has been proposed as an important gut microbial strain to characterize and potentially inhibit in patients undergoing treatment for cardiovascular disease. Cardiac glycosides, derived from *Digitalis purpurea*, have been used for centuries to treat both heart failure and atrial fibrillation (235). Approximately 10% of those treated with cardiac glycosides harbor an intestinal microbiota capable of reducing the α,β -unsaturated butyrolactone ring, thereby inactivating the drug (Figure 3.1) (236). It has been shown that some strains of *E. lenta*, including the type strain, have the ability to reductively inactivate digitoxin (237). Within these active *E. lenta* strains, a two-gene locus termed the “cardiac glycoside reductase operon” (cgrAB) was found that encodes proteins resembling bacterial cytochromes that are associated

Figure 3.1: Diagram of reductive digoxin inactivation by *Eggerthella lenta*



Adapted from (236)

with the formation of reduced digoxin products from digoxin (238), although it has yet to be proven that this “cgr locus” encodes a digoxin reductase. These reduced digoxin products have reduced cardiac reactivity, likely due to a decreased affinity to the Na⁺/K⁺ ATPase in cardiomyocytes (239). The role of *E. lenta* in the formation of inactivated digoxin products on the availability of digoxin is important because of the narrow range at which digoxin is therapeutically effective before it becomes toxic (240).

In addition to the metabolism of cardiac glycosides, *E. lenta* has been shown to metabolize endogenous steroid molecules. Because of their metabolism of endogenous corticosteroids, *E. lenta* has been identified as a candidate to be linked to essential hypertension, although more work is necessary to delineate the extent of its involvement. The initial work of linking the gut microbiota to hypertension began in rats, where the development of hypertension could be attenuated by treatment with neomycin and vancomycin (241, 242). However, attempts to delineate the specific microbes responsible for this modulation at the time were unsuccessful and not pursued further (243). In the study of adults with 17-hydroxylase insufficiency, a genetic defect causing hypertension due to an increased level of deoxycorticosterone leading to renal sodium retention (244), it was found in urinary steroid analysis that 21-deoxycorticosterone was a major metabolite of corticosterone (245). Radiolabeled assays showed that 21-deoxycorticosterone was a direct metabolite of corticosterone, and that its production did not occur in germ free rats (245, 246). Around the same time it was discovered that *Eggerthella lenta* produced a 21-dehydroxylase capable of converting cortisone to 11 β -hydroxy-progesterone (247, 248). A major regulator of systemic blood pressure is aldosterone, which imparts its action by binding to the mineralocorticoid receptor in renal epithelial cells (249). This leads to the

expression of sodium reabsorption mechanisms, ultimately increasing extracellular volume (249). However, cortisol is a much more potent agonist for the mineralocorticoid receptor in renal epithelial cells and is in much higher concentrations in serum. The reason that aldosterone is the major systemic modulator of blood pressure is that renal cells also contain 11 β -hydroxysteroid dehydrogenase-2 (11 β -HSD2), which can inactivate cortisol once inside the cell, forming inactive cortisone (250). Therefore, 11 β -HSD2 acts as a modulator of cortisol activity. It has been shown that 11 β -hydroxy-progesterone is a competitive inhibitor for the 11 β -HSD2 enzyme (251). *E. lenta* is the only gut microbe reported to contain 21-dehydroxylase activity capable of converting cortisol to 11 β -hydroxy-progesterone, although not all strains harbor activity (248). In a model of hypertension caused by obstructive sleep apnea in rats, it was found that the gut microbiome of those with hypertension showed an increase in *Coriobacteriaceae*, which includes *E. lenta* (252).

Additionally, 11 β -hydroxysteroid dehydrogenase type 1 (11 β -HSD1) found in the liver and responsible for converting cortisone to activated cortisol (the reverse of 11 β -HSD2), has been shown to be competitively inhibited by oxo-bile acid derivatives of microbial bile acid metabolism, such as 7-oxo-lithocholic acid (198, 199), although more oxo-bile acid derivatives need to be screened. *E. lenta* has been reported to harbor 3 α -HSDH, 7 α -HSDH, and 12 α -HSDH activity, varying on the strain, which are involved in the formation of oxo-bile acids (151, 153).

Metabolism of corticosterone and bile acids by *E. lenta* may also have implications on CRC formation. 11 β -HSD2 is also found in colonocytes, the disruption of which has been shown to rescue APC knockout mice from tumor formation through a *Cox-2* dependent mechanism (253).

Therefore, the inhibition of 11β -HSD2 activity by *E. lenta*-derived corticosterone derivatives may alter prostaglandin synthesis and reduce colonic inflammation, both factors important to CRC development.

In addition, the metabolism of bile acids by *E. lenta* may lead to the formation of less toxic bile acid metabolites and affect CRC progression as well. As reviewed earlier, secondary bile acids DCA and to a lesser degree LCA, formed from primary bile acids CA and CDCA, have been associated with the formation of CRC. However, other secondary bile acids produced by gut microbes are less toxic. Ursodeoxycholic acid (UDCA) is formed by the oxidation and subsequent epimerization of the 7α hydroxyl group of CDCA via microbial 7α -HSDH and 7β -HSDH enzymes (125). UDCA has been shown to be less toxic to both microbial and host cells, and additionally have seen some use as therapeutic agents in liver and biliary disease. The β -configuration of the 7-hydroxyl group leads to a more hydrophilic molecule, leading to its reduced toxicity (254, 255). In addition to epimerization of the C7-hydroxyl group on CA, CDCA, and UDCA, the C3-hydroxyl group is also subject to isomerization by bacterial enzymes in the gut, including some produced by *E. lenta*. *E. lenta* has been found to encode both a 3α -HSDH and 3β -HSDH necessary to convert DCA to iso-DCA (150). The same work showed that iso-DCA was less toxic to other gut microbes than DCA, indicating it may be a detoxification mechanism (150). The effects of isomerized secondary bile acids on colonocytes remains unstudied, but it can be hypothesized that due to their increased hydrophilicity, iso-secondary bile acids would be less toxic than secondary bile acids. What was not established in this previous study was whether *E. lenta* could convert primary bile acids to 3β -epimers. Removal of the C7-hydroxyl group on primary bile acids requires the formation of a 3-oxo- Δ^4 -intermediate

and to date no 7α -dehydroxylating bacteria has been shown to encode a 3β -HSDH. Therefore, we predict that isomerization of primary bile acids would lead to formation of alternate bile acid metabolites and prevent 7α -dehydroxylation.

Studies identifying the makeup of the inhabitants of the gut microbiome have shown the two major represented phyla being Bacteroidetes and Firmicutes, making up on average 85% of the total phylotypes (256, 257). The next most represented phylum is Actinobacteria, of which *E. lenta* is a member. Even though it is found in lower relative abundance in the gut, *E. lenta* still has significant implications to both gut microbiome and host physiology. Studies of both germ-free mice and hamsters have indicated that OTUs identified as or closely related to *E. lenta* are associated with increased hepatic triglycerides, increased synthesis of primary bile acids via the alternative pathway, and increased liver cytochrome activity (258, 259). Interestingly, *E. lenta* and *Clostridium scindens*, both numerically minor constituents of the gut microbiome, which are nevertheless responsible for substantial metabolism of bile acids and steroid molecules, were shown to be associated with increased hepatic triglyceride synthesis in conventionalized ex-germ free mice (258). The bile acid composition (a switch to primary bile acids produced via the alternative pathway) as well as increased hepatic FXR and PXR signaling, suggesting a significant role of *E. lenta* in gut microbiome-modulated energy homeostasis via bile acid signaling pathways (258). A mechanism by which *E. lenta* may be exerting these effects is through activation of TGR5, leading to glucagon-like peptide-1 (GLP-1) release from neuroendocrine cells, leading to increased insulin release from the pancreas, which stimulates production of triglycerides by hepatocytes. However, it has been shown that secondary bile acids

DCA and LCA are the most potent activators of TGR-5 (170, 171) and *E. lenta* has not been shown to create these molecules.

Human studies have shown that diet substantially alters the structure and metabolic activity of the gut microbiome (226, 256). One such quantitative study of changes to gut microbial diversity based on varying diets showed *E. lenta* levels can vary in the same individual based purely on diet. A significant increase in *E. lenta* was observed in human subjects given a diet high in non-starch polysaccharides relative to other dietary polysaccharides, including resistant starch and a “weight loss” diet high in protein (260). Similarly, fecal concentrations of SCFAs acetate, propionate, butyrate, as well as succinate, were all significantly higher in the same patients eating a diet high in non-starch polysaccharides when compared to other diets (260). These results suggest that *E. lenta* thrives in an environment where anaerobic bacterial fermentation is occurring.

Based on the previous literature, it is apparent that *E. lenta* impacts both gut microbial and host physiology. However, a better understanding of the types of bile acid and steroid products it recognizes and the metabolites it creates is necessary. Furthermore, understanding how bile acids and steroids play into the overall metabolism of *E. lenta* may give insight into why bile acids and steroids are utilized in the more complex gut microbial environment. We set out to better understand *E. lenta* bile acid and steroid metabolism through characterization of a novel strain; C592, a human fecal isolate from a Japanese octogenarian. Comparison of steroid metabolism and genome sequence between the type strain *E. lenta* ATCC 25559 reveals important strain-dependent differences in the sterolbiome among *E. lenta* isolates. I discovered

that both these bacteria make unique patterns of oxidized bile acid and steroid metabolites, including a novel ability to metabolize testosterone. I show that the pattern of metabolites made can be altered based on the atmospheric gases present during their growth. Based on these observations, the full genome sequencing/annotation of C592, and preliminary fermentative end product analysis, I hypothesize that *Eggerthella lenta* is an acetogen able to link the metabolism of bile acids to the formation of acetate in order to maintain intracellular redox equilibrium. In addition, I show that the bile acid metabolites made by *E. lenta* ATCC 25559 and C592 inhibit subsequent 7 α -dehydroxylation by *Clostridium scindens*.

Results:

Initial screening of C592 primary bile acid metabolism

Strain C592 is a gram-positive, obligate anaerobe isolated from a human fecal sample from Dr. Fusae Takamine (University of Ryukyus) in Okinawa, Japan during a screen for fecal bile acid 7 α -dehydroxylating bacteria. However, the bile acid metabolites derived from whole-cell cholic acid-induced ^{14}C -cholic acid metabolism by the C592 strain had unique retardation factor (R_F) values as compared to known metabolites synthesized by 7 α -dehydroxylating bacteria (Figure 3.2). In comparison to both high-activity and low-activity 7 α -dehydroxylating strains, C592 CA metabolites do not comigrate with CA, DCA, or allodeoxycholic acid (ADCA), a 5 α -epimer of DCA (Figure 3.2). In addition, numerous secondary metabolites were generated from CA, whereas the major product from other 7 α -dehydroxylating strains comigrates with the DCA standard (Figure 3.2). These results suggested C592 is producing unique bile acid metabolites from CA. C592 CA metabolism screening was repeated, inducing with either CA or allocholic acid (ACA), a 5 α epimer of CA. Results showed that both CA and ACA-induced C592 cultures metabolized [^{14}C]-CA to secondary products unique from known 7 α -dehydroxylated metabolites DCA and ADCA (Figure 3.3). There was no difference in the migration of ^{14}C -CA metabolites between CA and ACA-induced C592 metabolism by TLC analysis. C592 was also screened for its ability to metabolize CDCA, the other primary bile acid produced by human hepatocytes. C592 CDCA-induced metabolism of [^{14}C]-CDCA showed formation of three secondary products (Figure 3.4). Experiments looking at C592 uninduced whole cell metabolism of [^{14}C]-CA and

Figure 3.2: TLC of whole cell extracts from various fecal bacterial strains induced by cholic acid to metabolize [24-¹⁴C]-cholic acid

First section of TLC plate includes cholic acid, deoxycholic acid, and allodeoxycholic acid TLC standards. The second section contains organic extracts from whole-cell cholic acid-induced [24-¹⁴C]-cholic acid metabolism. I10, SA19, C592, 19BHI, KS11, SO96, SO77 are all human fecal isolates previously screened for bile acid metabolizing potential. Cultures were grown overnight with 25µM cholic acid and 1µCi labeled cholic acid and separated on TLC as described in Materials and Methods. The major CA metabolite for I10, SA19, 19BHI, KS11, SO96, and SO77 comigrates with the DCA standard. However, the C592 metabolites appear to migrate separately with one migrating similarly to ADCA.

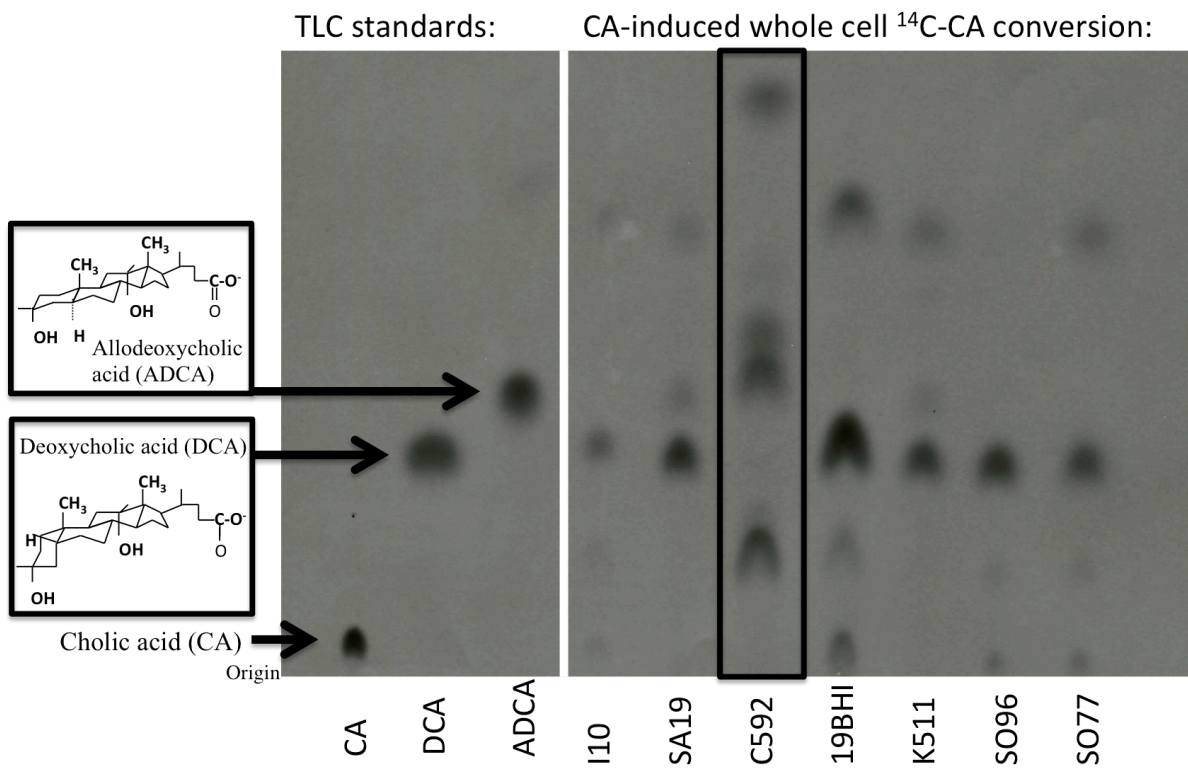


Figure 3.3: Conversion of [24-¹⁴C]-cholic acid by allocholic acid- and cholic acid-induced C592

First section of TLC plate includes cholic acid, deoxycholic acid, and allodeoxycholic acid TLC standards. The second section contains organic extracts from C592 whole-cell bile acid-induced [24-¹⁴C]-cholic acid metabolism. C592 was grown in the presence of either 25 μ M cholic acid or 25 μ M allocholic acid, along with 1 μ Ci cholic acid. Cultures were extracted and run on TLC as described in the Materials and Methods. C592 metabolizes [24-¹⁴C]-cholic acid to five secondary metabolites, with no apparent difference in the spectrum of metabolites when induced with either cholic or allocholic acid. No C592 CA metabolites comigrate with DCA or ADCA, suggesting they are not 7 α -dehydroxylated.

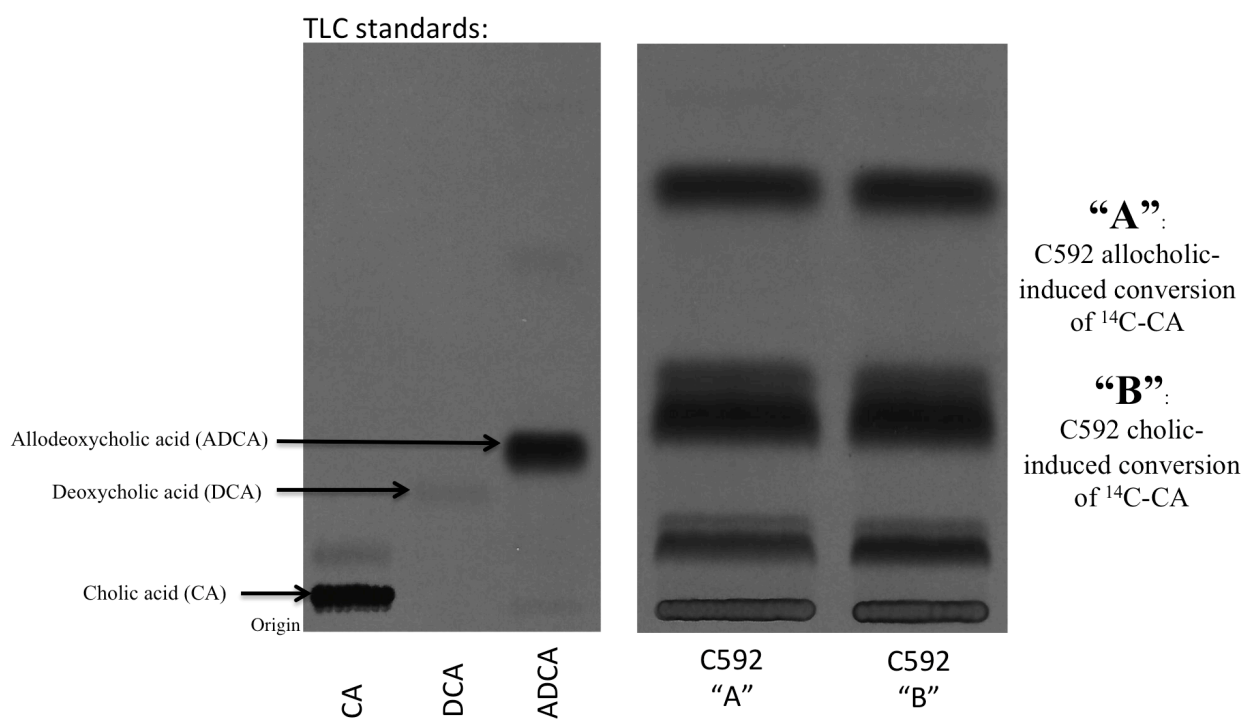
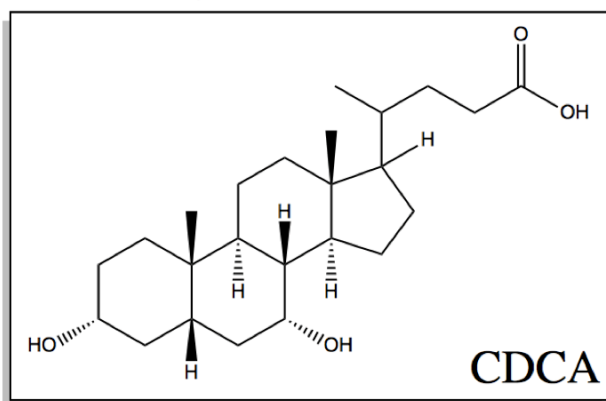


Figure 3.4: Conversion of [24-¹⁴C]-CDCA by CDCA-induced C592

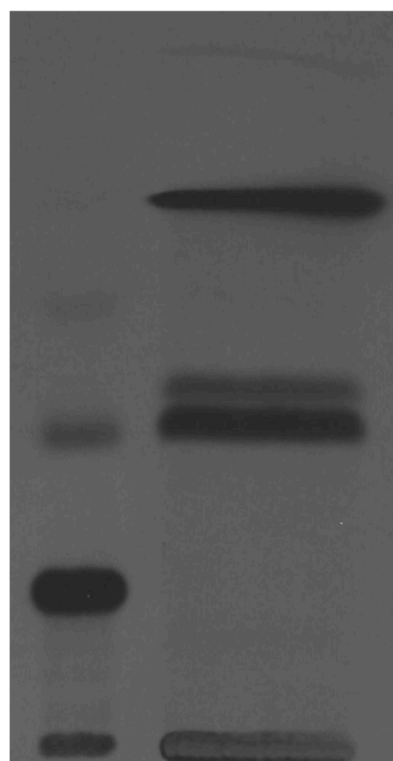
First spot on the TLC plate is the chenodeoxycholic acid TLC standard. The second spot contains the organic extracts from a C592 whole-cell chenodeoxycholic acid-induced [24-¹⁴C]-chenodeoxycholic acid metabolism. C592 was grown in the presence of 25µM chenodeoxycholic acid along with 1µCi chenodeoxycholic acid. Cultures were extracted and run on TLC as described in the Materials and Methods. C592 metabolizes [24-¹⁴C]-chenodeoxycholic acid to three secondary metabolites.

chenodeoxycholic acid

5 β -cholanic acid-3 α -7 α -ol



Origin



CDCA
TLC
standard

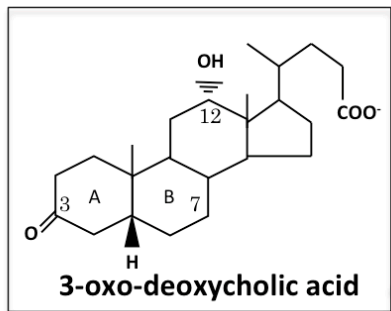
CDCA-induced
C592 + ¹⁴C-
CDCA

[¹⁴C]-CDCA as well as C592 whole cell protein extract metabolism of [¹⁴C]-CA and [¹⁴C]-CDCA showed no significant difference from the induced samples, indicating this was not an inducible phenomenon (data not shown).

Next C592 was compared against known bile acid 7 α -dehydroxylating and epimerizing bacterial whole-cell cultures. *Clostridium scindens* VPI 12708 is a known high-activity 7 α -dehydroxylating bacterium known to harbor a bile acid-inducible operon (bai-operon). The products created from CA-induced [¹⁴C]-CA metabolism in whole cell cultures are known, including 3-oxo-deoxycholic acid, DCA, and 7-oxo-cholic acid (Figure 3.5). Additionally, when induced with ACA, *C. scindens* VPI 12708 shifts its metabolic profile to create 3-oxo-allodeoxycholic acid and allodeoxycholic acid, in addition to some trace DCA (143) (Figure 3.5). Both whole cell extracts of 12708 [¹⁴C]-CA metabolism were used as comparisons to help determine possible C592 CA metabolites, although only 7-oxo-cholic acid appeared to comigrate, indicating C592 CA metabolites are not 7 α -dehydroxylated (Figure 3.5). In addition, C592 CDCA-induced [¹⁴C]-CDCA metabolism was compared against two other bacteria known to metabolize CDCA. *C. scindens* VPI 12708 is known to convert CDCA into several metabolites, including LCA, 3-oxo-lithocholic acid, 3-oxo-chenodeoxycholic acid, and 7-oxo-lithocholic acid (7-oxo-LCA) (Figure 3.6). *Clostridium absonum* was also screened, as it has been previously shown to harbor both a 7 α -HSDH and 7 β -HSDH, allowing it to epimerize CDCA at the 7-hydroxyl group forming ursodeoxycholic acid (146). *C. absonum* whole cell CDCA metabolism generated 7-oxo-lithocholic acid as well as ursodeoxycholic acid (Figure 3.6). When these known CDCA metabolites were compared to the three C592 CDCA

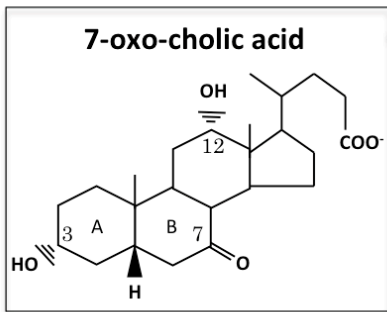
Figure 3.5: TLC separation of organic extracts from *C. scindens* VPI 12708 and C592 bile acid-induced whole cell conversions of [24-¹⁴C]-CA

The first spot on the TLC plate is a cholic acid TLC standard. The next three spots are organic extracts from whole-cell bile acid-induced [24-¹⁴C]-cholic acid metabolism screens in *C. scindens* VPI 12708 or C592. Based on previous literature, *C. scindens* VPI 12708 is known to differentially produce deoxycholic acid or allodeoxycholic acid from cholic acid when induced with either cholic acid or allocholic acid, respectively (143). In addition, *C. scindens* VPI 12708 bile acid induced cultures usually generate some 7-oxo-cholic acid and 3-oxo-deoxycholic acid (when induced with cholic acid) or 3-oxo-allodeoxycholic acid (when induced with allocholic acid), based on R_f (143). One C592 cholic acid metabolite appears to comigrate with allodeoxycholic acid and another with 7-oxo-cholic acid, but the rest have unique migration patterns.



Allodeoxycholic acid (ADCA)

Deoxycholic acid (DCA)



Origin

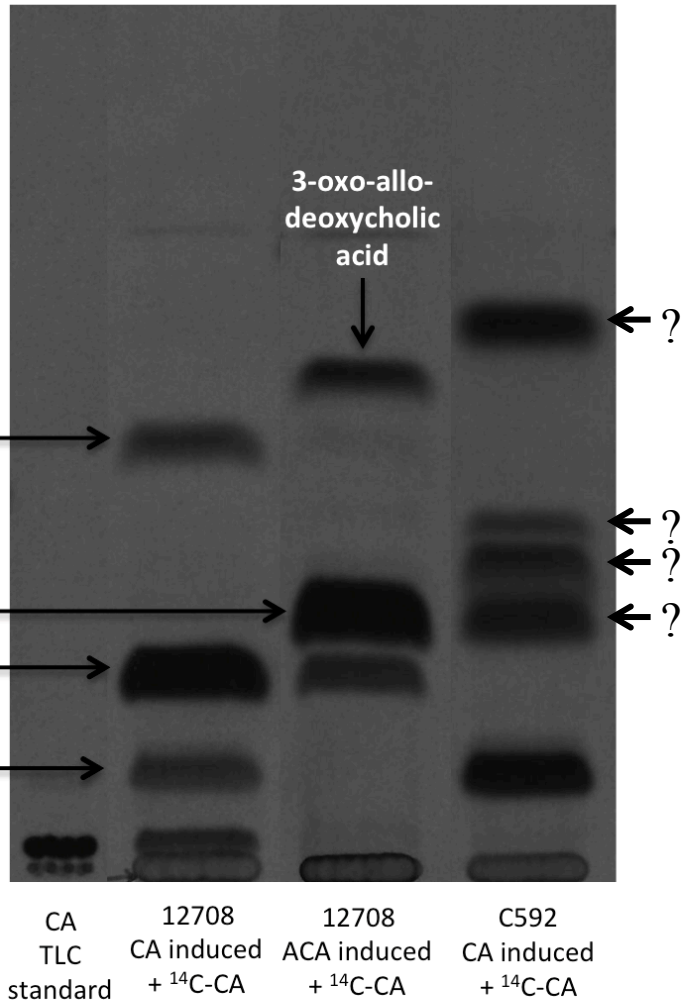
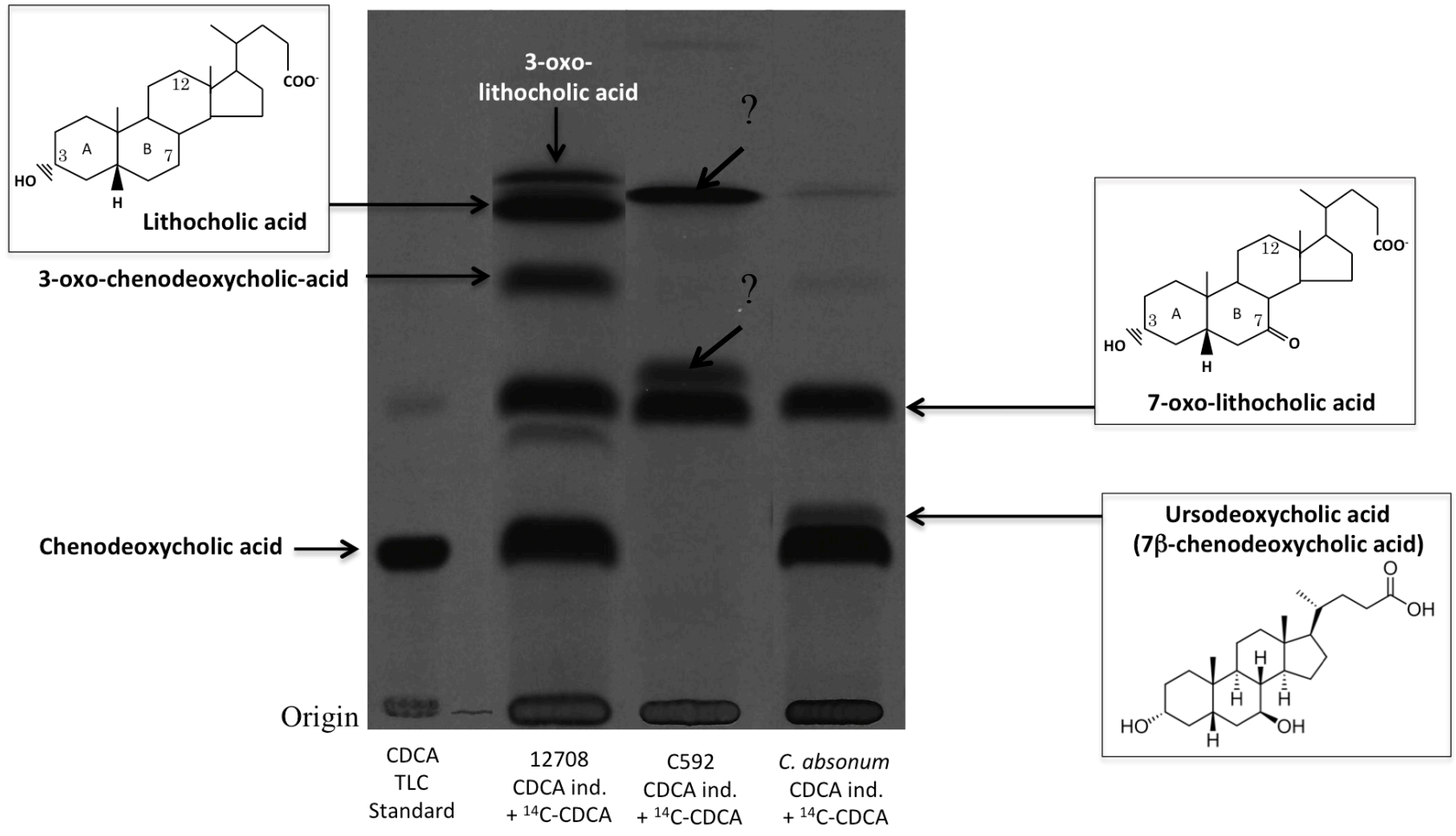


Figure 3.6: TLC separation of organic extracts from *C. scindens* VPI 12708, *C. absonum*, and C592 CDCA-induced whole cell conversions of [24-¹⁴C]-CDCA

The first spot on the TLC plate is a chenodeoxycholic acid TLC standard. The next three spots are organic extracts from whole-cell chenodeoxycholic acid-induced [24-¹⁴C]-chenodeoxycholic acid metabolism screens in *C. scindens* VPI 12708, *Clostridium absonum*, or C592. Previous literature has determined LCA as a major product of *C. scindens* VPI 12708 CDCA metabolism (261). Additionally, *C. absonum* is known to epimerize chenodeoxycholic acid to ursodeoxycholic acid via 7 α -HSDH and 7 β -HSDH reactions (146, 262). When whole cell conversion of CDCA of these two known CDCA metabolizers is compared to C592, one metabolite (7-oxo-lithocholic acid) comigrates while the two others do not.



metabolites, the only metabolites that shared a similar Rf was 7-oxo-LCA, indicating the other two compounds were unique CDCA metabolites.

Determination of C592 phylogeny based on 16S sequencing

C592 was confirmed to be pure through anaerobic BHI agar plate growth, colony isolation, and subsequent bile acid metabolism screening. There was no growth under aerobic BHI agar plating. Purified C592 was grown anaerobically in BHI broth overnight at 37°C for genomic DNA isolation and purification. Purified C592 genomic DNA was used as template for 16S sequence amplification using generic primers (Table 2.2). The ~1kb PCR product was run on a 1% agarose gel, isolated, purified, and sequenced. The resulting C592 16S DNA fragment had >99% sequence similarity to the *Eggerthella lenta* type strain.

Comparison of phenotypic similarities between C592 and *E. lenta* ATCC 25559

E. lenta ATCC 25559 (25559) was acquired from the American Type Culture Collection, plated anaerobically, and colonies picked for further analysis. Purified 25559 was grown anaerobically in BHI media and compared with C592 growth. Growth of C592 and 25559 was similar between both strains both with and without arginine, which has been shown to be stimulatory for *E. lenta* growth *in vitro* (Table 3.1). Both showed similar Gram-positive bacillus morphology (data not shown).

Comparison of C592 and 25559 metabolism of primary and secondary bile acids

Table 3.1: Overnight growth comparison between C592 and *E. lenta* ATCC 25559

Strain	OD600 w/ arginine (0.5% wt/vol)	OD600 w/out arginine
<i>E. lenta</i> ATCC 25559	0.431 ± 0.068	0.211 ± 0.025
C592-1	0.442 ± 0.058	0.209 ± 0.021

Since *E. lenta* is known to epimerize primary and secondary bile acids, we screened the ability of C592 and 25559 to metabolize numerous bile acids. Grown overnight in BHI broth under inert N₂ gas, C592 and 25559 both metabolize 25µM CDCA into three metabolites; CDCA-A, CDCA-B, and CDCA-C (Figure 3.7). CDCA-A has a similar R_f to 7-oxo-LCA, however, CDCA-B and CDCA-C do not share R_f values with previously described CDCA metabolites generated by bile acid 7α-dehydroxylating bacteria. Both strains metabolize CDCA to completion, leaving no remaining CDCA after 24 hours. In a time course experiment, CDCA metabolism begins in early-log phase, with no detectable CDCA remaining by mid-log phase (data not shown). In addition, both C592 and 25559 can grow in higher concentrations of CDCA (50µM and 500µM) as well as completely metabolizing the increased CDCA concentrations to the same three secondary metabolites (data not shown). C592 and 25559 also completely metabolize CA to six metabolites (Figure 3.8). One CA metabolite has a similar R_f value to 7-oxo-CA, however the rest do not match known CA metabolites based on R_f values.

E. lenta has been previously shown to isomerize secondary bile acids, so the ability for C592 to metabolize DCA and LCA was tested. In order to test secondary bile acid metabolism, ¹⁴C-secondary bile acids were synthesized biologically. *C. scindens* VPI 12708 was grown with CA and ¹⁴C-CA or CDCA and ¹⁴C-CDCA overnight and the resulting bile acid metabolites were separated on TLC, isolated, and quantified via liquid scintillation spectrometry. The resulting [¹⁴C]-secondary bile acids were used for whole cell metabolism assays. Both C592 and 25559 fully metabolize 25µM DCA to secondary metabolites, DCA-A and DCA-B (Figure 3.9). C592 also recognizes LCA, fully metabolizing it to a single secondary metabolite (data not shown).

Figure 3.7: TLC separation of CDCA-induced C592 and *Eggerthella lenta* ATCC 25559 whole cell metabolism of [24-¹⁴C]-CDCA

The first frame is a chenodeoxycholic acid TLC standard. The next two frames are organic extracts from whole-cell chenodeoxycholic acid-induced [24-¹⁴C]-chenodeoxycholic acid metabolism screens in C592 and *E. lenta* ATCC 25559. Both C592 and *E. lenta* ATCC 25559 metabolize CDCA to three metabolites; CDCA-A which comigrates with 7-oxo-lithocholic acid, CDCA-B and CDCA-C, which do not comigrate with known CDCA metabolites. CDCA metabolites CDCA-A, CDCA-B, and CDCA-C were isolated from TLC plates and used for further characterization

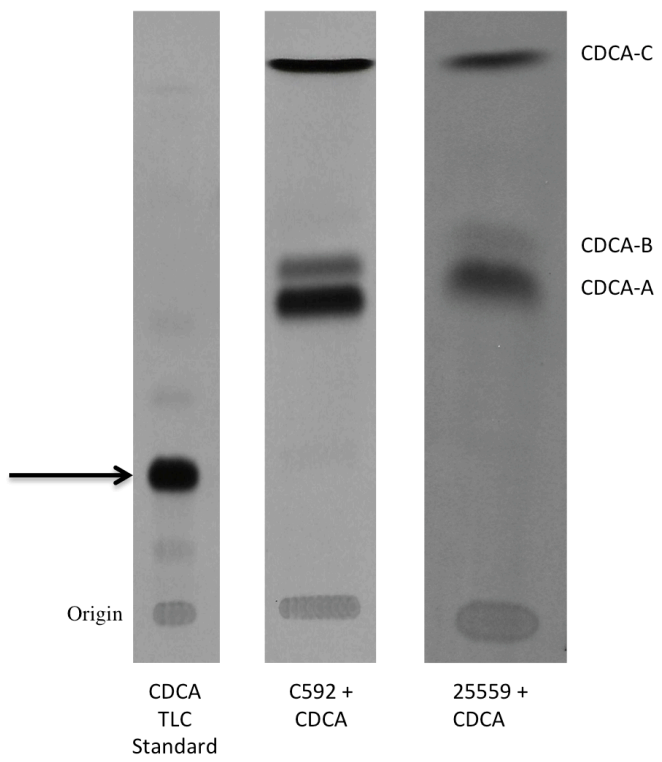
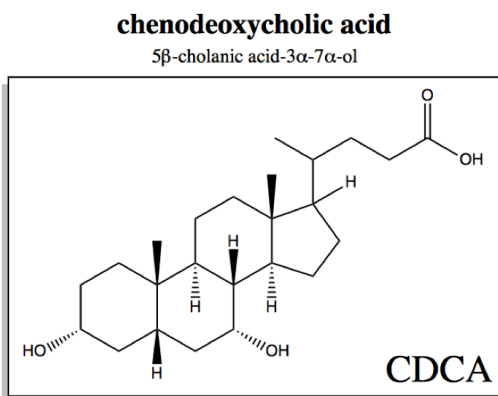
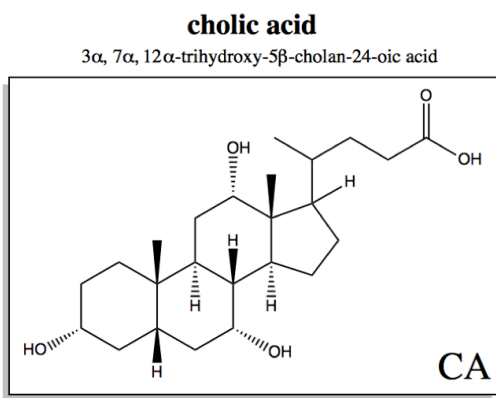


Figure 3.8: TLC separation of CA-induced C592 and *Eggerthella lenta* ATCC 25559 whole cell metabolism of [24-¹⁴C]-CA

The first frame is a cholic acid TLC standard. The next two frames are organic extracts from whole-cell cholic acid-induced [24-¹⁴C]-cholic acid metabolism screens in C592 and *E. lenta* ATCC 25559. Both C592 and *E. lenta* ATCC 25559 metabolize CA to a similar pattern of metabolites.



Origin

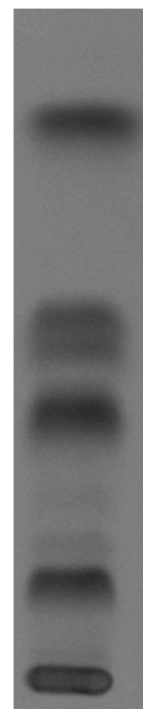
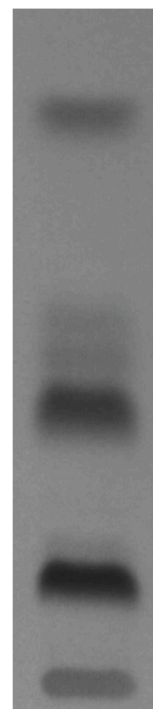
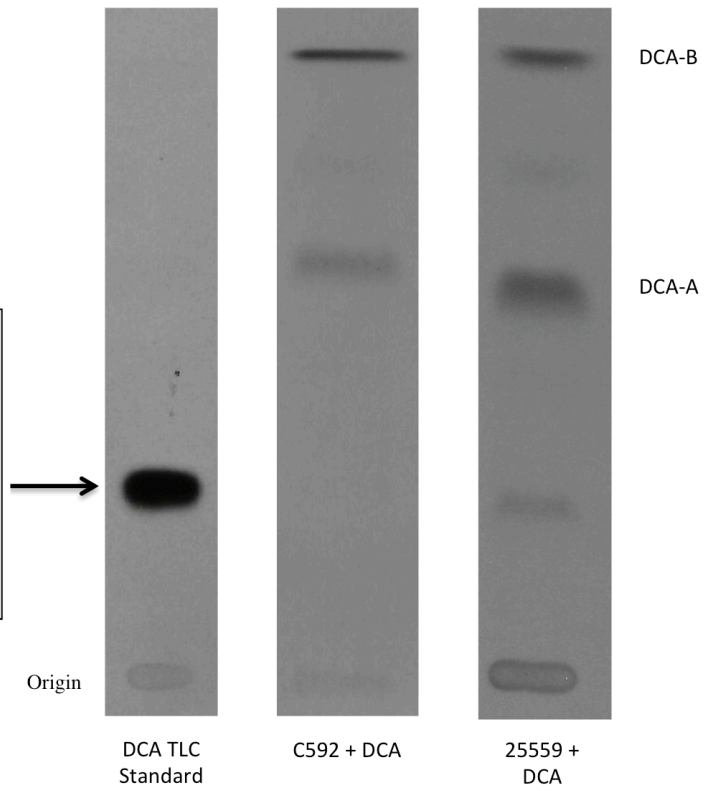
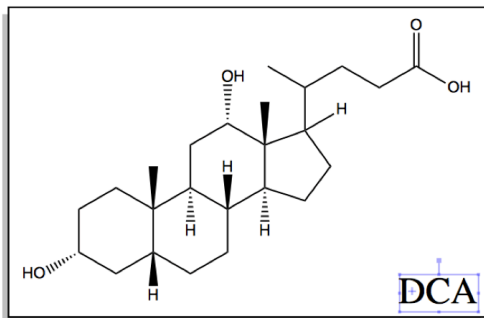


Figure 3.9: TLC separation of DCA-induced C592 and *Eggerthella lenta* ATCC 25559 whole cell metabolism of [24-¹⁴C]-DCA

The first frame is a deoxycholic acid TLC standard. The next two frames are organic extracts from whole-cell deoxycholic acid-induced [24-¹⁴C]-deoxycholic acid metabolism screens in C592 and *E. lenta* ATCC 25559. Deoxycholic acid was made biologically via metabolism of CA by *C. scindens* VPI 12708, as described in the Materials and Methods. Both C592 and *E. lenta* ATCC 25559 metabolize DCA to in a similar pattern to two distinct metabolites, DCA-A and DCA-B. These two metabolites were isolated from the TLC plate and used for further analysis.

deoxycholic acid
5 β -cholanic acid-3 α -12 α -ol



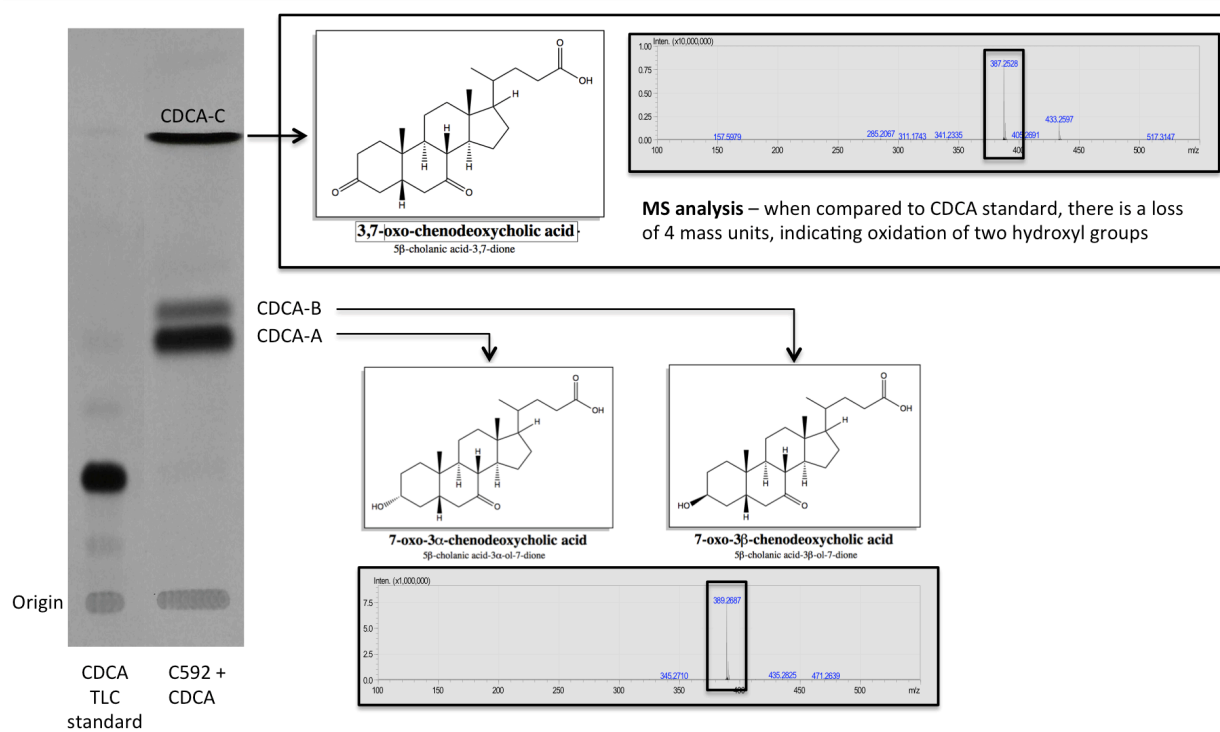
C592 and 25559 metabolism of CDCA was also tested in the presence of varying molecules which were hypothesized to alter the pattern of bile acid metabolism. Arginine, at a concentration of 0.5% wt/vol, did not inhibit formation of CDCA metabolites (data not shown). Neither pyruvate nor glutamate (100 μ M final concentration) altered C592 metabolism of CDCA (data not shown).

Mass spectrometry characterization of C592 CDCA and DCA metabolites

C592 metabolism of CDCA and DCA was repeated in a larger volume in order to obtain enough of each metabolite to perform MS analysis. 100mL C592 BHI cultures were grown anaerobically overnight under inert N₂ gas in the presence of 25 μ M CDCA. The metabolites were separated on TLC alongside C592 ¹⁴C-CDCA whole cell metabolism extracts and the corresponding bands for unlabeled CDCA-A, CDCA-B, and CDCA-C were isolated. MS analysis on the resulting bands was performed. MS analysis of authentic CDCA was performed resulting in a mass/charge of 392.57m/z. CDCA-A and CDCA-B metabolites saw a loss of two mass units (390m/z) on MS analysis, indicating oxidation of a single hydroxyl-group (Figure 3.10). CDCA-C was four mass units less than CDCA (388m/z), indicating probable oxidation of two hydroxyl groups (Figure 3.10). CDCA is a dihydroxy bile acid (C3, C7) and a loss of 4 AMU is consistent with CDCA-C being identified as 3,7-dioxo-5 β -cholanoic acid. CDCA-A has a similar R_f to 7-oxo-LCA and shows the expected mass on MS analysis. Additionally, when CDCA-A was treated with purified 3 α -HSDH from *Pseudomonas testosteroni* in the presence of NAD⁺, a single product migrating with the same R_f value of 3,7-dioxo-5 β -cholanoic acid is observed. Taken together, these results suggest CDCA-A is 3 α -hydroxy-7-oxo-5 β -cholanoic acid.

Figure 3.10: C592 CDCA metabolite separation and subsequent MS characterization

C592 CDCA metabolites were separated as previously described on TLC both with and without [24-¹⁴C]-radiolabel. Isolated unlabeled substrates then underwent MS analysis as described in the Materials and Methods. Both CDCA-A and CDCA-B exhibited mass/charge ratios of 390m/z, suggesting a loss of 2 AMU when compared to CDCA, consistent with the oxidation of a single hydroxyl group. CDCA-C exhibited a loss of 4 AMU (388m/z) when compared to CDCA, consistent with the oxidation of two hydroxyl groups. Correlating this data with TLC and 3 α -HSDH treatment data, the putative identities of these metabolites are: CDCA-A - 3 α -hydroxy-7-oxo-5 β -cholanoic acid, CDCA-B - 3 β -hydroxy-7-oxo-5 β -cholanoic acid, CDCA-C - 3,7-dioxo-5 β -cholanoic acid.



CDCA-B has the same mass as CDCA-A. However, the R_f matches neither 7-oxo-LCA nor 3-oxo-CDCA. In addition, when treated with purified 3 α -HSDH in the presence of NAD⁺, there is no product formed. These results suggest that CDCA-B is 3 β -hydroxy-7-oxo-5 β -cholanoic acid.

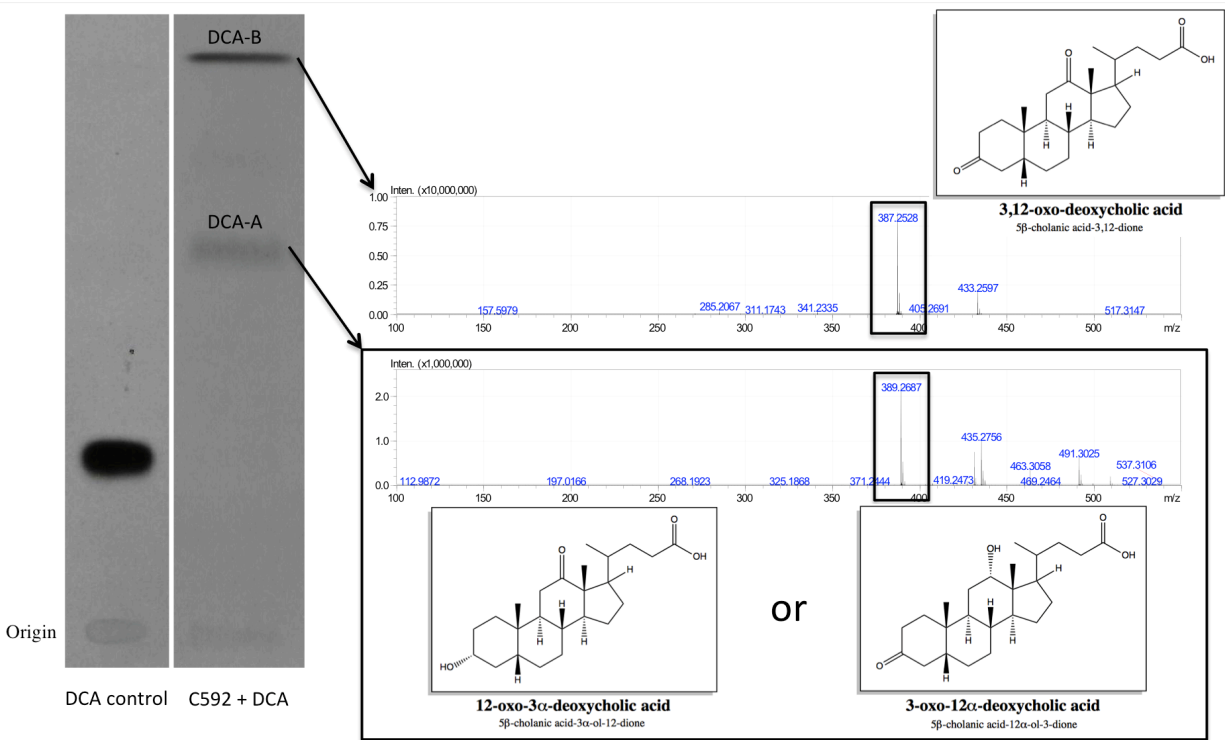
The same procedure was used to perform MS analysis on the C592 DCA metabolites. MS analysis for DCA has been performed previously with a resulting mass of 392.57m/z. When compared to the mass of DCA, C592 DCA metabolite DCA-A shows a loss of two mass units (390m/z), indicating the oxidation of a single hydroxyl group (Figure 3.11). DCA-B shows a loss of four mass units (388m/z), indicating the oxidation of two hydroxyl groups (Figure 3.10). Similarly to CDCA, DCA only contains two hydroxyl groups, one at the 3rd and 12th carbons. Therefore, DCA-B can be identified as 3,12-dioxo-5 β -cholanoic acid. DCA-A is likely either 3-oxo-DCA or 12-oxo-DCA, the specific oxidized hydroxyl group was not determined.

Comparison of steroid metabolism by C592 and 25559

Since *E. lenta* type strain has previously been shown to metabolize neutral steroids such as deoxycortisone, deoxycortisol, and dehydrocorticosterone (248), we determined substrate specificity for C592 and 25559 metabolism of numerous compounds sharing the steroid backbone. C592 and 25559 were grown overnight anaerobically in BHI broth in the presence of 25 μ M androstenedione and its 17 α / β -reduced end products, epitestosterone and testosterone, respectively. Cultures were extracted and the metabolites separated on reverse phase column HPLC and monitored at 240nm. Neither androstenedione nor epitestosterone were metabolized to a secondary metabolite (data not shown). However, both C592 and 25559 metabolized

Figure 3.11: C592 DCA metabolite separation and subsequent MS characterization

C592 DCA metabolites were separated as previously described on TLC both with and without [24-¹⁴C]-radiolabel. Isolated unlabeled substrates then underwent MS analysis as described in the Materials and Methods. DCA-A exhibited mass/charge ratio of 390m/z, suggesting a loss of 2 AMU when compared to DCA, consistent with the oxidation of a single hydroxyl group. DCA-B exhibited a loss of 4 AMU (388m/z) when compared to DCA, consistent with the oxidation of two hydroxyl groups. DCA-A is hypothesized to be either- 3 α -hydroxy-12-oxo-5 β -cholanoic acid or 12 α -hydroxy-3-oxo-5 β -cholanoic acid. DCA-B is predicted to be 3,12-dioxo-5 β -cholanoic acid.



testosterone to a secondary metabolite that comigrated with androstenedione (Figure 3.12). The data indicates that C592 and 25559 recognize the 17 β -hydroxyl group on testosterone and preferentially oxidize it. This is the first report of 17 β -HSDH activity in *E. lenta*. C592 and 25559 were also tested for their ability to metabolize hydrocortisone and cholesterol, however no products were detected under N₂ gas (data not shown). Taken together, it appears that under inert N₂ anaerobic growth, both C592 and 25559 preferentially oxidize bile acid and steroid hydroxyl groups (Figure 3.13).

Whole genomic sequencing of C592 and comparison to *E. lenta* type strain

In order to get a more comprehensive comparison of novel strain C592 and *E. lenta* 25559, the genome C592 was sequenced. Genomic DNA was isolated from C592 was sheared and converted to a Nanopore library. The library was then sequenced on SpotON Flowcell MK 1 for 48 hours using a MinION MK 1B sequencer. Poretools and FastQC was used to determine quality scores of the data set and reads from *E. coli* were removed via a Perl script. SPAdes-v3.9.0 was then used for de novo hybrid assembly of the reads. This resulted in five contigs >500bp, the top five of which were blasted to the NCBI NT database (Table 3.2). NODE_1 indicates the C592 genomic DNA, while four smaller contigs were also picked up likely indicating the presence of plasmids (Table 3.2). MUMmer v-3.23 was used to perform nucleotide level comparisons between the C592 NODE_1 contig and the *E. lenta* type strain closed genome (Table 3.3). This comparison showed that C592 and 25559 share approximately 88% base pair identity, however over 400k base pairs (>10%) were unaligned (Table 3.3). Mauve alignment

Figure 3.12: C592 metabolizes testosterone to androstenedione under inert N₂ gas

C592 was grown in the presence of 25mM testosterone and then extracted as described in the Materials and Methods. The organic extract was run on HPLC, monitoring at 240nm for absorption via UV-Vis. Based on both androstenedione and testosterone controls, C592 metabolizes testosterone to a product that comigrates with the androstenedione control yet maintains the 4-ene-3-oxo moiety required for 240nm absorption. This suggests the 17 β -hydroxyl group on testosterone is being oxidized by C592. Similar experiments run with epitestosterone did not show production of a secondary metabolite, suggesting this activity is specific to the β -configuration of the C17-hydroxyl group.

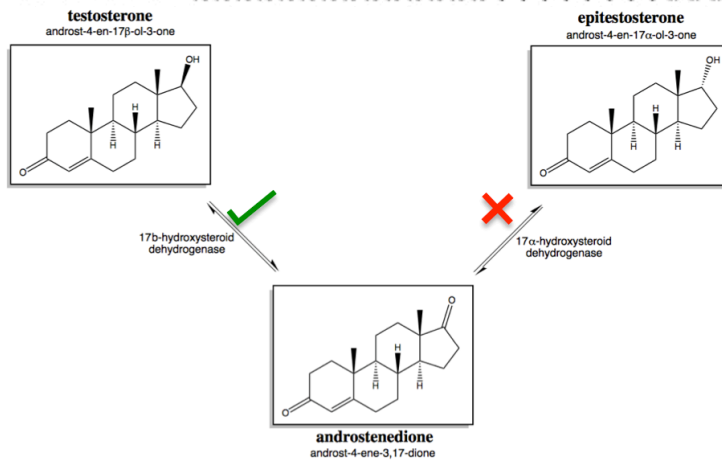
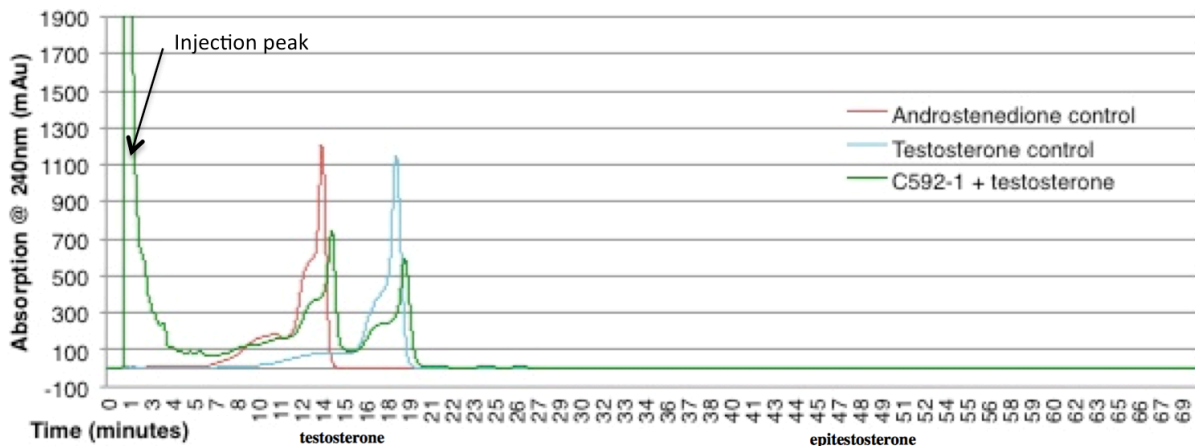


Figure 3.13: Summary of C592 and 25559 bile acid and neutral steroid metabolic potential

This diagram shows C592 bile acid and steroid metabolic potential. Based on the data presented so far, C592 has shown the potential for numerous biotransformations of the three hydroxyl groups found on primary and secondary bile acids, including 3 α -, 3 β -, 7 α -, 12 α -HSDH activity. Additionally, C592 has been shown to exhibit 17 β -HSDH activity.

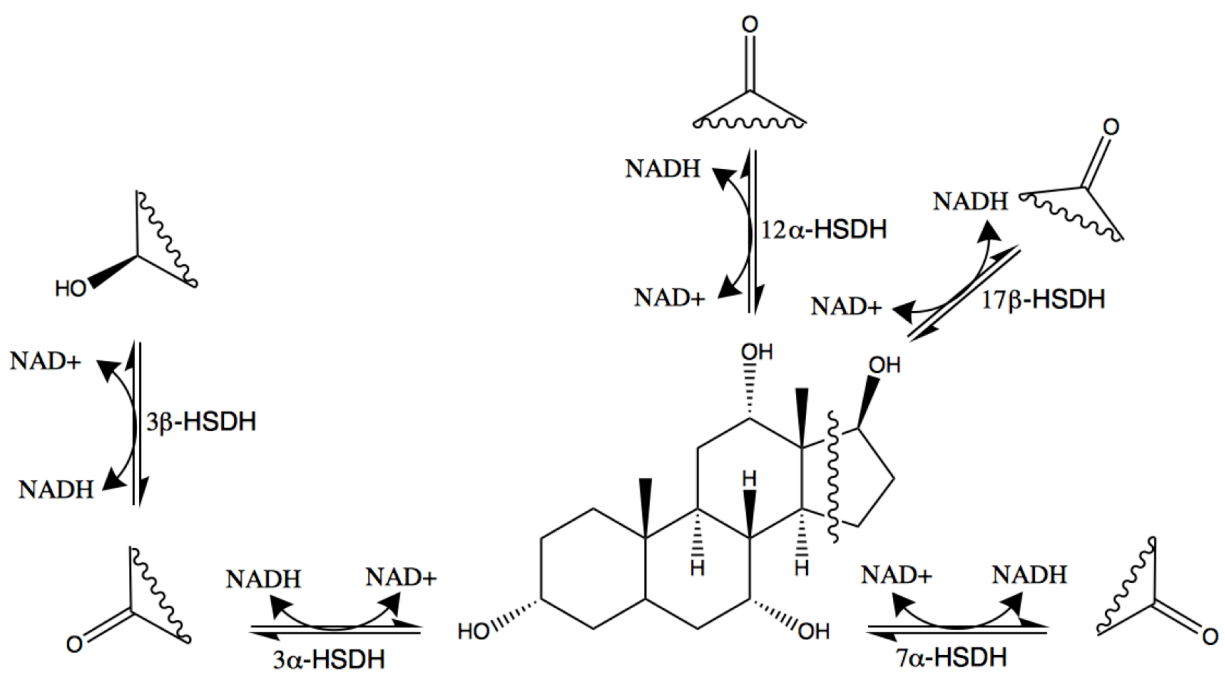


Table 3.2: De novo hybrid assembly of the five largest contigs from C592 genomic sequencing

SPAdes-v3.9.0 Hybrid Assembly			
Contig Name	Length	Coverage	BLAST Top Hits (NT database)
NODE_1	3,593,230	71x	Eggerthella lenta DSM 2243, complete genome
NODE_2	45,419	148x	Gordonibacter pamelaee 7-10-1-b draft genome
NODE_3	3,947	864x	Uncultured prokaryote from Rat gut metagenome metamobilome, <u>plasmid</u> pRGRH0595
NODE_4	2,749	1663x	Uncultured prokaryote from Rat gut metagenome metamobilome, <u>plasmid</u> pRGRH0074
NODE_5	2,231	1780.77	Uncultured prokaryote from Rat gut metagenome metamobilome, <u>plasmid</u> pRGRH0074
Total	3,647,576		

Table 3.3: Nucleotide level comparisons between C592 NODE_1 contig and the *E. lenta* type strain closed genome

	Eggerthella lenta DSM 2243 genome	C592 NODE_1
Sequences		
TotalSeqs	1	1
AlignedSeqs	1(100.00%)	1(100.00%)
TotalBases	3,632,260	3,593,230
AlignedBases	3,196,021(87.99%)	3,188,117(88.73%)
UnalignedBases	436,239(12.01%)	405,113(11.27%)
Alignments		
1-to-1	220	220
TotalLength	3,172,629	3,172,428
AvgIdentity	98.66	98.66
[Feature Estimates]		
Breakpoints	554	554
Relocations	26	35
Translocations	0	0
Inversions	14	14
InsertionSum	466,071	434,221
InsertionAvg	2,118.50	1,929.87
TandemIns	0	2
TandemInsSum	0	255
TandemInsAvg	0.00	127.50
[SNPs]		
TotalSNPs	35,383	35,383
TotalGSNPs	8,237	8,237
TotalIndels	4,555	4,555
TotalGIndels	99	99

of the C592 and 25559 genomes was performed, showing significant rearrangement but high similarity between the two genomes (Figure 3.14). Comparison of annotations were performed between C592 and the *E. lenta* type strain and showed that C592 encodes 3047 proteins, while 25559 encodes 3110 proteins (Table 3.4). Taken together, although C592 and 25559 appear to have similar bile acid metabolic profiles and highly conserved genomic regions, their genomes also harbor significant differences.

Searching the C592 genome for an explanation for the production of oxo-bile acid derivatives under anaerobic conditions

The production of oxo-bile acids under anaerobic condition is unique, since most anaerobic bacteria scavenge for electron acceptors to regenerate their oxidized metabolic cofactors, such as pyridine nucleotides and ferredoxin. Conversely, the oxidation of bile acids would generate reduced pyridine nucleotides. Therefore, we sought to determine a reason C592 would be carrying out such a reaction in an anaerobic environment. Using the genetic information gained from C592 genomic sequencing, KEGG maps were populated with enzymes annotated to be present in C592 based on KEGG gene ontology using BlastKOALA and pathway mapping tools. Of the entirety of encoding sequences in C592, only 1340 (42%) matched KEGG annotations (Figure 3.15). Sixty-one enzymes were annotated to be involved in carbon metabolism. C592 contains genes for the glycolysis pathway, an incomplete TCA cycle (missing succinyl-CoA synthetase), and a pyruvate:ferredoxin oxidoreductase capable of creating acetyl-CoA from pyruvate. Interestingly, annotation of the complete genome sequence of C592 and comparative genomics against *E. lenta* ATCC 25559 suggests that both

Figure 3.14: Mauve alignment of C592 and *E. lenta* type strain genomes

Mauve gene alignment was performed between the longest C592 contig from sequencing and the *E. lenta* type strain closed genome and visualized using Circos as described in the Materials and Methods. There are some gaps in this alignment both within the localized collinear blocks (LCB) and in between LCBs.

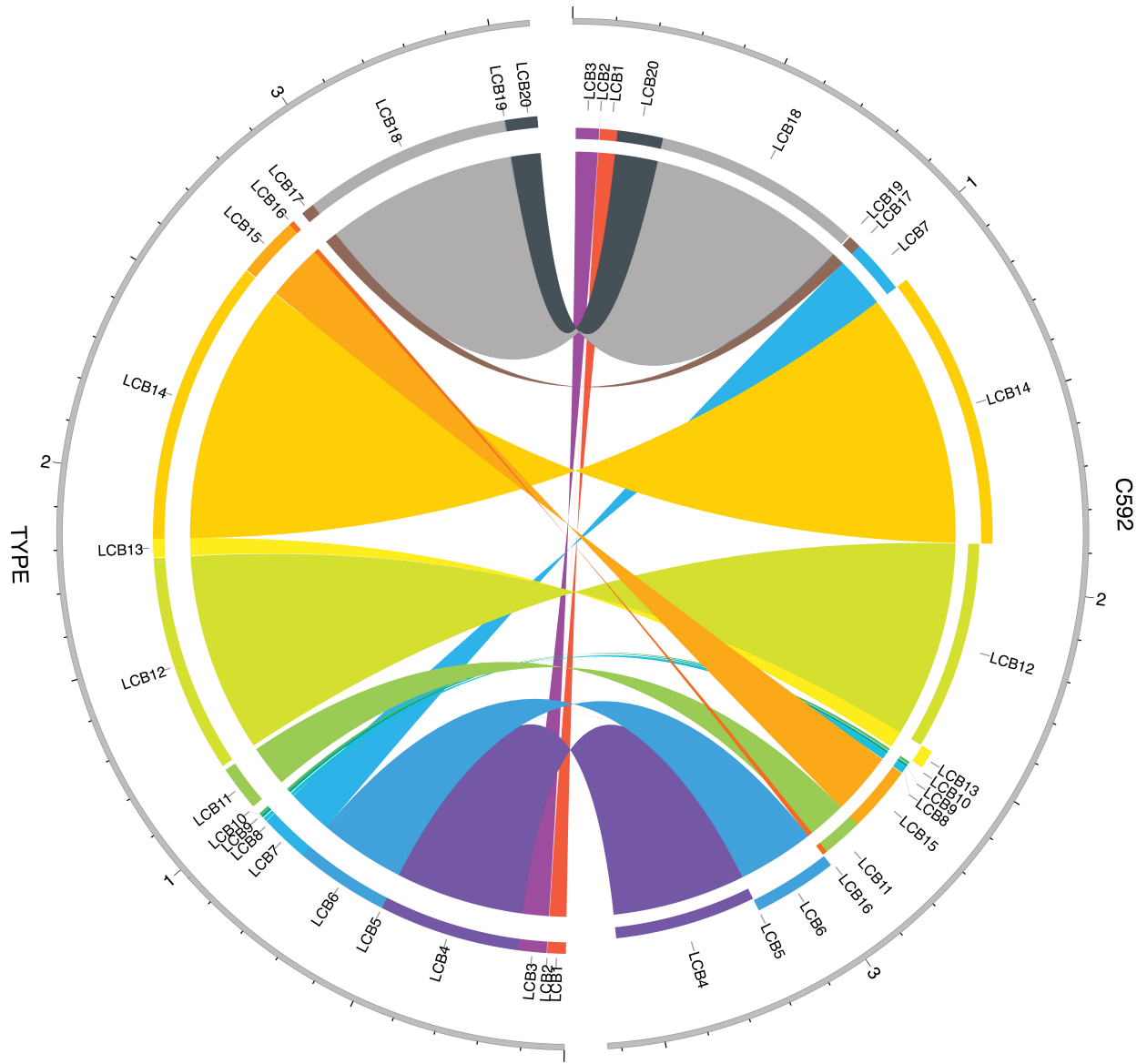


Table 3.4: CDS protein annotation comparison between C592 and *Eggerthella lenta* type strain

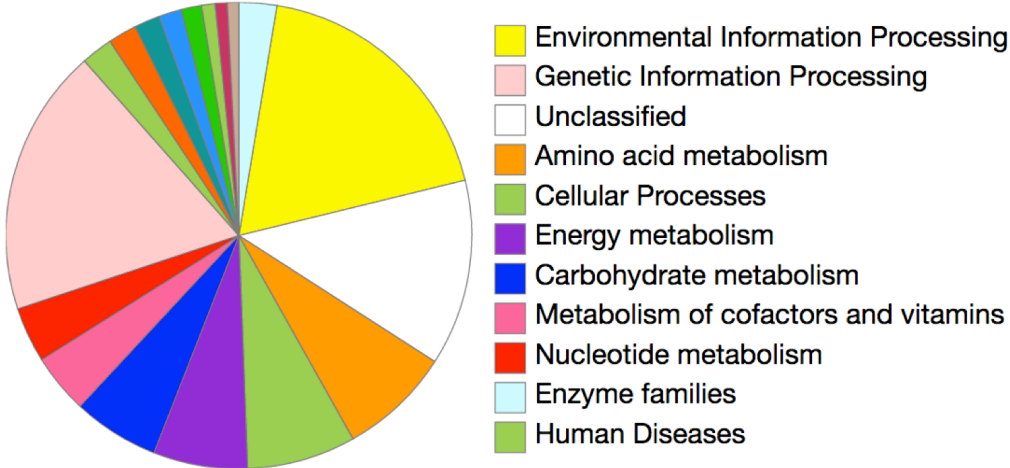
	Eggerthella_lenta_DSM_2243	New Assembly
contig	contigs: 1	contigs: 1
bases:	3,632,260	3,593,230
tmRNA:	1	1
tRNA:	54	54
rRNA:	6	6
Repeat region:	1	1
CDS:	3110	3047

Figure 3.15: Overall C592 BlastKOALA results

Annotated sequences from the C592 genomic data in FASTA format were further analyzed using the KEGG Orthology and Links Annotation (BlastKOALA) (223). C592 KEGG maps were generated using KEGG mapping software. 42.1% of the total C592 annotated genes were recognized by the BlastKOALA algorithm and populated to relevant KEGG maps. Overall breakdown of the recognized C592 sequences shows that the two largest groups represented by KEGG maps were environmental information processing and genetic information processing, with numerous other groups represented as well.

Summary 1340 entries (42.1%) annotated

Functional category



strains encode a near complete Wood-Ljungdahl pathway for generation of acetate from CO₂ (Figure 3.16). Of the nine enzymes in this pathway, KEGG annotation located six of the genes in C592. Further searching of C592 genomic data showed putative genes for two of the remaining three genes in the pathway (Table 3.5). These results gave a possible explanation for the requirement of reducing equivalents from bile acids, as the fixation of CO₂ to acetate requires multiple reducing equivalents.

In addition to carbon metabolism, C592 was shown to have numerous other metabolic pathways of interest. Of note, it contains genes required for the metabolism of arginine, as the *E. lenta* type strain is reported to have (263). C592 is annotated to have genes allowing it to convert arginine to form ornithine, ammonia, and CO₂ while generating ATP from ADP (Figure 3.16). In addition, it has genes allowing it to interconvert arginine and fumarate, likely depending on its energetic needs (Figure 3.17). This shows energy conservation gene pathways in *E. lenta* are maintained in C592.

Identifying gene clusters of interest in C592 and 25559

Work on the characterization of genes in the *E. lenta* type strain encoding bile acid isomerization enzymes has been done previously (150). Devlin et al. screened numerous *E. lenta* short-chain dehydrogenase/reductase enzymes (SDR) for bile acid 3 α -HSDH and 3 β -HSDH activity, focusing on their ability to isomerize DCA. However, of all ten genes tested, only three were found to be active. Six of the seven tested were found in high homology in C592, including the two confirmed 3 β -HSDH and one 3 α -HSDH (Table 3.6). Additional SDR, oxidoreductases,

Figure 3.16: C592 encodes genes annotated to be involved in the Wood Ljungdahl pathway

C592 KEGG annotated data generated from BlastKOALA was used with the KEGG Mapper Reconstruct Pathway tool, utilizing data from the KEGG Atlas (264). Green lines indicate genes present in C592 that match the relevant annotation in the pathway. C592 has genes annotated to be part of the Wood-Ljungdahl pathway. These include formate dehydrogenase, formyl-tetrahydrofolate synthetase, formyl-tetrahydrofolate cyclohydrolase, methylene-tetrahydrofolate reductase, phosphotransacetylase, and acetate kinase. Three genes in this pathway were not annotated via KEGG mapping, but two had similar candidates found through searching the C592 genome for similar enzymes. These include a methylene-tetrahydrofolate reductase, and the carbon monoxide dehydrogenase. A methyltransferase/acetyl-CoA synthase was not located in the C592 genome. All of these identified C592 genes are also highly conserved in the *E. lenta* ATCC 25559 type strain. Table 3.6 contains the ascension numbers for the relevant Wood-Ljungdahl pathway genes in C592 and their corresponding genes in *E. lenta* ATCC 25559.

Enzymes not annotated:

#1 – methylenetetrahydrofolate reductase responsible for converting 5,10-Methylene-THF to 5-Methyl-THF

#2 – carbon monoxide dehydrogenase

#3 – methyltransferase/acetyl-CoA synthase; forms acetyl-CoA from 5-methyl-THF and CO

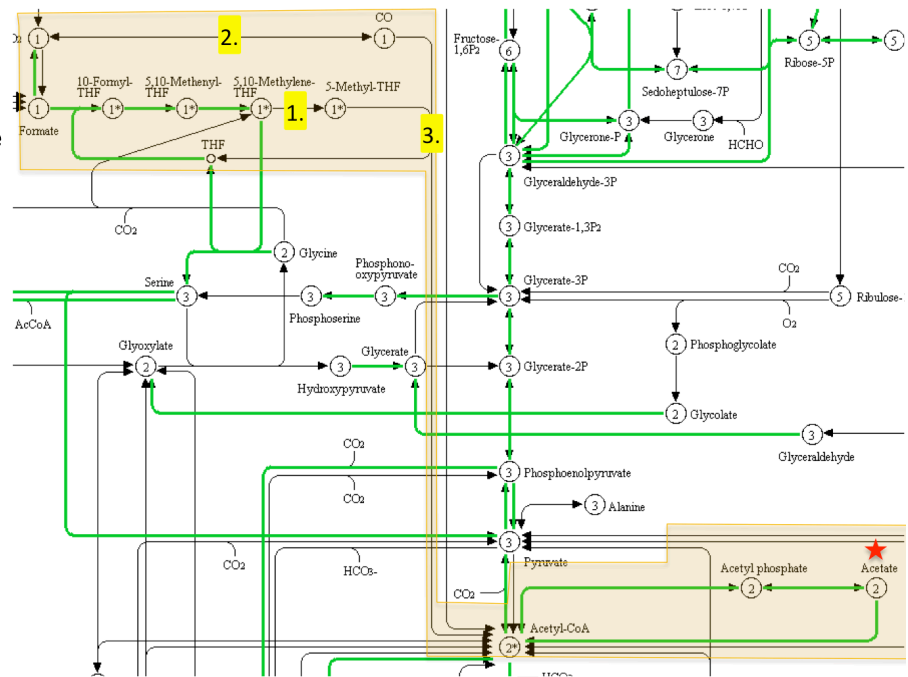
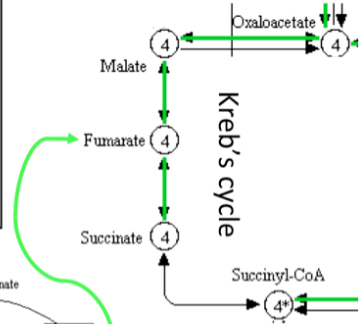
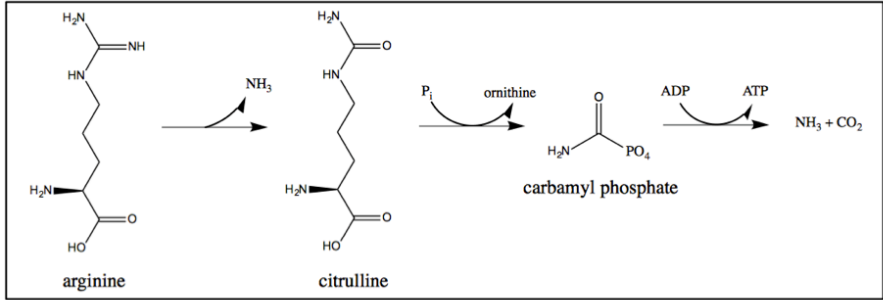


Table 3.5: Wood Ljungdahl Pathway Homologous Genes in C592 and *E. lenta* ATCC 25559

Wood-Ljungdahl Pathway Homologous Genes					
<i>Formate-tetrahydrofolate synthetase</i>					
C592:			Type Strain:		
Name	db_xref	Length	Name	db_xref	Length
Formate--tetrahydrofolate ligase (EC 6.3.4.3) CDS	SEED:fig 6666666.209054.peg.396	1,668	formate--tetrahydrofolate ligase CDS	GI:506241661	1,668
<i>Formyl-tetrahydrofolate cyclohydrolase / methylene-tetrahydrofolate dehydrogenase</i>					
C592:			Type Strain:		
Name	db_xref	Length	Name	db_xref	Length
Methylenetetrahydrofolate dehydrogenase (NADP+) (EC 1.5.1.5) / Methenyltetrahydrofolate cyclohydrolase (EC 3.5.4.9) CDS	SEED:fig 6666666.209054.peg.400	870	tetrahydrofolate dehydrogenase CDS	GI:497294816	870
<i>Methylene-tetrahydrofolate reductase</i>					
C592:			Type Strain:		
Name	db_xref	Length	Name	db_xref	Length
bifunctional homocysteine S-methyltransferase/5,10-methylenetetrahydrofolate reductase protein CDS	SEED:fig 6666666.209054.peg.677	903	methionine synthase CDS	GI:497295229	903
<i>Carbon monoxide dehydrogenase</i>					
C592:			Type Strain:		
Name	db_xref	Length			
Xanthine dehydrogenase, molybdenum binding subunit (EC 1.17.1.4) CDS	SEED:fig 6666666.209054.peg.1780	2,298	(Did not show up in Mauve alignment)		
<i>Phosphate acetyltransferase and acetate kinase</i>					
C592:			Type Strain:		
Name	db_xref	Length	Name	db_xref	Length
Phosphate acetyltransferase (EC 2.3.1.8) CDS	SEED:fig 6666666.209054.peg.1464	999	phosphate acetyltransferase CDS	GI:496664653	999
Acetate kinase (EC 2.7.2.1) CDS	SEED:fig 6666666.209054.peg.1463	1,215	acetate kinase CDS	GI:496664654	1,215

Figure 3.17: KEGG map of C592 arginine metabolism genes and the link to Kreb's cycle

C592 KEGG annotated data generated from BlastKOALA was used with the KEGG Mapper Reconstruct Pathway tool, utilizing data from the KEGG Atlas (264). Green lines indicate genes present in C592 that match the relevant annotation in the pathway. C592 encodes genes allowing it to metabolize arginine to ammonia while generating ATP, CO₂, and ornithine. This pathway of ATP generation in the *E. lenta* type strain, outlined in the box, was first described by Sperry et al and was described as necessary for optimal *E. lenta* growth (263). C592 additionally encodes enzymes that allow it to generate fumarate from arginine, which can then be utilized as an electron acceptor to form succinate. C592 encodes numerous redundant fumarate reductases throughout its genome.



ARGININE BIOSYNTHESIS

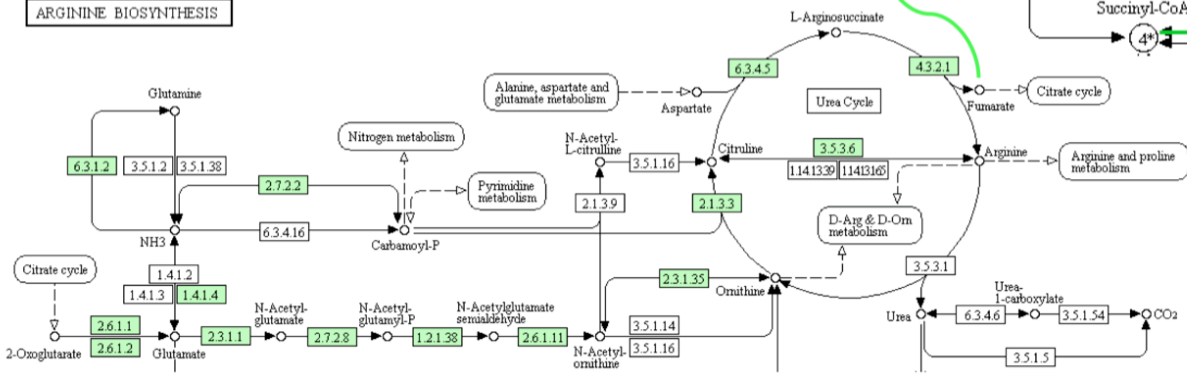


Table 3.6: Annotated reductases in C592 and *E. lenta* ATCC 25559 genomes

Reductase genes tested in Devlin et. al 2015					
C592:		<i>E. lenta</i> type strain:			
Name	db_xref	Name	db_xref		Confirmed activity?
3-oxoacyl-[acyl-carrier protein] reductase (EC 1.1.1.100) CDS	SEED:fig 6666666.209054.peg.735	short-chain dehydrogenase CDS	GI:496664150	Elen_2515	
Sorbitol-6-phosphate 2-dehydrogenase (EC 1.1.1.140) CDS	SEED:fig 6666666.209054.peg.1846	3-ketoacyl-ACP reductase CDS	GI:506240750	Elen_1325	3 β -HSDH
Dehydrogenases with different specificities (related to short-chain alcohol dehydrogenases) CDS	SEED:fig 6666666.209054.peg.1011	short-chain dehydrogenase CDS	GI:496663880	Elen_2188	
3-oxoacyl-[acyl-carrier protein] reductase (EC 1.1.1.100) CDS	SEED:fig 6666666.209054.peg.879	short-chain dehydrogenase CDS	GI:496663981	Elen_0690	3 α -HSDH
3-oxoacyl-[acyl-carrier protein] reductase (EC 1.1.1.100) CDS	SEED:fig 6666666.209054.peg.1230	beta-ketoacyl-ACP reductase CDS	GI:496661655	Elen_1987	
Glucose 1-dehydrogenase (EC 1.1.1.47) CDS	SEED:fig 6666666.209054.peg.3084	glucose-1-dehydrogenase CDS	GI:506240102	Elen_0198	3 β -HSDH
? Gap in Mauve Alignment		short-chain dehydrogenase/reductase SDR CDS	GI:506240693	Elen_1208	
Other reductases in C592 and <i>E. lenta</i> type strain genome					
C592:		<i>E. lenta</i> type strain:			
Name	db_xref	Name	db_xref		
2,4-dienoyl-CoA reductase [NADPH] (EC 1.3.1.34) CDS	SEED:fig 6666666.209054.peg.377	NADH:flavin oxidoreductase CDS	GI:497294813		
putative Fe-S oxidoreductase CDS	SEED:fig 6666666.209054.peg.412	hypothetical protein CDS	GI:506241657		
oxidoreductase FAD/NAD(P)-binding CDS	SEED:fig 6666666.209054.peg.516	ferredoxin-NADP+ reductase subunit alpha CDS	GI:506241633		
3-oxoacyl-[acyl-carrier protein] reductase (EC 1.1.1.100) CDS	SEED:fig 6666666.209054.peg.735	short-chain dehydrogenase CDS	GI:496664150		
Short-chain dehydrogenase/reductase SDR CDS	SEED:fig 6666666.209054.peg.851	short-chain dehydrogenase CDS	GI:496664009		
oxidoreductase of aldo/keto reductase family, subgroup 1 CDS	SEED:fig 6666666.209054.peg.1492	2,5-diketo-D-gluconic acid reductase CDS	GI:506240950		
FIG00624394: hypothetical protein CDS	SEED:fig 6666666.209054.peg.1692	FAD-dependent oxidoreductase CDS	GI:497294359		

Periplasmic aromatic aldehyde oxidoreductase, FAD binding subunit YagS CDS	SEED:fig 6666666.209054.peg.1779	Gap in Mauve Alignment	
Xanthine dehydrogenase, molybdenum binding subunit (EC 1.17.1.4) CDS	SEED:fig 6666666.209054.peg.1780	Gap in Mauve Alignment	
Periplasmic aromatic aldehyde oxidoreductase, iron-sulfur subunit YagT CDS	SEED:fig 6666666.209054.peg.1781	Gap in Mauve Alignment	
Fe-S oxidoreductase, related to NifB/MoaA family with PDZ N-terminal domain CDS	SEED:fig 6666666.209054.peg.1835	hypothetical protein CDS	GI:506240759
predicted NADPH-dependent reductase CDS	SEED:fig 6666666.209054.peg.1898	FMN reductase CDS	GI:496662103
FIG092679: Fe-S oxidoreductase CDS	SEED:fig 6666666.209054.peg.1914	B12-binding domain-containing radical SAM protein CDS	GI:506240718
Heterodisulfide reductase, cytochrome reductase subunit CDS	SEED:fig 6666666.209054.peg.1923	oxidoreductase CDS	GI:496662126
Sarcosine oxidase alpha subunit (EC 1.5.3.1) CDS	SEED:fig 6666666.209054.peg.1944	FAD-dependent oxidoreductase CDS	GI:497294180
Flavin reductase-like, FMN-binding:Rubredoxin-type Fe(Cys) ₄ protein CDS	SEED:fig 6666666.209054.peg.2052	flavin reductase CDS	GI:496662252
Aldo/keto reductase:4Fe-4S ferredoxin, iron-sulfur binding CDS	SEED:fig 6666666.209054.peg.2122	Fe-S oxidoreductase CDS	GI:506240601
NAD(FAD)-utilizing dehydrogenase, sll0175 homolog CDS	SEED:fig 6666666.209054.peg.2164	FAD-dependent oxidoreductase CDS	GI:506240573
Fe-S OXIDOREDUCTASE (1.8.-.-) CDS	SEED:fig 6666666.209054.peg.2424	YgiQ family radical SAM protein CDS	GI:506241324
Fe-S oxidoreductase CDS	SEED:fig 6666666.209054.peg.2654	radical SAM protein CDS	GI:497295255
putative NADH-dependent flavin oxidoreductase CDS	SEED:fig 6666666.209054.peg.2823	NADH:flavin oxidoreductase CDS	GI:506240206
FMN-dependent NADH-azoreductase CDS	SEED:fig 6666666.209054.peg.2883	NAD(P)H dehydrogenase (quinone) CDS	GI:496663491
Aldo/keto reductase:4Fe-4S ferredoxin, iron-sulfur binding CDS	SEED:fig 6666666.209054.peg.3057	Fe-S oxidoreductase CDS	GI:497293772
Gap in Mauve Alignment		oxidoreductase CDS	GI:496664037
Gap in Mauve Alignment		FAD-dependent oxidoreductase CDS	GI:496661933
Gap in Mauve Alignment		NADH:flavin oxidoreductase CDS	GI:496661830
Gap in Mauve Alignment		short-chain dehydrogenase CDS	GI:506240690

and dehydrogenases were identified in both C592 and 25559, totaling 26, although not all are identified in both genomes via the Mauve alignment (Table 3.6). Of interest, Devlin et al. identified a “bai-like” operon in the *E. lenta* type strain containing numerous SDR enzymes reductases in an operon (150). C592 contains the same operon in high homology, but is missing a key enzyme in the pathway, directly downstream of the three SDR enzymes (Figure 3.18). It has been hypothesized that this missing gene directly downstream of three SDR enzymes is the gene for the 21-dehydroxylase enzyme, indicating that C592 may not 21-dehydroxylate corticoids.

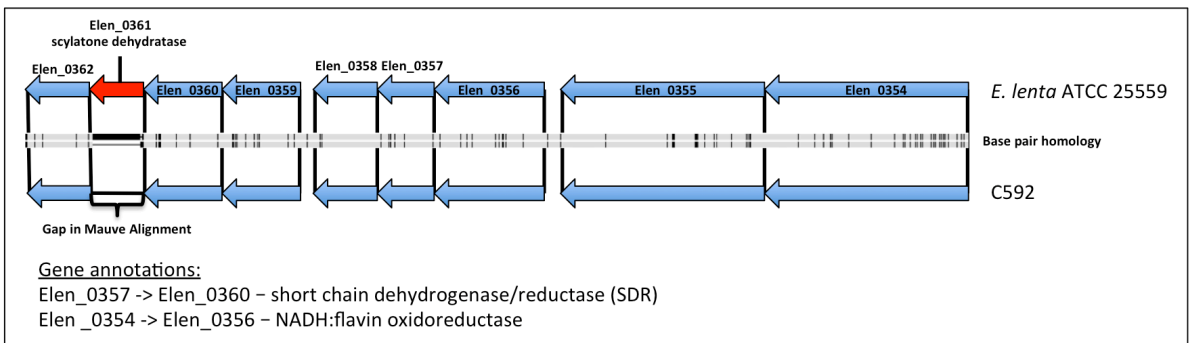
In the determination of cardiac glycoside reductase activity in the *E. lenta* type strain, a putative gene cluster responsible for this activity was identified based on RNAseq results (238). However, when searching the aligned genome of C592, this two-gene cluster is absent (Figure 3.19). This suggests that C592 should not exhibit digoxin reductase activity. Alternatively, if digoxin reductase activity is measured, it is likely this two-gene cluster in the type strain is not responsible for producing the enzymes responsible.

When searching the KEGG maps based on C592, it was found that many genes in the Wood-Ljungdahl acetogenesis pathway are present. These same genes are also present in the *E. lenta* type strain genome. In addition, both genomes encode membrane-energization gene clusters responsible for producing multi-subunit hydrogenases capable of functioning as an electron transport chain while generating a proton or Na⁺ gradient. A *Rhodococcus* nitrogen fixation (RNF) complex, found in acetogens as a means of coupling ATP generation to the Wood-Ljungdahl pathway (95-97), is also found in both C592 and 25559 (Figure 3.20). Not all

Figure 3.18: Gene cluster alignment of “bai-like” operon from C592 and 25559

A. Alignment of a gene cluster in C592 and 25559 that contains numerous reductases. Within this series of reductases in the type strain is a gene annotated as a scytalone dehydratase. It shares that annotation to the 7α -dehydratase from *C. scindens* (265). We hypothesize that this gene encodes the enzyme responsible for the 21-dehydroxylase enzyme. **B.** *E. lenta* type strain has been reported to have 21-dehydroxylase activity previously (247, 248). Interestingly, this putative gene is missing from C592 while the two flanking genes remain with high homology. C592 is currently being tested for its ability to 21-dehydroxylate deoxycortisone.

A.



B.

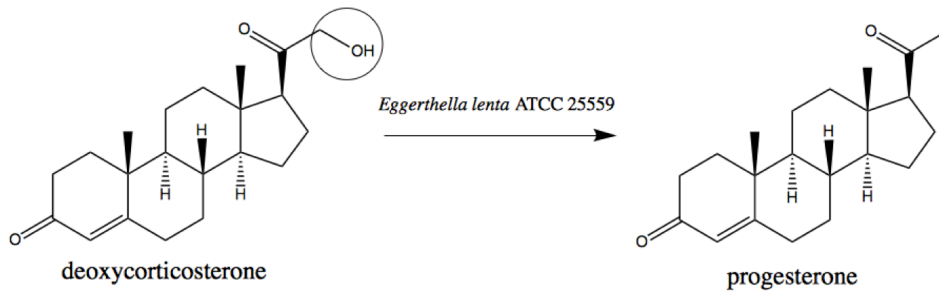


Figure 3.19: Gene cluster alignment of the putative cardiac glycoside reductase operon from C592 and 25559

Gene cluster identified by Haiser et al to encode the cardiac glycoside reductase in *Eggerthella lenta* ATCC 25559 is missing from C592. Homologous genes are not found elsewhere in the genome. C592 is currently being tested for cardiac glycoside reductase activity, although based on the absence of the genes predicted to encode activity, it is hypothesized it will not exhibit the phenotype.

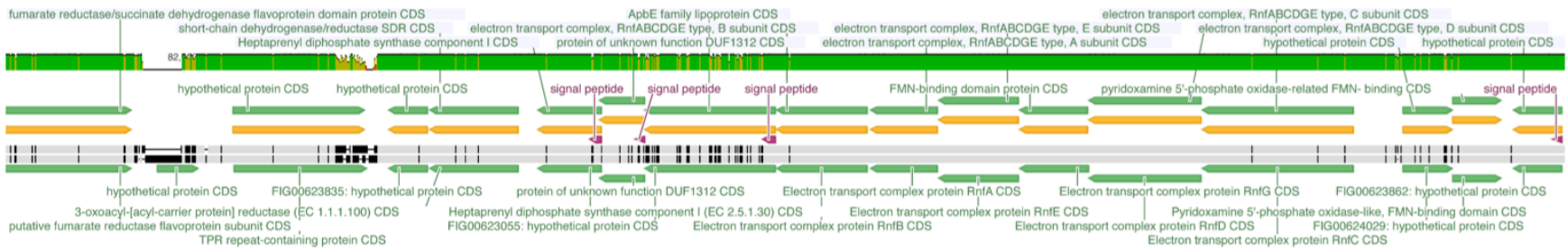
Type
C592



Figure 3.20: Gene cluster alignment of RNF complex operon from C592 and 25559

Gene clusters in C592 and 25559 annotated to encode an RNF complex are similar to those found in acetogens (95-97). Green bar above the mauve alignment indicates level of homology. Green indicates >90% homology, yellow indicates 30-90% homology, red indicates >30% homology. The operon encoding the RNF complex is highly conserved between the two strains.

Type



C592

acetogens harbor genes for an RNF complex, others instead encode “energy conserving hydrogenase” (Ech) complexes that similarly generate a proton gradient while generating H₂ from reduced ferredoxin (266). Both C592 and 25559 also harbor a putative Ech gene cluster (Figure 3.21). In addition, both strains harbor ATP synthase transmembrane complexes, able to utilize this proton gradient generated from RNF and Ech complexes to generate ATP from ADP (Figure 3.22). Taken together, these results strongly suggest that both C592 and 25559 share many genetic similarities to acetogens, especially with regard to redox balancing and ATP generating processes.

One important molecule for acetogenesis is CO₂, which can be quickly utilized in anaerobic environments. Therefore, the ability to form CO₂ independently would be evolutionarily advantageous for an acetogen. C592 has genes to metabolize arginine and agmatine to form a carbamoyl phosphate intermediate and carbamate kinases to ultimately generate ATP, CO₂, and ammonia (Table 3.7). In addition, C592 appears to harbor multiple amino acid decarboxylases. A gene encoding a putative glutamate decarboxylase was located next to a glutamate/gamma-aminobutyric acid (GABA) antiporter, indicating C592 could metabolize glutamate to GABA + CO₂ and then use CO₂ as an electron acceptor (Table 3.8). In addition, C592 is annotated to have a histidine decarboxylase, which would yield histamine and CO₂ from histidine (Table 3.8). Taken together, it is apparent that C592 has numerous avenues for generating its own CO₂ via intracellular processes, depending on substrate availability. Additionally, C592 appears to have the ability to make biogenic amines, such as GABA and histamine, which could have significant effects on host physiology.

Figure 3.21: Gene cluster alignment of energy-conserving hydrogenase operon from C592 and 25559

Gene clusters in C592 and 25559 annotated to encode an Ech complex are similar to those found in acetogens not harboring an RNF complex (98, 266). Green bar above the mauve alignment indicates level of homology. Green indicates >90% homology, yellow indicates 30-90% homology, red indicates >30% homology. The operon encoding the Ech complex is highly conserved between the two strains.

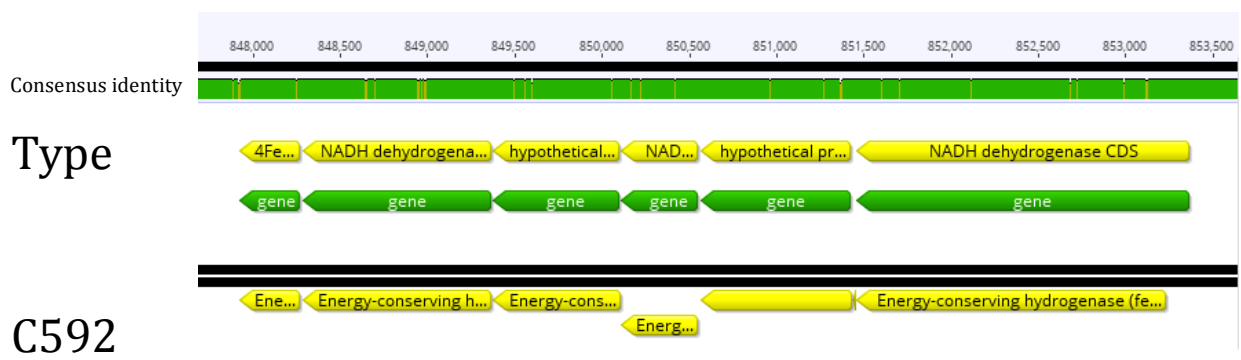
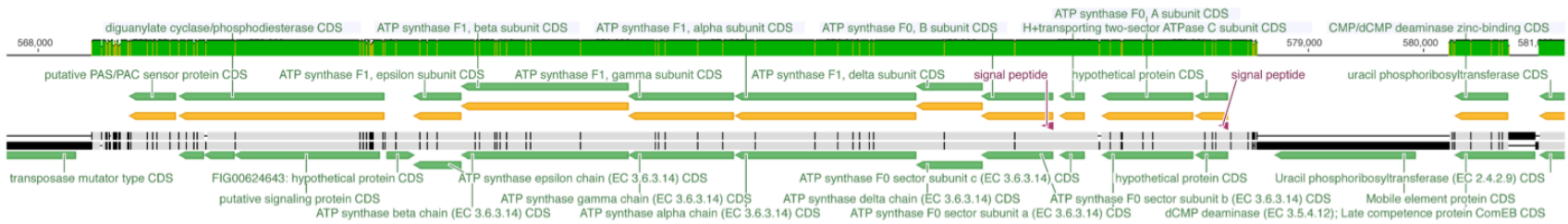


Figure 3.22: Gene cluster alignment of ATP synthase operon from *E. lenta* strains C592 and 25559

Gene clusters in C592 and 25559 annotated to encode an ATP synthase operon. This transmembrane protein would be able to utilize a putative proton gradient generated from either Ech- or RNF-complexes to generate ATP (93, 266).

Type



C592

Table 3.7: Annotated arginine and agmatine metabolism genes in *E. lenta* strain C592

Name	db_xref
Arginine deiminase (EC 3.5.3.6) CDS	SEED:fig 6666666.209054.peg.3131
Agmatine deiminase (EC 3.5.3.12) CDS	SEED:fig 6666666.209054.peg.2844
Arginine deiminase (EC 3.5.3.6) CDS	SEED:fig 6666666.209054.peg.1265
Agmatine deiminase (EC 3.5.3.12) CDS	SEED:fig 6666666.209054.peg.866
Agmatine deiminase (EC 3.5.3.12) CDS	SEED:fig 6666666.209054.peg.857
Ornithine carbamoyltransferase (EC 2.1.3.3) CDS	SEED:fig 6666666.209054.peg.2843
Aspartate carbamoyltransferase (EC 2.1.3.2) CDS	SEED:fig 6666666.209054.peg.1518
Ornithine carbamoyltransferase (EC 2.1.3.3) CDS	SEED:fig 6666666.209054.peg.1266
Putrescine carbamoyltransferase (EC 2.1.3.6) CDS	SEED:fig 6666666.209054.peg.864
Putrescine carbamoyltransferase (EC 2.1.3.6) CDS	SEED:fig 6666666.209054.peg.855
Ornithine carbamoyltransferase (EC 2.1.3.3) CDS	SEED:fig 6666666.209054.peg.593
Carbamate kinase (EC 2.7.2.2) CDS	SEED:fig 6666666.209054.peg.1267
Carbamate kinase (EC 2.7.2.2) CDS	SEED:fig 6666666.209054.peg.867
Carbamate kinase (EC 2.7.2.2) CDS	SEED:fig 6666666.209054.peg.858

Table 3.8: Annotated glutamate and histidine decarboxylation genes in *E. lenta* strain C592

Name	db_xref
Probable glutamate/gamma-aminobutyrate antiporter CDS	SEED:fig 6666666.209054.peg.3136
Glutamate decarboxylase (EC 4.1.1.15) CDS	SEED:fig 6666666.209054.peg.3135
histidine decarboxylase, pyruvyl type(EC:4.1.1.22) CDS	SEED:fig 6666666.209054.peg.753

Within the realm of carbon metabolism, C592 has genes encoding an incomplete TCA cycle (Table 3.9). Of particular interest, C592 appears to encode duplicate genes for fumarate reductase, a mechanism by which anaerobic bacteria are able to deposit reducing equivalents onto fumarate to generate succinate. Additionally, the C592 genome encodes genes for generating fumarate from arginine, including an arginosuccinate synthase and arginosuccinate lyase (Table 3.10). Fumarate is widely utilized anaerobically as a potential electron acceptor, leading to the formation of succinate (36). Previous work with the type strain of *E. lenta* as well as preliminary fermentative end product analysis (data not shown) suggest that both C592 and 25559 generate succinate as well as acetate as their major fermentative end products. The incomplete TCA cycle of C592 (ending at succinate), the multitude of fumarate reductases, and the ability to shift arginine to fumarate, suggests fumarate is a major electron acceptor in *E. lenta*. C592 also has genes that encode various other electron-accepting reactions, such as dimethyl sulfoxide reduction and nitrogen reduction (data not shown). Acetogens are described as being a heterogenous group of organisms, specifically with regard to their utilization of various electron donors and electron acceptors (93). These results correlate with those findings in other acetogenic bacteria, as both C592 and *E. lenta* appear to utilize numerous bile acids and steroids as electron donors and various other molecules as electron acceptors.

Varying atmospheric gases changes C592 and 25559 bile acid and steroid metabolism

Since both 25559 and C592 appear to be acetogens based on genetic composition and previous fermentative end product analysis, next we tested the effects altered atmospheric gases would have on bile acid metabolism. It was hypothesized since hydroxyl groups on bile acids were

Table 3.9: Annotated genes from the Krebs's cycle in *E. lenta* strain C592

Gene Name	db_xref
Citrate synthase (si) (EC 2.3.3.1) CDS	SEED:fig 6666666.209054.peg.20
Aconitate hydratase (EC 4.2.1.3) CDS	SEED:fig 6666666.209054.peg.2429
Isocitrate dehydrogenase [NAD] (EC 1.1.1.41) CDS	SEED:fig 6666666.209054.peg.2430
Isocitrate dehydrogenase [NADP] (EC 1.1.1.42) CDS	SEED:fig 6666666.209054.peg.1697
2-oxoglutarate oxidoreductase, gamma subunit (EC 1.2.7.3) CDS	SEED:fig 6666666.209054.peg.1488
2-oxoglutarate oxidoreductase, beta subunit (EC 1.2.7.3) CDS	SEED:fig 6666666.209054.peg.1487
2-oxoglutarate oxidoreductase, alpha subunit (EC 1.2.7.3) CDS	SEED:fig 6666666.209054.peg.1486
2-oxoglutarate oxidoreductase, delta subunit, putative (EC 1.2.7.3) CDS	SEED:fig 6666666.209054.peg.1485
Malate dehydrogenase (EC 1.1.1.37) CDS	SEED:fig 6666666.209054.peg.2038
fumarate hydratase CDS	SEED:fig 6666666.209054.peg.2035
Fumarate hydratase class I, aerobic (EC 4.2.1.2); L(+)-tartrate dehydratase beta subunit (EC 4.2.1.32) CDS	SEED:fig 6666666.209054.peg.2034
Succinate dehydrogenase flavoprotein subunit (EC 1.3.99.1) CDS	SEED:fig 6666666.209054.peg.3027
Succinate dehydrogenase iron-sulfur protein (EC 1.3.99.1) CDS	SEED:fig 6666666.209054.peg.3026
fumarate reductase/succinate dehydrogenase flavoprotein domain protein CDS	SEED:fig 6666666.209054.peg.2659
Succinate dehydrogenase flavoprotein subunit (EC 1.3.99.1) CDS	SEED:fig 6666666.209054.peg.36
Fumarate reductase flavoprotein subunit (EC 1.3.99.1) CDS	SEED:fig 6666666.209054.peg.3180
Fumarate reductase flavoprotein subunit (EC 1.3.99.1) CDS	SEED:fig 6666666.209054.peg.3162
Fumarate reductase flavoprotein subunit (EC 1.3.99.1) CDS	SEED:fig 6666666.209054.peg.3118
Fumarate reductase flavoprotein subunit (EC 1.3.99.1) CDS	SEED:fig 6666666.209054.peg.3101
Fumarate reductase flavoprotein subunit (EC 1.3.99.1) CDS	SEED:fig 6666666.209054.peg.3100
Fumarate reductase flavoprotein subunit (EC 1.3.99.1) CDS	SEED:fig 6666666.209054.peg.3074
Fumarate reductase flavoprotein subunit (EC 1.3.99.1) CDS	SEED:fig 6666666.209054.peg.2904

1.3.99.1) CDS	
Fumarate reductase flavoprotein subunit (EC 1.3.99.1) CDS	SEED:fig 6666666.209054.peg.2860
Fumarate reductase flavoprotein subunit (EC 1.3.99.1) CDS	SEED:fig 6666666.209054.peg.2775
Fumarate reductase flavoprotein subunit (EC 1.3.99.1) CDS	SEED:fig 6666666.209054.peg.2772
putative fumarate reductase flavoprotein subunit CDS	SEED:fig 6666666.209054.peg.2742
putative fumarate reductase flavoprotein subunit CDS	SEED:fig 6666666.209054.peg.2736
Fumarate reductase flavoprotein subunit (EC 1.3.99.1) CDS	SEED:fig 6666666.209054.peg.2731
Fumarate reductase flavoprotein subunit (EC 1.3.99.1) CDS	SEED:fig 6666666.209054.peg.2727
Fumarate reductase flavoprotein subunit (EC 1.3.99.1) CDS	SEED:fig 6666666.209054.peg.2679
fumarate reductase/succinate dehydrogenase flavoprotein domain protein CDS	SEED:fig 6666666.209054.peg.2659
Fumarate reductase flavoprotein subunit (EC 1.3.99.1) CDS	SEED:fig 6666666.209054.peg.2633
Fumarate reductase flavoprotein subunit (EC 1.3.99.1) CDS	SEED:fig 6666666.209054.peg.2449
Fumarate reductase flavoprotein subunit (EC 1.3.99.1) CDS	SEED:fig 6666666.209054.peg.2385
Fumarate reductase flavoprotein subunit (EC 1.3.99.1) CDS	SEED:fig 6666666.209054.peg.2353
Fumarate reductase flavoprotein subunit (EC 1.3.99.1) CDS	SEED:fig 6666666.209054.peg.2301
Fumarate reductase flavoprotein subunit (EC 1.3.99.1) CDS	SEED:fig 6666666.209054.peg.2227
Fumarate reductase flavoprotein subunit (EC 1.3.99.1) CDS	SEED:fig 6666666.209054.peg.2195
Fumarate reductase flavoprotein subunit (EC 1.3.99.1) CDS	SEED:fig 6666666.209054.peg.1967
Fumarate reductase flavoprotein subunit (EC 1.3.99.1) CDS	SEED:fig 6666666.209054.peg.1768
Fumarate reductase flavoprotein subunit (EC 1.3.99.1) CDS	SEED:fig 6666666.209054.peg.1642
Fumarate reductase flavoprotein subunit (EC 1.3.99.1) CDS	SEED:fig 6666666.209054.peg.1095
Fumarate reductase flavoprotein subunit (EC 1.3.99.1) CDS	SEED:fig 6666666.209054.peg.1084

putative fumarate reductase flavoprotein subunit CDS	SEED:fig 6666666.209054.peg.875
Fumarate reductase flavoprotein subunit (EC 1.3.99.1) CDS	SEED:fig 6666666.209054.peg.695
Fumarate reductase flavoprotein subunit (EC 1.3.99.1) CDS	SEED:fig 6666666.209054.peg.656
Fumarate reductase flavoprotein subunit (EC 1.3.99.1) CDS	SEED:fig 6666666.209054.peg.613
Fumarate reductase flavoprotein subunit (EC 1.3.99.1) CDS	SEED:fig 6666666.209054.peg.606
Fumarate reductase flavoprotein subunit (EC 1.3.99.1) CDS	SEED:fig 6666666.209054.peg.561
Fumarate reductase flavoprotein subunit (EC 1.3.99.1) CDS	SEED:fig 6666666.209054.peg.545
Fumarate reductase flavoprotein subunit (EC 1.3.99.1) CDS	SEED:fig 6666666.209054.peg.522
Fumarate reductase flavoprotein subunit (EC 1.3.99.1) CDS	SEED:fig 6666666.209054.peg.480
Fumarate reductase flavoprotein subunit (EC 1.3.99.1) CDS	SEED:fig 6666666.209054.peg.472
putative fumarate reductase flavoprotein subunit CDS	SEED:fig 6666666.209054.peg.471
Fumarate reductase flavoprotein subunit (EC 1.3.99.1) CDS	SEED:fig 6666666.209054.peg.364
Fumarate reductase flavoprotein subunit (EC 1.3.99.1) CDS	SEED:fig 6666666.209054.peg.243
Fumarate reductase flavoprotein subunit (EC 1.3.99.1) CDS	SEED:fig 6666666.209054.peg.217
Fumarate reductase flavoprotein subunit (EC 1.3.99.1) CDS	SEED:fig 6666666.209054.peg.19

Table 3.10: Annotated genes for arginine biosynthesis in *E. lenta* strain C592

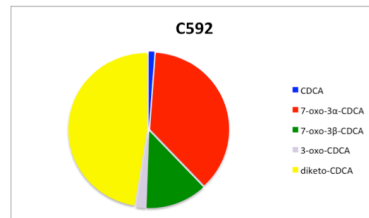
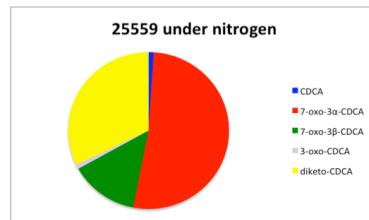
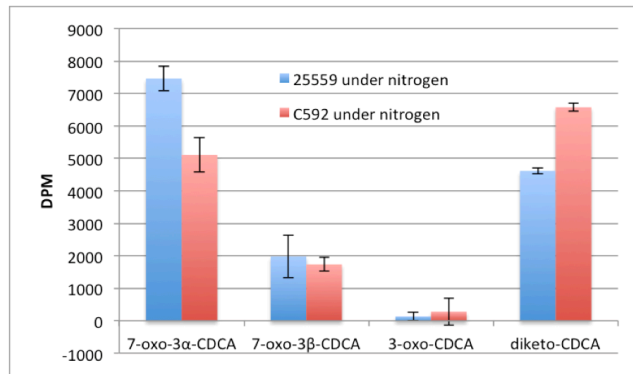
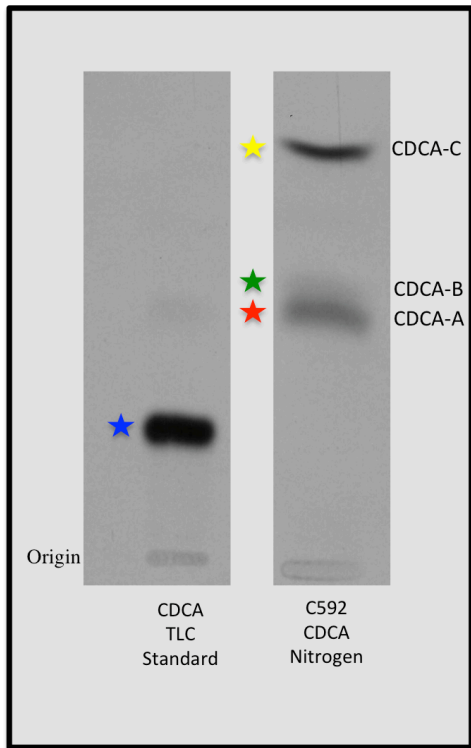
Name	db_xref
Argininosuccinate synthase (EC 6.3.4.5) CDS	SEED:fig 6666666.209054.peg.2435
Argininosuccinate lyase (EC 4.3.2.1) CDS	SEED:fig 6666666.209054.peg.2434

being used as electron donors, if a more energetically favorable electron donor was present then C592 and 25559 would shift to utilizing that electron donor and the oxidation of bile acids would be inhibited. Both C592 and 25559 encode membrane-associated and cytoplasmic ferredoxin hydrogenases (including and Ech complex described above) capable of utilizing hydrogen to reduce oxidized ferredoxin. The RNF complex, as well as other electron-bifurcating enzymes not yet identified in C592 or *E. lenta*, can then move electrons from reduced ferredoxin to oxidized NAD⁺, thereby generating reduced NADH, which would ultimately inhibit bile acid oxidation. C592 and 25559 metabolism of CDCA was tested under inert nitrogen, carbon dioxide, and hydrogen gas to mimic gases that might be present to varying degrees in the human intestinal tract to see if any changes in bile acid or steroid metabolism occurred. Under inert N₂ gas, C592 and 25559 completely metabolize CDCA into mostly CDCA-A and CDCA-C, although the relative amount is different between strains (Figure 3.23). When grown in the presence of CO₂ gas, CDCA was completely metabolized to the same three CDCA metabolites found under N₂ gas culture conditions, although CDCA-A is the major metabolite for both strains (Figure 3.24). When grown in the presence of H₂ gas, CDCA metabolism by both C592 and 25559 is significantly inhibited (Figure 3.25). While there was some production of 7-oxo-CDCA and 3-oxo-CDCA, the majority of the CDCA remains unutilized in the cell cultures. These experiments were repeated for both C592 and 25559 metabolism of testosterone. Under H₂, both C592 and 25559 have their metabolism of testosterone completely inhibited (data not shown). These results show that C592 and 25559 are able to shift their electron donors, and ultimately bile acid and steroid metabolism, based on substrate availability, preferring to use the most energetically favorable substrate possible. Such an ability to be flexible with redox balancing is beneficial for any microbe living in the competitive environment of the human intestinal tract.

Figure 3.23: Quantitation of C592 and 25559 metabolites of CDCA when grown overnight under inert N₂ gas

C592 and *E. lenta* ATCC 25559 were grown overnight in the presence of 25µM CDCA and 1µCi [24-¹⁴C]-CDCA under inert N₂, extracted, and run on TLC as previously described. Bands corresponding to CDCA metabolites were scraped and the relative amounts of each were determined through liquid scintillation spectrometry. Representative TLC on left. Top right indicates relative amount of each of the metabolites with pie charts to show amounts relative to total radioactivity detected from lane, experiment run in triplicate. The major product for 25559 under N₂ is 7-oxo-3α-chenodeoxycholic acid, whereas for C592 it is 3,7-dioxo-chenodeoxycholic acid.

Under 100% Nitrogen (inert) gas



Major product:

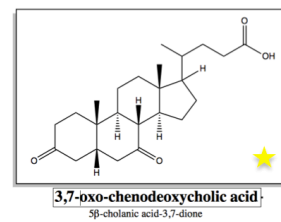
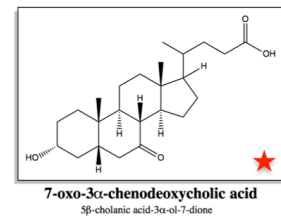
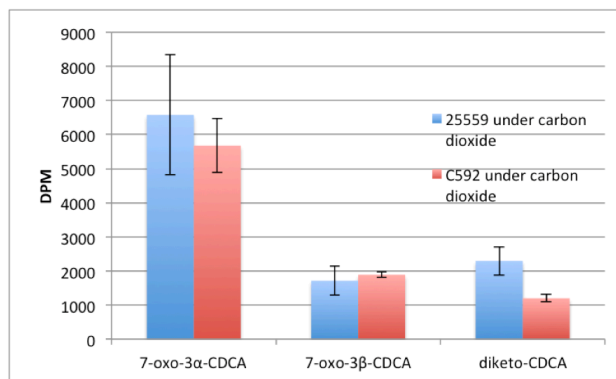
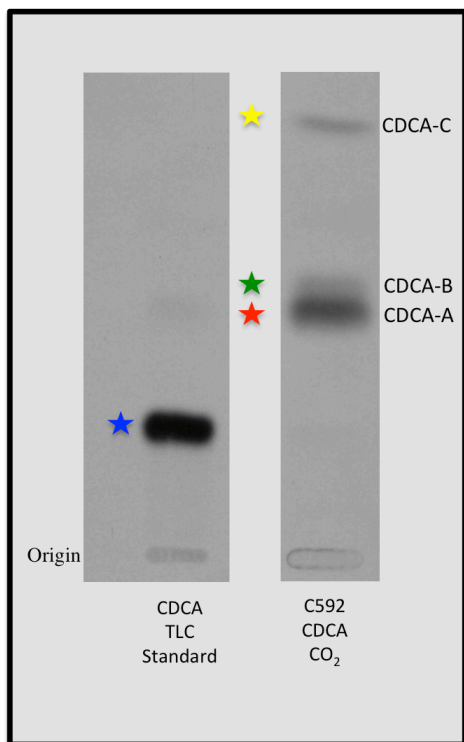


Figure 3.24: Quantitation of C592 and 25559 metabolites of CDCA when grown overnight under CO₂ gas

C592 and *E. lenta* ATCC 25559 were grown overnight in the presence of 25µM CDCA and 1µCi [24-¹⁴C]-CDCA under CO₂, extracted, and run on TLC as previously described. Bands corresponding to CDCA metabolites were scraped and the relative amounts of each were determined through liquid scintillation spectrometry. Representative TLC on left. Top right indicates relative amount of each of the metabolites with pie charts to show amounts relative to total radioactivity detected from lane, experiment run in triplicate. The major product for 25559 and C592 CDCA metabolism under CO₂ is 7-oxo-3α-chenodeoxycholic acid.

Under 100% CO₂ gas



Major product:

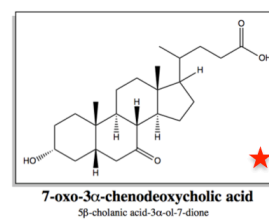
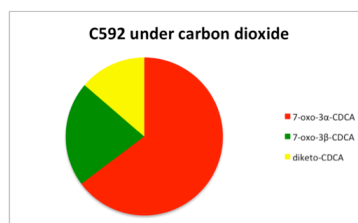
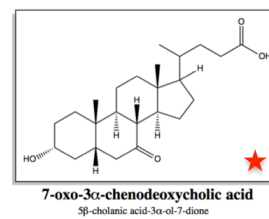
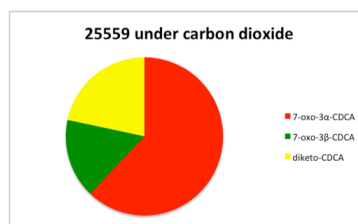
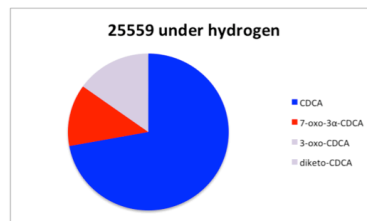
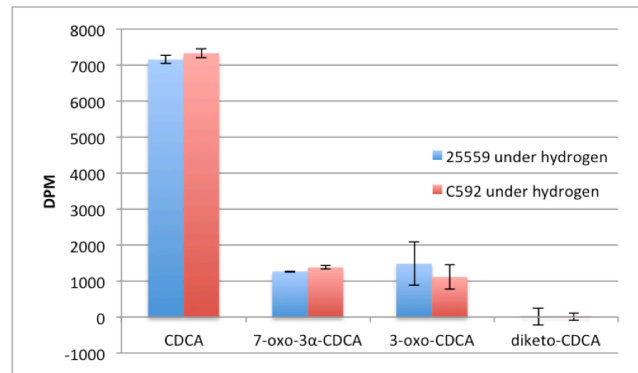
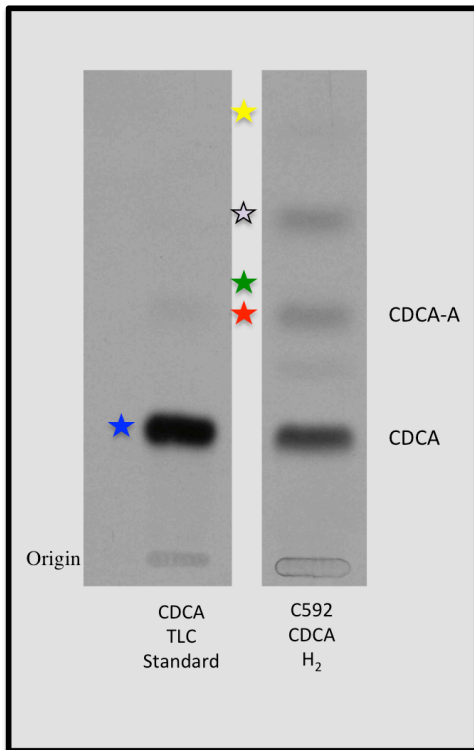


Figure 3.25: Quantitation of C592 and 25559 metabolites of CDCA when grown overnight under H₂ gas

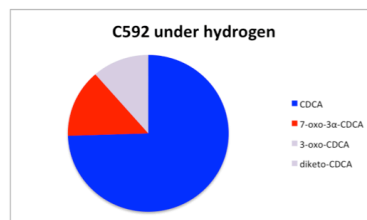
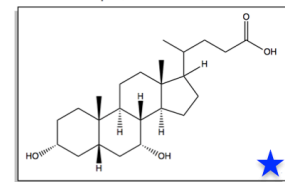
C592 and *E. lenta* ATCC 25559 were grown overnight in the presence of 25µM CDCA and 1µCi [24-¹⁴C]-CDCA under CO₂, extracted, and run on TLC as previously described. Bands corresponding to CDCA metabolites were scraped and the relative amounts of each were determined through liquid scintillation spectrometry. Representative TLC on left. Top right indicates relative amount of each of the metabolites with pie charts to show amounts relative to total radioactivity detected from lane, experiment run in triplicate. The major product for 25559 and C592 CDCA metabolism under CO₂ is 7-oxo-3α-chenodeoxycholic acid.

Under 100% H₂ gas

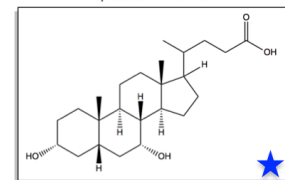


Major product:

chenodeoxycholic acid
5β-choleic acid-3α,7α-ol



chenodeoxycholic acid
5β-choleic acid-3α,7α-ol

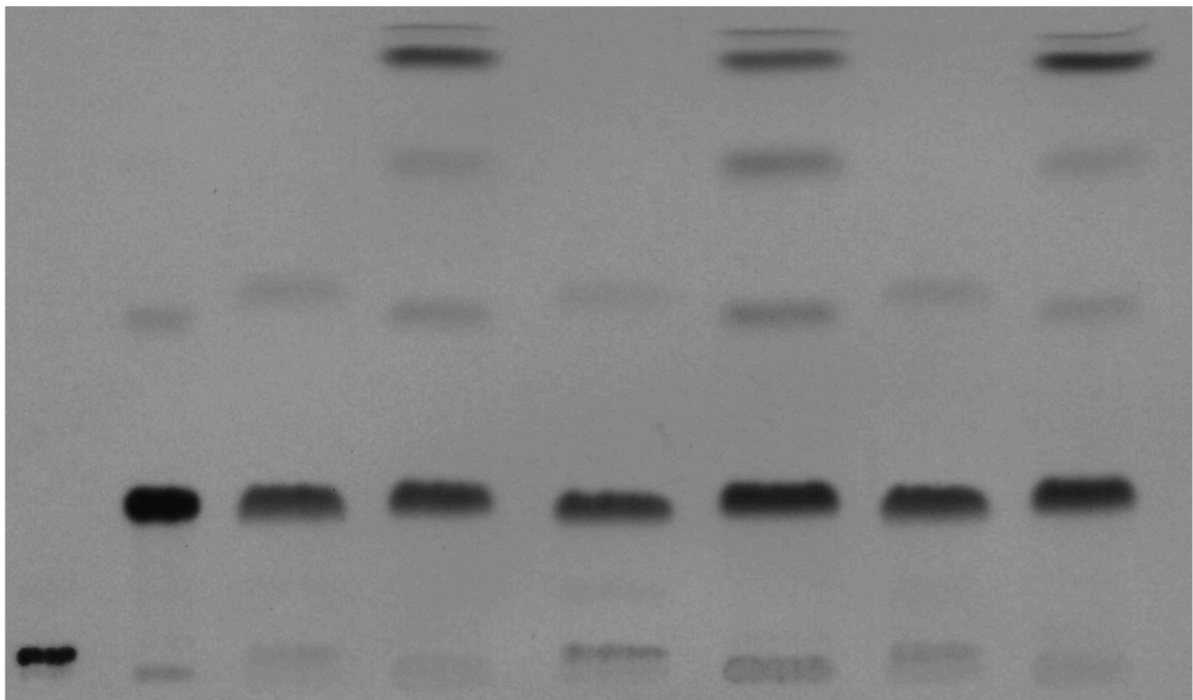


C592 oxo-bile acid derivatives inhibit 7 α -dehydroxylation *in vitro*

Since C592 and 25559 both exhibited significant changes in bile acid metabolism based on atmospheric gas composition, we first wanted to test if a similar effect occurred with 7 α -dehydroxylating bacteria. We performed the same bile acid metabolism test as above using the 7 α -dehydroxylating bacteria *Clostridium scindens* VPI 12708 (12708). There was no significant effect of CO₂ or H₂ gas atmosphere on CA or CDCA 7 α -dehydroxylation by 12708 (Figure 3.26). Next we tested the impact of the formation of oxo-bile acids on the 7 α -dehydroxylation of primary bile acids by 12708. We isolated [¹⁴C]-labeled CDCA metabolites (CDCA-A, CDCA-B, CDCA-C) and introduced them into a growing culture of 12708. After 24 hours, 12708 was able to reduce CDCA-A back to CDCA and subsequently 7 α -dehydroxylate a portion of the newly formed CDCA (Figure 3.27). Over the same time course, 12708 metabolized 7-oxo-3 β -chenodeoxycholic acid (CDCA-B) to a product whose R_f matched iso-CDCA (3 β -CDCA), but was unable to subsequently 7 α -dehydroxylate (Figure 3.26). *C. scindens* VPI 12708 is known to have 3 α -HSDH and 7 α -HSDH activity (148) but has never reported to have 3 β -HSDH activity, possibly explaining the lack of 7 α -dehydroxylation of the 3 β CDCA-B metabolite. When CDCA-C was added to growing cultures of 12708, it was only partially reduced back to a mixture of CDCA and 3-oxo-CDCA (Figure 3.27). These results suggest *in vitro*, two of the three major bile acid products from C592 and 25559 metabolism of CDCA prevent effective 7 α -dehydroxylation by 12708. When C592 and 12708 were grown in a mixed culture containing CDCA, the pattern of CDCA metabolites suggested a significant decrease in 7 α -dehydroxylation when compared to the results of a 12708 pure culture (Figure 3.28). Likely

Figure 3.26: *C. scindens* VPI 12708 metabolism of CA and CDCA does not change under anaerobic CO₂ or H₂ atmospheric gas

Clostridium scindens VPI 12708 was grown overnight in anaerobic BHI in the presence of 25mM CA or CDCA and 1 μ Ci CA or CDCA under varying atmospheric conditions (N₂, CO₂, or H₂). Cultures were extracted and run on TLC plates as described in Materials and Methods. *C. scindens* VPI 12708 did not alter its metabolism of CA or CDCA under any of the varying atmospheric gases.



CA TLC Standard	CDCA TLC Standard	12708 + CA Nitrogen	12708 + CDCA Nitrogen	12708 + CA CO ₂	12708 + CDCA CO ₂	12708 + CA H ₂	12708 + CDCA H ₂
-----------------------	-------------------------	---------------------------	-----------------------------	----------------------------------	------------------------------------	---------------------------------	-----------------------------------

Figure 3.27: *C. scindens* VPI 12708 recognizes C592 CDCA metabolites but is unable to effectively 7 α -dehydroxylate

A. First spot is a CDCA TLC standard. Next two spots are C592/12708 overnight cell culture conversions of CDCA. C592 generates three products as described above. 12708 generates one major metabolite, lithocholic acid (LCA), indicated by the black star. **B.** The three CDCA metabolites were isolated, concentrated, and added to 12708 overnight cultures at approximately 25 μ M final concentration. 7-oxo-3 α -CDCA (red star) was reduced back to CDCA by 12708. Some trace LCA is formed, but not as significant as 12708 + CDCA cell culture. **C.** 12708 reduces 7-oxo-3 β -CDCA (green star) to a band that does not comigrate with CDCA. This band has a similar R_f to 3 β -CDCA (iso-CDCA), suggesting 12708 reduces this metabolite back to iso-CDCA. However, 7 α -dehydroxylation does not appear to occur, suggesting 12708 is unable to 7 α -dehydroxylate the 3 β -epimer. **D.** 12708 recognizes 3,7-dioxo-CDCA (yellow star) and produces two major metabolites. One metabolite comigrates with CDCA, while the other comigrates with 3-oxo-CDCA. There does not appear to be any metabolite formed that comigrates with LCA.

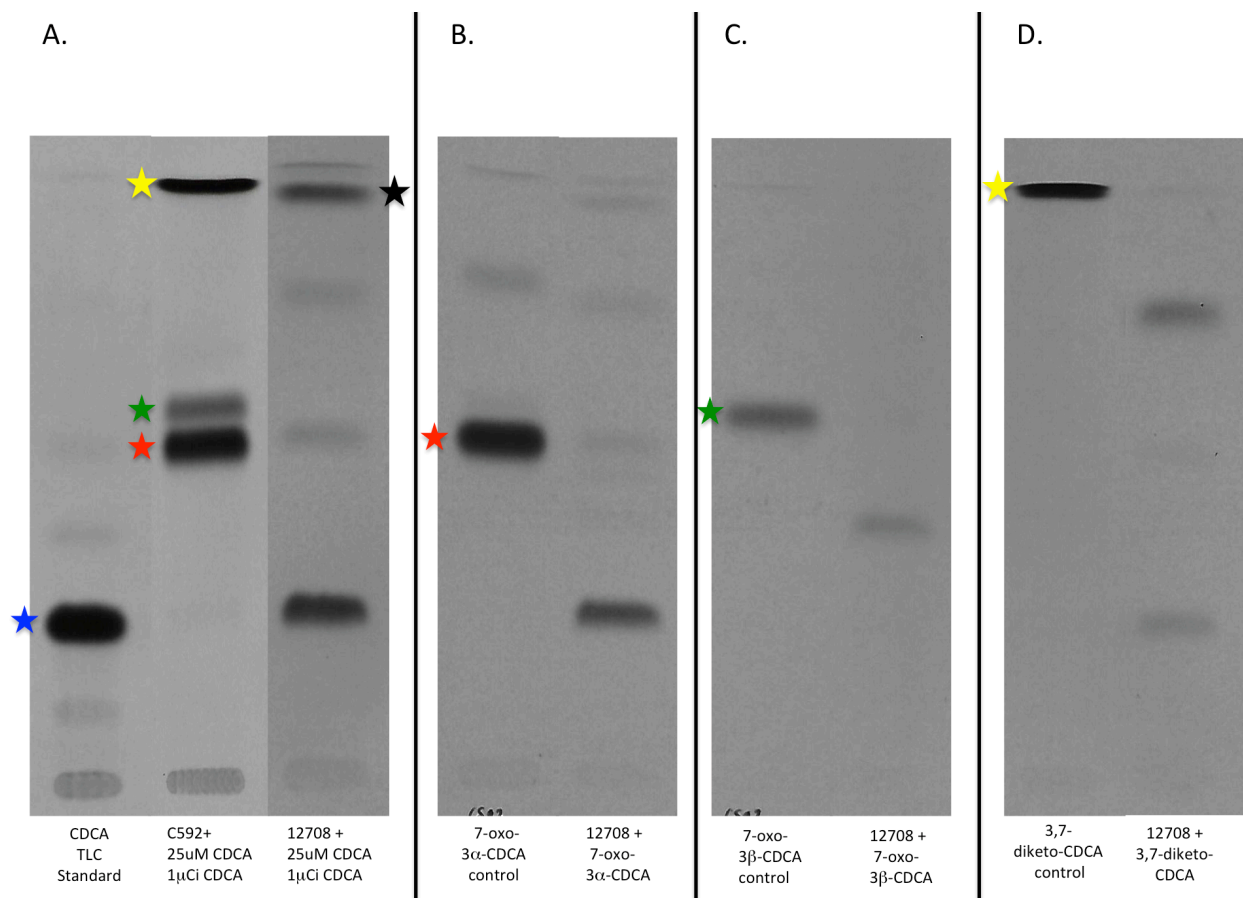
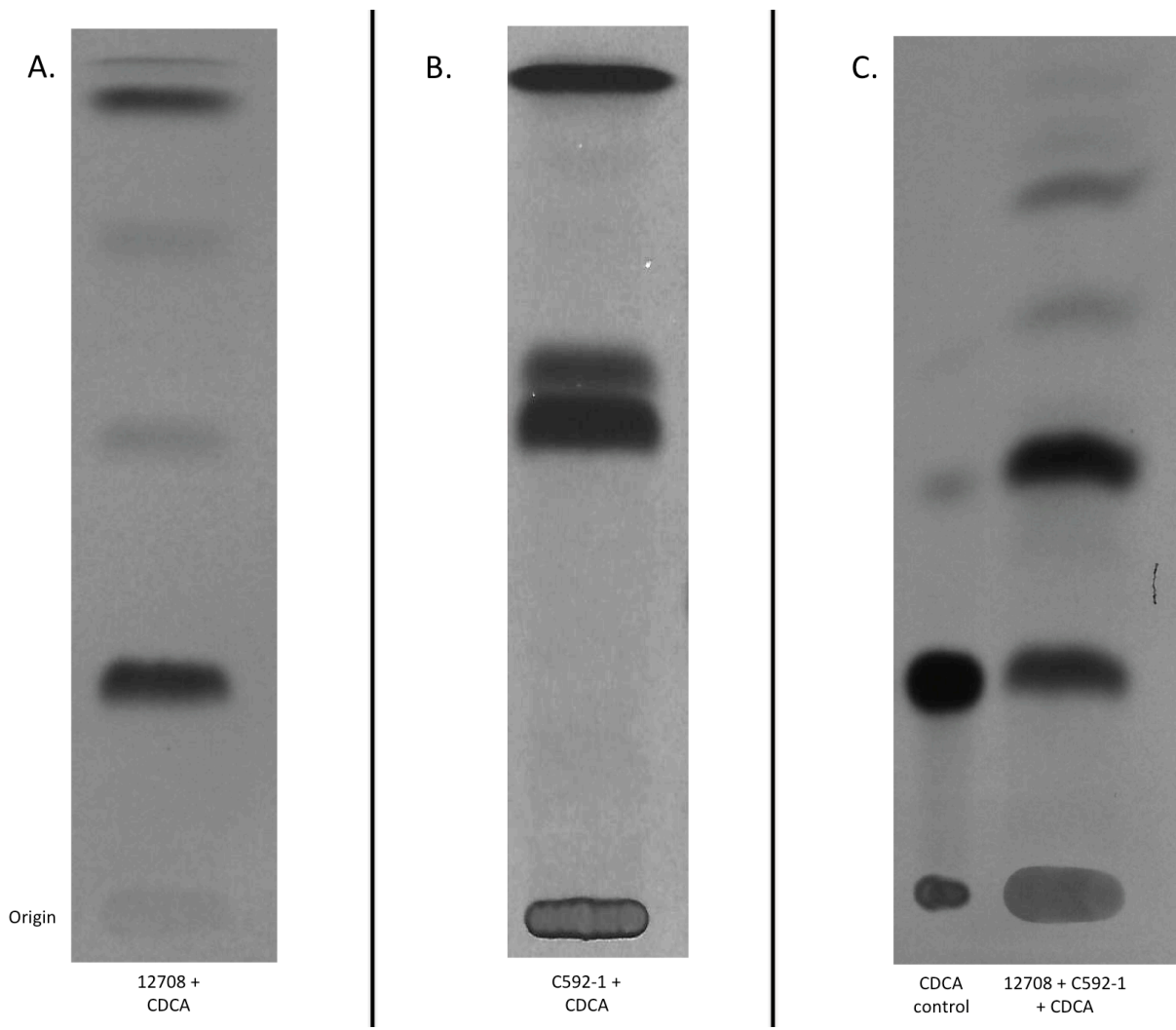


Figure 3.28: Coculture of *C. scindens* VPI 12708 and C592 inhibits 7 α -dehydroxylation of CDCA

A. *C. scindens* VPI 12708 whole cell conversion of CDCA. **B.** C592 whole cell conversion of CDCA. **C.** 10mL anaerobic BHI broth under N₂ was inoculated with 1% overnight culture of both 12708 and C592 along with 25mM CDCA and 1mCi [24-¹⁴C]-CDCA. This coculture was grown overnight at 37°C and then extracted and run on TLC as described above. The coculture CDCA pattern of metabolites matches neither the C592 nor 12708 patterns. A significant amount of CDCA remains, while the other major product comigrates with 7-oxo-3 α -CDCA. This suggests that in coculture, C592 and 12708 cycle CDCA back and forth between an oxidized and 3 α -reduced C7-oxo group.



these two gut bacteria cycle between oxidation and reduction of hydroxyl groups on the bile acids regulating secondary bile acid formation.

Discussion:

E. lenta is a normal inhabitant of the human intestinal microbiome. It has been studied due to its propensity to metabolize bile acids and steroids, including the isomerization of primary and secondary bile acids at the 3-hydroxyl group (150) and the 21-dehydroxylation of corticoids (248). The effects of these biotransformations are significant for both the gut microbiome as a whole and the host. *E. lenta*-derived glucocorticoid metabolites can inhibit renal cells ability to modulate response to cortisol, ultimately leading to fluid retention and hypertension (251). Isomerized secondary bile acids, such as iso-DCA, have been shown to be less toxic to other members of the gut microbiome at physiological concentrations (150). Additionally, isomerized secondary bile acids have been hypothesized to be less toxic to colonocytes. However, the pattern of isomerization requires what would at the surface appear to be an energetically unfavorable oxidation of a hydroxyl group in an anaerobic environment. Oxidized bile acids (oxo-BA), or bile acids with a ketone hydroxyl moiety, were thought to be intermediates in the ultimate bile acid metabolism profile. However, oxidized bile acids are known to be present in significant amounts in serum, portal blood, fecal water, and fecal pellets (158-163, 267). Cholecystectomized patients are reported to have increased oxo-BA in portal circulation, likely due to more primary bile acids escaping into the large intestine and undergoing metabolism by gut microbes (165). Oxo-BA have been shown to have differing agonistic properties than their fully reduced counterparts for host nuclear and G-protein coupled receptors. For instance, 3-oxo-LCA is the most potent bile acid VDR receptor agonist (175). However, oxo-BA receptor activation remains to be fully tested for other known receptors that respond to bile acids. Additionally, how the oxidation of the hydroxyl groups of bile acids by *E. lenta* plays into its

general host metabolism is not known, instead the studies focused on the effects of the fully reduced end products. Additionally, the effects of oxidation or epimerization of hydroxyl groups on other gut microbes, specifically those that are known to metabolize bile acids, had not been previously studied.

In the current study, a novel strain of *Eggerthella lenta*, C592, was characterized, with an emphasis on the composition of its genome as well as its steroid and bile acid metabolism profile. C592 was originally isolated from the fecal sample from Okinawa, Japan. Initially suspected to be a 7α -dehydroxylating bacterium, C592 was shown to create both mono- and di-keto bile acid metabolites from CDCA. Additionally, it was shown to completely metabolize secondary bile acids DCA and LCA to numerous secondary metabolites. When compared to high activity and low activity 7α -dehydroxylating bacteria, most are not able to completely convert CA and CDCA to secondary metabolites. Conversely, C592 was shown to convert concentrations of CDCA that can inhibit the growth of other bacteria ($500\mu\text{M}$) to secondary metabolites. This pattern of metabolites initially suggested an irreversible conversion of primary bile acids, such as 7α -dehydroxylation. However, MS analysis confirmed the CDCA and DCA C592 metabolites lost two or four mass units, indicating oxidation of one or two hydroxyl groups, respectively.

C592 was subsequently determined to have high 16S sequence similarity to the *Eggerthella lenta* type strain. Various *E. lenta* strains had been shown previously to have 3α -HSDH, 7α -HSDH, and 12α -HSDH activity (151, 153). However, complete oxidation of primary and secondary bile acids by *E. lenta* was not noted in the literature. Additionally, the accumulation of dioxo-

primary or secondary bile acids in *E. lenta* whole cell extracts, such as 3,7-dioxo-CDCA or 3,12-oxo-DCA, was not reported. This study also shows that both C592 and the *E. lenta* type strain have 17 β -HSDH activity, capable of converting testosterone to its precursor, androstenedione. While *E. lenta* has been reported to metabolize some steroids, 17 β -HSDH activity has never before been reported. Testosterone and other androgens are known to be excreted in the bile and become substrates for metabolism by gut microbes (268). Additionally, androgens may undergo passive diffusion across colonocytes. The effects of bacterial inactivation of androgens on host physiology is not known, however the conservation of these genes in numerous strains of *E. lenta* indicate they give some evolutionary advantage.

In this study, a full, closed genomic sequence for the novel C592 *E. lenta* strain was determined. Impressively, it maintains high genomic and metabolic similarities to the *Eggerthella lenta* type strain isolated from a patient in Europe in the 1930s. This strong homology over both temporal and geographical differences emphasizes the importance of its set of genes, especially those for bile acid metabolism, in its ability to grow in the niche environment of the human intestinal tract. However, some differences between C592 and the type strain arose. For instance, the *cgr* gene locus reported to encode the gene for digoxin reductase was not found in C592. Current testing of C592 is underway in order to ascertain its ability to reduce digoxin *in vitro*. The results of these future experiments will be important, as the clear lack of the described “cgr locus” from the type strain should indicate C592 would not have the ability to reduce digoxin. However, if it is able to successfully reduce digoxin, it is likely this gene cluster does not in fact encode the enzymes responsible for catalyzing this reaction

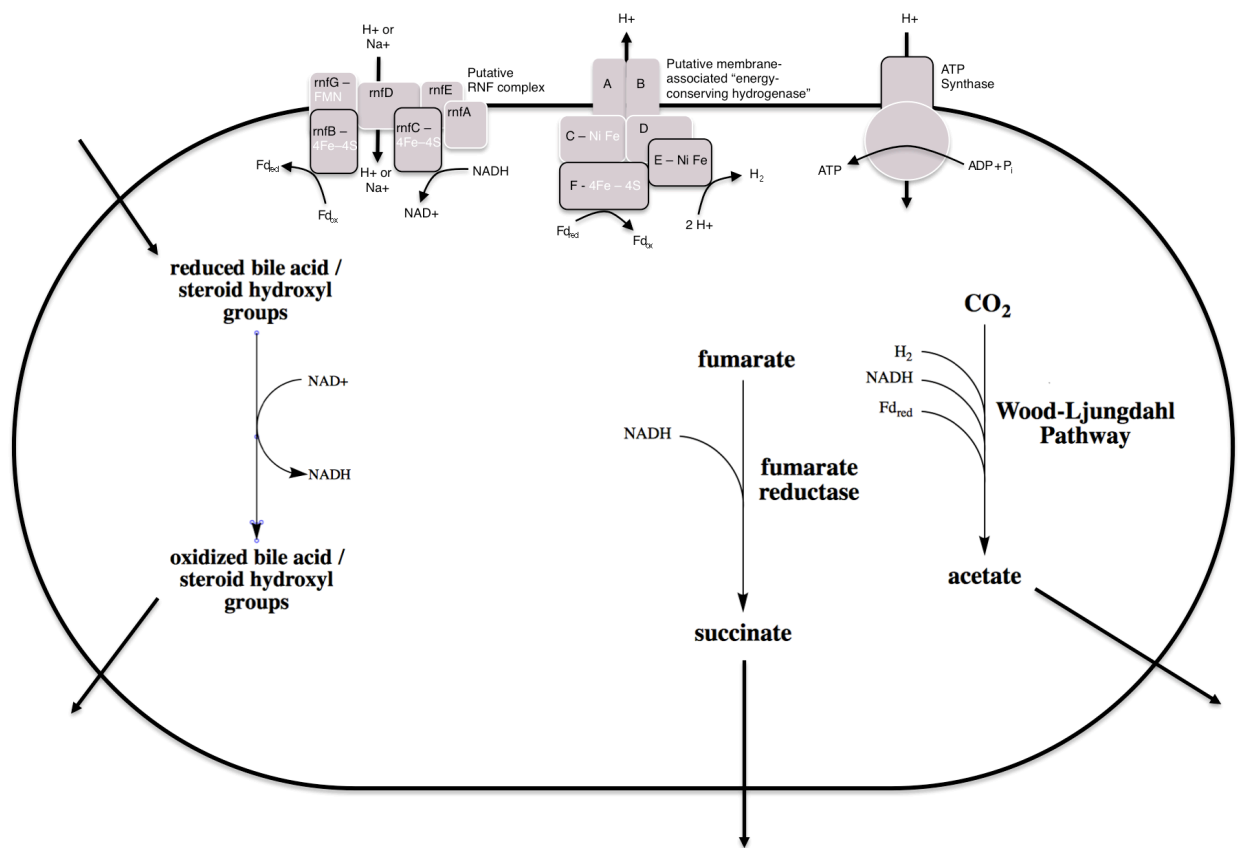
Additionally, a bai-like operon in *E. lenta* was identified in the Devlin et al. study describing the enzymes responsible for 3 α -hydroxyl epimerization of bile acids (150). Within this operon and downstream of three SDR family enzymes is a gene that is currently being analyzed by collaborators as the putative 21-dehydroxylase, the enzyme responsible for 21-dehydroxylation of glucocorticoids. The gene responsible for the production of this enzyme has not been previously reported. However, this gene is conspicuously absent from C592. In fact, both genes flanking this putative 21-dehydroxylase are there with high similarity. This suggests that C592 may not have 21-dehydroxylase activity *in vitro*. Experiments to ascertain C592's ability to perform the 21-dehydroxylase reaction are ongoing, although preliminary results suggest it does not have the activity (data not shown).

Whole genome sequencing of C592 allowed for better determination of the reasoning behind the formation of these oxo-bile acid derivatives. The anaerobic environment in the colon has a very low redox potential, therefore the oxidation of bile acid hydroxyl groups would appear to be energetically unfavorable. However, numerous previous observations gave us direction, including *E. lenta* production of acetate and succinate as its only fermentative end products (VPI Anaerobe Laboratory Manual) and its propensity to utilize CO₂ gas from its headspace during growth (VPI Anaerobe Laboratory Manual, past laboratory observations). It was found that C592, along with the type strain, harbor genes encoding the majority of the enzymes in the Wood-Ljungdahl pathway. This pathway of fixing CO₂ to produce acetate requires numerous reducing equivalents, including reduced ferredoxin and NADH (93) and is an explanation as to why C592 was preferentially oxidizing bile acids (Figure 3.29). Under inert nitrogen gas, C592/25559 oxidation of bile acids would generate reduced pyridine nucleotides.

Figure 3.29: Illustration of C592 whole cell redox balancing with bile acids under low H₂ partial pressure

C592, under low H₂ partial pressure, preferentially oxidizes bile acids. This would lead to an increased level of reduced pyridine nucleotides, which could either be cycled through the RNF complex to generate reduced ferredoxin or be used in other metabolic processes, such as the Wood-Ljungdahl pathway.

Under low H₂ partial pressure



These reduced pyridine nucleotides could then be transferred to oxidized ferredoxin while utilizing a H⁺ or Na⁺ gradient via the putative RNF complex, also located in C592 and *E. lenta* type strain. Reduced ferredoxin could then be used in the Wood-Ljungdahl pathway to generate acetate. Additionally, the reduced ferredoxin could be used to generate a H⁺ gradient via the putative Ech complex located in both C592 and *E. lenta* type strain genome. Ultimately, under inert gas, C592 and 25559 use bile acids as electron donors for various other metabolic pathways.

This study showed that the tendency of *E. lenta* strains to oxidize bile acids is sensitive to the atmospheric gases present. When the atmospheric gas in the headspace was changed to 100% hydrogen, oxidation of bile acids was significantly inhibited. The reasoning behind this shift gives further insight into why C592 and 25559 oxidize bile acids. C592 and 25559 encode numerous genes annotated to be ferredoxin oxidoreductases. This family of enzymes is able to utilize H₂ to reduce ferredoxin. Additionally, the membrane-bound Ech complex, also present in both C592 and 25559, can perform a similar reaction while utilizing a proton gradient. The RNF complex can utilize reduced ferredoxin to generate a proton gradient and reduced NADH. Reduced NADH can be utilized in various metabolic pathways, including the Wood-Ljungdahl pathway to create acetate. The proton gradient generated from the RNF complex can be used to generate ATP via ATP synthase. Energetically, the oxidation of H₂ to form reduced ferredoxin is a more favorable reaction than the oxidation of bile acid hydroxyl groups, as H₂ has a redox potential (E°') of -0.421 V while NADH is -0.315 V (41). Therefore, when H₂ is abundant, C592 is able to switch to the higher energy electron donor to regenerate both reduced ferredoxin and NADH, while generating a H⁺ gradient for ATP generation (Figure 3.29). More

experimentation about this putative link between bile acid metabolism and acetogenesis in *E. lenta* should be performed, including the confirmation of acetate generation from CO₂ utilizing radiolabeled CO₂ gas. Collaborators are currently testing the fermentative end products produced by both C592 and 25559 under the various gas atmospheres used to screen bile acid metabolism. Additionally, the presence or absence of bile acids will be tested to see its impacts on the amount of fermentative end products, as we hypothesize if *E. lenta* has more access to electron donors, then it will produce quantitatively more acetate.

Another important observation was the effect that oxo-bile acid production by *E. lenta* strains has on other bacteria that metabolize bile acids. The ability for high-activity 7 α -dehydroxylating bacteria to produce LCA from oxo-CDCA metabolites was impaired. Additionally, co-culturing of C592 and 12708 prevented formation of LCA, even though in pure cultures C592 grows to only two tenths the optical density of 12708 in the same time frame (data not shown). The two major bands from the coculture assay were CDCA and 7-oxo-CDCA, indicating both strains cycle the bile acid hydroxyl groups between oxidation and reduction. Taken together, these results suggest that in the human colon, under conditions of low available H₂, that *E. lenta* strains could prevent 7 α -dehydroxylation of primary bile acids (Figure 3.29).

This has significant implications for C592 and *E. lenta* bile acid metabolism *in vivo*. The composition of gas in the colon, specifically with regard to H₂, can vary significantly. Both methanogens and sulfidogens utilize H₂ and have higher affinity to H₂ than acetogens. However, the amount of methanogens found in colonic samples can vary on individuals to be undetectable to over 10⁹ CFU/g stool (47). Additionally, even if hydrogen sulfide producing bacteria are

present, sulfidogenesis requires the presence of sulfate or sulfite to occur. Some patients who have a very high level of bacterial fermentation occurring in their colon, such as native Africans eating a diet rich in complex carbohydrates, can have additional H₂ in their colon above what is already being utilized by methanogens and sulfidogens (14, 269). Therefore, *E. lenta* strains' ability to oxidize bile acids, if solely determined by availability of H₂, could be altered based on the amount of bacterial fermentation, presence of methanogens, presence of sulfidogens, and presence of sulfate/sulfite in the colon (Figure 3.30). This ability to metabolize primary bile acids would then affect the ability for 7 α -dehydroxylating bacteria to product more toxic secondary bile acids.

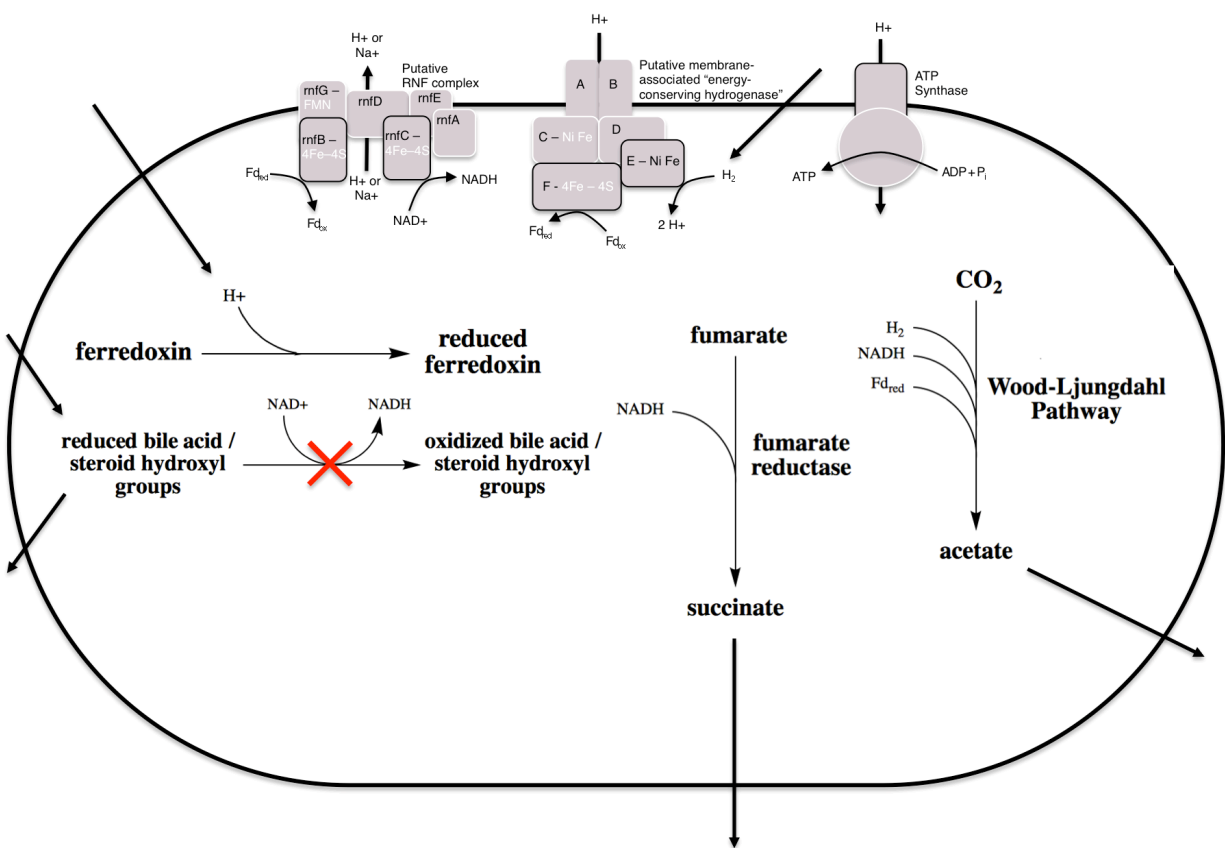
Current metrics for measuring the “metabolic potential” of an individual’s gut microbiome relies on OTUs, or groups of bacteria able to carry out specific metabolic reactions. However, this method lacks the resolution to see both differences between members of the same OTUs, such as C592 vs. other strains of *E. lenta*. Additionally, it cannot adequately take into account other variables that may affect microbial metabolism *in vivo* more than whether or not the genes are present, demonstrated by C592 and *E. lenta* bile acid oxidation reliance on a lack of available higher-energy electron donors.

Since secondary bile acids have been shown to be toxic molecules involved in many pathophysiological gastrointestinal disorders, *E. lenta* may turn out to be a very desirable bacterium in the colon, under the right circumstances. However, not all *E. lenta* strains were created equal. A strain such as C592, which does not contain the cardiac glycoside reductase operon nor the putative 21-dehydroxylase gene, may be a better probiotic candidate.

Figure 3.30: Illustration of C592 whole cell redox balancing with bile acids under high H₂ partial pressure

C592, under high H₂ partial pressure, significantly cuts back on its metabolism of bile acids. This is likely due to the fact that H₂ is able to directly reduce oxidized ferredoxin via cytoplasmic and membrane bound ferredoxin oxidoreductases. Reduced ferredoxin could then either be cycled through the RNF complex to generate reduced pyridine nucleotides or be used in other metabolic processes, such as the Wood-Ljungdahl pathway. Increased concentration of intracellular reduced pyridine nucleotides would inhibit the oxidation of bile acids.

Under high H₂ partial pressure



Additionally, it has been shown that metabolism of primary bile acids has been associated with a resistance to antibiotic-induced *C. difficile* infection (209). However, the effects of oxo-bile acid derivatives have not been studied. Future experiments are warranted to look at the possible protective effects oxo-bile acids could have to prevent *C. difficile* spore germination.

The major products of C592 and *E. lenta* bile acid metabolism determined in this study, oxo-bile acids, may be the explanation behind previous studies involving *E. lenta*. In a study of conventionalized ex-germ free mice, Claus et al. found that both the *C. scindens* and *E. lenta* OTUs were correlated with significant increases in hepatic triglyceride levels. The authors hypothesized that secondary bile acids DCA and LCA, produced by gut microbes such as *C. scindens*, were responsible for this increase since they are the most potent bile acid activators for TGR-5, which can ultimately lead to GLP-1 production, pancreatic insulin release, and hepatic triglyceride synthesis. However, *E. lenta* is not shown to make secondary bile acids DCA or LCA, which was also confirmed by this study. This suggests that other bile acid derivatives made by *E. lenta*, such as oxo-bile acids, have a significant role in modulating host physiology. More studies are needed to see the effects of varying oxidation states of the various hydroxyl groups on primary bile acids CA and CDCA to further understand this interaction.

The studies described in this report give insight into how *E. lenta* and novel strain C592 are able to link bile acid metabolism to redox balancing. It is the first report of acetogenic gene clusters in *E. lenta* and asserts its role as an acetogen in the gut microbiome. The formation of oxo-bile acid derivatives is also shown to inhibit microbial 7α -dehydroxylation. More studies, like those outlined above, are needed to understand the complex interactions between *E. lenta*, other gut

microbes, and the host under varying conditions which might alter its bile acid and steroid metabolic profile. However, it is apparent that oxo-bile acids, often overlooked as metabolic intermediates, are important molecules both for gut microbial physiology and for host physiology.

Chapter 4: *Clostridium scindens* ATCC 35704 Δ 4,6 reductase gene discovery

Introduction:

The human liver synthesizes two primary bile acids from cholesterol, cholic acid (3 α , 7 α , 12 α -trihydroxy-5 β -cholan-24-oic acid; CA) and chenodeoxycholic acid (3 α , 7 α -dihydroxy-5 β -cholan-24-oic acid; CDCA). Bile acids are conjugated to either taurine or glycine and secreted into the gallbladder where they form a major constituent of bile. Meal induced hormonal stimulation of the gallbladder results in secretion of bile into the small bowel where bile salts function to solubilize lipids and lipid-soluble vitamins. When bile salts reach the terminal ileum, they are actively transported across the epithelium and return to the liver in the portal circulation. This process is termed the enterohepatic circulation and is 95% efficient (113). However, roughly 400-800 mg of bile salts escape into the large bowel where they encounter a population of microbes whose functional gene capacity dwarfs that of the host. Indeed, 99% of functional genes in the human are microbial and most of these reside in the gut microbiome (132). Of these functional genes, there are two classes of enzymes that have the capacity to alter bile salt structure and thereby change the composition of the bile acid pool (270).

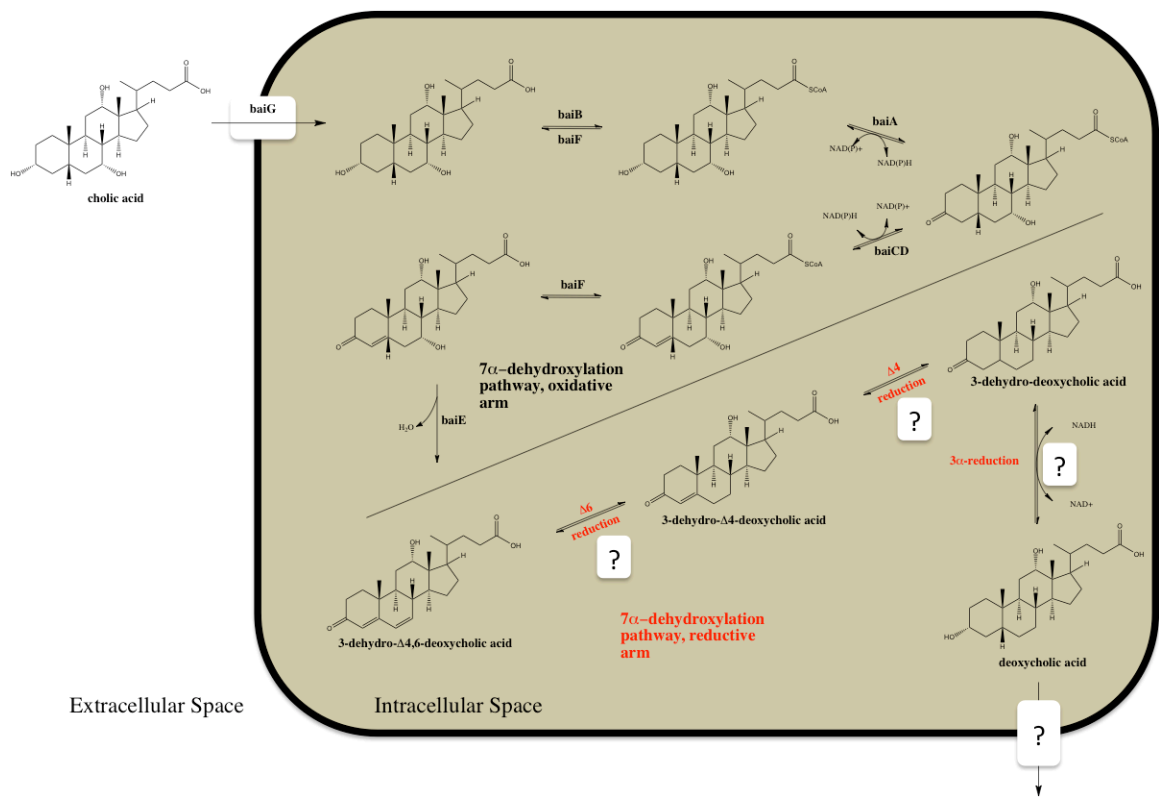
When bile salts encounter the gut microbiome, they are rapidly deconjugated to free bile acids and taurine or glycine by an enzyme encoded by the bile salt hydrolase (BSH) gene. BSH is widespread among members of the gut microbiome (116). Once the free bile acid is liberated, it becomes a substrate for bile acid 7 α -dehydroxylation (BA7). BA7 is a multi-enzyme biochemical pathway that results in the removal of the 7 α -hydroxy group through a series of oxidation

reactions (Figure 4.1). Unlike BSH, BA7 is found in only a few species within the genus *Clostridium* (125). Studies in numerous *Clostridia* strains led to the discovery of an eight-gene operon that was upregulated in the presence of primary unconjugated bile acids (262, 265, 271-277). Work on determining the enzymes in this bile acid-induced operon (*bai* operon) and the genes responsible for their production has yielded significant insight into the inner workings of this process (Figure 4.2). Primary bile acids are transported into the bacterial cell by a proton-dependent bile acid transporter encoded by the *baiG* gene (275). Once inside the cell, the first step of BA7 of primary bile acids is their ligation to CoA in an ATP-dependent fashion (273, 274, 276). After CoA ligation, the C3-hydroxyl group undergoes oxidation via the *baiA* gene (278), which is specific for CoA conjugates. Next, a C=C bond is formed between the fourth and fifth carbon by a NADH:flavin-dependent oxidoreductase encoded by the *baiCD* gene (262). The rate-limiting, non-reversible step of the reaction occurs next, the bile acid 7 α -dehydration. The gene encoding the enzyme for the 7 α -dehydratase is *baiE* (265), and the resulting bile acid products are 3-dehydro- Δ 4,6-deoxycholyl-CoA or 3-dehydro- Δ 4,6-lithocholyl-CoA, based on the starting metabolite (279). The 3-dehydro- Δ 4,6 bile acid intermediates then undergo three successive reductive steps leading to LCA or DCA. The genes responsible for the production of these enzymes have yet to be determined. Secondary bile acids are then exported from the cell, although the gene encoding the bile acid exporter has not yet been identified.

Our lab recently reported the structure and catalytic mechanism of the rate-limiting enzyme, the bile acid 7 α -dehydroxylase, encoded by the *baiE* gene, that converts 7 α ,12 α -dihydroxy-5 β -3-dehydro-chol-4-en-24-oic acid to 12 α -dihydroxy-5 β -3-dehydro-chol-4,6 dien-24-oic acid (279). The bile acid reaction product of the BaiE undergoes three reductions at C4- C5, C6-C7 and

Figure 4.1: Schematic of 7 α -dehydroxylation pathway in *Clostridium scindens* ATCC 35704.

This multi-step enzymatic process to remove the C7 α -hydroxyl group contains an oxidative arm, an irreversible 7 α -dehydration step, and a reductive arm that ultimately forms deoxycholic acid from cholic acid. The enzymes that constitute the reductive arm of this pathway are currently unidentified, although a Δ 4 and a Δ 6 reduction are two of the three proposed reaction steps in the pathway.



Adapted from (125)

finally the 3-oxo-group is converted to a 3 α -hydroxy forming DCA, a major secondary bile acid produced in the vertebrate gut. Genes in the “oxidative” arm have been identified and characterized (113), while genes in the “reductive” arm have yet to be identified. Here, we report the identification and initial characterization of a recombinant flavoprotein involved in the metabolism of 3-dehydro-DCA. Our phylogenetic analysis identified this gene in other bile acid BA7 bacteria. Mass spectrometric analysis of the product revealed a loss of four atomic mass units (amu) suggesting the formation of two double bonds. We suggest likely end products generated by this novel enzyme.

Results

Previous work in our laboratory identified bile acid intermediates in the “reductive arm” of the bile acid pathway including a 3-oxo-4 and a 3-oxo-4,6-intermediate (143). We also showed that oxidation of 3-dehydro-CDCA (7 α -hydroxy) and 3-dehydro-UDCA (7 β -hydroxy) prior to bile acid 7 α -dehydroxylation is catalyzed by stereo-specific NAD-dependent flavin oxidoreductases encoded by the *baiCD* and *baiH* genes, respectively (262). Therefore, we searched the annotated genome of *C. scindens* ATCC 35704 for “flavin oxidoreductase”. Our search identified 24 genes annotated as containing flavin-binding domains (Table 4.1). The BaiCD and BaiH proteins were identified in the search, previously demonstrated to oxidize the C₄-C₅ of primary bile acids prior to 7 α -dehydration (262). One ORF in particular, EDS08212.1, was selected for further analysis. The deduced amino acid sequence is in the HpnE squalene-associated FAD-dependent desaturase domain family, an enzyme involved in the mammalian cholesterol biosynthesis pathway (Figure 4.2). Taken together, this suggests that EDS08212.1 is a flavoprotein similar to those that metabolize sterols and may be involved in bile acid metabolism.

We overexpressed EDS08212.1 as a C-terminal streptavidin-tagged recombinant protein (rEDS08212) in *E. coli* BL21 (DE3) RIL. The predicted amino acid sequence is 44.5 kDa, and we observed a single band by SDS-PAGE after streptactin affinity chromatography at 46.5 \pm 2 kDa (Figure 4.3). After binding crude *E. coli* extracts overexpressing rEDS08212.1 and washing with binding buffer (see Materials and Methods), we observed a bright yellow protein that eluted during the desthiobiotin elution step (Figure 4.3). The rEDS08212.1 was stable only for <12 hrs

Table 4.1: Flavin reductases identified in the genome of *Clostridium scindens* ATCC 35704

Accession Number	Annotation	Regions/folds	Deduced Mr (kDa)
EDS06786.1	flavin reductase-like protein	Pyridoxine 5'-phosphate oxidase-like and flavin reductase-like proteins	24.2
EDS08212.1	flavoprotein family protein	squalene-associated FAD-dependent desaturase	45.5
EDS07700.1	flavin reductase-like protein	NADH-FMN oxidoreductase RutF, flavin reductase(DIM6/NTAB) family	21.1
EDS08305.1	flavin reductase	Multimeric flavodoxin WrbA	28.7
EDS06663.1	flavin reductase	NAD(P)H dehydrogenase, quinone family	19.8
EDS08737.1	pyridine nucleotide-disulfide oxidoreductase	Uncharacterized NAD(FAD)-dependent dehydrogenases	70.8
EDS08749.1	rubredoxin	rubredoxin	23.7
EDS07050.1	Nitroreductase	Nitro_FMN_reductase	20.3
EDS06718.1	rubredoxin	rubredoxin_SM	79
	oxidoreductase, 2-nitropropane dioxygenase family protein	Dioxygenases related to 2-nitropropane dioxygenase	38.4
EDS06682.1			
EDS05114.1	4Fe-4S binding domain protein	NAD(P)H-flavin oxidoreductase	30.1
EDS08567.1	Rubrerhythrin	rubredoxin_SM	23.4
EDS08382.1	pyridine nucleotide-disulfide oxidoreductase	Uncharacterized NAD(FAD)-dependent dehydrogenases	69.5
EDS08369.1	nitroreductase family protein	NAD(P)H-flavin oxidoreductase	21.7
EDS07342.1	hypothetical protein	NADH-FMN oxidoreductase RutF, flavin reductase(DIM6/NTAB) family	19.7
EDS07048.1	hypothetical protein	Nitroimidazol reductase NimA or a related FMN-containing flavoprotein	19.6
EDS06690.1	putative enoyl-[acyl-carrier-protein] reductase II	Dioxygenases related to 2-nitropropane dioxygenase	33.2
EDS06281.1	rubredoxin	Rubrerhythrin	19.8
EDS06280.1	Rubrerhythrin	Rubrerhythrin	22.2
EDS06153.1	NADH oxidase	OYE_like_FMN_family	70.1
EDS05767.1	pyridine nucleotide-disulfide oxidoreductase (BaiCD)	ADH oxidase (NoxB-2)	70.1
EDS05762.1	pyridine nucleotide-disulfide oxidoreductase (BaiH)	noxB-1; NADH oxidase	72
WP_004604785.1	flavin reductase	rubredoxin	23.6
WP_039909174.1	2,4-dienoyl-CoA reductase	OYE_like_FMN_family	72.5

Figure 4.2: Schematic representation of the reaction catalyzed by squalene-desaturase and the oxidation of 3-dehydro-4-DCA to 3-dehydro-DCA in the 7 α -dehydroxylation pathway.

A gene encoding a putative flavoprotein (EDS08212.1) in the FAD-dependent squalene-desaturase family is hypothesized to be involved in the “reductive arm” of the bile acid 7 α -dehydroxylating pathway.

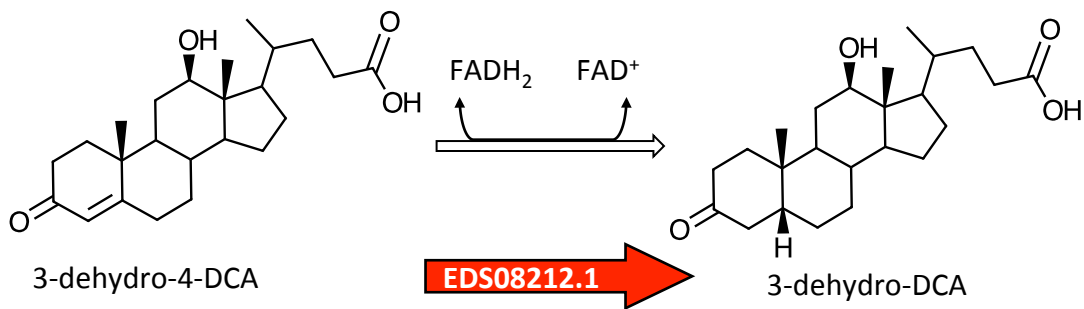
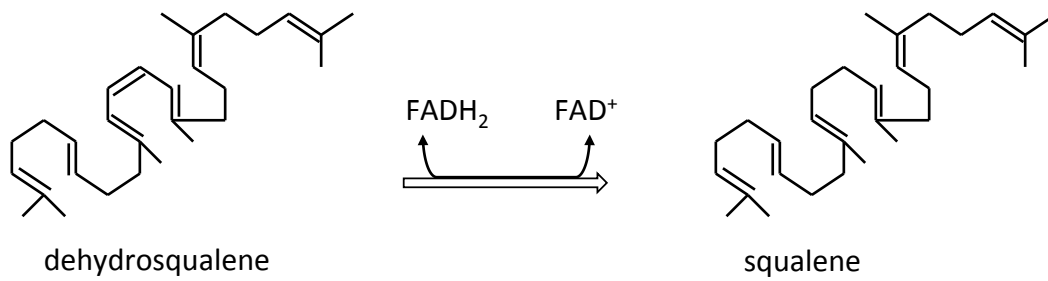
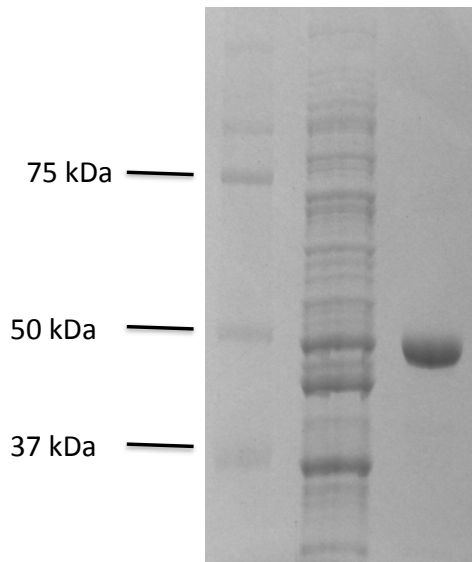


Figure 4.3: Overexpression and purification of rEDS08212.1 from *C. scindens* ATCC 35704

A: Lane “M” is the protein marker, lane “1” is the soluble crude extract (30 µg), lane “2” is the eluent following streptavidin affinity chromatography (2 µg). **B:** rEDS08212.1 bound to streptavidin column after thorough washing displaying distinctive yellow pigmentation.

A.



B.



after which visible precipitation was evident. Storage at -20°C in 50% glycerol did not improve solubility.

We detected formation of a single product on TLC after incubation with rEDS08212.1 (0.5 µg) in the presence of 3-dehydro-DCA, but not DCA, at pH 7.0 (Figure 4.4). We did not observe formation of this product with heat-killed enzyme (70°C 1 min). This reaction occurred in the presence or absence of pyridine nucleotides (NAD⁺, NADH, NADP⁺, NADPH), suggesting that this reaction proceeds by bile acid-dependent flavin reduction followed by regeneration of FAD⁺ via chemical oxidation via molecular oxygen (data not shown).

Next, the reaction substrate ($R_f=0.78$) and product ($R_f=0.40$) were scraped from the TLC plate, extracted from the silica gel by ethyl acetate, and dried under nitrogen gas for mass spectrometry analysis. The substrate had a retention time of 25 minutes and a major mass ion was detected in positive mode at 391.2878 m/z and 389.2559 m/z in negative mode, as predicted (Figure 4.5).

The product retention time was 22.5 minutes with a major mass ion in positive mode of 387.1681 m/z and 385.1739 m/z in negative mode. These data suggest that the substrate lost four atomic mass units (amu) and may potentially be involved in the metabolism of two carbon-carbon double bonds. This observation was repeated in three separate reactions and confirmed.

In order to investigate the most likely origin of the *C. scindens* ATCC 35704 EDS08212.1 gene, we have performed a wide-scale maximum-likelihood phylogenetic analysis involving all protein sequences from the public databases displaying a reasonable level of similarity to the protein

Figure 4.4: Autoradiograph of thin layer chromatography separation of rEDS08212.1 reaction products from [24-¹⁴C] 3-dehydro-DCA.

A. [24-¹⁴C] DCA TLC standard, **B.** [24-¹⁴C] 3-dehydro-DCA TLC standard, **C.** [24-¹⁴C] 3-dehydro-DCA + rEDS08212.1 + 150 μM NAD⁺, **D.** 3-dehydro-DCA + rEDS08212.1 + 150 μM NAD⁺ biological replicate, **E.** [24-¹⁴C] DCA standard, **F.** [24-¹⁴C] 3-dehydro-DCA + heat-killed rEDS08212.1, **G.** [24-¹⁴C] 3-dehydro-DCA + heat-killed rEDS08212.1 + 150 μM NAD⁺.

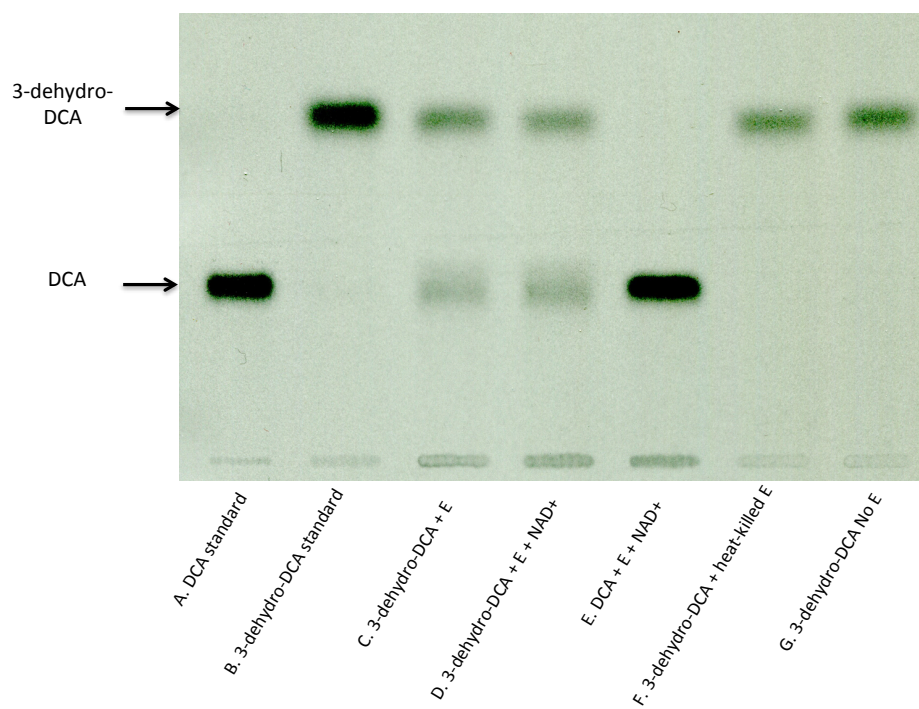
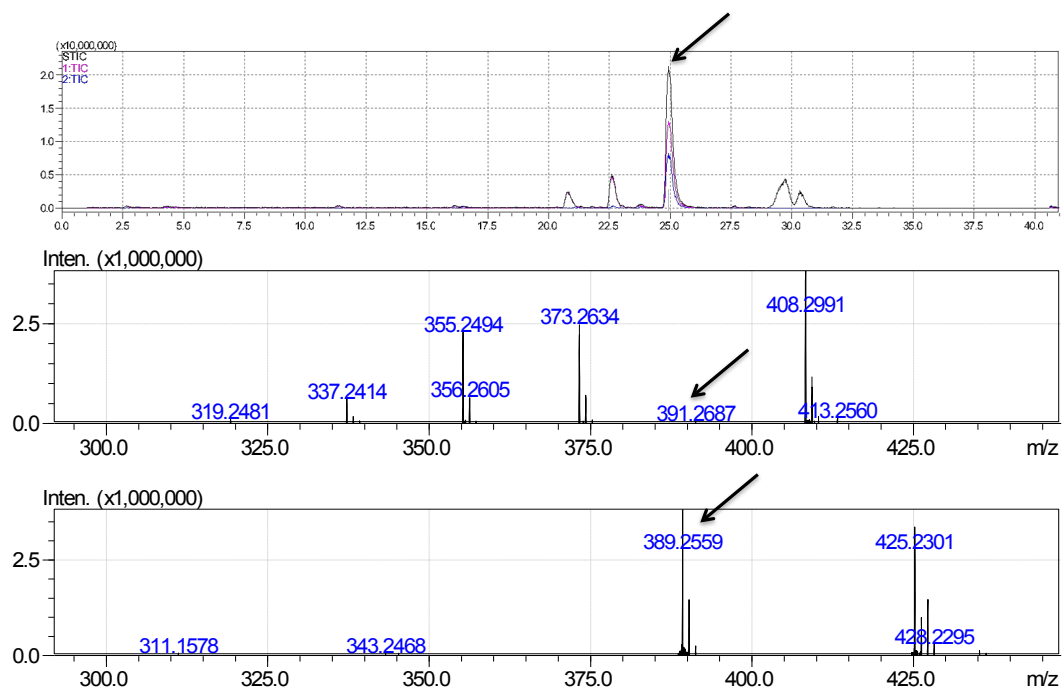


Figure 4.5: LCMS-IT-TOF analysis of rEDS08212.1 reaction products.

Substrate and product were separated from TLC, scraped and bile acids extracted from silica, concentrated and analyzed by LCMS. A. From top-bottom, UPLC profile with major peak identified at R_T 25 minutes (substrate), Positive mode analysis of R_T 25 minutes peak, Negative mode analysis of R_T 25 minutes peak. B. From top-bottom, UPLC profile with major peak identified at R_T 22.5 minutes (product), Positive mode analysis of R_T 25 minutes peak, Negative mode analysis of R_T 22.5 minutes peak.

A.



characterized herein. Our final alignment involved 1,273 protein sequences from a diverse assemblage of bacterial groups, as well as some eukaryotic sequences.

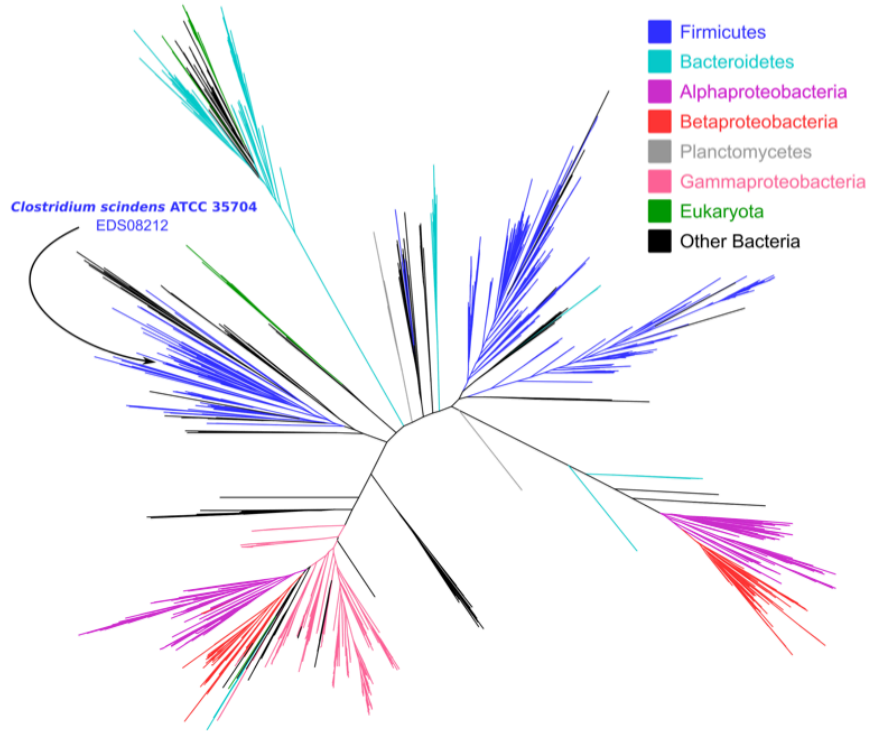
A previously determined sequence, from Clostridiales bacterium VE202-26 (280), is identical to the one for *C. scindens* VPI 12708, at the nucleotide as well as the amino acid level. Thus, as expected, they group in the tree with branch lengths of zero and bootstrap support of 100. The sequence for *C. scindens* ATCC 35704 clusters very closely to these two other sequences, also with the highest bootstrap support. The other *Clostridium* sequence nearest in the tree belongs to *C. hylemonae* DSM 15053, a bacterium previously shown to harbor the *bai* pathway (272).

The EDS08212.1 gene and homologous genes from the strains analyzed here grouped deep within a large group of Firmicutes bacteria (Figure 4.6) and, as seen in Figure 4.6-B, group with a number of bacteria from the Lachnospiraceae and Ruminococcaceae families, as seen previously in a phylogenomic analysis of 20 single-copy protein-coding genes that were present in 99 Firmicutes genomes (217). Thus, the EDS08212.1 gene in *C. scindens* strains does not seem to have been derived from a horizontal gene transfer event, since its phylogeny agrees closely with the species phylogeny.

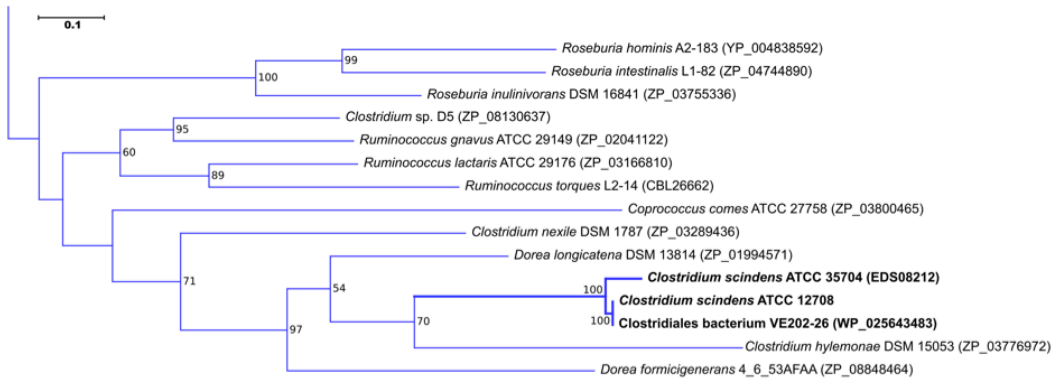
Figure 4.6: Maximum likelihood phylogenetic tree of EDS08212.1 from *Clostridium scindens* ATCC 35704.

A. Wide-scale phylogeny (1,273 protein sequences). **B.** Details of the region of the tree containing EDS08212.1. Values on nodes represent bootstrap support (only 50 or higher shown).

A.



B.



Discussion:

The conversion of primary to secondary bile acids such as DCA and LCA is implicated in diseases of the GI tract, including liver (179) and colorectal cancer (67, 281). The bile acid 7 α -dehydroxylation pathway has only been reported in a few species of intestinal clostridia, including *C. scindens* (113, 125). The genes encoding the enzymes for the oxidative half of the pathway have been delineated in numerous *Clostridium* species (113). However, the enzymes catalyzing the final three reductive reactions have not yet been identified (Figure 4.1).

In the current study, we identified a likely candidate for the first two reductive steps following 7 α -dehydration. The gene encoding EDS08212.1 in *C. scindens* ATCC 35704 is predicted to encode a flavin-dependent squalene desaturase, a reaction that is analogous to the oxidation/reduction of secondary bile acids. We cloned and overexpressed rEDS08212.1 in *E. coli* and purified the enzyme to apparent electrophoretic homogeneity. The enzyme yielded a bright yellow color, indicative of flavin-binding. The enzyme was active against 3-dehydro-DCA but not DCA, suggesting specificity for the A-ring. We observed a loss of 4 amu from the substrate after purification of the reaction products by TLC and then UPLC-IT-TOF-MS. This suggests that two oxidations are occurring, strongly indicating the formation of the 3-dehydro-4,6-DCA intermediate. Alternatively, the aerobic degradation of cholic acid to carbon dioxide by soil microorganisms, particularly by *Comamonas testosteroni*, results in the formation of a 3-dehydro-1,4-intermediate, which also requires two oxidations (282).

Further work is underway to confirm the specific activity of EDS08212.1, although the lack of commercial availability of substrates makes this further characterization difficult. However, we are currently testing the utilization of 3-dehydro- Δ 4,6-LCA by EDS08212.1 as a substrate for reduction under anaerobic conditions. If EDS08212.1 is confirmed to make 3-dehydro-LCA from this substrate, it will confirm the enzyme acts on the Δ 4,6 double bonds in bile acids formed during the 7α -dehydroxylation pathway. Additionally, EDS08212.1 is being tested for its pyridine nucleotide specificity, as we predict that under anaerobic conditions, NADH would be required to reduce the bound FAD/FMN.

Chapter 5: *Clostridium scindens* VPI 12708 RNAseq and 17 α -HSDH gene discovery

Introduction:

Bile acids are not the only steroidal compounds excreted by the liver that undergo enterohepatic circulation. Sharing the same four cycloalkane rings as bile acids, endogenously produced steroid hormones are conjugated to glucuronate or sulfate and then can be excreted into bile (283). The levels of excreted steroid hormones in bile are higher in females, as estrogen secretion into bile is a major mechanism used to modulate host serum levels (284). Once inside the lumen of the intestines, conjugated steroid hormones are deconjugated via hydrolysis by both host epithelial and bacterial deconjugating enzymes, such as glucuronidases and sulfatases, and deconjugated hormones can then be reabsorbed or enter the large intestine (268). Glucuronidase activity is found in some of the most abundant microbes in the gut microbiome, including *Bacteroides* species (285). After deconjugation, most steroid hormones reenter the circulation where they are eventually permanently excreted in urine. Studies have shown that treatment with broad-spectrum antibiotics increased fecal secretion of steroid hormones and decreased renal excretion, likely due to the lack of deconjugation and subsequently increased loss of steroid hormones in the feces (286). Interestingly, dietary changes such as increased fiber or decreased dietary fat have also been associated with increased fecal excretion and decreased levels of circulating androgenic steroid hormones (284). Both increased fiber and a vegetarian diet low in fat have been shown to be associated with reduced fecal bacteria β -glucuronidase activity, which would result in a decreased reuptake of excreted steroid hormones (287, 288).

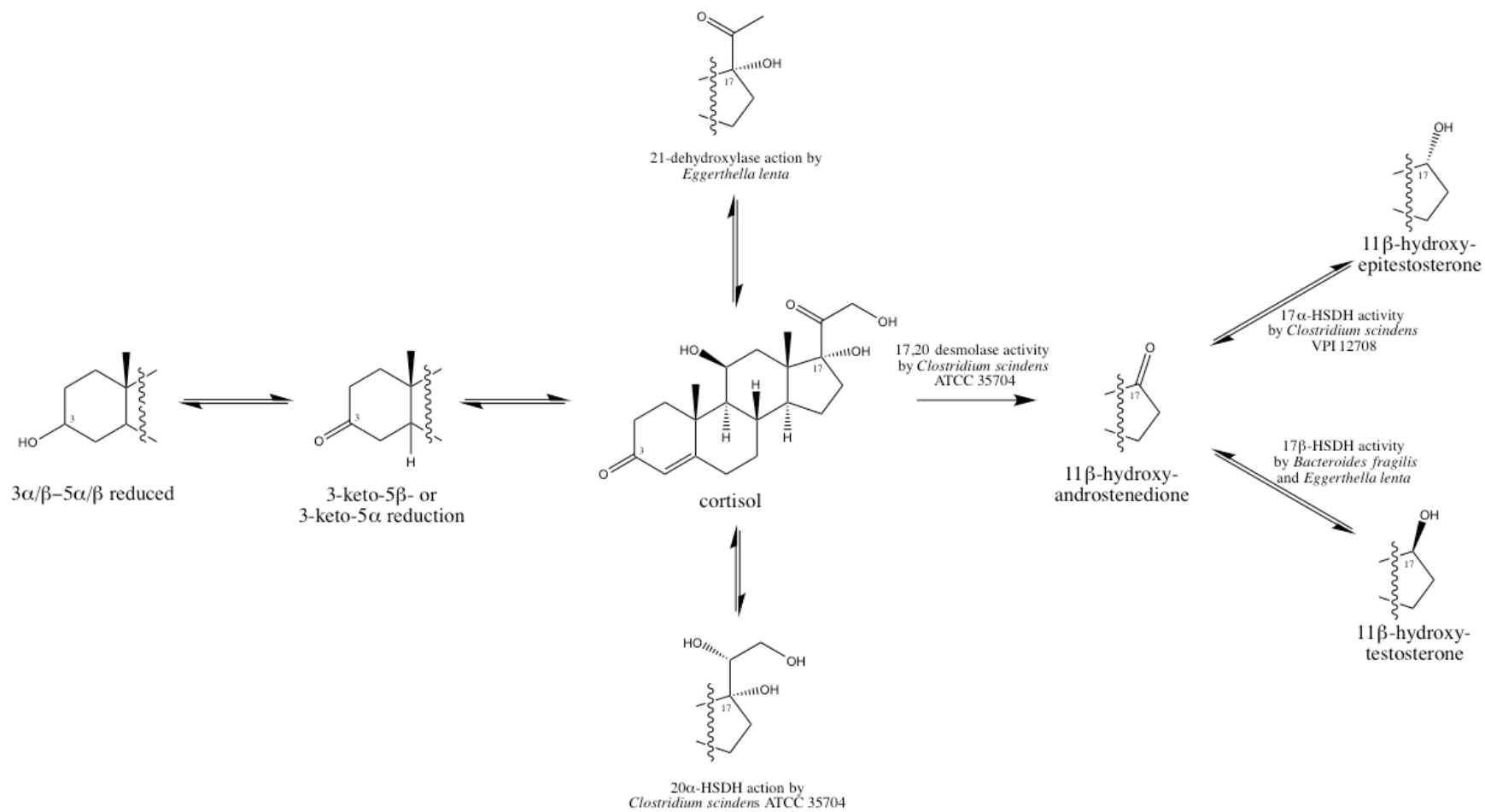
Once deconjugated, steroid hormones that escape reabsorption in the intestines, similarly to bile acids, become substrates for various bacterial biotransformations. In the anaerobic environment of the large intestine, the majority of bacterial steroid conversions are hydrolytic and reductive in nature. On C₂₁ and C₁₇ steroid hormones, the 4-ene-3-keto moiety can be reduced to either 3 α / β and 5 α / β , leading to a variety of differing metabolites (289-291). The reduction of this moiety generally leads to less biologically active molecules (268). The majority of bacteria shown to have this activity are within the *Clostridium* genus.

Other bacterial conversions target the side-chain of glucocorticoids (Figure 5.1). As discussed previously, *Eggerthella lenta* has been shown to have 21-dehydroxylase activity (247, 248, 292). This bacterium is able to convert deoxycortisone to progesterone. Other bacterial species within the genus *Clostridia* have been shown to have 17,20 desmolase activity capable of performing side-chain cleavage of glucocorticoids to form androgens. A recent study identified a gene cluster in *Clostridium scindens* ATCC 35704 encoding the steroid-17,20-desmolase, which is inducible by cortisol (217). In *C. scindens*, it was shown through RNAseq analysis that the 17,20-desmolase may feed the two carbons released from cortisol into the pentose-phosphate pathway for cellular growth and maintenance (217).

The product of 17,20-desmolase metabolism of cortisol, 11 β -hydroxy-androstenedione, and endogenously produced androgens such as testosterone and its precursor androstenedione harbor a C17-hydroxyl group that can undergo bacterial metabolism in the colon. The C17-keto group of androstenedione and 11 β -hydroxy-androstenedione can be reduced by *Bacteroides fragilis* to testosterone and 11 β -hydroxy-testosterone, respectively (291). Additionally, the same C17-keto

Figure 5.1: Biotransformations of cortisol by gut microbes.

Cortisol can undergo numerous biotransformations. Numerous strains of bacteria have been shown to $3\alpha/\beta$ and $5\alpha/\beta$ reduce the 4-ene-3-keto moiety of cortisol. *Clostridium scindens* ATCC 35704 has been shown to harbor 20α -HSDH activity on cortisol. *Eggerthella lenta* has been shown to have 21-dehydroxylase activity on cortisol. *Clostridium scindens* ATCC 35704 encodes a 17,20 desmolase able to convert cortisol to 11β -hydroxy-androstenedione. *Clostridium scindens* VPI 12708 has been shown to have 17α -HSDH activity on C17 steroid molecules. *Bacteroides fragilis* and, in this work, *Eggerthella lenta* has been shown to have 17β -HSDH activity on C17 steroids.



Adapted from (217)

group on androstenedione can be reduced to epitestosterone by *Clostridium scindens* VPI 12708 (228). Unpublished results from our lab have also shown that *C. scindens* VPI 12708 recognizes 11 β -hydroxy-androstenedione. Since both of these bacterial strains are present in the colon, it is possible that strains would be able to epimerize the C17-hydroxyl group on these molecules, interconverting these molecules between androgenically active (testosterone) and inactive (epitestosterone) compounds. The physiological purpose behind these biotransformation reactions is still unknown, but both interkingdom signaling and microbe-microbe signaling are valid hypotheses for why the enzymatic potential to interconvert these androgenic compounds persists in the colon.

The androgenic steroid molecules that are excreted in bile, become unconjugated and substrates for further bacterial metabolism can be physiologically active on host tissue even at nanomolar concentrations. This physiological activity can vary based on the presence, stereospecificity, and reductive state of the functional groups on the steroid core (293). It is important therefore to find the genes responsible for encoding enzymes that recognize androgens in the microbes that are known members of the gut microbiome. *Clostridium scindens* VPI 12708 has been shown to have 17 α -hydroxysteroid dehydrogenase activity, but the gene responsible for its production has never been found (de Prada 1994). Additionally, a very similar strain, *Clostridium scindens* ATCC 35704 was recently shown to metabolize endogenous steroid compounds, but not have 17 α -HSDH activity (217). I therefore set out to locate the gene in *Clostridium scindens* VPI 12708 responsible for the production of the 17 α -HSDH enzyme.

Results:

Previous work in *Clostridium scindens* VPI 12708 suggested that its 17α -hydroxysteroid dehydrogenase activity was inducible by androstenedione (228). We therefore set out to confirm that *C. scindens* 12708 had androstenedione-inducible 17α -HSDH activity. *C. scindens* VPI 12708 was grown overnight and induced with $100\mu\text{M}$ androstenedione. Overnight cultures were then centrifuged, the pellets washed with buffer, and then incubated with radiolabeled 11β -hydroxy-androstenedione (11β -OHAD). Results showed that over the course of two hours, androstenedione-induced *C. scindens* VPI 12708 generated reduced 11β -OHAD (Figure 5.2). Uninduced *C. scindens* VPI 12708 did not form a product from 11β -OHAD over the same time period (Figure 5.2). This suggested that metabolism of androstenedione was an inducible trait in this bacterium.

We also wanted to confirm that the product of androstenedione metabolism was epitestosterone, a 17α -reduced compound. Overnight cultures of *C. scindens* VPI 12708 were inoculated with $100\mu\text{M}$ androstenedione and allowed to grow overnight. Cultures were then extracted with ethyl acetate and the resulting organic layer was concentrated and run on HPLC using a reverse-phase C18 column. The formation of a secondary product was monitored at 240nm and fractionally collected (Figure 5.3). This isolated metabolite of androstenedione was then sent for NMR analysis. The resulting NMR structure confirmed that *C. scindens* VPI 12708 produced epitestosterone from androstenedione (Figure 5.4).

Figure 5.2: *Clostridium scindens* VPI 12708 exhibits inducible 17 α -HSDH activity

Clostridium scindens VPI 12708 was grown in the presence of 100 μ M androstenedione (induced) or without androstenedione (uninduced) overnight and then cells pelleted, washed, and exposed to fresh radiolabeled 11 β -hydroxyl-androstenedione. Conversion was tracked overtime with 1mL aliquots taken out and quenched with ethyl acetate. Organic extracts were run on TLC and the formation of a secondary metabolite was visualized over time only in the induced whole cell samples.

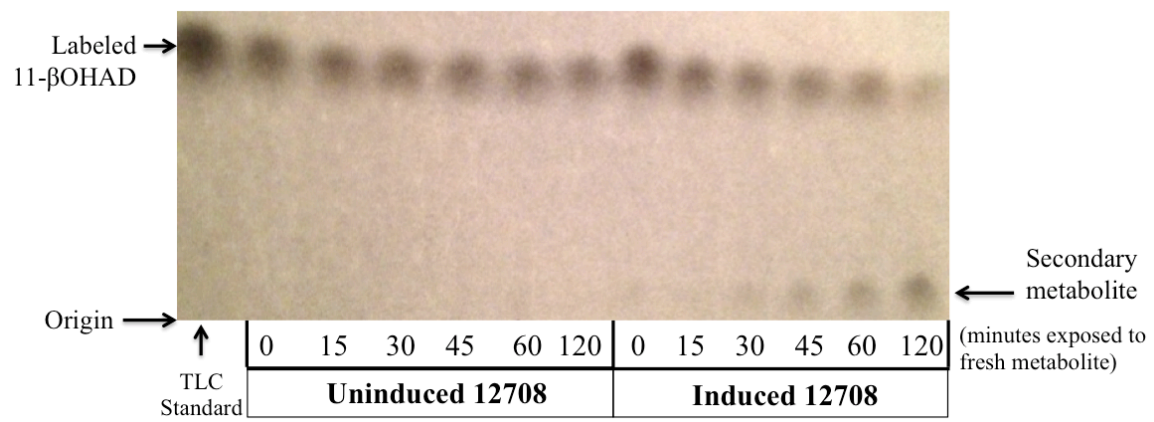


Figure 5.3: *Clostridium scindens* VPI 12708 produces a secondary metabolite from androstenedione that maintains the 4-ene-3-keto moiety

Clostridium scindens VPI 12708 was grown overnight in 10mL BHI in the presence of 100mM androstenedione and then extracted with ethyl acetate. 20% of the total organic extract was run on HPLC to separate androstenedione from its metabolite. Other than the injection peak, which is visible on all injections and corresponds with an influx of 100% methanol, the two peaks absorbing at 240nm correspond to the two steroids. Androstenedione, based on control data, elutes around 30 minutes. The secondary metabolite eluted at approximately 52 minutes. This elution also matched that of commercially obtained epitestosterone. The collected sample was subsequently sent for NMR analysis.

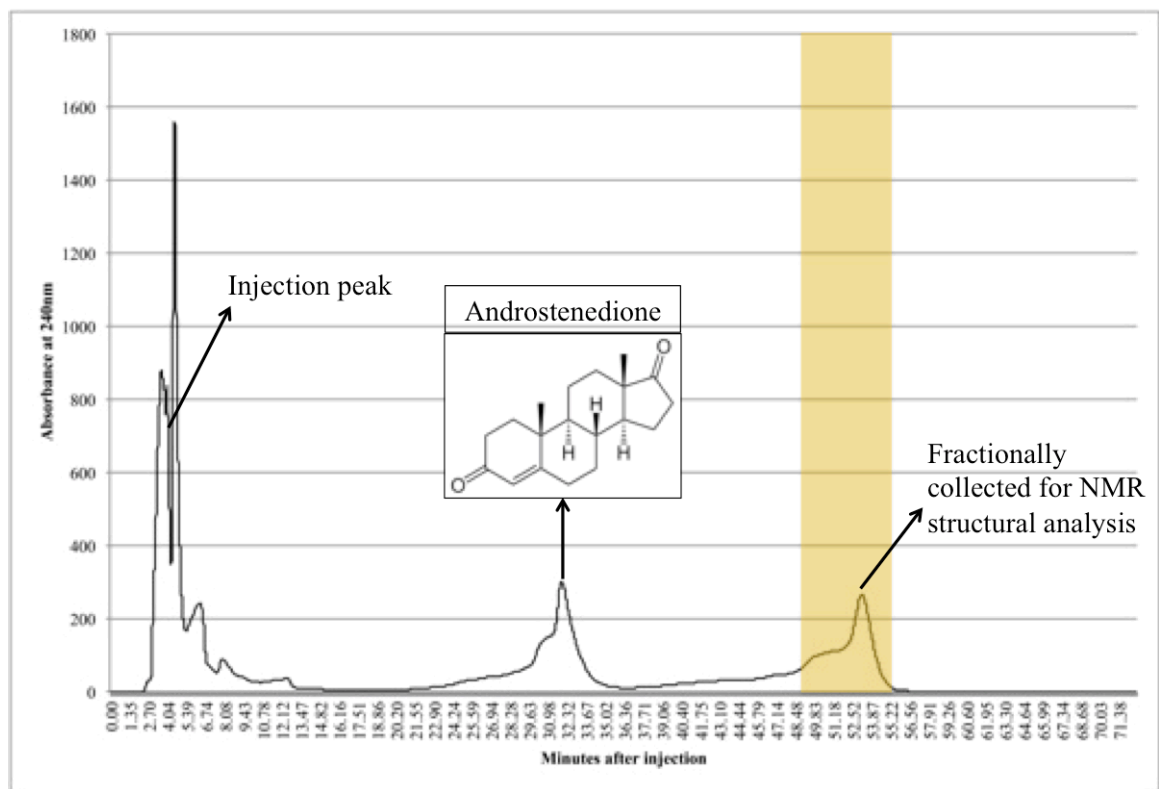
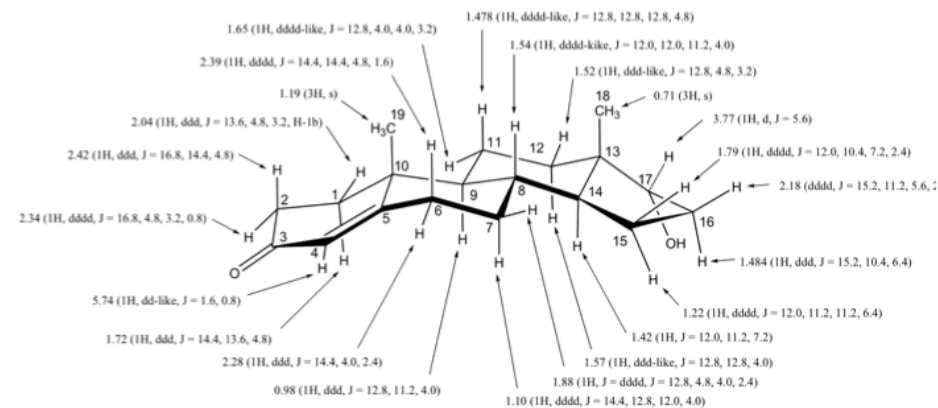


Figure 5.4: NMR analysis of the *Clostridium scindens* VPI 12708 androstenedione metabolite confirms epitestosterone formation

NMR analysis confirmed epitestosterone was being formed by *Clostridium scindens* VPI 12708. NMR analysis was performed on the fractionally collected *C. scindens* VPI 12708 androstenedione metabolite (see Figure 5.3). NMR analysis was performed as described previously (217). Table on left denotes hydrogen positioning. Table on right compares chemical shift, in ppm, as compared to two previous NMR spectrums of epitestosterone from literature (294, 295). Both findings are congruent with the *C. scindens* VPI 12708 metabolite being identified as epitestosterone.



H-1ax	1.72 (1H, ddd-like, J = 14.4, 13.6, 4.8, H-1a)
H-1eq	2.04 (1H, ddd, J = 13.6, 4.8, 3.2, H-1b)
H-2ax	2.42 (1H, ddd, J = 16.8, 14.4, 4.8, H-2b)
H-2eq	2.34 (1H, dddd, J = 16.8, 4.8, 3.2, 0.8, H-2a)
H-4	5.74 (1H, dd-like, J = 1.6, 0.8, H-4)
H-6ax	2.39 (1H, dddd, J = 14.4, 14.4, 4.8, 1.6, H-6b)
H-6eq	2.28 (1H, ddd, J = 14.4, 4.0, 2.4, H-6a)
H-7ax	1.10 (1H, dddd, J = 14.4, 12.8, 12.0, 4.0, H-7a)
H-7eq	1.88 (1H, J = dddd, J = 12.8, 4.8, 4.0, 2.4, H-7b)
H-8	1.54 (1H, dddd-like, J = 12.0, 12.0, 11.2, 4.0, H-8)
H-9	0.98 (1H, ddd, J = 12.8, 11.2, 4.0, H-9)
H-11ax	1.478 (1H, dddd-like, J = 12.8, 12.8, 12.8, 4.8, H-11a)
H-11eq	1.65 (1H, dddd-like, J = 12.8, 4.0, 4.0, 3.2, H-11b)
H-12ax	1.57 (1H, ddd-like, J = 12.8, 12.8, 4.0, H-12b)
H-12eq	1.52 (1H, ddd-like, J = 12.8, 4.8, 3.2, H-12a)
H-14	1.42 (1H, J = 12.0, 11.2, 7.2, H-14)
H-15a	1.22 (1H, dddd, J = 12.0, 11.2, 11.2, 6.4, H-15a)
H-15b	1.79 (1H, dddd, J = 12.0, 10.4, 7.2, 2.4, H-15b)
H-16a	1.484 (1H, ddd, J = 15.2, 10.4, 6.4, H-16a)
H-16b	2.18 (ddd, J = 15.2, 11.2, 5.6, 2.4, H-16b)
H-17	3.77 (1H, d, J = 5.6, H-17)
18-CH3	0.71 (3H, s, H-18)
19-CH3	1.19 (3H, s, H-19)

	Sample 17-epi-testosterone	Testosterone ¹	Testosterone ²
C1	35.8	36.1	35.6
C2	33.9	34.1	33.8
C3	199.5	198.0	199.4
C4	123.9	124.2	123.6
C5	171.3	170.4	171.0
C6	32.9	32.8	32.7
C7	32.3	32.2	31.5
C8	35.9	36.1	35.0
C9	53.6	54.6	53.9
C10	38.7	39.0	38.6
C11	20.6	21.2	20.6
C12	31.2	37.1	36.4
C13	45.1	43.2	42.7
C14	48.2	51.1	50.4
C15	24.6	23.8	23.2
C16	32.4	30.7	30.1
C17	79.7	81.3	81.0
C18	16.9	11.3	11.0
C19	17.4	17.3	17.3

1) 25.2 MHz [JOC, 46, 1127 (1981)]

2) 25.2 MHz [JCS, Perkin 1, 1956 (1975)]

After confirming *C. scindens* VPI 12708 has inducible 17 α -HSDH activity, we next set out to find the gene encoding the respective enzyme. RNA-seq had been used previously to great effect in identifying the cortisol-induced 17,20 desmolase operon in a highly similar strain of *Clostridium scindens* (ATCC 35704) (217). Therefore, we set out to use the same technique for the identifying the *C. scindens* VPI 12708 17 α -HSDH. Additionally, RNAseq could be used simultaneously to study the changes in the overall transcriptome when certain steroid hormones and bile acids are present. In this aim, *C. scindens* VPI 12708 cultures were grown to mid-log phase under varying inducing conditions, including cortisol, androstenedione, cholic acid, and allocholic acid. The cells were pelleted and frozen at -80°C and the supernatants were extracted and run on TLC to confirm substrate metabolism (data not shown). Total RNA was then isolated from cell pellets following methods derived from Ridlon et al., including the enrichment of mRNA using custom designed biotinylated polynucleotides (217). rRNA depleted samples were used to generate libraries for sequencing using NEBNext Ultra RNA Library Prep Kit for Illumina and sequenced using the MiSeq 2 x 300 bp protocol. Reads were then populated to a previously sequenced *Clostridium scindens* VPI 12708 genome (unpublished). Results indicated that in the cholic acid-induced and allocholic acid-induced samples, the bile acid operon (bai-operon) was significantly induced versus uninduced control (Table 5.1). These results functioned as a positive internal control, showing the quality of the RNA in these samples was high enough to determine induction of various genes against uninduced controls. Interestingly, although cortisol, androstenedione, cholic acid, and allocholic acid all share a similar steroidal backbone, their effects on the overall transcriptomic pattern in *C. scindens* VPI 12708 are

Table 5.1: Induction of bile acid inducible operon in *Clostridium scindens* VPI 12708 by cholic acid (CA) and allocholic acid (ACA)

Cholic acid-induced vs. uninduced “bai operon” Illumina MiSeq Reads						
locus	Uninduced Reads	CA-induced reads	log ₂ (fold_change)	p_value	q_value	significant
Cs12708_c00003_00018	8.28709	924.929	6.80233	0.0167	0.0894583	no
Cs12708_c00003_00019	8.4592	1268.97	7.22892	0.0018	0.0176897	yes
Cs12708_c00003_00020	0	1624.22	inf	5.00E-05	0.000844444	yes
Cs12708_c00003_00021	12.077	1433.27	6.8909	0.0654	0.210908	no
Cs12708_c00003_00022	12.5373	1431.1	6.83476	0.0167	0.0894583	no
Cs12708_c00003_00024	8.97984	1240.13	7.10958	0.0167	0.0894583	no
Cs12708_c00003_00026	12.2184	1535.93	6.97392	0.00025	0.00367742	yes
Cs12708_c00003_00027	42.0197	2020.16	5.58726	0.0167	0.0894583	no
Allocholic acid-induced vs. uninduced “bai operon” Illumina MiSeq Reads						
locus	Uninduced Reads	ACA-induced reads	log ₂ (fold_change)	p_value	q_value	significant
Cs12708_c00003_00018	8.31544	140.121	4.07474	0.0019	0.0156222	yes
Cs12708_c00003_00019	8.48946	135.107	3.99229	0.00035	0.00390943	yes
Cs12708_c00003_00020	0	174.78	inf	5.00E-05	0.000700592	yes
Cs12708_c00003_00021	12.1164	109.976	3.18216	0.11395	0.283439	no
Cs12708_c00003_00022	12.5816	132.8	3.39987	0.001	0.00935968	yes
Cs12708_c00003_00024	9.01056	89.4478	3.31136	0.00625	0.0396766	yes
Cs12708_c00003_00026	12.2606	119.024	3.27915	5.00E-05	0.000700592	yes
Cs12708_c00003_00027	42.1566	133.286	1.6607	0.0541	0.17104	no

striking (Figure 5.5). Cholic acid-induced *C. scindens* VPI 12708 transcriptomic pattern appears to cluster separately from allocholic, androstenedione, and cortisol induced transcriptomic patterns (Figure 5.5). This observation is interesting, as the only difference between cholic acid and its epimer allocholic acid is the position of the hydrogen on the fifth carbon. With hydrogen in the α -configuration, the steroid backbone of allocholic acid more closely resembles a planar steroid hormone than a bile acid. Therefore, it appears that because of this change, *C. scindens* VPI 12708 responds to it more as a steroid hormone than a bile acid, although the bai-operon is still induced, although to a lower level than what is seen from cholic acid induction (Figure 5.4).

From previous studies and unpublished data, we knew that the 17α -HSDH should have the following characteristics: be annotated to be within the SDR family or alcohol polyol dehydrogenase family; encode a polypeptide sequence around 40kDa; be induced by androstenedione and cholic acid; should have a metal binding and pyridine nucleotide binding site; not be found in similar strain *Clostridium scindens* ATCC 35704 (de Prada 1994). In contrast to the cholic acid-induced sample, there were not very many significantly induced genes in the androstenedione-induced sample (Table 5.2). Putative genes that matched the 17α -HSDH criteria were chosen for further analysis (Table 5.3).

Genes that were chosen based on the RNAseq analysis were successfully cloned into expression vectors, overexpressed in *E. coli*, purified, and tested for their 17α -HSDH activity. Constructs were made with either a C- or N-terminal streptavidin tag for column purification, or no tag in the case of whole cell extract assays, and constructs were checked for nucleotide fidelity by sequencing. Purified enzymes, whole cell extracts, and induced whole cell transformed *E. coli*

Table 5.2: Genes upregulated in *Clostridium scindens* VPI 12708 in response to androstenedione induction

Locus	Uninduced Reads	Androstenedione induced reads	log₂ (fold change)	p value	q value	significant
Cs12708_c00002_00026:0-663	225.526	969.11	2.10337	5.00E-05	0.00110607	yes
Cs12708_c00043_00034:0-1050	114.12	391.381	1.77803	5.00E-05	0.00110607	yes
Cs12708_c00073_00017:0-1962	180.598	393.201	1.12249	5.00E-05	0.00110607	yes
Cs12708_c00056_00017:0-1014	222.157	460.616	1.05198	5.00E-05	0.00110607	yes
Cs12708_c00163_00001:0-657	2456.39	4786.56	0.962446	5.00E-05	0.00110607	yes
Cs12708_c00001_00068:0-1086	211.009	409.538	0.956696	5.00E-05	0.00110607	yes
Cs12708_c00117_00003:0-840	641.622	1184.81	0.884863	5.00E-05	0.00110607	yes
Cs12708_c00060_00011:0-888	3375.83	6031.37	0.837242	5.00E-05	0.00110607	yes
Cs12708_c00002_00029:0-543	12527.7	21981.3	0.811153	5.00E-05	0.00110607	yes
Cs12708_c00064_00002:0-2043	354.865	622.498	0.810802	5.00E-05	0.00110607	yes
Cs12708_c00022_00007:0-1275	257.052	449.644	0.806724	5.00E-05	0.00110607	yes
Cs12708_c00005_00015:0-1062	442.204	760.787	0.782782	5.00E-05	0.00110607	yes
Cs12708_c00005_00016:0-1014	411.663	705.56	0.777307	5.00E-05	0.00110607	yes
Cs12708_c00005_00013:0-759	555.471	951.575	0.776607	5.00E-05	0.00110607	yes
Cs12708_c00065_00020:0-1551	628.777	1056.69	0.748936	5.00E-05	0.00110607	yes
Cs12708_c00119_00005:0-1446	273.459	459.123	0.747557	5.00E-05	0.00110607	yes
Cs12708_c00039_00001:2-2760	94.0148	157.74	0.746587	5.00E-05	0.00110607	yes
Cs12708_c00060_00013:0-657	603.456	1004.75	0.735521	5.00E-05	0.00110607	yes
Cs12708_c00038_00001:0-1506	2022.81	3350.23	0.727895	5.00E-05	0.00110607	yes

Cs12708_c00214_00001:0-555	1403.85	2300.25	0.712406	5.00E-05	0.0011 0607	yes
Cs12708_c00043_00033:0-1422	242.143	383.461	0.663222	5.00E-05	0.0011 0607	yes
Cs12708_c00002_00028:0-537	5594.94	8752.84	0.645628	5.00E-05	0.0011 0607	yes
Cs12708_c00131_00003:0-1344	405.984	628.224	0.629855	5.00E-05	0.0011 0607	yes
Cs12708_c00060_00010:0-771	2460.73	3740.22	0.604038	5.00E-05	0.0011 0607	yes
Cs12708_c00144_00011:0-627	1277.69	1914.51	0.583437	5.00E-05	0.0011 0607	yes
Cs12708_c00146_00003:0-1326	766.735	1145.99	0.57979	5.00E-05	0.0011 0607	yes
Cs12708_c00007_00064:0-2184	1370.67	2031.96	0.567989	5.00E-05	0.0011 0607	yes
Cs12708_c00075_00015:0-936	717.297	1050.21	0.550039	5.00E-05	0.0011 0607	yes
Cs12708_c00001_00016:0-1740	886.114	1295.91	0.548396	5.00E-05	0.0011 0607	yes
Cs12708_c00103_00014:0-2139	1801.65	2626.09	0.543598	5.00E-05	0.0011 0607	yes
Cs12708_c00060_00012:0-1533	583.929	850.414	0.542371	5.00E-05	0.0011 0607	yes
Cs12708_c00202_00002:0-1311	661.761	963.585	0.542102	5.00E-05	0.0011 0607	yes
Cs12708_c00149_00007:0-1335	444.439	643.149	0.533168	5.00E-05	0.0011 0607	yes
Cs12708_c00195_00007:0-828	658.498	936.879	0.508683	5.00E-05	0.0011 0607	yes
Cs12708_c00076_00015:0-1035	5197.37	7209.73	0.472162	5.00E-05	0.0011 0607	yes
Cs12708_c00023_00037:0-657	4351.25	5896.36	0.438396	5.00E-05	0.0011 0607	yes
Cs12708_c00013_00036:0-1314	642.023	860.493	0.422539	5.00E-05	0.0011 0607	yes
Cs12708_c00059_00020:0-375	32471.2	43056.3	0.407062	5.00E-05	0.0011 0607	yes
Cs12708_c00114_00009:0-768	32.2213	422.962	3.71444	0.0001	0.0019 8908	yes
Cs12708_c00194_00002:0-489	233.608	598.168	1.35646	0.00015	0.0027 9567	yes

Cs12708_c00064_00017:0-1359	44.4706	112.038	1.33307	0.00015	0.0027 9567	yes
Cs12708_c00008_00038:0-396	1091.75	1948.95	0.836058	0.0002	0.0035 594	yes
Cs12708_c00058_00001:0-492	271.411	517.127	0.93004	0.0031	0.0320 424	yes
Cs12708_c00166_00003:0-786	124.227	229.998	0.888637	0.00405	0.0389 689	yes
Cs12708_c00151_00009:0-924	101.621	182.081	0.841384	0.00405	0.0389 689	yes
Cs12708_c00022_00038:0-501	199.674	412.743	1.0476	0.00465	0.0435 042	yes
Cs12708_c00081_00005:0-624	83.9893	208.062	1.30874	0.00495	0.0457 682	yes
Cs12708_c00005_00027:0-1767	26.5059	55.6576	1.07027	0.005	0.0460 506	yes

Figure 5.5: Overall transcriptomic heatmap of *Clostridium scindens* VPI 12708 induced with numerous bile acid and steroid molecules

C. scindens VPI 12708 was grown in the presence of 50 μ M cortisol, androstenedione, allocholic acid, or cholic acid. mRNA was isolated, purified, and then sequenced for each sample.

RNAseq results were used to generate heat maps of induction using a distance metric of 1-(abs(pearson correlation)). Results show that the *C. scindens* VPI 12708 transcriptomic pattern in response to cortisol, androstenedione, and allocholic acid cluster together and separately from the cholic acid induced transcriptomic pattern.

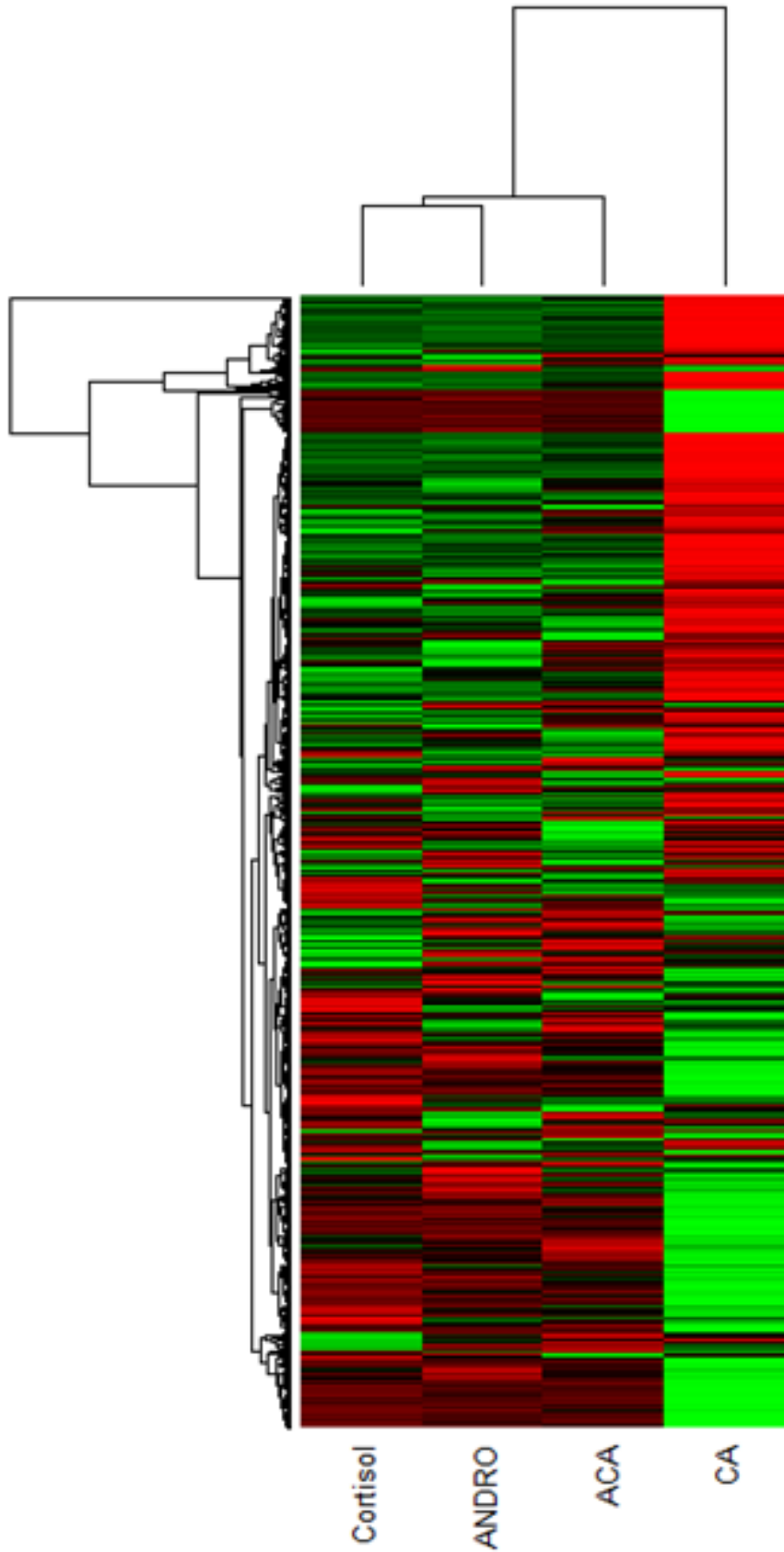


Table 5.3: Putative 17 α -HSDH genes from *Clostridium scindens* VPI 12708 screened for activity

Locus	Annotation based on blastp results	Size	Presence in 35704 strain	Metal binding site	NAD(P) binding site	Induction by androstenedione	Induction by cholic acid	17 α -HSDH activity	Other information of interest
Cs12708_00064_00018	Glycerol dehydrogenase	39.1 kDa	No	Yes	Yes	Yes	Yes	No	Part of operon, including membrane-spanning protein, that is upregulated by androstenedione and cholic acid
Cs12708_00005_00084	“Old yellow enzyme”, NADH flavin oxidoreductase	70.5 kDa	No	Not annotated	Yes	Yes	No	No	Alignment with previously characterized 12708 baiCD (262) shows conservation of catalytically necessary cysteine residues
Cs12708_00124_00009	Short chain dehydrogenase /reductase (SDR)	31.3 kDa	No	Not annotated	Yes	Yes	No	No	Has bacterial 3 α -HSDH conserved domain (via NCBI protein blast, ascension = cd05328)
Cs12708_00114_00009	Short chain dehydrogenase /reductase (SDR)	27.6 kDa	No	Not annotated	Yes	Yes	No	No	

cultures were tested for 17 α -HSDH activity. Assays were performed both aerobically and anaerobically (under N₂ stream). Reduction of androstenedione or oxidation of epitestosterone was measured spectrophotometrically for the change in NAD⁺/NADH oxidation state or via organic extraction and HPLC separation of products. Under all these experimental conditions, none of the tested enzymes exhibited 17 α -HSDH activity. At this point, there were no more candidate genes left from the RNAseq analysis.

Discussion:

Gaining a better understanding of our gut microbiome's ability to metabolize numerous endogenous and exogenous molecules to secondary molecules of varying physiological relevance is an important area of study. Bacterial bile acid and steroid metabolites have been shown on numerous occasions to have important physiological effects on the host. Finding the genes responsible for the production of genes that encode steroid/bile acid metabolizing enzymes is important in order to get a better understanding of why microbes utilize these substrates *in vivo*. Of equal importance, as the era of "personalized medicine" approaches, it is becoming more important to be able to predict metabolic potential of an individual's gut microbiome as it may pertain to other pathophysiological disorders. In this aim, it is important to have more a more robust understanding of specific enzymes in the "sterolbiome", as it makes predictive annotation and therefore the prediction of an individual's gut microbiome's "metabolic potential" more accurate. Therefore, we set out to find the gene in *Clostridium scindens* VPI 12708 responsible for the synthesis of a 17 α -HSDH enzyme able to interconvert androstenedione and epitestosterone. In concert with other bacteria known to have 17 β -activity such as *B. fragilis* (291), this would allow the gut microbiota to interconvert active testosterone to anti-androgenic epitestosterone, and vice versa.

We were able to confirm that *C. scindens* VPI 12708 has inducible 17 α -HSDH activity, able to convert androstenedione to epitestosterone *in vitro*. We performed RNAseq analysis on differentially induced *C. scindens* VPI 12708 samples and showed interesting differences in whole transcriptomic changes under these varying conditions. After finding candidate genes, we

tested them for their 17 α -HSDH activity using numerous experimental conditions. Ultimately the gene responsible for the production of the *C. scindens* VPI 12708 17 α -HSDH was not found.

There are numerous potential explanations for this outcome. One explanation is that the *C. scindens* VPI 12708 genomic data used as reference for the RNAseq data was not a closed genome. Therefore, if the gene for the 17 α -HSDH was not sequenced in the genomic sequencing, it would not have been identified through RNAseq analysis. Alternatively, it is possible that any of the putative 17 α -HSDH purified enzymes lost activity at some stage in their production or purification. However, we took every precaution to prevent this including using various expression vectors, confirming fidelity of the inserts, confirming production of protein, testing whole cell extracts and transformed cell cultures for activity, testing enzymes activity aerobically and anaerobically using two separate metrics for screening, and testing both the oxidation of epitestosterone and reduction of androstenedione.

It is possible that in producing these *Clostridial* proteins in a different genus (*Escherichia*) that an additional component, such as differing molecular chaperones, are necessary for the proper maturation of the 17 α -HSDH. A way of getting around this difficulty would be to knock out genes of interest directly in *C. scindens*. Unfortunately, a mechanism for directly knocking out genes in *Clostridium scindens* has not been developed, however not for a lack of effort. Most recently, work on developing a Crispr-Cas9 knockout system in *Clostridium scindens* is underway in a collaborating lab. Such a system in *Clostridium scindens* would be a huge accomplishment and widely utilized. The production of secondary bile acids by *Clostridium scindens* have been differentially implicated to be associated with CRC (67, 281) as well as with

protection against post-antibiotic *Clostridium difficile* infection (209). If one was able to knock out the bai-operon responsible for producing secondary bile acids in *Clostridium scindens*, the contributions of secondary bile acids to these disease processes could be more accurately determined.

Until either more cost-effective means of screening transcriptomic data for prokaryotes or a genetic knockout system for *Clostridium scindens* is developed, the gene encoding 17 α -HSDH will continue to elude us. A future direction may be to screen other fecal isolates for 17 α -HSDH activity on androstenedione and then comparing the genomic data to more accurately search for a putative gene. This experiment would be interesting, as the prevalence of microbial 17 α -HSDH activity in human fecal samples is unknown.

The work on identifying the 17 α -HSDH gene in *C. scindens* VPI 12708 did provide some interesting results. It showed how differently *C. scindens* VPI 12708 recognizes steroid compounds with the same steroidal backbone. Additionally, based on the clustering of heat maps of the four treatment groups, *C. scindens* VPI 12708 appears to recognize cholic acid differently from allocholic acid, androstenedione, and cortisol (Figure 5.4). Since allocholic acid is a 5 α -epimer of cholic acid, these results suggest that the planar orientation of the A ring on the steroid backbone on these molecules is an important regulator of its molecular function. To make better use of this data, I recommend the resequencing of *C. scindens* VPI 12708 genome using more up to date annotation techniques. That way, the transcriptomic data from the RNAseq analysis we performed can give more insight into how these steroid molecules impact the overall cell metabolism. Additionally, it could test one of the possible reasons for the

inability to identify the 17α -HSDH gene. Ultimately, this work gives interesting preliminary data for future studies, as well as a list of genes not to screen for 17α -HSDH activity in subsequent studies.

Chapter 6: Summary and Perspectives

The human gut microbiome is a diverse ecosystem of microbial organisms that inhabit our gastrointestinal tract. The concentration of living cells, approximately 10^{11} /g feces, is of the highest density found in nature. The study of the human gut microbiome has undergone a renaissance in the past decade with the advent of next-generation sequencing techniques (2). High-throughput analysis of the constituents of the gut microbiome has given significant insights into human health and changed how we study the general makeup of the gut microbiome. Changes to certain characteristics of the gut microbiome, such as the quantities of specific bacterial species or changes in the presence and levels of microbial-derived metabolites, have been associated with a wide range of pathophysiological conditions. Obesity (226, 256, 296), cardiovascular disease (297), hypertension (242, 252), inflammatory bowel disease (66, 84), colorectal cancer (67, 281), liver cancer (179), cirrhosis (298, 299), and post-antibiotic *C. difficile* infection (209) have all been associated with changes to the gut microbiome or the various metabolites it produces. There are, however, limitations to the conclusions we can draw from 16S, COG, and KEGG DNA and transcriptomic analysis. 16S screens of fecal bacteria do not delineate differences that may exist within different strains of the same species. The reference genomes that guide the predictive annotation for shotgun sequencing, such as COG and KEGG, account for only a third of all genomic data that is obtained (227).

This problem is evident when looking at specific aspects of gut microbial metabolism such as the “sterolbiome”, or the prokaryotic genes that encode enzymes metabolizing bile acids within the gut microbiome. Numerous bacterial strains within the Firmicutes and Actinobacteria phyla, two

of the three most prevalent phyla present in the GI tract, encode enzymes responsible for biotransformations of both bile acids and other steroid molecules. A small subset of bacteria within the *Clostridium* genus have been shown to have genes encoding enzymes in a multi-step 7α -dehydroxylation pathway, making them capable of turning endogenously produced primary bile acids CA and CDCA into secondary bile acids DCA and LCA, respectively (113). Production of secondary bile acids have been reported to be qualitatively the most common bioconversion of bile acids in the colon, as the majority of primary bile acids that escape enterohepatic circulation end up 7α -dehydroxylated in the large intestine (133). The genes encoding enzymes in the oxidative arm of the 7α -dehydroxylation pathway have been characterized in numerous *Clostridium* species (113). However, the genes encoding the enzymes for the three successive reductive steps have not been identified. In the current study, evidence is presented that the *Clostridium scindens* ATCC 35704 gene EDS08212.1 encodes a $\Delta 4,6$ reductase that catalyzes the two reductive steps immediately following 7α -dehydration. This gene is closely related to genes found in other 7α -dehydroxylating strains. It is unique in its ability to catalyze two reductive reactions on both the A and B ring of bile acids (both the $C_4=C_5$ and $C_6=C_7$ bonds). Ultimately this work helps to further characterize a very important biochemical pathway within the “sterolbiome” and will ultimately serve to help us better understand the entirety of the 7α -dehydroxylation pathway.

While 7α -dehydroxylation of primary bile acids is the most studied bacterial bile acid metabolic pathway, other biotransformations do occur. One such set of reactions is the oxidation and epimerization of bile acid hydroxyl groups. Oxidation of the α -hydroxyl groups on the 3rd, 7th, and 12th carbon of bile acids leads to the formation of an oxo-moiety. Microbial oxidation of

bile acids occurs regularly in the large intestine, as previous analysis of fecal samples and portal circulation show the accumulation of oxo-bile acids to varying degrees (158-163, 165, 267)

Once epimerized, these oxo-bile acids can undergo further biotransformations. They can be reduced back to an α -configuration by bacterial or host hepatic α -HSDHs. Alternatively, they can be epimerized to the β -configuration. Numerous gut-associated microbes have been shown to harbor bile acid C3- and C7-hydroxyl- β -HSDHs (146, 150, 157). Epimerized bile acids have been shown to be less toxic to other gut microbes that inhabit the large intestine (150). As such, if an individual harbors gut microbes that can epimerize bile acids, the makeup of their gut microbiome may be different from an individual who does not, although that has not been experimentally proven. Additionally, epimerized bile acids pose a problem for bacteria that otherwise utilize primary bile acids. These 7α -dehydroxylating bacteria were not induced to 7α -dehydroxylate primary bile acids by ursodeoxycholic acid, although they are capable of 7β -dehydroxylation if induced by 7α -bile acids (261). Additionally, ursodeoxycholic acid has been shown to inhibit the germination and vegetative growth of *Clostridium difficile* spores and be protective against recurrent infection (216). It is clear that the epimerization of bile acids forms less toxic secondary metabolites. However, the role of oxo-bile acids, the “intermediate” molecule in this process, is less well characterized.

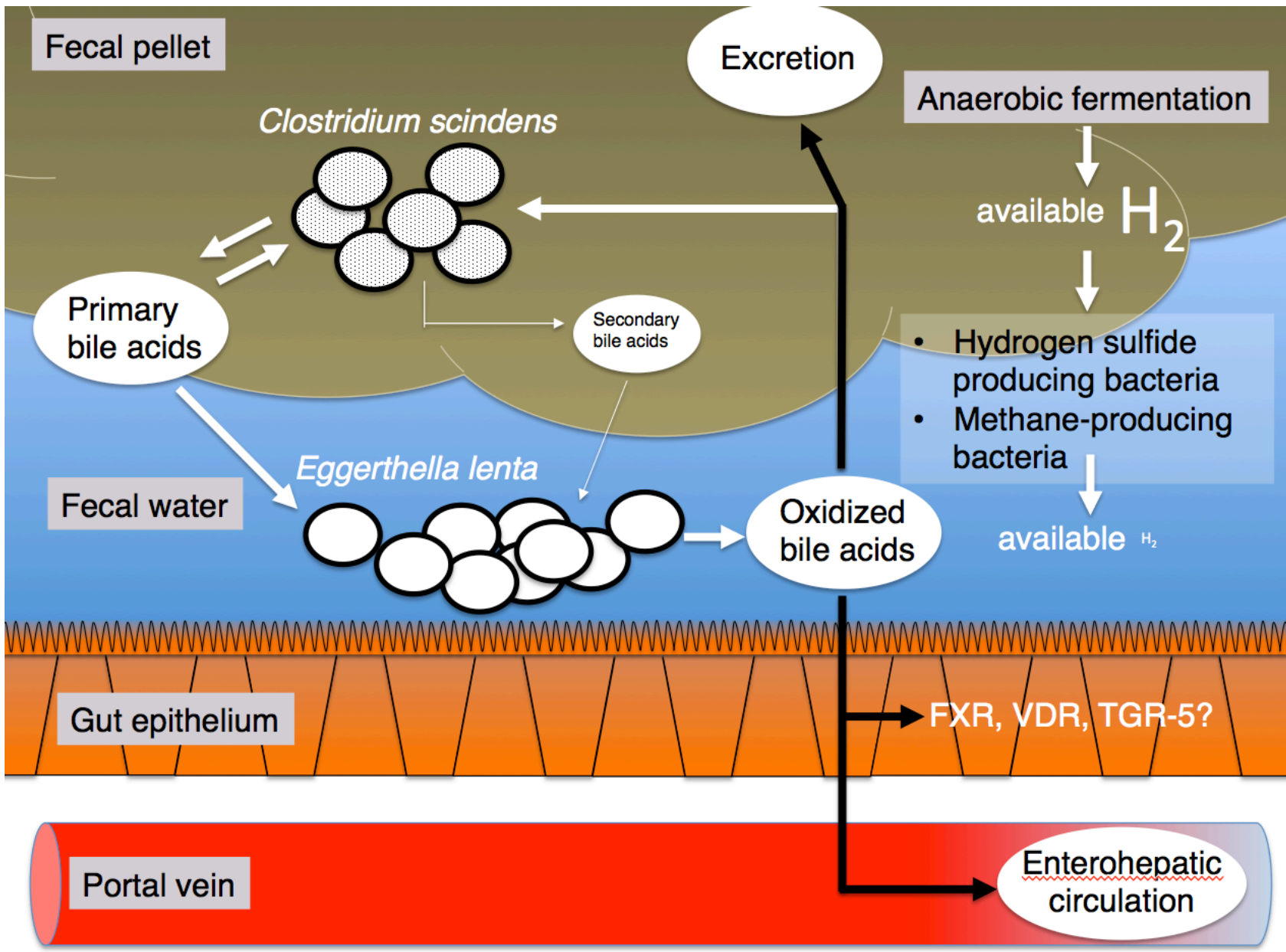
In the current study, we show evidence that 7α -dehydroxylation can be inhibited by the formation of oxo-bile acid derivatives. *Clostridium scindens* VPI 12708 (12708) was unable to effectively 7α -dehydroxylate the three CDCA metabolites produced by *E. lenta* C592. Two of the metabolites (7-oxo-3 α -hydroxy-CDCA and 3,7-dioxo-CDCA) were partially reduced back to

CDCA, although 7 α -dehydroxylation did not occur to the same extent as fully reduced CDCA. Additionally, the 7-oxo-3 β -hydroxy-CDCA metabolite was reduced by *C. scindens* VPI 12708 back to isoCDCA, but was not 7 α -dehydroxylated. Taken together, this shows that *C. scindens* VPI 12708 does not recognize isoCDCA as a substrate for 7 α -dehydroxylation, possibly due to the absence of a 3 β -HSDH. Additionally, the oxidation of hydroxyl groups appears to inhibit the 7 α -dehydroxylation of primary bile acids, even if *C. scindens* is able to reduce the oxo-bile acid metabolites back to the original primary bile acid. One potential explanation for these findings is that oxo-bile acids do not induce the “bai” operon, similar to ursodeoxycholic acid (261). Therefore, in the *C. scindens* VPI 12708 oxo-bile acid metabolism analysis, the oxo-bile acids are reduced but 7 α -dehydroxylated products do not form because they require induction of the bai operon. Further experimentation should be done to test *C. scindens* “bai” gene expression via qPCR when induced with the various oxo-bile acid derivatives made by C592.

In coculture experiments, *E. lenta* C592 and *C. scindens* 12708 appear to cycle CDCA back and forth between 7 α -CDCA and 7-oxo-CDCA, but LCA does not appear to accumulate. This experiment gives insight into what might happen if both *C. scindens* 12708 and *E. lenta* C592 were in the large intestine under low H₂ partial pressure and suggests a mechanism by which secondary bile acid formation may be inhibited *in vivo* by another member of the gut microbiome (Figure 6.1). Future experimentation on this point is warranted. *In vivo* experiments of humanized mice (mice designed to have a humanized gut microbiome), could be designed to include supplementation with *E. lenta* strains to see if secondary bile acid formation is inhibited. Additionally, the effect of diet, such as the supplementation of complex carbohydrates that could lead to an excess of H₂ gas in the colon and thus inhibit *E. lenta* bile acid metabolism, could be

Figure 6.1: Model of *Eggerthella lenta* C592 bile acid metabolism *in vivo*.

In the lumen of the large intestine, both *Clostridium scindens* and *Eggerthella lenta* would be competing for the same pool of primary bile acids. *C. scindens* preferentially 7 α -dehydroxylates primary bile acids to secondary bile acids. At the same time, *E. lenta* would be competing for the same primary bile acids to use as electron donors. These oxidized bile acids would be reduced by *C. scindens* back to primary bile acids, leading to a cycle of oxidation-reduction between the two strains. This cycle would inhibit the build up of secondary bile acids in the colon. However, the ability for *E. lenta* to oxidize bile acids would be dependent on the availability of H₂ gas. The availability of H₂ gas in the lumen of the colon is dependent on two factors; the rate of production via anaerobic fermentation and the rate of utilization by H₂ utilizers. Other gut microbial H₂ utilizers, sulfidogens and methanogens, have higher affinity to H₂ than acetogens. Therefore if sulfidogens or methanogens were present and their preferred substrates for reduction were available, the amount of H₂ for utilization by *E. lenta* would be low. With a paucity of available H₂, *E. lenta* would use bile acids as electron donors, leading to the formation of oxo-bile acids. Alternatively, if H₂ production outpaces the H₂ utilization or if methanogenesis and sulfidogenesis are not occurring, *E. lenta* would switch to utilizing H₂ as an electron donor and cease to oxidize bile acids. This would allow *C. scindens* to properly 7 α -dehydroxylate primary bile acids, leading to an accumulation of secondary bile acids.



tested in this model. Within this framework, other strains could be added as well, such as hydrogen sulfide gas producing bacteria (both with and without sulfate substrates) or methanogens, to see if their presence with *E. lenta* impacts the formation of secondary bile acids. Given the *in vitro* data generated in this work, it would be expected that *E. lenta* might inhibit 7 α -dehydroxylation by *C. scindens* strains and that excess H₂ formation could counteract this inhibition. However, given recent studies showing that secondary bile acids are directly linked to resistance against post-antibiotic CDI, the question arises as to whether limiting the formation of secondary bile acids should be viewed as a therapeutic target.

Recent literature has suggested that *C. scindens*, specifically the formation of secondary bile acids, is protective against post-AB CDI in both human patients and animal models (209). However, little data is available showing a mechanism linking secondary bile acids to the inhibition of either *C. difficile* spore germination or vegetative growth. Perhaps the most promising link is the study identifying the *C. difficile* germination receptor CspC is specifically activated by 12 α -hydroxyl bile acids (214). Work presented in this study shows that the 12 α -hydroxyl group on DCA is oxidized during *E. lenta* C592 DCA metabolism. Future experimentation should look to the effects that 12-oxo-DCA has on both *C. difficile* growth and spore germination, as well as its ability to be recognized by the CspC receptor.

The effects these oxo-bile acid metabolites have are not limited to other members of the gut microbiome. Host tissues are significantly affected by numerous bacterial metabolites, particularly bile acids. Oxo-bile acid derivatives have been shown to have varying effects, although they have not been thoroughly tested as well as their fully reduced counterparts. 7-oxo-

CDCA, coincidentally a major product of *E. lenta* C592 CDCA metabolism, has been shown previously to be a competitive inhibitor for hepatic 11 β -HSDH1 (198, 199). This inhibition prevents effective reduction of inactive cortisone to cortisol. The extent to which this inhibition affects overall host physiology has not been tested. Additionally, bile acids are known to activate host G-protein coupled and nuclear receptors to varying extents based on the regio and stereo positioning of the functional groups attached to their steroid cores and side chains. 3-oxo-LCA, the most likely product of *E. lenta* C592 LCA metabolism, has been shown to be the most potent vitamin D receptor agonist (175). Additionally, 7-oxo-CDCA and 3,7-oxo-CDCA have both been shown to be less potent agonists for FXR than their α -reduced counterparts, but more potent than β -reduced epimers (167). Oxo-bile acids, therefore, already have an established role in host physiology unique from their α - and β -reduced sister molecules. However, the full spectrum of primary and secondary oxo-bile acid derivatives has not been tested for agonist properties on various bile acid-sensitive receptors. Of particular interest would be to determine oxo-bile acids' ability to activate TGR-5, as this is implicated in significantly altering host metabolism. Previous literature has suggested *C. scindens* is associated with increased hepatic triglyceride levels (258), which is a downstream effect of secondary bile acid activation of TGR-5 (173). Secondary bile acids DCA and LCA are the most potent activators of TGR-5 (170). *E. lenta* was also shown to be associated with increased hepatic triglyceride levels (258), but they do not perform 7 α -dehydroxylation. Therefore, this suggests that oxo-bile acid derivatives made by *E. lenta* are performing similar activities to secondary bile acids, potentially through the activation of TGR-5.

Epimerized bile acids, such as ursodeoxycholic acid, have been shown to be less toxic to colonocytes (254, 255). The toxicity of oxo-bile acid derivatives has not been studied, but would likely be different from fully reduced bile acids. Previous studies have shown that varying the configuration of hydroxyl groups on bile acids directly affects their hydrophobicity (254), which is a major contributor to bile acid toxicity. However, the hydrophobicity of oxo-bile acid derivatives has not been assessed.

The formation of oxo-bile acids by *E. lenta* strains could have many effects, both to other gut microbes and to various host tissues. The extent of these effects have yet to be fully elucidated, likely owing to the fact that oxo-bile acids have been seen as intermediates in the epimerization of bile acids. However recent published studies, as well as the work presented here, suggest that oxo-bile acids could be key actors in modulating host and gut microbial physiology. Evidence has been presented that *E. lenta* strains share many qualities with acetogens, and how bile acid oxidation play into their whole cell redox balancing and energy production. Additionally, our studies show that atmospheric gases play a key role in determining the extent of *E. lenta* bile acid metabolism. Both the *E. lenta* strains and oxo-bile acids warrant further exploration as possible therapeutic agents. However, this comes with a warning, since recent studies have suggested an important role of secondary bile acids in the prevention of CDI. Therefore, it is important to acquire a better understanding of the mechanism by which secondary bile acids prevent CDI before suggesting for their diminution in patients. Ultimately, this work makes a case for *E. lenta* strains to be considered acetogens, for the formation of oxo-bile acids as a means to prevent 7 α -dehydroxylation, and serves as a baseline to direct future study of oxo-bile acid formation *in vivo*.

References Cited

1. Savage DC. Microbial ecology of the gastrointestinal tract. Annual review of microbiology. 1977;31:107-33. Epub 1977/01/01. doi: 10.1146/annurev.mi.31.100177.000543. PubMed PMID: 334036.
2. Structure, function and diversity of the healthy human microbiome. Nature. 2012;486(7402):207-14. Epub 2012/06/16. doi: 10.1038/nature11234. PubMed PMID: 22699609; PubMed Central PMCID: PMC3564958.
3. Nebe-von-Caron G, Stephens PJ, Hewitt CJ, Powell JR, Badley RA. Analysis of bacterial function by multi-colour fluorescence flow cytometry and single cell sorting. J Microbiol Methods. 2000;42(1):97-114. PubMed PMID: 11000436.
4. Tyson GW, Chapman J, Hugenholtz P, Allen EE, Ram RJ, Richardson PM, et al. Community structure and metabolism through reconstruction of microbial genomes from the environment. Nature. 2004;428(6978):37-43. doi: 10.1038/nature02340. PubMed PMID: 14961025.
5. Durot M, Bourguignon PY, Schachter V. Genome-scale models of bacterial metabolism: reconstruction and applications. FEMS Microbiol Rev. 2009;33(1):164-90. doi: 10.1111/j.1574-6976.2008.00146.x. PubMed PMID: 19067749; PubMed Central PMCID: PMC32704943.
6. Whitman WB, Coleman DC, Wiebe WJ. Prokaryotes: the unseen majority. Proceedings of the National Academy of Sciences of the United States of America. 1998;95(12):6578-83. Epub 1998/06/17. PubMed PMID: 9618454; PubMed Central PMCID: PMC33863.
7. McNeil NI. The contribution of the large intestine to energy supplies in man. Am J Clin Nutr. 1984;39(2):338-42. PubMed PMID: 6320630.
8. Gill SR, Pop M, Deboy RT, Eckburg PB, Turnbaugh PJ, Samuel BS, et al. Metagenomic analysis of the human distal gut microbiome. Science. 2006;312(5778):1355-9. doi: 10.1126/science.1124234. PubMed PMID: 16741115; PubMed Central PMCID: PMC3027896.
9. Round JL, Mazmanian SK. The gut microbiota shapes intestinal immune responses during health and disease. Nat Rev Immunol. 2009;9(5):313-23. doi: 10.1038/nri2515. PubMed PMID: 19343057; PubMed Central PMCID: PMC34095778.
10. Flint HJ, Scott KP, Louis P, Duncan SH. The role of the gut microbiota in nutrition and health. Nat Rev Gastroenterol Hepatol. 2012;9(10):577-89. doi: 10.1038/nrgastro.2012.156. PubMed PMID: 22945443.
11. Miller TL, Wolin MJ. Pathways of acetate, propionate, and butyrate formation by the human fecal microbial flora. Applied and environmental microbiology. 1996;62(5):1589-92. PubMed PMID: 8633856; PubMed Central PMCID: PMC3167932.
12. Cummings JH, Pomare EW, Branch WJ, Naylor CP, Macfarlane GT. Short chain fatty acids in human large intestine, portal, hepatic and venous blood. Gut. 1987;28(10):1221-7. PubMed PMID: 3678950; PubMed Central PMCID: PMC31433442.
13. Sleeth ML, Thompson EL, Ford HE, Zac-Varghese SE, Frost G. Free fatty acid receptor 2 and nutrient sensing: a proposed role for fibre, fermentable carbohydrates and short-chain fatty acids in appetite regulation. Nutr Res Rev. 2010;23(1):135-45. doi: 10.1017/S0954422410000089. PubMed PMID: 20482937.

14. Carbonero F, Benefiel AC, Gaskins HR. Contributions of the microbial hydrogen economy to colonic homeostasis. *Nat Rev Gastroenterol Hepatol.* 2012;9(9):504-18. doi: 10.1038/nrgastro.2012.85. PubMed PMID: 22585131.
15. Lewis SJ, Heaton KW. Increasing butyrate concentration in the distal colon by accelerating intestinal transit. *Gut.* 1997;41(2):245-51. PubMed PMID: 9301506; PubMed Central PMCID: PMCPMC1891451.
16. El Oufir L, Flourie B, Bruley des Varannes S, Barry JL, Cloarec D, Bornet F, et al. Relations between transit time, fermentation products, and hydrogen consuming flora in healthy humans. *Gut.* 1996;38(6):870-7. PubMed PMID: 8984026; PubMed Central PMCID: PMCPMC1383195.
17. O'Keefe SJ. The African way of life and colon cancer risk. *Am J Gastroenterol.* 2001;96(11):3220-1. doi: 10.1111/j.1572-0241.2001.05296.x. PubMed PMID: 11721790.
18. Ou J, Carbonero F, Zoetendal EG, DeLany JP, Wang M, Newton K, et al. Diet, microbiota, and microbial metabolites in colon cancer risk in rural Africans and African Americans. *Am J Clin Nutr.* 2013;98(1):111-20. doi: 10.3945/ajcn.112.056689. PubMed PMID: 23719549; PubMed Central PMCID: PMCPMC3683814.
19. Willemsen LE, Koetsier MA, van Deventer SJ, van Tol EA. Short chain fatty acids stimulate epithelial mucin 2 expression through differential effects on prostaglandin E(1) and E(2) production by intestinal myofibroblasts. *Gut.* 2003;52(10):1442-7. PubMed PMID: 12970137; PubMed Central PMCID: PMCPMC1773837.
20. Gaudier E, Jarry A, Blottiere HM, de Coppet P, Buisine MP, Aubert JP, et al. Butyrate specifically modulates MUC gene expression in intestinal epithelial goblet cells deprived of glucose. *American journal of physiology Gastrointestinal and liver physiology.* 2004;287(6):G1168-74. doi: 10.1152/ajpgi.00219.2004. PubMed PMID: 15308471.
21. Rooks MG, Garrett WS. Gut microbiota, metabolites and host immunity. *Nat Rev Immunol.* 2016;16(6):341-52. doi: 10.1038/nri.2016.42. PubMed PMID: 27231050.
22. Kripke SA, Fox AD, Berman JM, Settle RG, Rombeau JL. Stimulation of intestinal mucosal growth with intracolonic infusion of short-chain fatty acids. *JPEN J Parenter Enteral Nutr.* 1989;13(2):109-16. doi: 10.1177/0148607189013002109. PubMed PMID: 2496241.
23. Topping DL, Clifton PM. Short-chain fatty acids and human colonic function: roles of resistant starch and nonstarch polysaccharides. *Physiol Rev.* 2001;81(3):1031-64. PubMed PMID: 11427691.
24. Wilson AJ, Chueh AC, Togel L, Corner GA, Ahmed N, Goel S, et al. Apoptotic sensitivity of colon cancer cells to histone deacetylase inhibitors is mediated by an Sp1/Sp3-activated transcriptional program involving immediate-early gene induction. *Cancer Res.* 2010;70(2):609-20. doi: 10.1158/0008-5472.CAN-09-2327. PubMed PMID: 20068171; PubMed Central PMCID: PMCPMC2939837.
25. Fung KY, Cosgrove L, Lockett T, Head R, Topping DL. A review of the potential mechanisms for the lowering of colorectal oncogenesis by butyrate. *Br J Nutr.* 2012;108(5):820-31. doi: 10.1017/S0007114512001948. PubMed PMID: 22676885.
26. Tao R, de Zoeten EF, Ozkaynak E, Chen C, Wang L, Porrett PM, et al. Deacetylase inhibition promotes the generation and function of regulatory T cells. *Nat Med.* 2007;13(11):1299-307. doi: 10.1038/nm1652. PubMed PMID: 17922010.
27. Suarez F, Furne J, Springfield J, Levitt M. Insights into human colonic physiology obtained from the study of flatus composition. *Am J Physiol.* 1997;272(5 Pt 1):G1028-33. PubMed PMID: 9176210.

28. Christl SU, Murgatroyd PR, Gibson GR, Cummings JH. Production, metabolism, and excretion of hydrogen in the large intestine. *Gastroenterology*. 1992;102(4 Pt 1):1269-77. PubMed PMID: 1551534.
29. Levitt MD. Production and excretion of hydrogen gas in man. *N Engl J Med*. 1969;281(3):122-7. doi: 10.1056/NEJM196907172810303. PubMed PMID: 5790483.
30. Hartmann L, Taras D, Kamlage B, Blaut M. A new technique to determine hydrogen excreted by gnotobiotic rats. *Lab Anim*. 2000;34(2):162-70. doi: 10.1258/002367700780457617. PubMed PMID: 10817455.
31. Duncan SH, Hold GL, Barcenilla A, Stewart CS, Flint HJ. *Roseburia intestinalis* sp. nov., a novel saccharolytic, butyrate-producing bacterium from human faeces. *Int J Syst Evol Microbiol*. 2002;52(Pt 5):1615-20. doi: 10.1099/00207713-52-5-1615. PubMed PMID: 12361264.
32. Miller TL, Wolin MJ. Formation of hydrogen and formate by *Ruminococcus albus*. *Journal of bacteriology*. 1973;116(2):836-46. PubMed PMID: 4745433; PubMed Central PMCID: PMCPMC285454.
33. Duncan SH, Flint HJ. Proposal of a neotype strain (A1-86) for *Eubacterium rectale*. Request for an opinion. *Int J Syst Evol Microbiol*. 2008;58(Pt 7):1735-6. doi: 10.1099/ijs.0.2008/004580-0. PubMed PMID: 18599726.
34. Steer T, Collins MD, Gibson GR, Hippe H, Lawson PA. *Clostridium hathewayi* sp. nov., from human faeces. *Syst Appl Microbiol*. 2001;24(3):353-7. doi: 10.1078/0723-2020-00044. PubMed PMID: 11822669.
35. Kamlage B, Gruhl B, Blaut M. Isolation and characterization of two new homoacetogenic hydrogen-utilizing bacteria from the human intestinal tract that are closely related to *Clostridium coccoides*. *Applied and environmental microbiology*. 1997;63(5):1732-8. PubMed PMID: 9143110; PubMed Central PMCID: PMCPMC168470.
36. Wolf PG, Biswas A, Morales SE, Greening C, Gaskins HR. H₂ metabolism is widespread and diverse among human colonic microbes. *Gut microbes*. 2016;7(3):235-45. Epub 2016/04/29. doi: 10.1080/19490976.2016.1182288. PubMed PMID: 27123663; PubMed Central PMCID: PMCPMC4939926.
37. Thauer RK. Biochemistry of methanogenesis: a tribute to Marjory Stephenson. 1998 Marjory Stephenson Prize Lecture. *Microbiology (Reading, England)*. 1998;144 (Pt 9):2377-406. doi: 10.1099/00221287-144-9-2377. PubMed PMID: 9782487.
38. Miller TL, Wolin MJ. Methanogens in human and animal intestinal Tracts. *Systematic and Applied Microbiology*. 1986;7(2):223-9. doi: [http://dx.doi.org/10.1016/S0723-2020\(86\)80010-8](http://dx.doi.org/10.1016/S0723-2020(86)80010-8).
39. Costa KC, Leigh JA. Metabolic versatility in methanogens. *Curr Opin Biotechnol*. 2014;29:70-5. doi: 10.1016/j.copbio.2014.02.012. PubMed PMID: 24662145.
40. Gottschalk G, Thauer RK. The Na⁽⁺⁾-translocating methyltransferase complex from methanogenic archaea. *Biochim Biophys Acta*. 2001;1505(1):28-36. PubMed PMID: 11248186.
41. Thauer RK, Jungermann K, Decker K. Energy conservation in chemotrophic anaerobic bacteria. *Bacteriol Rev*. 1977;41(1):100-80. PubMed PMID: 860983; PubMed Central PMCID: PMCPMC413997.
42. Miller TL, Wolin MJ, Conway de Macario E, Macario AJ. Isolation of *Methanobrevibacter smithii* from human feces. *Applied and environmental microbiology*. 1982;43(1):227-32. PubMed PMID: 6798932; PubMed Central PMCID: PMCPMC241804.

43. Hansen EE, Lozupone CA, Rey FE, Wu M, Guruge JL, Narra A, et al. Pan-genome of the dominant human gut-associated archaeon, *Methanobrevibacter smithii*, studied in twins. *Proceedings of the National Academy of Sciences of the United States of America*. 2011;108 Suppl 1:4599-606. doi: 10.1073/pnas.1000071108. PubMed PMID: 21317366; PubMed Central PMCID: PMC3063581.
44. Thauer RK, Hedderich R, Fischer R. Reactions and Enzymes Involved in Methanogenesis from CO₂ and H₂. In: Ferry JG, editor. *Methanogenesis: Ecology, Physiology, Biochemistry & Genetics*. Boston, MA: Springer US; 1993. p. 209-52.
45. Calloway DH. Respiratory hydrogen and methane as affected by consumption of gas-forming foods. *Gastroenterology*. 1966;51(3):383-9. PubMed PMID: 5945818.
46. Pochart P, Dore J, Lemann F, Goderel I, Rambaud JC. Interrelations between populations of methanogenic archaea and sulfate-reducing bacteria in the human colon. *FEMS Microbiol Lett*. 1992;77(1-3):225-8. PubMed PMID: 1459413.
47. Scanlan PD, Shanahan F, Marchesi JR. Human methanogen diversity and incidence in healthy and diseased colonic groups using *mcrA* gene analysis. *BMC Microbiol*. 2008;8:79. doi: 10.1186/1471-2180-8-79. PubMed PMID: 18492229; PubMed Central PMCID: PMC2408590.
48. Mihajlovski A, Alric M, Brugere JF. A putative new order of methanogenic Archaea inhabiting the human gut, as revealed by molecular analyses of the *mcrA* gene. *Res Microbiol*. 2008;159(7-8):516-21. doi: 10.1016/j.resmic.2008.06.007. PubMed PMID: 18644435.
49. Nava GM, Carbonero F, Croix JA, Greenberg E, Gaskins HR. Abundance and diversity of mucosa-associated hydrogenotrophic microbes in the healthy human colon. *The ISME journal*. 2012;6(1):57-70. doi: 10.1038/ismej.2011.90. PubMed PMID: 21753800; PubMed Central PMCID: PMC3246246.
50. Bjorneklett A, Jenssen E. Relationships between hydrogen (H₂) and methane (CH₄) production in man. *Scand J Gastroenterol*. 1982;17(8):985-92. PubMed PMID: 7167741.
51. Bjorneklett A, Fausa O, Midtvedt T. Bacterial overgrowth in jejunal and ileal disease. *Scand J Gastroenterol*. 1983;18(2):289-98. PubMed PMID: 6369510.
52. McKay LF, Eastwood MA, Brydon WG. Methane excretion in man--a study of breath, flatus, and faeces. *Gut*. 1985;26(1):69-74. PubMed PMID: 3965369; PubMed Central PMCID: PMC1432392.
53. Peled Y, Weinberg D, Hallak A, Gilat T. Factors affecting methane production in humans. *Gastrointestinal diseases and alterations of colonic flora*. *Dig Dis Sci*. 1987;32(3):267-71. PubMed PMID: 3816480.
54. Pimentel M, Mayer AG, Park S, Chow EJ, Hasan A, Kong Y. Methane production during lactulose breath test is associated with gastrointestinal disease presentation. *Dig Dis Sci*. 2003;48(1):86-92. PubMed PMID: 12645795.
55. Pique JM, Pallares M, Cuso E, Vilar-Bonet J, Gassull MA. Methane production and colon cancer. *Gastroenterology*. 1984;87(3):601-5. PubMed PMID: 6745612.
56. Karlin DA, Jones RD, Stroehlein JR, Mastromarino AJ, Potter GD. Breath methane excretion in patients with unresected colorectal cancer. *J Natl Cancer Inst*. 1982;69(3):573-6. PubMed PMID: 6955554.
57. Kashtan H, Rabau M, Peled Y, Milstein A, Wiznitzer T. Methane production in patients with colorectal carcinoma. *Isr J Med Sci*. 1989;25(11):614-6. PubMed PMID: 2592175.
58. Sivertsen SM, Bjorneklett A, Gullestad HP, Nygaard K. Breath methane and colorectal cancer. *Scand J Gastroenterol*. 1992;27(1):25-8. PubMed PMID: 1736338.

59. Gibson GR. Physiology and ecology of the sulphate-reducing bacteria. *J Appl Bacteriol.* 1990;69(6):769-97. PubMed PMID: 2286579.
60. Gibson GR, Cummings JH, Macfarlane GT, Allison C, Segal I, Vorster HH, et al. Alternative pathways for hydrogen disposal during fermentation in the human colon. *Gut.* 1990;31(6):679-83. PubMed PMID: 2379871; PubMed Central PMCID: PMCPMC1378495.
61. Liamleam W, Annachatre AP. Electron donors for biological sulfate reduction. *Biotechnol Adv.* 2007;25(5):452-63. doi: 10.1016/j.biotechadv.2007.05.002. PubMed PMID: 17572039.
62. Peck HD, Jr. Enzymatic basis for assimilatory and dissimilatory sulfate reduction. *Journal of bacteriology.* 1961;82:933-9. PubMed PMID: 14484818; PubMed Central PMCID: PMCPMC279279.
63. Carbonero F, Benefiel AC, Alizadeh-Ghamsari AH, Gaskins HR. Microbial pathways in colonic sulfur metabolism and links with health and disease. *Front Physiol.* 2012;3:448. doi: 10.3389/fphys.2012.00448. PubMed PMID: 23226130; PubMed Central PMCID: PMCPMC3508456.
64. Florin T, Neale G, Gibson GR, Christl SU, Cummings JH. Metabolism of dietary sulphate: absorption and excretion in humans. *Gut.* 1991;32(7):766-73. PubMed PMID: 1855683; PubMed Central PMCID: PMCPMC1378993.
65. Fite A, Macfarlane GT, Cummings JH, Hopkins MJ, Kong SC, Furrie E, et al. Identification and quantitation of mucosal and faecal desulfovibrios using real time polymerase chain reaction. *Gut.* 2004;53(4):523-9. PubMed PMID: 15016746; PubMed Central PMCID: PMCPMC1774019.
66. Zinkevich VV, Beech IB. Screening of sulfate-reducing bacteria in colonoscopy samples from healthy and colitic human gut mucosa. *FEMS Microbiol Ecol.* 2000;34(2):147-55. PubMed PMID: 11102692.
67. McGarr SE, Ridlon JM, Hylemon PB. Diet, anaerobic bacterial metabolism, and colon cancer: a review of the literature. *Journal of clinical gastroenterology.* 2005;39(2):98-109. Epub 2005/02/01. PubMed PMID: 15681903.
68. Devkota S, Wang Y, Musch MW, Leone V, Fehlner-Peach H, Nadimpalli A, et al. Dietary-fat-induced taurocholic acid promotes pathobiont expansion and colitis in I110-/- mice. *Nature.* 2012;487(7405):104-8. doi: 10.1038/nature11225. PubMed PMID: 22722865; PubMed Central PMCID: PMCPMC3393783.
69. Stocchi A, Ellis CJ, Levitt MD. Use of metabolic inhibitors to study H₂ consumption by human feces: evidence for a pathway other than methanogenesis and sulfate reduction. *J Lab Clin Med.* 1993;121(2):320-7. PubMed PMID: 8433043.
70. Lewis S, Cochrane S. Alteration of sulfate and hydrogen metabolism in the human colon by changing intestinal transit rate. *Am J Gastroenterol.* 2007;102(3):624-33. doi: 10.1111/j.1572-0241.2006.01020.x. PubMed PMID: 17156141.
71. Christl SU, Gibson GR, Cummings JH. Role of dietary sulphate in the regulation of methanogenesis in the human large intestine. *Gut.* 1992;33(9):1234-8. PubMed PMID: 1427377; PubMed Central PMCID: PMCPMC1379493.
72. Gibson GR, Cummings JH, Macfarlane GT. Growth and activities of sulphate-reducing bacteria in gut contents of healthy subjects and patients with ulcerative colitis. *FEMS Microbiology Letters.* 1991;86(2):103-11. doi: 10.1111/j.1574-6968.1991.tb04799.x.

73. Levine J, Ellis CJ, Furne JK, Springfield J, Levitt MD. Fecal hydrogen sulfide production in ulcerative colitis. *Am J Gastroenterol*. 1998;93(1):83-7. doi: 10.1111/j.1572-0241.1998.083_c.x. PubMed PMID: 9448181.
74. Moore J, Babidge W, Millard S, Roediger W. Colonic luminal hydrogen sulfide is not elevated in ulcerative colitis. *Dig Dis Sci*. 1998;43(1):162-5. PubMed PMID: 9508519.
75. Truelove SC. Ulcerative colitis provoked by milk. *Br Med J*. 1961;1(5220):154-60. PubMed PMID: 13778258; PubMed Central PMCID: PMCPMC1952962.
76. Jowett SL, Seal CJ, Pearce MS, Phillips E, Gregory W, Barton JR, et al. Influence of dietary factors on the clinical course of ulcerative colitis: a prospective cohort study. *Gut*. 2004;53(10):1479-84. doi: 10.1136/gut.2003.024828. PubMed PMID: 15361498; PubMed Central PMCID: PMCPMC1774231.
77. Sjovall J. Dietary glycine and taurine on bile acid conjugation in man; bile acids and steroids 75. *Proc Soc Exp Biol Med*. 1959;100(4):676-8. PubMed PMID: 13645682.
78. Hardison WG. Hepatic taurine concentration and dietary taurine as regulators of bile acid conjugation with taurine. *Gastroenterology*. 1978;75(1):71-5. PubMed PMID: 401099.
79. Yamada M, Ohkusa T, Okayasu I. Occurrence of dysplasia and adenocarcinoma after experimental chronic ulcerative colitis in hamsters induced by dextran sulphate sodium. *Gut*. 1992;33(11):1521-7. PubMed PMID: 1333439; PubMed Central PMCID: PMCPMC1379539.
80. Kanazawa K, Konishi F, Mitsuoka T, Terada A, Itoh K, Narushima S, et al. Factors influencing the development of sigmoid colon cancer. *Bacteriologic and biochemical studies. Cancer*. 1996;77(8 Suppl):1701-6. doi: 10.1002/(SICI)1097-0142(19960415)77:8<1701::AID-CNCR42>3.0.CO;2-0. PubMed PMID: 8608565.
81. Balamurugan R, Rajendiran E, George S, Samuel GV, Ramakrishna BS. Real-time polymerase chain reaction quantification of specific butyrate-producing bacteria, *Desulfovibrio* and *Enterococcus faecalis* in the feces of patients with colorectal cancer. *J Gastroenterol Hepatol*. 2008;23(8 Pt 1):1298-303. doi: 10.1111/j.1440-1746.2008.05490.x. PubMed PMID: 18624900.
82. Scanlan PD, Shanahan F, Marchesi JR. Culture-independent analysis of desulfovibrios in the human distal colon of healthy, colorectal cancer and polypectomized individuals. *FEMS Microbiol Ecol*. 2009;69(2):213-21. doi: 10.1111/j.1574-6941.2009.00709.x. PubMed PMID: 19496818.
83. Shaw L, Engel PC. CoA-persulphide: a possible in vivo inhibitor of mammalian short-chain acyl-CoA dehydrogenase. *Biochim Biophys Acta*. 1987;919(2):171-4. PubMed PMID: 3580384.
84. Christl SU, Eisner HD, Dusel G, Kasper H, Scheppach W. Antagonistic effects of sulfide and butyrate on proliferation of colonic mucosa: a potential role for these agents in the pathogenesis of ulcerative colitis. *Dig Dis Sci*. 1996;41(12):2477-81. PubMed PMID: 9011461.
85. Roediger WE, Moore J, Babidge W. Colonic sulfide in pathogenesis and treatment of ulcerative colitis. *Dig Dis Sci*. 1997;42(8):1571-9. PubMed PMID: 9286219.
86. Attene-Ramos MS, Wagner ED, Plewa MJ, Gaskins HR. Evidence that hydrogen sulfide is a genotoxic agent. *Mol Cancer Res*. 2006;4(1):9-14. Epub 2006/02/01. doi: 10.1158/1541-7786.mcr-05-0126. PubMed PMID: 16446402.
87. Attene-Ramos MS, Wagner ED, Gaskins HR, Plewa MJ. Hydrogen sulfide induces direct radical-associated DNA damage. *Mol Cancer Res*. 2007;5(5):455-9. doi: 10.1158/1541-7786.MCR-06-0439. PubMed PMID: 17475672.
88. Attene-Ramos MS, Nava GM, Muellner MG, Wagner ED, Plewa MJ, Gaskins HR. DNA damage and toxicogenomic analyses of hydrogen sulfide in human intestinal epithelial FHs 74

- Int cells. Environ Mol Mutagen. 2010;51(4):304-14. doi: 10.1002/em.20546. PubMed PMID: 20120018.
89. Ramasamy S, Singh S, Taniere P, Langman MJ, Eggo MC. Sulfide-detoxifying enzymes in the human colon are decreased in cancer and upregulated in differentiation. *American journal of physiology Gastrointestinal and liver physiology*. 2006;291(2):G288-96. doi: 10.1152/ajpgi.00324.2005. PubMed PMID: 16500920.
 90. Fontaine FE, Peterson WH, McCoy E, Johnson MJ, Ritter GJ. A New Type of Glucose Fermentation by *Clostridium thermoaceticum*. *Journal of bacteriology*. 1942;43(6):701-15. PubMed PMID: 16560531; PubMed Central PMCID: PMCPMC373636.
 91. Wood H, Ljungdahl L. Autotrophic character of the acetogenic bacteria. *Variations in autotrophic life*. 1991;1:201-50.
 92. Schaupp A, Ljungdahl LG. Purification and properties of acetate kinase from *Clostridium thermoaceticum*. *Arch Microbiol*. 1974;100(2):121-9. PubMed PMID: 4447427.
 93. Schuchmann K, Muller V. Energetics and Application of Heterotrophy in Acetogenic Bacteria. *Applied and environmental microbiology*. 2016;82(14):4056-69. Epub 2016/05/22. doi: 10.1128/aem.00882-16. PubMed PMID: 27208103; PubMed Central PMCID: PMCPMC4959221.
 94. Drake HL, Gossner AS, Daniel SL. Old acetogens, new light. *Ann N Y Acad Sci*. 2008;1125:100-28. doi: 10.1196/annals.1419.016. PubMed PMID: 18378590.
 95. Poehlein A, Bengelsdorf FR, Schiel-Bengelsdorf B, Gottschalk G, Daniel R, Durre P. Complete Genome Sequence of Rnf- and Cytochrome-Containing Autotrophic Acetogen *Clostridium aceticum* DSM 1496. *Genome announcements*. 2015;3(4). Epub 2015/07/18. doi: 10.1128/genomeA.00786-15. PubMed PMID: 26184942; PubMed Central PMCID: PMCPMC4505130.
 96. Poehlein A, Cebulla M, Ilg MM, Bengelsdorf FR, Schiel-Bengelsdorf B, Whited G, et al. The Complete Genome Sequence of *Clostridium aceticum*: a Missing Link between Rnf- and Cytochrome-Containing Autotrophic Acetogens. *mBio*. 2015;6(5):e01168-15. Epub 2015/09/10. doi: 10.1128/mBio.01168-15. PubMed PMID: 26350967; PubMed Central PMCID: PMCPMC4600107.
 97. Tremblay PL, Zhang T, Dar SA, Leang C, Lovley DR. The Rnf complex of *Clostridium ljungdahlii* is a proton-translocating ferredoxin:NAD⁺ oxidoreductase essential for autotrophic growth. *mBio*. 2012;4(1):e00406-12. Epub 2012/12/28. doi: 10.1128/mBio.00406-12. PubMed PMID: 23269825; PubMed Central PMCID: PMCPMC3531802.
 98. Martin WF. Hydrogen, metals, bifurcating electrons, and proton gradients: the early evolution of biological energy conservation. *FEBS letters*. 2012;586(5):485-93. Epub 2011/10/08. doi: 10.1016/j.febslet.2011.09.031. PubMed PMID: 21978488.
 99. Hess V, Schuchmann K, Muller V. The ferredoxin:NAD⁺ oxidoreductase (Rnf) from the acetogen *Acetobacterium woodii* requires Na⁺ and is reversibly coupled to the membrane potential. *J Biol Chem*. 2013;288(44):31496-502. doi: 10.1074/jbc.M113.510255. PubMed PMID: 24045950; PubMed Central PMCID: PMCPMC3814746.
 100. Hess V, Gallegos R, Jones JA, Barquera B, Malamy MH, Muller V. Occurrence of ferredoxin:NAD(+) oxidoreductase activity and its ion specificity in several Gram-positive and Gram-negative bacteria. *PeerJ*. 2016;4:e1515. Epub 2016/01/23. doi: 10.7717/peerj.1515. PubMed PMID: 26793417; PubMed Central PMCID: PMCPMC4715464.

101. Ragsdale SW, Pierce E. Acetogenesis and the Wood-Ljungdahl pathway of CO₂ fixation. *Biochim Biophys Acta*. 2008;1784(12):1873-98. doi: 10.1016/j.bbapap.2008.08.012. PubMed PMID: 18801467; PubMed Central PMCID: PMCPMC2646786.
102. Pierce E, Xie G, Barabote RD, Saunders E, Han CS, Detter JC, et al. The complete genome sequence of *Moorella thermoacetica* (f. *Clostridium thermoaceticum*). *Environmental microbiology*. 2008;10(10):2550-73. Epub 2008/07/18. doi: 10.1111/j.1462-2920.2008.01679.x. PubMed PMID: 18631365; PubMed Central PMCID: PMCPMC2575129.
103. Schuchmann K, Muller V. Autotrophy at the thermodynamic limit of life: a model for energy conservation in acetogenic bacteria. *Nature reviews Microbiology*. 2014;12(12):809-21. Epub 2014/11/11. doi: 10.1038/nrmicro3365. PubMed PMID: 25383604.
104. Moss AR, Jouany J-P, Newbold J, editors. *Methane production by ruminants: its contribution to global warming*. *Annales de zootechnie*; 2000: EDP Sciences.
105. McAllister T, Newbold C. Redirecting rumen fermentation to reduce methanogenesis. *Animal Production Science*. 2008;48(2):7-13.
106. Rey FE, Faith JJ, Bain J, Muehlbauer MJ, Stevens RD, Newgard CB, et al. Dissecting the in vivo metabolic potential of two human gut acetogens. *J Biol Chem*. 2010;285(29):22082-90. doi: 10.1074/jbc.M110.117713. PubMed PMID: 20444704; PubMed Central PMCID: PMCPMC2903421.
107. Schink B. Diversity, ecology, and isolation of acetogenic bacteria. *Acetogenesis*: Springer; 1994. p. 197-235.
108. Gerloff T, Stieger B, Hagenbuch B, Madon J, Landmann L, Roth J, et al. The sister of P-glycoprotein represents the canalicular bile salt export pump of mammalian liver. *J Biol Chem*. 1998;273(16):10046-50. PubMed PMID: 9545351.
109. Ivy A, Oldberg E. A hormone mechanism for gall-bladder contraction and evacuation. *American Journal of Physiology--Legacy Content*. 1928;86(3):599-613.
110. Hofmann AF. The continuing importance of bile acids in liver and intestinal disease. *Arch Intern Med*. 1999;159(22):2647-58. PubMed PMID: 10597755.
111. Gallo-Torres HE. Obligatory role of bile for the intestinal absorption of vitamin E. *Lipids*. 1970;5(4):379-84. PubMed PMID: 5447010.
112. Borgström B. On the interactions between pancreatic lipase and colipase and the substrate, and the importance of bile salts. *Journal of lipid research*. 1975;16(6):411-7.
113. Ridlon JM, Kang DJ, Hylemon PB. Bile salt biotransformations by human intestinal bacteria. *J Lipid Res*. 2006;47(2):241-59. Epub 2005/11/22. doi: 10.1194/jlr.R500013-JLR200. PubMed PMID: 16299351.
114. Dawson PA, Hubbert M, Haywood J, Craddock AL, Zerangue N, Christian WV, et al. The heteromeric organic solute transporter alpha-beta, Ostalpha-Ostbeta, is an ileal basolateral bile acid transporter. *J Biol Chem*. 2005;280(8):6960-8. doi: 10.1074/jbc.M412752200. PubMed PMID: 15563450; PubMed Central PMCID: PMCPMC1224727.
115. Hagenbuch B, Stieger B, Foguet M, Lubbert H, Meier PJ. Functional expression cloning and characterization of the hepatocyte Na⁺/bile acid cotransport system. *Proceedings of the National Academy of Sciences of the United States of America*. 1991;88(23):10629-33. PubMed PMID: 1961729; PubMed Central PMCID: PMCPMC52983.
116. Jones BV, Begley M, Hill C, Gahan CG, Marchesi JR. Functional and comparative metagenomic analysis of bile salt hydrolase activity in the human gut microbiome. *Proceedings of the National Academy of Sciences of the United States of America*. 2008;105(36):13580-5.

- Epub 2008/09/02. doi: 10.1073/pnas.0804437105. PubMed PMID: 18757757; PubMed Central PMCID: PMC2533232.
117. Gopal-Srivastava R, Hylemon PB. Purification and characterization of bile salt hydrolase from *Clostridium perfringens*. *J Lipid Res.* 1988;29(8):1079-85. PubMed PMID: 2903208.
 118. Masuda N. Deconjugation of bile salts by Bacteroids and *Clostridium*. *Microbiol Immunol.* 1981;25(1):1-11. PubMed PMID: 6265737.
 119. Wijaya A, Hermann A, Abriouel H, Specht I, Yousif NM, Holzapfel WH, et al. Cloning of the bile salt hydrolase (bsh) gene from *Enterococcus faecium* FAIR-E 345 and chromosomal location of bsh genes in food enterococci. *J Food Prot.* 2004;67(12):2772-8. PubMed PMID: 15633685.
 120. Jarocki P, Targoński Z. Genetic diversity of bile salt hydrolases among human intestinal bifidobacteria. *Current microbiology.* 2013;67(3):286-92.
 121. Tanaka H, Hashiba H, Kok J, Mierau I. Bile salt hydrolase of *Bifidobacterium longum*-biochemical and genetic characterization. *Applied and environmental microbiology.* 2000;66(6):2502-12. PubMed PMID: 10831430; PubMed Central PMCID: PMC110569.
 122. Oh HK, Lee JY, Lim SJ, Kim MJ, Kim GB, Kim JH, et al. Molecular cloning and characterization of a bile salt hydrolase from *Lactobacillus acidophilus* PF01. *J Microbiol Biotechnol.* 2008;18(3):449-56. PubMed PMID: 18388461.
 123. De Smet I, Van Hoorde L, Vande Woestyne M, Christiaens H, Verstraete W. Significance of bile salt hydrolytic activities of lactobacilli. *J Appl Bacteriol.* 1995;79(3):292-301. PubMed PMID: 7592123.
 124. Stellwag EJ, Hylemon PB. Purification and characterization of bile salt hydrolase from *Bacteroides fragilis* subsp. *fragilis*. *Biochim Biophys Acta.* 1976;452(1):165-76. PubMed PMID: 10993.
 125. Ridlon JM, Harris SC, Bhowmik S, Kang DJ, Hylemon PB. Consequences of bile salt biotransformations by intestinal bacteria. *Gut microbes.* 2016;7(1):22-39. Epub 2016/03/05. doi: 10.1080/19490976.2015.1127483. PubMed PMID: 26939849; PubMed Central PMCID: PMC4856454.
 126. Kim GB, Miyamoto CM, Meighen EA, Lee BH. Cloning and characterization of the bile salt hydrolase genes (bsh) from *Bifidobacterium bifidum* strains. *Applied and environmental microbiology.* 2004;70(9):5603-12. doi: 10.1128/AEM.70.9.5603-5612.2004. PubMed PMID: 15345449; PubMed Central PMCID: PMC520925.
 127. Kumar RS, Brannigan JA, Prabhune AA, Pundle AV, Dodson GG, Dodson EJ, et al. Structural and functional analysis of a conjugated bile salt hydrolase from *Bifidobacterium longum* reveals an evolutionary relationship with penicillin V acylase. *J Biol Chem.* 2006;281(43):32516-25. doi: 10.1074/jbc.M604172200. PubMed PMID: 16905539.
 128. Coleman JP, Hudson LL. Cloning and characterization of a conjugated bile acid hydrolase gene from *Clostridium perfringens*. *Applied and environmental microbiology.* 1995;61(7):2514-20. PubMed PMID: 7618863; PubMed Central PMCID: PMC167523.
 129. Gustafsson BE, Midtvedt T, Norman A. Metabolism of cholic acid in germfree animals after the establishment in the intestinal tract of deconjugating and 7 alpha-dehydroxylating bacteria. *Acta Pathol Microbiol Scand.* 1968;72(3):433-43. PubMed PMID: 4297296.
 130. Narushima S, Itoha K, Miyamoto Y, Park SH, Nagata K, Kuruma K, et al. Deoxycholic acid formation in gnotobiotic mice associated with human intestinal bacteria. *Lipids.* 2006;41(9):835-43. PubMed PMID: 17152920.

131. Wells JE, Berr F, Thomas LA, Dowling RH, Hylemon PB. Isolation and characterization of cholic acid 7 α -dehydroxylating fecal bacteria from cholesterol gallstone patients. *J Hepatol.* 2000;32(1):4-10. PubMed PMID: 10673060.
132. Qin J, Li R, Raes J, Arumugam M, Burgdorf KS, Manichanh C, et al. A human gut microbial gene catalogue established by metagenomic sequencing. *Nature.* 2010;464(7285):59-65. Epub 2010/03/06. doi: 10.1038/nature08821. PubMed PMID: 20203603; PubMed Central PMCID: PMC3779803.
133. Hamilton JP, Xie G, Raufman JP, Hogan S, Griffin TL, Packard CA, et al. Human cecal bile acids: concentration and spectrum. *American journal of physiology Gastrointestinal and liver physiology.* 2007;293(1):G256-63. Epub 2007/04/07. doi: 10.1152/ajpgi.00027.2007. PubMed PMID: 17412828.
134. Hofmann AF, Hagey LR. Key discoveries in bile acid chemistry and biology and their clinical applications: history of the last eight decades. *J Lipid Res.* 2014;55(8):1553-95. doi: 10.1194/jlr.R049437. PubMed PMID: 24838141; PubMed Central PMCID: PMC4109754.
135. Sarett LH. Partial synthesis of pregnene-4-triol-17 (β), 20 (β), 21-dione-3, 11 and pregnene-4-diol-17 (β), 21-trione-3, 11, 20 monoacetate. *Journal of Biological Chemistry.* 1946;162(3):601-31.
136. Hench PS, Kendall EC, Slocumb CH, Polley HF. The effect of a hormone of the adrenal cortex (17-hydroxy-11-dehydrocorticosterone: compound E) and of pituitary adrenocortical hormone in arthritis: preliminary report. *Annals of the rheumatic diseases.* 1949;8(2):97-104.
137. Hillier SG. Diamonds are forever: the cortisone legacy. *J Endocrinol.* 2007;195(1):1-6. doi: 10.1677/JOE-07-0309. PubMed PMID: 17911391.
138. Bergstrom S, Danielsson H, Kazuno T. Bile acids and steroids. 98. The metabolism of bile acids in python and constrictor snakes. *J Biol Chem.* 1960;235:983-8. PubMed PMID: 13799458.
139. Sjovall J. Fifty years with bile acids and steroids in health and disease. *Lipids.* 2004;39(8):703-22. PubMed PMID: 15638239.
140. Norman A, Sjovall J. On the transformation and enterohepatic circulation of cholic acid in the rat: bile acids and steroids 68. *J Biol Chem.* 1958;233(4):872-85. PubMed PMID: 13587508.
141. Norman A, Shorb MS. In vitro Formation of Deoxycholic and Lithocholic Acid by Human Intestinal Microorganisms.*. *Proceedings of the Society for Experimental Biology and Medicine.* 1962;110(3):552-5.
142. Samuelsson B. Bile acids and steroids 96. On the mechanism of the biological formation of deoxycholic acid from cholic acid. *Journal of Biological Chemistry.* 1960;235(2):361-6.
143. Hylemon PB, Melone PD, Franklund CV, Lund E, Bjorkhem I. Mechanism of intestinal 7 α -dehydroxylation of cholic acid: evidence that allo-deoxycholic acid is an inducible side-product. *J Lipid Res.* 1991;32(1):89-96. Epub 1991/01/01. PubMed PMID: 2010697.
144. Bennett MJ, McKnight SL, Coleman JP. Cloning and characterization of the NAD-dependent 7 α -Hydroxysteroid dehydrogenase from *Bacteroides fragilis*. *Curr Microbiol.* 2003;47(6):475-84. PubMed PMID: 14756531.
145. Sherrod JA, Hylemon PB. Partial purification and characterization of NAD-dependent 7 α -hydroxysteroid dehydrogenase from *Bacteroides thetaiotaomicron*. *Biochim Biophys Acta.* 1977;486(2):351-8. PubMed PMID: 189820.

146. Macdonald IA, Hutchison DM, Forrest TP. Formation of urso- and ursodeoxy-cholic acids from primary bile acids by *Clostridium absonum*. *J Lipid Res.* 1981;22(3):458-66. PubMed PMID: 6940948.
147. Macdonald IA, Meier EC, Mahony DE, Costain GA. 3 α -, 7 α - and 12 α -hydroxysteroid dehydrogenase activities from *Clostridium perfringens*. *Biochim Biophys Acta.* 1976;450(2):142-53. PubMed PMID: 10985.
148. Franklund CV, de Prada P, Hylemon PB. Purification and characterization of a microbial, NADP-dependent bile acid 7 α -hydroxysteroid dehydrogenase. *J Biol Chem.* 1990;265(17):9842-9. PubMed PMID: 2351678.
149. Yoshimoto T, Higashi H, Kanatani A, Lin XS, Nagai H, Oyama H, et al. Cloning and sequencing of the 7 α -hydroxysteroid dehydrogenase gene from *Escherichia coli* HB101 and characterization of the expressed enzyme. *Journal of bacteriology.* 1991;173(7):2173-9. PubMed PMID: 2007545; PubMed Central PMCID: PMCPMC207764.
150. Devlin AS, Fischbach MA. A biosynthetic pathway for a prominent class of microbiota-derived bile acids. *Nat Chem Biol.* 2015;11(9):685-90. Epub 2015/07/21. doi: 10.1038/nchembio.1864. PubMed PMID: 26192599; PubMed Central PMCID: PMCPMC4543561.
151. Hirano S, Masuda N. Transformation of bile acids by *Eubacterium lentum*. *Applied and environmental microbiology.* 1981;42(5):912-5. Epub 1981/11/01. PubMed PMID: 6947718; PubMed Central PMCID: PMCPMC244126.
152. MacDonald IA, Mahony DE, Jellett JF, Meier CE. NAD-dependent 3 α - and 12 α -hydroxysteroid dehydrogenase activities from *Eubacterium lentum* ATCC no. 25559. *Biochim Biophys Acta.* 1977;489(3):466-76. Epub 1977/12/21. PubMed PMID: 201289.
153. MacDonald IA, Jellett JF, Mahony DE, Holdeman LV. Bile salt 3 α - and 12 α -hydroxysteroid dehydrogenases from *Eubacterium lentum* and related organisms. *Applied and environmental microbiology.* 1979;37(5):992-1000. Epub 1979/05/01. PubMed PMID: 39496; PubMed Central PMCID: PMCPMC243337.
154. Eyssen H, Verhulst A. Biotransformation of linoleic acid and bile acids by *Eubacterium lentum*. *Applied and environmental microbiology.* 1984;47(1):39-43. Epub 1984/01/01. PubMed PMID: 6582800; PubMed Central PMCID: PMCPMC239608.
155. Edenharder R, Pfütznner A, Hammann R. Characterization of NAD-dependent 3 α - and 3 β -hydroxysteroid dehydrogenase and of NADP-dependent 7 β -hydroxysteroid dehydrogenase from *Peptostreptococcus productus*. *Biochimica et Biophysica Acta (BBA)-Lipids and Lipid Metabolism.* 1989;1004(2):230-8.
156. Taiko A, Teruaki A, HATTORI M, NAMBA T, KOBASHI K. 3 β -Hydroxysteroid Dehydrogenase of *Ruminococcus* sp. from Human Intestinal Bacteria. *Journal of biochemistry.* 1986;99(5):1425-31.
157. Lee JY, Arai H, Nakamura Y, Fukiya S, Wada M, Yokota A. Contribution of the 7 β -hydroxysteroid dehydrogenase from *Ruminococcus gnavus* N53 to ursodeoxycholic acid formation in the human colon. *J Lipid Res.* 2013;54(11):3062-9. doi: 10.1194/jlr.M039834. PubMed PMID: 23729502; PubMed Central PMCID: PMCPMC3793610.
158. Tandon R, Axelson M, Sjovall J. Selective liquid chromatographic isolation and gas chromatographic-mass spectrometric analysis of ketonic bile acids in faeces. *Journal of chromatography.* 1984;302:1-14. Epub 1984/10/19. PubMed PMID: 6501503.

159. Eneroth P, Gordon B, Ryhage R, Sjovall J. Identification of mono- and dihydroxy bile acids in human feces by gas-liquid chromatography and mass spectrometry. *J Lipid Res.* 1966;7(4):511-23. Epub 1966/07/01. PubMed PMID: 5966634.
160. Eneroth P, Gordon B, Sjovall J. Characterization of trisubstituted cholanoic acids in human feces. *J Lipid Res.* 1966;7(4):524-30. Epub 1966/07/01. PubMed PMID: 5965294.
161. Bjorkhem I, Angelin B, Einarsson K, Ewerth S. Fasting levels of monoketonic bile acids in human peripheral and portal circulation. *J Lipid Res.* 1982;23(7):1020-5. Epub 1982/09/01. PubMed PMID: 7142811.
162. Bjorkhem I, Liljeqvist L, Nilsell K, Einarsson K. Oxidoreduction of different hydroxyl groups in bile acids during their enterohepatic circulation in man. *J Lipid Res.* 1986;27(2):177-82. Epub 1986/02/01. PubMed PMID: 3958620.
163. Eguchi T, Miyazaki H, Nakayama F. Simultaneous determination of keto and non-keto bile acids in human serum by gas chromatography with selected ion monitoring. *Journal of chromatography.* 1990;525(1):25-42. Epub 1990/01/26. PubMed PMID: 2338448.
164. MacDonald IA, Williams CN, Mahony DE. A 3α - and 7α -hydroxysteroid dehydrogenase assay for conjugated dihydroxy-bile acid mixtures. *Analytical biochemistry.* 1974;57(1):127-36.
165. Einarsson K, Nilsell K, Bjorkhem I. Increased oxidoreduction of deoxycholic acid in cholecystectomised patients. *Gut.* 1989;30(9):1275-8. Epub 1989/09/01. PubMed PMID: 2806996; PubMed Central PMCID: PMCPMC1434232.
166. Parks DJ, Blanchard SG, Bledsoe RK, Chandra G, Consler TG, Kliewer SA, et al. Bile acids: natural ligands for an orphan nuclear receptor. *Science.* 1999;284(5418):1365-8. PubMed PMID: 10334993.
167. Wang H, Chen J, Hollister K, Sowers LC, Forman BM. Endogenous bile acids are ligands for the nuclear receptor FXR/BAR. *Mol Cell.* 1999;3(5):543-53. PubMed PMID: 10360171.
168. Inagaki T, Choi M, Moschetta A, Peng L, Cummins CL, McDonald JG, et al. Fibroblast growth factor 15 functions as an enterohepatic signal to regulate bile acid homeostasis. *Cell metabolism.* 2005;2(4):217-25.
169. Jung D, Inagaki T, Gerard RD, Dawson PA, Kliewer SA, Mangelsdorf DJ, et al. FXR agonists and FGF15 reduce fecal bile acid excretion in a mouse model of bile acid malabsorption. *J Lipid Res.* 2007;48(12):2693-700. doi: 10.1194/jlr.M700351-JLR200. PubMed PMID: 17823457.
170. Kawamata Y, Fujii R, Hosoya M, Harada M, Yoshida H, Miwa M, et al. A G protein-coupled receptor responsive to bile acids. *J Biol Chem.* 2003;278(11):9435-40. doi: 10.1074/jbc.M209706200. PubMed PMID: 12524422.
171. Maruyama T, Miyamoto Y, Nakamura T, Tamai Y, Okada H, Sugiyama E, et al. Identification of membrane-type receptor for bile acids (M-BAR). *Biochem Biophys Res Commun.* 2002;298(5):714-9. PubMed PMID: 12419312.
172. Duboc H, Tache Y, Hofmann AF. The bile acid TGR5 membrane receptor: from basic research to clinical application. *Dig Liver Dis.* 2014;46(4):302-12. doi: 10.1016/j.dld.2013.10.021. PubMed PMID: 24411485.
173. Thomas C, Gioiello A, Noriega L, Strehle A, Oury J, Rizzo G, et al. TGR5-mediated bile acid sensing controls glucose homeostasis. *Cell Metab.* 2009;10(3):167-77. doi: 10.1016/j.cmet.2009.08.001. PubMed PMID: 19723493; PubMed Central PMCID: PMCPMC2739652.

174. Kliewer SA, Goodwin B, Willson TM. The nuclear pregnane X receptor: a key regulator of xenobiotic metabolism. *Endocr Rev.* 2002;23(5):687-702. doi: 10.1210/er.2001-0038. PubMed PMID: 12372848.
175. Makishima M, Lu TT, Xie W, Whitfield GK, Domoto H, Evans RM, et al. Vitamin D receptor as an intestinal bile acid sensor. *Science.* 2002;296(5571):1313-6. doi: 10.1126/science.1070477. PubMed PMID: 12016314.
176. Studer E, Zhou X, Zhao R, Wang Y, Takabe K, Nagahashi M, et al. Conjugated bile acids activate the sphingosine-1-phosphate receptor 2 in primary rodent hepatocytes. *Hepatology.* 2012;55(1):267-76. doi: 10.1002/hep.24681. PubMed PMID: 21932398; PubMed Central PMCID: PMC3245352.
177. Raufman JP, Cheng K, Zimniak P. Activation of muscarinic receptor signaling by bile acids: physiological and medical implications. *Dig Dis Sci.* 2003;48(8):1431-44. PubMed PMID: 12924634.
178. Zhou H, Hylemon PB. Bile acids are nutrient signaling hormones. *Steroids.* 2014;86:62-8. doi: 10.1016/j.steroids.2014.04.016. PubMed PMID: 24819989; PubMed Central PMCID: PMC4073476.
179. Yoshimoto S, Loo TM, Atarashi K, Kanda H, Sato S, Oyadomari S, et al. Obesity-induced gut microbial metabolite promotes liver cancer through senescence secretome. *Nature.* 2013;499(7456):97-101. Epub 2013/06/28. doi: 10.1038/nature12347. PubMed PMID: 23803760.
180. Gill CI, Rowland IR. Diet and cancer: assessing the risk. *Br J Nutr.* 2002;88 Suppl 1:S73-87. doi: 10.1079/BJN2002632. PubMed PMID: 12215186.
181. Kawalek JC, Hallmark RK, Andrews AW. Effect of lithocholic acid on the mutagenicity of some substituted aromatic amines. *J Natl Cancer Inst.* 1983;71(2):293-8. PubMed PMID: 6348361.
182. Shibuya N, Nakadaira H, Ohta T, Nakamura K, Hori Y, Yamamoto M, et al. Co-mutagenicity of glyco- and tauro-deoxycholic acids in the Ames test. *Mutat Res.* 1997;395(1):1-7. PubMed PMID: 9465909.
183. Reddy BS, Narasawa T, Weisburger JH, Wynder EL. Promoting effect of sodium deoxycholate on colon adenocarcinomas in germfree rats. *J Natl Cancer Inst.* 1976;56(2):441-2. PubMed PMID: 1255778.
184. Islam KB, Fukiya S, Hagio M, Fujii N, Ishizuka S, Ooka T, et al. Bile acid is a host factor that regulates the composition of the cecal microbiota in rats. *Gastroenterology.* 2011;141(5):1773-81. doi: 10.1053/j.gastro.2011.07.046. PubMed PMID: 21839040.
185. Majer F, Sharma R, Mullins C, Keogh L, Phipps S, Duggan S, et al. New highly toxic bile acids derived from deoxycholic acid, chenodeoxycholic acid and lithocholic acid. *Bioorg Med Chem.* 2014;22(1):256-68. doi: 10.1016/j.bmc.2013.11.029. PubMed PMID: 24332653.
186. Barrasa JI, Olmo N, Lizarbe MA, Turnay J. Bile acids in the colon, from healthy to cytotoxic molecules. *Toxicol In Vitro.* 2013;27(2):964-77. doi: 10.1016/j.tiv.2012.12.020. PubMed PMID: 23274766.
187. Rao YP, Studer EJ, Stravitz RT, Gupta S, Qiao L, Dent P, et al. Activation of the Raf-1/MEK/ERK cascade by bile acids occurs via the epidermal growth factor receptor in primary rat hepatocytes. *Hepatology.* 2002;35(2):307-14. doi: 10.1053/jhep.2002.31104. PubMed PMID: 11826403.

188. Bernstein H, Bernstein C, Payne CM, Dvorak K. Bile acids as endogenous etiologic agents in gastrointestinal cancer. *World J Gastroenterol*. 2009;15(27):3329-40. PubMed PMID: 19610133; PubMed Central PMCID: PMCPMC2712893.
189. Hamada K, Umemoto A, Kajikawa A, Seraj MJ, Monden Y. In vitro formation of DNA adducts with bile acids. *Carcinogenesis*. 1994;15(9):1911-5. PubMed PMID: 7923585.
190. Da Silva M, Jagers GK, Verstraeten SV, Erlejan AG, Fraga CG, Oteiza PI. Large procyanidins prevent bile-acid-induced oxidant production and membrane-initiated ERK1/2, p38, and Akt activation in Caco-2 cells. *Free Radic Biol Med*. 2012;52(1):151-9. doi: 10.1016/j.freeradbiomed.2011.10.436. PubMed PMID: 22074817.
191. Muhlbauer M, Allard B, Bosserhoff AK, Kiessling S, Herfarth H, Rogler G, et al. Differential effects of deoxycholic acid and taurodeoxycholic acid on NF-kappa B signal transduction and IL-8 gene expression in colonic epithelial cells. *American journal of physiology Gastrointestinal and liver physiology*. 2004;286(6):G1000-8. doi: 10.1152/ajpgi.00338.2003. PubMed PMID: 14726307.
192. Payne CM, Weber C, Crowley-Skillicorn C, Dvorak K, Bernstein H, Bernstein C, et al. Deoxycholate induces mitochondrial oxidative stress and activates NF-kappaB through multiple mechanisms in HCT-116 colon epithelial cells. *Carcinogenesis*. 2007;28(1):215-22. doi: 10.1093/carcin/bgl139. PubMed PMID: 16887864.
193. Zhu Y, Hua P, Rafiq S, Waffner EJ, Duffey ME, Lance P. Ca²⁺- and PKC-dependent stimulation of PGE₂ synthesis by deoxycholic acid in human colonic fibroblasts. *American journal of physiology Gastrointestinal and liver physiology*. 2002;283(3):G503-10. doi: 10.1152/ajpgi.00525.2001. PubMed PMID: 12181161.
194. Pereira MA, Wang W, Kramer PM, Tao L. DNA hypomethylation induced by non-genotoxic carcinogens in mouse and rat colon. *Cancer Lett*. 2004;212(2):145-51. doi: 10.1016/j.canlet.2004.03.024. PubMed PMID: 15279894.
195. Pai R, Tarnawski AS, Tran T. Deoxycholic acid activates β -catenin signaling pathway and increases colon cell cancer growth and invasiveness. *Molecular biology of the cell*. 2004;15(5):2156-63.
196. Im E, Martinez JD. Ursodeoxycholic acid (UDCA) can inhibit deoxycholic acid (DCA)-induced apoptosis via modulation of EGFR/Raf-1/ERK signaling in human colon cancer cells. *The Journal of nutrition*. 2004;134(2):483-6.
197. Shant J, Cheng K, Marasa BS, Wang J-Y, Raufman J-P. Akt-dependent NF- κ B activation is required for bile acids to rescue colon cancer cells from stress-induced apoptosis. *Experimental cell research*. 2009;315(3):432-50.
198. Odermatt A, Da Cunha T, Penno CA, Chandsawangbhuwana C, Reichert C, Wolf A, et al. Hepatic reduction of the secondary bile acid 7-oxolithocholic acid is mediated by 11 β -hydroxysteroid dehydrogenase 1. *Biochem J*. 2011;436(3):621-9. doi: 10.1042/BJ20110022. PubMed PMID: 21453287.
199. Odermatt A, Klusonova P. 11 β -Hydroxysteroid dehydrogenase 1: Regeneration of active glucocorticoids is only part of the story. *J Steroid Biochem Mol Biol*. 2015;151:85-92. doi: 10.1016/j.jsbmb.2014.08.011. PubMed PMID: 25151952.
200. Huijghebaert SM, Eyssen HJ. Specificity of bile salt sulfatase activity from *Clostridium* sp. strains S1. *Applied and environmental microbiology*. 1982;44(5):1030-4. PubMed PMID: 7181500; PubMed Central PMCID: PMCPMC242143.

201. Van Eldere J, Celis P, De Pauw G, Lesaffre E, Eyssen H. Tauroconjugation of cholic acid stimulates 7 alpha-dehydroxylation by fecal bacteria. *Applied and environmental microbiology*. 1996;62(2):656-61. PubMed PMID: 8593067; PubMed Central PMCID: PMCPMC167832.
202. Rupnik M, Wilcox MH, Gerding DN. Clostridium difficile infection: new developments in epidemiology and pathogenesis. *Nature reviews Microbiology*. 2009;7(7):526-36. doi: 10.1038/nrmicro2164. PubMed PMID: 19528959.
203. Lessa FC, Mu Y, Bamberg WM, Beldavs ZG, Dumyati GK, Dunn JR, et al. Burden of Clostridium difficile infection in the United States. *N Engl J Med*. 2015;372(9):825-34. doi: 10.1056/NEJMoa1408913. PubMed PMID: 25714160.
204. Furuya-Kanamori L, Marquess J, Yakob L, Riley TV, Paterson DL, Foster NF, et al. Asymptomatic Clostridium difficile colonization: epidemiology and clinical implications. *BMC Infect Dis*. 2015;15:516. doi: 10.1186/s12879-015-1258-4. PubMed PMID: 26573915; PubMed Central PMCID: PMCPMC4647607.
205. Wilson KH, Perini F. Role of competition for nutrients in suppression of Clostridium difficile by the colonic microflora. *Infect Immun*. 1988;56(10):2610-4. PubMed PMID: 3417352; PubMed Central PMCID: PMCPMC259619.
206. Kuehne SA, Cartman ST, Heap JT, Kelly ML, Cockayne A, Minton NP. The role of toxin A and toxin B in Clostridium difficile infection. *Nature*. 2010;467(7316):711-3. doi: 10.1038/nature09397. PubMed PMID: 20844489.
207. Zar FA, Bakkanagari SR, Moorthi KM, Davis MB. A comparison of vancomycin and metronidazole for the treatment of Clostridium difficile-associated diarrhea, stratified by disease severity. *Clin Infect Dis*. 2007;45(3):302-7. doi: 10.1086/519265. PubMed PMID: 17599306.
208. van Nood E, Vrieze A, Nieuwdorp M, Fuentes S, Zoetendal EG, de Vos WM, et al. Duodenal infusion of donor feces for recurrent Clostridium difficile. *N Engl J Med*. 2013;368(5):407-15. doi: 10.1056/NEJMoa1205037. PubMed PMID: 23323867.
209. Buffie CG, Bucci V, Stein RR, McKenney PT, Ling L, Gorboun A, et al. Precision microbiome reconstitution restores bile acid mediated resistance to Clostridium difficile. *Nature*. 2015;517(7533):205-8. doi: 10.1038/nature13828. PubMed PMID: 25337874; PubMed Central PMCID: PMCPMC4354891.
210. Wilson KH. Efficiency of various bile salt preparations for stimulation of Clostridium difficile spore germination. *Journal of clinical microbiology*. 1983;18(4):1017-9. PubMed PMID: 6630458; PubMed Central PMCID: PMCPMC270959.
211. Wilson KH, Kennedy MJ, Fekety FR. Use of sodium taurocholate to enhance spore recovery on a medium selective for Clostridium difficile. *Journal of clinical microbiology*. 1982;15(3):443-6. PubMed PMID: 7076817; PubMed Central PMCID: PMCPMC272115.
212. Sorg JA, Sonenshein AL. Bile salts and glycine as cogerminants for Clostridium difficile spores. *Journal of bacteriology*. 2008;190(7):2505-12. doi: 10.1128/JB.01765-07. PubMed PMID: 18245298; PubMed Central PMCID: PMCPMC2293200.
213. Sorg JA, Sonenshein AL. Inhibiting the initiation of Clostridium difficile spore germination using analogs of chenodeoxycholic acid, a bile acid. *Journal of bacteriology*. 2010;192(19):4983-90. doi: 10.1128/JB.00610-10. PubMed PMID: 20675492; PubMed Central PMCID: PMCPMC2944524.
214. Francis MB, Allen CA, Shrestha R, Sorg JA. Bile acid recognition by the Clostridium difficile germinant receptor, CspC, is important for establishing infection. *PLoS Pathog*. 2013;9(5):e1003356. doi: 10.1371/journal.ppat.1003356. PubMed PMID: 23675301; PubMed Central PMCID: PMCPMC3649964.

215. Lewis BB, Carter RA, Pamer EG. Bile acid sensitivity and in vivo virulence of clinical *Clostridium difficile* isolates. *Anaerobe*. 2016;41:32-6. doi: 10.1016/j.anaerobe.2016.05.010. PubMed PMID: 27241781; PubMed Central PMCID: PMCPMC505091.
216. Weingarden AR, Chen C, Zhang N, Graiziger CT, Dosa PI, Steer CJ, et al. Ursodeoxycholic Acid Inhibits *Clostridium difficile* Spore Germination and Vegetative Growth, and Prevents the Recurrence of Ileal Pouchitis Associated With the Infection. *Journal of clinical gastroenterology*. 2016;50(8):624-30. doi: 10.1097/MCG.0000000000000427. PubMed PMID: 26485102; PubMed Central PMCID: PMCPMC4834285.
217. Ridlon JM, Ikegawa S, Alves JM, Zhou B, Kobayashi A, Iida T, et al. *Clostridium scindens*: a human gut microbe with a high potential to convert glucocorticoids into androgens. *J Lipid Res*. 2013;54(9):2437-49. Epub 2013/06/19. doi: 10.1194/jlr.M038869. PubMed PMID: 23772041; PubMed Central PMCID: PMCPMC3735941.
218. Ridlon JM, McGarr SE, Hylemon PB. Development of methods for the detection and quantification of 7 α -dehydroxylating clostridia, *Desulfovibrio vulgaris*, *Methanobrevibacter smithii*, and *Lactobacillus plantarum* in human feces. *Clin Chim Acta*. 2005;357(1):55-64. doi: 10.1016/j.cccn.2005.02.004. PubMed PMID: 15963794.
219. Loman NJ, Quinlan AR. Poretools: a toolkit for analyzing nanopore sequence data. *Bioinformatics (Oxford, England)*. 2014;30(23):3399-401. doi: 10.1093/bioinformatics/btu555. PubMed PMID: 25143291; PubMed Central PMCID: PMCPMC4296151.
220. Bankevich A, Nurk S, Antipov D, Gurevich AA, Dvorkin M, Kulikov AS, et al. SPAdes: a new genome assembly algorithm and its applications to single-cell sequencing. *J Comput Biol*. 2012;19(5):455-77. doi: 10.1089/cmb.2012.0021. PubMed PMID: 22506599; PubMed Central PMCID: PMCPMC3342519.
221. Kurtz S, Phillippy A, Delcher AL, Smoot M, Shumway M, Antonescu C, et al. Versatile and open software for comparing large genomes. *Genome Biol*. 2004;5(2):R12. doi: 10.1186/gb-2004-5-2-r12. PubMed PMID: 14759262; PubMed Central PMCID: PMCPMC395750.
222. Seemann T. Prokka: rapid prokaryotic genome annotation. *Bioinformatics (Oxford, England)*. 2014;30(14):2068-9. doi: 10.1093/bioinformatics/btu153. PubMed PMID: 24642063.
223. Kanehisa M, Sato Y, Morishima K. BlastKOALA and GhostKOALA: KEGG Tools for Functional Characterization of Genome and Metagenome Sequences. *J Mol Biol*. 2016;428(4):726-31. doi: 10.1016/j.jmb.2015.11.006. PubMed PMID: 26585406.
224. Stamatakis A. RAxML-VI-HPC: maximum likelihood-based phylogenetic analyses with thousands of taxa and mixed models. *Bioinformatics (Oxford, England)*. 2006;22(21):2688-90. Epub 2006/08/25. doi: 10.1093/bioinformatics/btl446. PubMed PMID: 16928733.
225. Huson DH, Richter DC, Rausch C, Dezulian T, Franz M, Rupp R. Dendroscope: An interactive viewer for large phylogenetic trees. *BMC bioinformatics*. 2007;8:460. Epub 2007/11/24. doi: 10.1186/1471-2105-8-460. PubMed PMID: 18034891; PubMed Central PMCID: PMCPMC2216043.
226. Turnbaugh PJ, Ley RE, Mahowald MA, Magrini V, Mardis ER, Gordon JI. An obesity-associated gut microbiome with increased capacity for energy harvest. *Nature*. 2006;444(7122):1027-31. doi: 10.1038/nature05414. PubMed PMID: 17183312.
227. Cho I, Blaser MJ. The human microbiome: at the interface of health and disease. *Nat Rev Genet*. 2012;13(4):260-70. doi: 10.1038/nrg3182. PubMed PMID: 22411464; PubMed Central PMCID: PMCPMC3418802.

228. de Prada P, Setchell KD, Hylemon PB. Purification and characterization of a novel 17 alpha-hydroxysteroid dehydrogenase from an intestinal Eubacterium sp. VPI 12708. *J Lipid Res.* 1994;35(5):922-9. Epub 1994/05/01. PubMed PMID: 8071614.
229. Macdonald IA, Bokkenheuser VD, Winter J, McLernon AM, Mosbach EH. Degradation of steroids in the human gut. *J Lipid Res.* 1983;24(6):675-700. PubMed PMID: 6350517.
230. Pellicciari R, Costantino G, Camaioni E, Sadeghpour BM, Entrena A, Willson TM, et al. Bile acid derivatives as ligands of the farnesoid X receptor. Synthesis, evaluation, and structure-activity relationship of a series of body and side chain modified analogues of chenodeoxycholic acid. *J Med Chem.* 2004;47(18):4559-69. doi: 10.1021/jm049904b. PubMed PMID: 15317466.
231. MOORE WEC, CATO EP, HOLDEMAN LV. *Eubacterium lentum* (Eggerth) Prévot 1938: Emendation of Description and Designation of the Neotype Strain. *International Journal of Systematic and Evolutionary Microbiology.* 1971;21(4):299-303. doi: doi:10.1099/00207713-21-4-299.
232. Eggerth AH. The Gram-positive Non-spore-bearing Anaerobic Bacilli of Human Feces. *Journal of bacteriology.* 1935;30(3):277-99. PubMed PMID: 16559837; PubMed Central PMCID: PMC543656.
233. Wade WG, Downes J, Dymock D, Hiom SJ, Weightman AJ, Dewhurst FE, et al. The family Coriobacteriaceae: reclassification of *Eubacterium exiguum* (Poco et al. 1996) and *Peptostreptococcus heliotrinireducens* (Lanigan 1976) as *Slackia exigua* gen. nov., comb. nov. and *Slackia heliotrinireducens* gen. nov., comb. nov., and *Eubacterium lentum* (Prevot 1938) as *Eggerthella lenta* gen. nov., comb. nov. *Int J Syst Bacteriol.* 1999;49 Pt 2:595-600. doi: 10.1099/00207713-49-2-595. PubMed PMID: 10319481.
234. Kageyama A, Benno Y, Nakase T. Phylogenetic evidence for the transfer of *Eubacterium lentum* to the genus *Eggerthella* as *Eggerthella lenta* gen. nov., comb. nov. *Int J Syst Bacteriol.* 1999;49 Pt 4:1725-32. doi: 10.1099/00207713-49-4-1725. PubMed PMID: 10555354.
235. Silverman ME. William Withering and An Account of the Foxglove. *Clin Cardiol.* 1989;12(7):415-8. PubMed PMID: 2663265.
236. Lindenbaum J, Rund DG, Butler VP, Jr., Tse-Eng D, Saha JR. Inactivation of digoxin by the gut flora: reversal by antibiotic therapy. *N Engl J Med.* 1981;305(14):789-94. doi: 10.1056/NEJM198110013051403. PubMed PMID: 7266632.
237. Chandrasekaran A, Robertson LW, Reuning RH. Reductive inactivation of digitoxin by *Eubacterium lentum* cultures. *Applied and environmental microbiology.* 1987;53(4):901-4. PubMed PMID: 3579289; PubMed Central PMCID: PMC203778.
238. Haiser HJ, Gootenberg DB, Chatman K, Sirasani G, Balskus EP, Turnbaugh PJ. Predicting and manipulating cardiac drug inactivation by the human gut bacterium *Eggerthella lenta*. *Science.* 2013;341(6143):295-8. Epub 2013/07/23. doi: 10.1126/science.1235872. PubMed PMID: 23869020; PubMed Central PMCID: PMC3736355.
239. Erdmann E, Schoner W. Ouabain-receptor interactions in (Na + +K +)-ATPase preparations from different tissues and species. Determination of kinetic constants and dissociation constants. *Biochim Biophys Acta.* 1973;307(2):386-98. PubMed PMID: 4268076.
240. Doherty JE, Kane JJ. Clinical pharmacology and therapeutics use of digitalis glycosides. *Drugs.* 1973;6(3):182-221. PubMed PMID: 4273255.
241. Honour J. The possible involvement of intestinal bacteria in steroidal hypertension. *Endocrinology.* 1982;110(1):285-7. doi: 10.1210/endo-110-1-285. PubMed PMID: 7053989.
242. Honour JW, Borriello SP, Ganten U, Honour P. Antibiotics attenuate experimental hypertension in rats. *J Endocrinol.* 1985;105(3):347-50. PubMed PMID: 2987388.

243. Honour JW. Historical perspective: gut dysbiosis and hypertension. *Physiol Genomics*. 2015;47(10):443-6. doi: 10.1152/physiolgenomics.00063.2015. PubMed PMID: 26199399.
244. Biglieri EG, Herron MA, Brust N. 17-hydroxylation deficiency in man. *The Journal of clinical investigation*. 1966;45(12):1946-54. doi: 10.1172/JCI105499. PubMed PMID: 4288776; PubMed Central PMCID: PMCPMC292880.
245. Shackleton CH, Biglieri EG, Roitman E, Honour JW. Metabolism of radiolabeled corticosterone in an adult with the 17 alpha-hydroxylase deficiency syndrome. *J Clin Endocrinol Metab*. 1979;48(6):976-82. doi: 10.1210/jcem-48-6-976. PubMed PMID: 312808.
246. Eriksson H, Gustafsson JA, Sjoval J. Steroids in germfree and conventional rats. 21-dehydroxylation by intestinal microorganisms. *Eur J Biochem*. 1969;9(4):550-4. PubMed PMID: 5806503.
247. Feighner SD, Bokkenheuser VD, Winter J, Hylemon PB. Characterization of a C21 neutral steroid hormone transforming enzyme, 21-dehydroxylase, in crude cell extracts of *Eubacterium lentum*. *Biochim Biophys Acta*. 1979;574(1):154-63. Epub 1979/07/27. PubMed PMID: 38850.
248. Feighner SD, Hylemon PB. Characterization of a corticosteroid 21-dehydroxylase from the intestinal anaerobic bacterium, *Eubacterium lentum*. *J Lipid Res*. 1980;21(5):585-93. Epub 1980/07/01. PubMed PMID: 6967506.
249. Funder JW. Mineralocorticoid receptors: distribution and activation. *Heart Fail Rev*. 2005;10(1):15-22. doi: 10.1007/s10741-005-2344-2. PubMed PMID: 15947887.
250. Edwards CR, Stewart PM, Burt D, Brett L, McIntyre MA, Sutanto WS, et al. Localisation of 11 beta-hydroxysteroid dehydrogenase--tissue specific protector of the mineralocorticoid receptor. *Lancet*. 1988;2(8618):986-9. PubMed PMID: 2902493.
251. Souness GW, Morris DJ. 11 alpha- and 11 beta-hydroxyprogesterone, potent inhibitors of 11 beta-hydroxysteroid dehydrogenase, possess hypertensinogenic activity in the rat. *Hypertension*. 1996;27(3 Pt 1):421-5. PubMed PMID: 8698448.
252. Durgan DJ, Ganesh BP, Cope JL, Ajami NJ, Phillips SC, Petrosino JF, et al. Role of the Gut Microbiome in Obstructive Sleep Apnea-Induced Hypertension. *Hypertension*. 2016;67(2):469-74. doi: 10.1161/HYPERTENSIONAHA.115.06672. PubMed PMID: 26711739; PubMed Central PMCID: PMCPMC4713369.
253. Jiang L, Yang S, Yin H, Fan X, Wang S, Yao B, et al. Epithelial-specific deletion of 11beta-HSD2 hinders *Apc^{min}/+* mouse tumorigenesis. *Mol Cancer Res*. 2013;11(9):1040-50. doi: 10.1158/1541-7786.MCR-13-0084-T. PubMed PMID: 23741059; PubMed Central PMCID: PMCPMC3778073.
254. Heuman DM. Quantitative estimation of the hydrophilic-hydrophobic balance of mixed bile salt solutions. *J Lipid Res*. 1989;30(5):719-30. PubMed PMID: 2760545.
255. Matsuoka K, Moroi Y. Micelle formation of sodium deoxycholate and sodium ursodeoxycholate (part 1). *Biochim Biophys Acta*. 2002;1580(2-3):189-99. PubMed PMID: 11880243.
256. Ley RE, Backhed F, Turnbaugh P, Lozupone CA, Knight RD, Gordon JI. Obesity alters gut microbial ecology. *Proceedings of the National Academy of Sciences of the United States of America*. 2005;102(31):11070-5. doi: 10.1073/pnas.0504978102. PubMed PMID: 16033867; PubMed Central PMCID: PMCPMC1176910.
257. Eckburg PB, Bik EM, Bernstein CN, Purdom E, Dethlefsen L, Sargent M, et al. Diversity of the human intestinal microbial flora. *Science*. 2005;308(5728):1635-8. doi:

- 10.1126/science.1110591. PubMed PMID: 15831718; PubMed Central PMCID: PMCPMC1395357.
258. Claus SP, Ellero SL, Berger B, Krause L, Bruttin A, Molina J, et al. Colonization-induced host-gut microbial metabolic interaction. *mBio*. 2011;2(2):e00271-10. doi: 10.1128/mBio.00271-10. PubMed PMID: 21363910; PubMed Central PMCID: PMCPMC3045766.
259. Martinez I, Wallace G, Zhang C, Legge R, Benson AK, Carr TP, et al. Diet-induced metabolic improvements in a hamster model of hypercholesterolemia are strongly linked to alterations of the gut microbiota. *Applied and environmental microbiology*. 2009;75(12):4175-84. doi: 10.1128/AEM.00380-09. PubMed PMID: 19411417; PubMed Central PMCID: PMCPMC2698331.
260. Salonen A, Lahti L, Salojarvi J, Holtrop G, Korpela K, Duncan SH, et al. Impact of diet and individual variation on intestinal microbiota composition and fermentation products in obese men. *The ISME journal*. 2014;8(11):2218-30. Epub 2014/04/26. doi: 10.1038/ismej.2014.63. PubMed PMID: 24763370; PubMed Central PMCID: PMCPMC4992075.
261. White BA, Fricke RJ, Hylemon PB. 7 beta-Dehydroxylation of ursodeoxycholic acid by whole cells and cell extracts of the intestinal anaerobic bacterium, *Eubacterium* species V.P.I. 12708. *J Lipid Res*. 1982;23(1):145-53. PubMed PMID: 7057103.
262. Kang DJ, Ridlon JM, Moore DR, 2nd, Barnes S, Hylemon PB. *Clostridium scindens* baiCD and baiH genes encode stereo-specific 7 α /7 β -hydroxy-3-oxo- Δ 4-cholenoic acid oxidoreductases. *Biochim Biophys Acta*. 2008;1781(1-2):16-25. Epub 2007/12/01. doi: 10.1016/j.bbali.2007.10.008. PubMed PMID: 18047844; PubMed Central PMCID: PMCPMC2275164.
263. Sperry JF, Wilkins TD. Arginine, a growth-limiting factor for *Eubacterium lentum*. *Journal of bacteriology*. 1976;127(2):780-4. Epub 1976/08/01. PubMed PMID: 182668; PubMed Central PMCID: PMCPMC232984.
264. Okuda S, Yamada T, Hamajima M, Itoh M, Katayama T, Bork P, et al. KEGG Atlas mapping for global analysis of metabolic pathways. *Nucleic Acids Res*. 2008;36(Web Server issue):W423-6. doi: 10.1093/nar/gkn282. PubMed PMID: 18477636; PubMed Central PMCID: PMCPMC2447737.
265. Dawson JA, Mallonee DH, Bjorkhem I, Hylemon PB. Expression and characterization of a C24 bile acid 7 α -dehydratase from *Eubacterium* sp. strain VPI 12708 in *Escherichia coli*. *J Lipid Res*. 1996;37(6):1258-67. PubMed PMID: 8808760.
266. Buckel W, Thauer RK. Energy conservation via electron bifurcating ferredoxin reduction and proton/Na⁺ translocating ferredoxin oxidation. *Biochim Biophys Acta*. 2013;1827(2):94-113. Epub 2012/07/18. doi: 10.1016/j.bbabi.2012.07.002. PubMed PMID: 22800682.
267. Soloway RD, Hofmann AF, Thomas PJ, Schoenfield LJ, Klein PD. Triketocholanoic (dehydrocholic) acid. Hepatic metabolism and effect on bile flow and biliary lipid secretion in man. *The Journal of clinical investigation*. 1973;52(3):715-24. Epub 1973/03/01. doi: 10.1172/jci107233. PubMed PMID: 4685091; PubMed Central PMCID: PMCPMC302310.
268. Winter J, Bokkenheuser VD. Bacterial metabolism of natural and synthetic sex hormones undergoing enterohepatic circulation. *J Steroid Biochem*. 1987;27(4-6):1145-9. PubMed PMID: 3320550.
269. Nava GM, Carbonero F, Ou J, Benefiel AC, O'Keefe SJ, Gaskins HR. Hydrogenotrophic microbiota distinguish native Africans from African and European Americans. *Environ*

- Microbiol Rep. 2012;4(3):307-15. doi: 10.1111/j.1758-2229.2012.00334.x. PubMed PMID: 23760794; PubMed Central PMCID: PMC4258901.
270. Ridlon JM, Kang DJ, Hylemon PB, Bajaj JS. Bile acids and the gut microbiome. *Current opinion in gastroenterology*. 2014;30(3):332-8. Epub 2014/03/15. doi: 10.1097/mog.000000000000057. PubMed PMID: 24625896; PubMed Central PMCID: PMC4215539.
271. Wells JE, Hylemon PB. Identification and characterization of a bile acid 7alpha-dehydroxylation operon in *Clostridium* sp. strain TO-931, a highly active 7alpha-dehydroxylating strain isolated from human feces. *Applied and environmental microbiology*. 2000;66(3):1107-13. Epub 2000/03/04. PubMed PMID: 10698778; PubMed Central PMCID: PMC91949.
272. Ridlon JM, Kang DJ, Hylemon PB. Isolation and characterization of a bile acid inducible 7alpha-dehydroxylating operon in *Clostridium hylemonae* TN271. *Anaerobe*. 2010;16(2):137-46. Epub 2009/05/26. doi: 10.1016/j.anaerobe.2009.05.004. PubMed PMID: 19464381.
273. Ye HQ, Mallonee DH, Wells JE, Bjorkhem I, Hylemon PB. The bile acid-inducible baiF gene from *Eubacterium* sp. strain VPI 12708 encodes a bile acid-coenzyme A hydrolase. *J Lipid Res*. 1999;40(1):17-23. Epub 1998/12/31. PubMed PMID: 9869646.
274. Ridlon JM, Hylemon PB. Identification and characterization of two bile acid coenzyme A transferases from *Clostridium scindens*, a bile acid 7alpha-dehydroxylating intestinal bacterium. *J Lipid Res*. 2012;53(1):66-76. Epub 2011/10/25. doi: 10.1194/jlr.M020313. PubMed PMID: 22021638; PubMed Central PMCID: PMC3243482.
275. Mallonee DH, Hylemon PB. Sequencing and expression of a gene encoding a bile acid transporter from *Eubacterium* sp. strain VPI 12708. *Journal of bacteriology*. 1996;178(24):7053-8. Epub 1996/12/01. PubMed PMID: 8955384; PubMed Central PMCID: PMC178615.
276. Mallonee DH, Adams JL, Hylemon PB. The bile acid-inducible baiB gene from *Eubacterium* sp. strain VPI 12708 encodes a bile acid-coenzyme A ligase. *Journal of bacteriology*. 1992;174(7):2065-71. Epub 1992/04/01. PubMed PMID: 1551828; PubMed Central PMCID: PMC205821.
277. Mallonee DH, White WB, Hylemon PB. Cloning and sequencing of a bile acid-inducible operon from *Eubacterium* sp. strain VPI 12708. *Journal of bacteriology*. 1990;172(12):7011-9. PubMed PMID: 2254270; PubMed Central PMCID: PMC210822.
278. Mallonee DH, Lijewski MA, Hylemon PB. Expression in *Escherichia coli* and characterization of a bile acid-inducible 3 alpha-hydroxysteroid dehydrogenase from *Eubacterium* sp. strain VPI 12708. *Curr Microbiol*. 1995;30(5):259-63. PubMed PMID: 7766153.
279. Bhowmik S, Chiu HP, Jones DH, Chiu HJ, Miller MD, Xu Q, et al. Structure and functional characterization of a bile acid 7alpha dehydratase BaiE in secondary bile acid synthesis. *Proteins*. 2016;84(3):316-31. Epub 2015/12/10. doi: 10.1002/prot.24971. PubMed PMID: 26650892; PubMed Central PMCID: PMC4755848.
280. Atarashi K, Tanoue T, Oshima K, Suda W, Nagano Y, Nishikawa H, et al. Treg induction by a rationally selected mixture of *Clostridia* strains from the human microbiota. *Nature*. 2013;500(7461):232-6. Epub 2013/07/12. doi: 10.1038/nature12331. PubMed PMID: 23842501.
281. Ridlon JM, Wolf PG, Gaskins HR. Taurocholic acid metabolism by gut microbes and colon cancer. *Gut microbes*. 2016;7(3):201-15. Epub 2016/03/24. doi: 10.1080/19490976.2016.1150414. PubMed PMID: 27003186; PubMed Central PMCID: PMC4939921.

282. Horinouchi M, Hayashi T, Kudo T. Steroid degradation in *Comamonas testosteroni*. *J Steroid Biochem Mol Biol*. 2012;129(1-2):4-14. Epub 2010/11/09. doi: 10.1016/j.jsbmb.2010.10.008. PubMed PMID: 21056662.
283. Eriksson H, Gustafsson JA. Excretion of steroid hormones in adults. *Steroids in faeces from adults*. *Eur J Biochem*. 1971;18(1):146-50. PubMed PMID: 5540510.
284. Adlercreutz H, Hockerstedt K, Bannwart C, Bloigu S, Hamalainen E, Fotsis T, et al. Effect of dietary components, including lignans and phytoestrogens, on enterohepatic circulation and liver metabolism of estrogens and on sex hormone binding globulin (SHBG). *J Steroid Biochem*. 1987;27(4-6):1135-44. PubMed PMID: 2826899.
285. Lombardi P, Goldin B, Boutin E, Gorbach SL. Metabolism of androgens and estrogens by human fecal microorganisms. *J Steroid Biochem*. 1978;9(8):795-801. PubMed PMID: 713557.
286. Adlercreutz H, Martin F, Jarvenpaa P, Fotsis T. Steroid absorption and enterohepatic recycling. *Contraception*. 1979;20(3):201-23. PubMed PMID: 389544.
287. Goldin BR, Adlercreutz H, Gorbach SL, Warram JH, Dwyer JT, Swenson L, et al. Estrogen excretion patterns and plasma levels in vegetarian and omnivorous women. *N Engl J Med*. 1982;307(25):1542-7. doi: 10.1056/NEJM198212163072502. PubMed PMID: 7144835.
288. Adlercreutz H, Fotsis T, Bannwart C, Hamalainen E, Bloigu S, Ollus A. Urinary estrogen profile determination in young Finnish vegetarian and omnivorous women. *J Steroid Biochem*. 1986;24(1):289-96. PubMed PMID: 3009980.
289. Bokkenheuser VD, Winter J, Cohen BI, O'Rourke S, Mosbach EH. Inactivation of contraceptive steroid hormones by human intestinal clostridia. *Journal of clinical microbiology*. 1983;18(3):500-4. PubMed PMID: 6630441; PubMed Central PMCID: PMCPMC270842.
290. Winter J, Shackleton CH, O'Rourke S, Bokkenheuser VD. Bacterial formation of aldosterone metabolites. *J Steroid Biochem*. 1984;21(5):563-9. PubMed PMID: 6513554.
291. Winter J, O'Rourke-Lo Cascio S, Bokkenheuser VD, Mosbach EH, Cohen BI. Reduction of 17-keto steroids by anaerobic microorganisms isolated from human fecal flora. *Biochim Biophys Acta*. 1984;795(2):208-11. PubMed PMID: 6477942.
292. Winter J, Bokkenheuser VD, Ponticorvo L. Bacterial metabolism of corticoids with particular reference to the 21-dehydroxylation. *J Biol Chem*. 1979;254(8):2626-9. Epub 1979/04/25. PubMed PMID: 429305.
293. Donova MV, Egorova OV. Microbial steroid transformations: current state and prospects. *Appl Microbiol Biotechnol*. 2012;94(6):1423-47. doi: 10.1007/s00253-012-4078-0. PubMed PMID: 22562163.
294. Rendle DF, Trotter J. The crystal and molecular structure of a novel steroidal rearrangement product, C₁₉H₂₆O₅. H₂O. *Acta Crystallographica Section B: Structural Crystallography and Crystal Chemistry*. 1975;31(6):1678-83.
295. Kerb U, Stahnke M, Schulze PE, Wiechert R. A novel entry to corticoids. *Angewandte Chemie International Edition in English*. 1981;20(1):88-9.
296. Turnbaugh PJ, Hamady M, Yatsunenko T, Cantarel BL, Duncan A, Ley RE, et al. A core gut microbiome in obese and lean twins. *Nature*. 2009;457(7228):480-4. doi: 10.1038/nature07540. PubMed PMID: 19043404; PubMed Central PMCID: PMCPMC2677729.
297. Neves AL, Chilloux J, Sarafian MH, Rahim MB, Boulange CL, Dumas ME. The microbiome and its pharmacological targets: therapeutic avenues in cardiometabolic diseases. *Current opinion in pharmacology*. 2015;25:36-44. Epub 2015/11/05. doi: 10.1016/j.coph.2015.09.013. PubMed PMID: 26531326.

298. Kakiyama G, Pandak WM, Gillevet PM, Hylemon PB, Heuman DM, Daita K, et al. Modulation of the fecal bile acid profile by gut microbiota in cirrhosis. *J Hepatol.* 2013;58(5):949-55. doi: 10.1016/j.jhep.2013.01.003. PubMed PMID: 23333527; PubMed Central PMCID: PMC3936319.
299. Ridlon JM, Alves JM, Hylemon PB, Bajaj JS. Cirrhosis, bile acids and gut microbiota: unraveling a complex relationship. *Gut microbes.* 2013;4(5):382-7. Epub 2013/07/16. doi: 10.4161/gmic.25723. PubMed PMID: 23851335; PubMed Central PMCID: PMC3839982.

Vita

Spencer Harris was born on September 7th, 1989 in Harrisburg, Pennsylvania. He graduated from Lower Dauphin High School in 2007. He attended the University of Richmond and graduated *magna cum laude* in 2011 with a Bachelors of Science in Biology. He matriculated into the MD-PhD program at the Virginia Commonwealth University in 2011.

AWARDS

Mary P. Coleman Award, 2015

Virginia Commonwealth University Department of Microbiology and Immunology

POSTERS/ABSTRACTS

Spencer C. Harris, Jason M. Ridlon, João M. P. Alves, Myrna Serrano, Shigeo Ikegawa, Takashi Iida, Gregory A. Buck, Phillip B. Hylemon. “Application of RNA-Seq in discovery of a gene involved in formation of allodeoxycholic acid by the human gut microbe *Clostridium scindens* ATCC 35704.” Rowett-INRA Joint Symposium in Aberdeen, Scotland, June 2014.

Jason M. Ridlon, **Spencer C. Harris**, Dae-Joong Kang, Runping Lui, Phillip Hylemon “Metabolomic analysis in a gnotobiotic mice colonized by human gut microbes *Clostridium scindens* and *Bacteroides vulgatus*” Rowett-INRA Joint Symposium in Aberdeen, Scotland, June 2014.

Spencer C. Harris, Jason M. Ridlon, Patricia Cooper, Shigeo Ikegawa, Kuniko Mitamura, Phillip B. Hylemon. “Biotransformation of androgenic precursors to epitestosterone and other 17α -hydroxy-steroids by commensal gut microbe *Clostridium scindens* VPI 12708.” National MD/PhD Student Conference in Keystone, Colorado, July 2014

Spencer C. Harris, Jason M. Ridlon, Dae-Joong Kang, Phillip B. Hylemon. “Newly characterized strain of *Eggerthella lenta* demonstrates link between bile acid metabolism and the acetogenesis pathway.” Gordon Archer Research Day in Richmond, Virginia, November 2016.

PUBLICATIONS

Ridlon J. M., **Harris S. C.**, Bhowmik S., Kang DJ., Hylemon P. B. (2016). Consequences of bile salt biotransformations by intestinal bacteria. *Gut Microbes* 7, 22–39.